



National Aeronautics and Space Administration

DO NOT DESTROY  
RETURN TO LIBRARY

CONFIGURATION DEVELOPMENT STUDY  
OF THE  
X-24C HYPERSONIC RESEARCH AIRPLANE  
- PHASE I

H G COMBS, et al  
Lockheed Aircraft Corporation  
Advanced Development Projects  
December 1976

8 SEP 1978  
MCDONNELL DOUGLAS  
RESEARCH & ENGINEERING LIBRARY  
ST. LOUIS

Prepared for

NATIONAL AERONAUTICS AND SPACE ADMINISTRATION  
Langley Research Center  
Hampton, Virginia 23665

NASA-CR-145032

M78-16775



National Aeronautics and  
Space Administration

**CONFIGURATION DEVELOPMENT STUDY  
OF THE  
X-24C HYPERSONIC RESEARCH AIRPLANE  
- PHASE I**

**H G COMBS, et al  
Lockheed Aircraft Corporation  
Advanced Development Projects  
December 1976**

**Prepared for  
NATIONAL AERONAUTICS AND SPACE ADMINISTRATION  
Langley Research Center  
Hampton, Virginia 23665**

1 Report No. NASA-CR-145032	2 Government Accession No.	3. Recipient's Catalog No	
4. Title and Subtitle CONFIGURATION DEVELOPMENT STUDY OF THE X-24C HYPERSONIC RESEARCH AIRPLANE - PHASE I		5 Report Date	
		6 Performing Organization Code	
7 Author(s) Henry G. Combs, et al		8. Performing Organization Report No SP-4499	
		10 Work Unit No	
9 Performing Organization Name and Address Advance Development Projects of The California Company, A Division of Lockheed Aircraft Corporation Burbank, CA 91520		11. Contract or Grant No NAS-1-14222	
		13. Type of Report and Period Covered Contractor Report Nov. 1975 thru March 1976	
12 Sponsoring Agency Name and Address National Aeronautics and Space Administration Washington, D.C. 20546		14 Sponsoring Agency Code	
15. Supplementary Notes			
16 Abstract  Four Hypersonic Research Airplane configurations found to be the most cost effective have been selected for further refinement in the Phase II Study. The selection was based on a systematic analysis and evaluation of realistic designs involving nine different configurations evolving from three different structural/thermal concepts coupled with existing rocket and sustainer engines. All configurations were constrained by the mission profiles, research requirements, aerodynamic envelope and maximum launch weight established by NASA.			
17 Key Words (Suggested by Author(s)) (STAR category underlined) Thermal Protection Systems Heat-Sink Structure Hypersonic Flight      Rocket Engines Lockalloy                      Research Ablator		18. Distribution Statement  Unclassified - Unlimited	
19 Security Classif (of this report) Unclassified	20. Security Classif. (of this page) Unclassified	21. No of Pages 351	22 Price*

\* Available from { The National Technical Information Service, Springfield, Virginia 22151  
{ STIF/NASA Scientific and Technical Information Facility, P O Box 33, College Park, MD 20740

## FOREWORD

This analytical study report is submitted to the National Aeronautics and Space Administration in accordance with NASA Contract NAS 1-14222. The work reported herein was performed between November 1975 through March 1976 culminating in an oral presentation at NASA LRC on 17 March 1976. The study was performed by the Advanced Development Projects "Skunk Works" of the California Company, a Division of Lockheed Aircraft, under the supervision of Mr. H.G. Combs, Study Manager. Engineering graphics and supporting text were developed under the direction of Messrs. D.H. Campbell (Propulsion and Thermodynamics), M.D. Cassidy (Aerodynamics), C.D. Sumpter (Structures), R.C. Murphy (Flight Dynamics), E.B. Seitz (Weight), G.J. Kachel and R.P. James (Vehicle Design), J. Walters and consulting services of J. Love (Maintenance), and R.T. Passon (Cost). The Program Monitor for NASA was Mr. J.D. Watts.

This study was a co-operative effort between the contractor and NASA in which data and frequent consultation, as well as program direction were provided by NASA.

## SUMMARY

Phase I analytical study was performed to determine the vehicle configuration most cost effective for refinement in Phase II and III of the NASA Configuration Development Study of the X-24C Hypersonic Research Airplane. The results permitted selection of cost-effective configurations for further refinement in the follow-on phases of the study.

Nine vehicle configurations, consisting of three different structure concepts in combination with three propulsion systems, were subjected to a systematic program involving development and evaluation of realistic design concepts coupled with propulsion and airframe integration. All configurations were constrained by predetermined mission profiles, aerodynamic shape and launch mass as specified by NASA.

Trade-off assessment of the thermal protection system clearly indicates the Lockalloy to be more cost-effective than the LI-900 RSI configuration, and to a lesser degree than the Ablator TPS. Both the Ablator configuration and Lockalloy configuration are recommended as the Phase II candidates.

Engine combination analysis concluded the kerosene fueled LR-105 engine with 12 LR-101 vernier engines to be the most effective combination as the Phase II study candidates. The LR-99 engine with two LR-11 engines is also recommended for the Phase II study.

Trade studies have systematically narrowed the configuration to the four most promising for the Phase II analytical study. In addition to meeting all requirements set forth by NASA for the X-24C they are the most cost-effective and provide the maximum payload mass capability for research activities.

Design refinement during the Phase II study will include analytical analysis to expand the selected configurations and an assessment of the impact to boost the vehicle to higher mach numbers.

## TABLE OF CONTENTS

	<u>Page</u>
Foreword	iii/iv
Summary	v/vi
Introduction	1
Basis for Design	3
Candidate Vehicles	8
Technical Approach	9
Mission Profiles	10
Realistic Designs	29
Load Analysis	31
Structural Analysis Models	36
Wing Analysis	60
Fuselage Analysis	91
Thermal Analysis	137
Landing Gear Selection	170
Propulsion System Installation	176
Propellant Tankage - Volumetric Analysis	186
Structural Arrangement	189
Functional Systems	207
Structural Dynamics Analysis	216
Mass Analysis	221
Cost Analysis	266
Flight Support and Maintenance Analysis	293
Research Capabilities	307
Risk Assessment	309
Trade Study Results	312
Trade Study Recommendations	315

## TABLE OF CONTENTS (Continued)

	<u>Page</u>
Review of Phase II and III Studies	316
References	317
APPENDICES	
A - NASA Statement of Work	323
B - NASTRAN Output - Unit Surface Loading and Shear Flows	341
C - Cost Trade Studies - Escalation Factor	347
D - X-24C Major Equipment Items	349

## LIST OF FIGURES

<u>Number</u>	<u>Title</u>	<u>Page</u>
A	Aerodynamic Configuration	4
1	Trim Lift Characteristics	12
2	Zero Lift Drag	13
3	Drag Due to Lift	13
4	Lift/Drag Characteristics with Scramjets	14
5	LR-99 Throttled Performance	16
6	LR-105 Throttled Performance	16
7	LR-105 DT Derated Thrust Performance	17
8	LR-105 ALC Thrust	17
9	LR-11 Thrust	18
10	LR-101's Throttled Performance	18
11	Launch/Boost Control by Pitch Attitude Schedule	20
12	Typical Boost Profile	21
13	Deceleration and Descent Path for Cross-Range	24
14	Deceleration Control	24
15	Mission Profiles - Altitude/Mach vs Time	25
16	Mission Profiles - $q$ , $N_z$ , $\alpha$ vs Time	25
17	Mission Profiles - Mach vs Altitude	27
18	Mission Profiles - Altitude vs Distance	27
19	Analysis Program	30
20	Wing Spanwise Load Intensities - Pullup after B-52 Launch (Aluminum Design)	35
21	Wing Spanwise Load Intensities - Subsonic Flight Negative One G (Aluminum Design)	35
22	Wing Surface Load Intensities - Pullup after B-52 Launch (Lockalloy Design)	38
23	Wing Surface Load Intensities - Maximum Temperature Gradients (Lockalloy Design)	38
24	Wing Surface Load Intensities - Comparison	39



LIST OF FIGURES (Continued)

<u>Number</u>	<u>Title</u>	<u>Page</u>
25	NASTRAN Model	40
26	NASTRAN Structural Model - Wing	43/44
27	NASTRAN Frame Model, F.S. 498	42
28	NASTRAN Frame Model, F.S. 553	42
29	NASTRAN Structural Model - Fuselage	45/46
30	NASTRAN Structural Model, F.S. 496 (Lockalloy Design)	48
31	Airframe Structural Arrangement - Aluminum	50
32	Fuselage Extensional and Shear Thicknesses Input into the Aluminum Design Structural Model	51
33	Wing Surface Extensional and Shear Thicknesses - Aluminum	52
34	Wing Rear Beam Vertical Displacement	53
35	Fuselage Lower Centerline Vertical Displacement	53
36	Wing Surface Load Intensities - Pullup	54
37	Wing Surface Load Intensities - Subsonic	54
38	Fuselage Load Intensities for Pullup After Launch	55
39	Fuselage Panel Thicknesses Input - Lockalloy	56
40	Wing Surface Extensional and Shear Thicknesses - Lockalloy Design	58
41	Wing Surface Load Intensities, Pullup - Lockalloy Design	58
42	Wing Surface Load Intensities, Maximum Maneuver - Lockalloy Design	59
43	Wing Surface Load Intensities, Maximum Temperature Gradient Condition - Lockalloy Design	59
44	Fuselage Thermal Stress	60
45	Wing Arrangement - Aluminum	64
46	Wing Arrangement - Lockalloy	64
47	Wing Point Design Regions	66

## LIST OF FIGURES (Continued)

<u>Number</u>	<u>Title</u>	<u>Page</u>
48	Wing Surface Load Intensities, Pullup - Aluminum Design	66
49	Wing Surface Load Intensities, Pullup - Lockalloy Design	67
50	Wing Surface Load Intensities, Maximum Temperature Gradient Condition - Lockalloy Design	67
51	Cross Sectional Geometry of Surface Panel Concepts	70
52	Notation of Panel Dimension and Loading	70
53	Temperature History - Aluminum/LI-900 Design	79
54	Temperature History - Aluminum/LI-900 Design	79
55	Insulation Thickness - LI-900 as Function of Temperature	80
56	Wing Box Unit Mass - Point Design Region 2	81
57	Estimated Ablator Thicknesses	84
58	Ablator Thicknesses as Function of Panel Thickness	84
59	Wing Box Unit Mass, Point Design - Aluminum/Ablator Design	85
60	Wing Upper Surface Panel Thicknesses	86
61	Wing Lower Surface Panel Thicknesses	86
62	Detail Mass Breakdown, Point Design - Lockalloy Design	88
63	Aluminum Design Critical Design Regions	89
64	Wing Rib/Spar Spacing - Aluminum Design	89
65	Wing Surface Effective Thickness Map - Aluminum/LI-900 Design	90
66	Wing Surface Effective Thickness Map - Aluminum/Ablator Design	90
67	Critical Design Regions - Lockalloy Design	92
68	Wing Rib/Spar Spacing - Lockalloy Design	92
69	Wing Surface Thickness Map - Lockalloy Design	93
70	X-24C General Arrangement	94

## LIST OF FIGURES (Continued)

<u>Number</u>	<u>Title</u>	<u>Page</u>
71	Fuselage Section - Aluminum Design	95
72	Fuselage Frame - Lockalloy Design	95
73	Critical Design Conditions - Aluminum Design	96
74	Critical Design Conditions - Lockalloy Design	96
75	Fuselage Surface Design Loads	97
76	Fuselage Surface Pressures - F. S. 300	98
77	Fuselage Surface Pressures - F. S. 400	98
78	Fuselage Surface Pressures - F. S. 525	99
79	Fuselage Shell Thickness	100
80	Fuselage Shell Thickness - LR-99 Mission	100
81	Skin Thickness Requirements, Side Panel - Lockalloy Design	106
82	Skin Thickness Requirements, Upper Surface - Lockalloy Design	106
83	Skin Thickness, 0.46 Meter Frames - Lockalloy Design	107
84	Surface Thickness, Typical Station - Lockalloy Design	107
85	NASTRAN Structural Model - F. S. 496	115
86	Frame for Lockalloy Vehicle	117
87	Frame for Aluminum Vehicle	117
88	Frame Load and Constraint Combination Configuration - F. S. 496	118
89	Simplified Frame Model	118
90	Frame Moments - F. S. 496	120
91	Fuselage Frames - Area Requirement	121
92	Frame Area - Titanium Frames	121
93	Fuselage Frame, Area Requirement - Upper Surface	122
94	Fuselage Frame, Area Requirement - Lower Surface	122
95	Frame Length Between Support for Frame - Stability Requirement	123
96	Frame Construction - Lockalloy Design	125

## LIST OF FIGURES (Continued)

<u>Number</u>	<u>Title</u>	<u>Page</u>
97	Lockalloy Supports - Lower Surface	125
98	Frame Thermal Stress vs Material	126
99	Thermal Stress with Rotational Constraint	129
100	Lockalloy Stresses and Strain During Heating and Cooling	129
101	Fuselage Skin Panel Time-Temperature History	130
102	Lockalloy Creep Allowances	132
103	Vehicle Heat Treat Element Numbers	138
104	Lockalloy Peak Temperature During Mission vs Skin Thickness - Lockalloy Design	140
105	Lockalloy Peak Temperature During Mission vs Skin Thickness - Lockalloy Design	140
106	Conical Half Angle	142
107	Axial Distance to Transition Location	142
108	Axial Distance to Midpoint of Transition - Nominal Flight	143
109	Axial Distance to Beginning of Transition - Nominal Flight	143
110	Temperature History, Fuselage Side - Aluminum/LI-900 Design	146
111	Temperature History, Wing Upper Surface - Aluminum/Li-900 Design	146
112	Temperature History, Fuselage Underside - Aluminum/LI-900 Design	147
113	Temperature History, Wing Lower Surface - Aluminum/LI-900 Design	147
114	Effects of Aerodynamic Heating on Ablator Charing Rate	150
115	Effects of Initial Char on Temperature - Aluminum/Ablator Design	151
116	Effects of Initial Char on Temperature - Aluminum/Ablator Design	151
117	Estimated Ablator Thickness - Elements 96 @ 106	152
118	Peak Temperature of Lockalloy Leading Edges	155

LIST OF FIGURES (Continued)

<u>Number</u>	<u>Title</u>	<u>Page</u>
119	Effect of Insulation on Aluminum Leading Edges	156
120	Thermal Response - Linkage Assembly	156
121	Lockalloy Supports - Top Surface	157
122	Lockalloy Supports - Side Surface	157
123	Lockalloy Supports - Lower Surface	158
124	Lockalloy Supports - Top Surface	158
125	Lockalloy/Titanium Frames - Side Surface	159
126	Lockalloy/Titanium Frames - Lower Surface	159
127	Effect of Heating Rate Uncertainty Factor on Skin Temperature - Shock Interference Area (Lockalloy Design)	163
128	Effect of Heating Rate Uncertainty Factor on Skin Temperature - Lower Centerline (Lockalloy Design)	163
129	Effect of Heating Rate Uncertainty Factor on Aluminum/LI-900 - Lower Centerline	164
130	Effect of Heating Rate Uncertainty Factor on Aluminum/LI-900 - Shock Interference Area	164
131	Effect of Heating Rate Uncertainty Factor on Aluminum/Ablator	165
132	Effect of Heating Rate Uncertainty Factor on Aluminum/Ablator - Shock Interference Area	165
133	Oxygen Tank Insulation Study	167
134	Oxygen Tank Insulation Study	167
135	Effects of Lockalloy Maximum Temperature on Windward Side of Elevon	169
136	Effect of LI-900 Thickness in Flow Reattachment Area of Rudder	171
137	Effect of Lockalloy Thickness in Flow Reattachment Area of Rudder	171
138	Effect of Ablator Thickness in Flow Reattachment Area - Speed Brake	172
139	Thermal Response of Lockalloy Rudder Flaps	172

## LIST OF FIGURES (Continued)

<u>Number</u>	<u>Title</u>	<u>Page</u>
140	Area/Periphery Curve	254
141	Landing Gear Arrangement	175
142	Nose Gear Installation	177
143	Main Landing Gear Installation	178
144	LR-99 Engine Installation	180
145	LR-105 Engine Installation	180
146	LR-11 Engine Installation	181
147	LR-101 Engine Installation	182
148	Engine Seal Criteria	183
149	Scramjet Structural Cavity	184
150	Scramjet Module Installation	185
151	Scramjet Seal Criteria	186
152	Propellant Tankage Arrangement - LR-99	188
153	Propellant Tankage Arrangement - LR-105	188
154	Propellant Tankage Arrangement - LR-105	189
155	Typical Tank Mounting	190
156	General Arrangement - Aluminum Design	192
157	Typical Frame - Aluminum Design	193
158	Midbody Section - Aluminum Design	193
159	Cockpit Area Structure - Aluminum Design	194
160	Lower Flap Installation	195
161	Payload Bay Structure - Aluminum Design	196
162	Wing Arrangement - Aluminum Design	196
163	Wing Attachment	197
164	General Arrangement - Lockalloy Design	198
165	Cockpit Area Structure - Lockalloy Design	199
166	Typical Fuselage Frame - Lockalloy Design	199
167	Midbody Structure - Lockalloy Design	200

## LIST OF FIGURES (Continued)

<u>Number</u>	<u>Title</u>	<u>Page</u>
168	Wing Arrangement - Lockalloy Design	200
169	Space Shuttle - LI-900 RSI Installation	201
170	Slip Joint Criteria	205
171	Avionic System	208
172	Flight Control System Pitch and Roll Axis	211
173	Electrical and Hydraulic System	214
174	Spars and Ribs	227
175	Rudder Envelope	235
176	Speed Brake Limit	236
177	Side Fin Envelope	242
178	Access Door Cutout	247
179	Side Wall Structure	251
180	Manpower Summary	297
181	Manpower Summary - Two Vehicles	297
182	Maintenance Hours Assignment, - Lockalloy	299
183	Maintenance Hours Assignment - LI-900	299
184	Maintenance Hours Assignment - Ablative	300
185	Base Support Summary	306
186	Risk Elements - LI-900	313
187	Risk Elements - Ablator	313
188	Risk Elements - Lockalloy	314
189	Risk Elements Summary	314

## LIST OF TABLES

<u>Number</u>	<u>Title</u>	<u>Page</u>
1	Performance of Propulsion System-Launch Mass - 25.85 Mg	28
2	Comparison Wing Inplane Load Intensities - Aluminum Design	34
3	Comparison Wing Inplane Load Intensities - Lockalloy Design	37
4	History of NASTRAN Internal Load Runs	41
5	Model Load Inputs	49
6	Mechanical and Physical Properties - Candidate Structural Materials	62
7	Wing Aerodynamic Pressure	68
8	Wing Point Design Load/Temperature Environment - Aluminum Design, Pullup	69
9	Wing Point Design Load/Temperature Environment - Aluminum Design, Subsonic	69
10	Wing Point Design Load/Temperature Environment - Lockalloy Design, Pullup	69
11	Wing Point Design Load/Temperature Environment - Lockalloy Design, Maximum Maneuver	69
12	Wing Panel Requirement - Aluminum/LI-900 Design	78
13	Insulation Requirements for Aluminum/LI-900 Design	78
14	Detail Mass Breakdown - Point Design - Aluminum/ LI-900 Design	81
15	Wing Surface Geometry - Aluminum/Ablator Design	83
16	Insulation Requirements - Aluminum/Ablator Design	83
17	Detail Mass Breakdown, Point Design - Aluminum/ Ablator Design	85
18	Wing Surface Panel Thickness - Lockalloy Design	85
19	Detail Mass Breakdown Point Design - Lockalloy Design	88
20	Thermal Stress Analysis Configuration	124
21	Limit Load State for Wing Surface Panels	134
22	Detail Creep Analysis - Lockalloy Design	134



## LIST OF TABLES (Continued)

<u>Number</u>	<u>Title</u>	<u>Page</u>
23	Summary of Creep Analysis - Wing Surface Panels - Lockalloy Design	135
24	LI-900 Insulation Thermal Results	145
25	Ablator Insulation Thermal Results	153
26	Shockwave and Boundary Layer Interaction	162
27	Group Mass Breakdown	222
28	Wing Structure Box - LI-900	226
29	Lower Skin Panels - LI-900	227
30	Spars and Ribs	227
31	Leading Edge Mass - LI-900	228
32	Elevon Mass - LI-900	228
33	Wing Summary - LI-900	229
34	Wing Summary - Ablator	229
35	Wing Structure Box - Lockalloy	230
36	Lower Skin Panels - Lockalloy	230
37	Leading Edge Mass - Lockalloy	231
38	Elevon Panel Thickness - Lockalloy	232
39	Elevon Mass - Lockalloy	232
40	Wing Summary - Lockalloy	234
41	Wing Structure Mass Summary	234
42	Speed Brake Design Conditions	235
43	Skin Panel Thickness	241
44	Skin Panel Mass	241
45	Skin Panel Criteria	244
46	Tail Structure Mass Summary	246
47	Forebody Skin Panel Mass - LI-900	247
48	Frame and Bulkhead Mass	249
49	Cockpit Structure Mass	251

## LIST OF TABLES (Continued)

<u>Number</u>	<u>Title</u>	<u>Page</u>
50	Side Wall Structure	252
51	Forebody Structure - LI-900	253
52	Forebody Structure - Ablator	253
53	Forebody Panel Mass	255
54	Frame/Bulkhead Mass - Lockalloy	257
55	Forebody Structure Mass - Lockalloy	259
56	Cockpit Secondary Structure Mass	259
57	Door/Nonstructure Panels Mass - Aluminum	260
58	Doors/Nonstructure Panels Mass - Lockalloy	260
59	Forebody Secondary Structure Mass	260
60	Payload Bay Mass Summary	261
61	Aft Body Mass Summary	262
62	Fuselage Structure Mass Summary	263
63	Propulsion System Mass Summary	264
64	Propellant System Mass Summary	265
65	Systems Mass Summary	266
66	Phase I Costing Tradeoff Study	268
67	Vehicle Price Summary	270
68	X-24C-101 Summary	271
69	X-24C-102 Summary	271
70	X-24C-103 Summary	272
71	X-24C-104 Summary	272
72	X-24C-105 Summary	273
73	X-24C-106 Summary	273
74	X-24C-107 Summary	274
75	X-24C-108 Summary	274
76	X-24C-109 Summary	275
77	Material and Equipment Cost Summary	277

## LIST OF TABLES (Continued)

<u>Number</u>	<u>Title</u>	<u>Page</u>
78	X-24C-101 Mass Breakdown	280
79	X-24C-102 Mass Breakdown	280
80	X-24C-103 Mass Breakdown	281
81	X-24C-104 Mass Breakdown	281
82	X-24C-105 Mass Breakdown	282
83	X-24C-106 Mass Breakdown	282
84	X-24C-107 Mass Breakdown	283
85	X-24C-108 Mass Breakdown	283
86	X-24C-109 Mass Breakdown	284
87	Propulsion System Alternatives	285
88	Propulsion System Alternatives - Lockalloy Configuration	285
89	Thermal Protection System Alternatives	287
90	TPS Comparison	289
91	TPS Alternatives	289
92	TPS Cost Comparison	290
93	Initial Spares and AGE Premises	291
94	Initial Investment	293
95	Initial Investment Cost Summary	294
96	Cost Estimate Accuracy	296
97	Vehicle Acquisition Cost Conclusion	295

## INTRODUCTION

During the past 15 years considerable progress has been made in ground-based R&D aimed at solving the critical problems of future high-speed aircraft. Many of these developments have reached the stage where they must be demonstrated in actual flight at large scale prior to applications. The research airplane provides focus and stimulus for ground-based research and development and demands a level of commitment which will guarantee worthy hardware. While it is evident that much of the value of a flight test program is derived from the focused laboratory development and testing which it generates, the actual flight demonstration in the real environment of large critical components enables decision makers to accept these technologies as proven options for future operational systems.\*

A number of special purpose research aircraft with limited objectives have been built, i. e., USAF X-24A and NASA HL-10 and M2F2 specifically to explore the piloting problems of the lifting-body reentry vehicles at low speeds and landing. The successful X-24A program was extended by the USAF to include a more slender shape, the X-24B, at speeds up to about Mach 2. Recently the USAF proposed a further extension to Mach 5 denoting the program X-24C.\*

While the proposed X-24 vehicle could accomplish some of the objectives for a high speed aircraft the question arose as whether some other low-cost derivative of the X-24 configuration could not be developed to accomplish all the major objectives of a new high speed research aircraft.\*

Since considerable interest was evident on the part of both USAF and NASA, an ad hoc study group was formed in May 1974. The study centered on the use of the X-24C concept to develop a flight vehicle which would fulfill USAF and NASA

---

\* From Reference 48

research objectives. The approach taken was to develop a flight research vehicle which has the inherent capability to be a test bed for a significant number of experiments, not only those which can be visualized now but the unknown experiments of the future.\*

The original research vehicle concept adopted as a starting point a research vehicle primarily intended to explore the aerodynamic and heating characteristics of a blended wing-body delta-planform vehicle in the Mach 2 to 5 speed regime and was conceived as a growth version of the X-24B.\*

From the joint NASA/USAF ad-hoc group studies, requirements for higher speeds and the ability to accommodate payloads of greater mass and larger payload volumes were established. In addition, the basic aerodynamic configuration, the mission performance and the research payload definition were established for a research vehicle which would provide maximum research versatility at minimum cost. Trade studies by the joint NASA/USAF group further outlined a number of configuration alternatives regarding propulsion, structures and thermal protection systems which the research vehicle could accommodate.

Since ultimate performance capabilities of the proposed research vehicle will largely depend on the final selection of the structure and thermal protection system, in addition to the propulsion system, a three part study expressly for the purpose of narrowing these design options was let out to industry.

Phase I of the study would provide cost and mass trade study results of the alternative structure, thermal protection system, and propulsion systems from which multiple concepts would emerge as the contender for review in Phase II. Phase II would look into the performance growth of the potential design concept(s), selected in Phase I, along with the attendant costs associated with the increased

---

\* From Reference 48

performance. Phase III would study the refinement of the NASA-USAF X-24C aerodynamic configuration and conceptual design of the vehicle which evolves from the design trades and growth potential evaluation, Phase I and II.

This report covers the Phase I analytical study conducted by the Advanced Development Projects of the California Company, a Division of Lockheed Aircraft Corporation. Aerodynamic, structural, thermal, mass and cost analysis based on realistic designs were conducted with sufficient depth to verify and support the trade study analysis configurations. Critical problem areas investigated include: (1) selection of thermal protection systems, (2) selection of propulsion systems, (3) scramjet integration, (4) definition of a stability and control system, and (5) initial and operational costs. Analytical studies include analysis of life-cycle costs of vehicle field maintenance and thermal protection system (TPS) field maintenance. The results from these systematic analysis narrowed the configuration alternatives down to the most cost-effective concepts, meeting the Phase I vehicle requirements, from which a selection for Phase II was possible.

### BASIS FOR DESIGN TRADES

The basic objective of the study effort was to determine, through a comprehensive, systematic trade study, a viable X-24C design concept that could proceed directly into the hardware phase. The amount of detail design which went into each of the configurations was of sufficient depth to support each of the trade study analysis, but entails further design effort before it could support a manufacturing program. The analytical study was performed on vehicle configurations, and missions established by NASA/USAF and meet the following salient input data as set forth by NASA/USAF:

Aerodynamic Configuration - The aerodynamic configuration for the X-24C (Figure A) with three Scramjet modules was supplied by Langley Research Center. Changes to the configuration developed during the study included: (1) shifting to

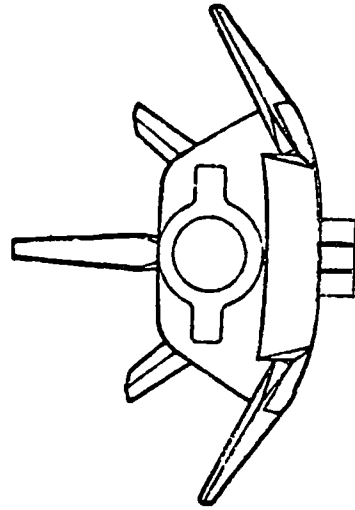
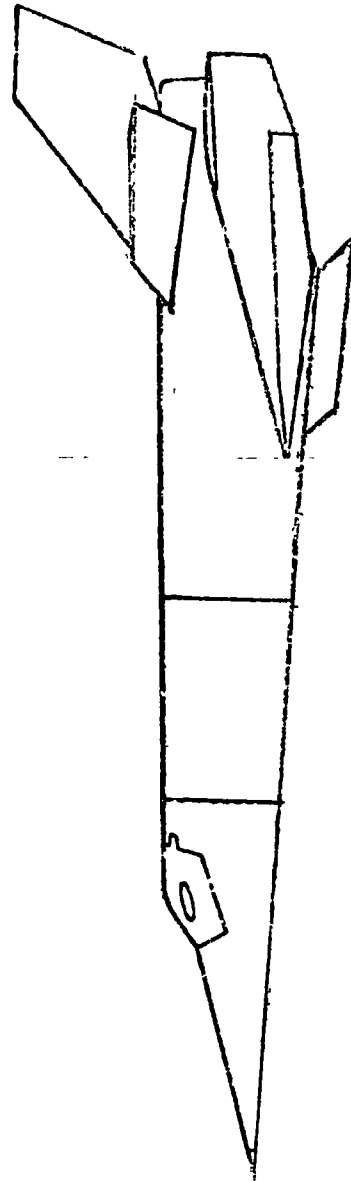
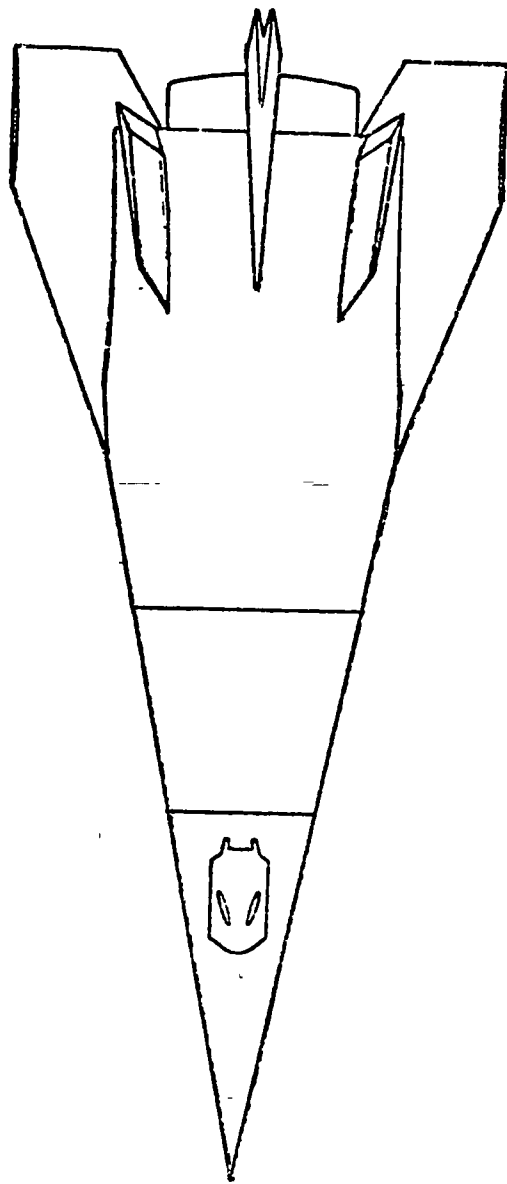


Figure A - Aerodynamic Configuration

vertical fin aft approximately 25.4 cm to align the fin rear spar with the fuselage aft-most frame, and (2) converting the flat bottom, side, and top surface to large radius of curvature to aid in carrying longitudinal axial loads in the Lockalloy monocoque shell configuration.

Performance - Performance defined for the Phase I study included:

- 1) 40 seconds cruise at  $M = 6.0$  and 47.9 kPa dynamic pressure (26930 m) with a 3 module Scramjet package installed.
- 2) Launch from a B-52 at  $M = 0.85$  and 13720 m.
- 3) Rocket performance supplied by the engine manufacturers.
- 4) Payload bay in the fuselage for research experiments including Scramjet hydrogen tanks and following payload bay options:
  - All rocket propellants to meet the performance to be carried in the primary propellant tanks, and
  - A portion of the rocket propellant may be carried in the payload section.

Research Requirements - Research requirements dictate the following vehicle features to be maintained:

- 1) The vehicle shall have a full-depth, replaceable 3.0 m long research payload bay provided by a section of the body structure between the cockpit and rocket propellant tanks.
- 2) The volume within the payload bay shall be used for research payloads, research structures, integral and nonintegral experimental hydrogen tanks, research instrumentation and equipment, and fuel for research propulsion systems such as the Scramjet.
- 3) The payload bay structure may be of conventional construction compatible with the rest of the vehicle and have transition sections at both



ends to allow a load path offset as required in 4 below. Field splices will be provided at each end of the bay to allow replacement of the bay structure with advanced research structure.

- 4) The payload bay shall have a heat shield type stand-off thermal protection system (TPS) with the same TPS concept as the vehicle itself and a mold line recessed 0.10 meter on the upper and side surfaces and 0.15 meter on the lower surface. This arrangement will allow partial or complete replacement of the payload bay stand-off TPS with advanced research TPS concepts.
- 5) The vehicle shall have removable and replaceable wings, fins, and stabilizers to allow testing of advanced aerodynamic surface structures. Slip joints or other appropriate interface structure shall be provided at the fuselage junction to enable testing of hot structures.
- 6) The vehicle shall have a lower surface designed to allow efficient aerodynamic integration of LRC Scramjet modules of sufficient size to cruise the aircraft at Mach 6. The integrated design concept utilizes the forebody of the vehicle as an inlet precompression surface and the aftbody as an external nozzle expansion surface.

Vehicle Operations - The X-24C vehicle shall be operated in the following manner during the flight research program:

- 1) B-52 Air Launch - The vehicle will be air-launched from B-52B S/N 008 at 13720 meter altitude and a Mach number of 0.85. The assumption is made that mass, c. g., and clearance constraints are the same as with the X-15A-2 vehicle.
- 2) Test Range - The NASA High Range test corridor in the Utah-Nevada-California area will be utilized for X-24C in the same manner as with the X-15. Existing radar, telemetry, and communications stations at Edwards AFB and Ely, Nevada, shall be considered satisfactory for the X-24C program.

- 3) **Flight Frequency** - For planning purposes and operational cost estimating, an average of 12 flights per vehicle per year will be used for the X-24C vehicle unless refurbishment or other characteristics of a particular design concept made this an unrealistic assumption. The flight research program will be assumed to consist of 100 flights per vehicle.
- 4) **Energy Management** - For the purposes of energy management in the flight operations of X-24C, a speed brake system is required.

Structural Design Criteria - The requirements for structural performance were established by NASA and delineated by Appendix A. Criteria were expanded during the study for the Lockalloy vehicle design corresponding to the time in flight when the maximum temperature differentials exist.

Costing Assumptions - The following assumptions were made regarding cost determinations:

- 1) The program philosophy is based on the need by both NASA and USAF to keep program costs to a minimum commensurate with accomplishing the research objectives.
- 2) The management approach shall be in the form of prototype management wherein the Contractor who builds the vehicle is given considerable freedom to accomplish the task with minimum Government control.
- 3) The operating mode shall be in a "classical" experimental shop or "Skunk Works" type wherein the engineering, design, and fabrication team is separate from normal corporate activity and is located in an atmosphere which is conducive to close communication and minimum red tape and paperwork.
- 4) All cost estimates and breakdowns (actuals) are provided in terms of January 1975 and January 1976 dollars.

- 5) Maximum usage of Government furnished equipment and off-the-shelf hardware has been made in the interest of minimizing cost. Estimates include the cost of GFE and identify the source and availability. Excepting for rocket engines, which will be procured and costed separately by the Government, the design effort and cost estimates include all other components of the primary propulsion system including installation of the rocket engines.
- 6) In order that dollar estimates are more representative of potential Government funding, a Contractor fee of 10% is included in all prices except for the cost of GFAE.

#### CANDIDATE VEHICLES

Considering the range of heat loads and mission profile anticipated for the X-24C vehicle, nine configurations emerged as candidates based on the spectrum of structural approaches and propulsion system combinations available to support the X-24C program schedule. The candidate configurations were based on the following:

Propulsion System - The X-24C vehicle requirement for acceleration to Mach 6 and cruise for 40 seconds dictated a rocket engine propulsion system. Additionally, since the steady state 40 second cruise requires lower thrust than acceleration, this leads to a throttleable propulsion system or separate cruise engines. These characteristics produced eight candidate propulsion systems for the analysis:

	MAX THRUST @ $\triangle 2$	ISP @ $\triangle 2$	MIN CRUISE THRUST @ $\triangle 3$
1. LR-99 EXT NOZZLE, $\triangle 1$	277.1 kN (62,300 LB)	285 SEC	131.2 kN (29,500 LB)
2. LR-105 $\triangle 1$	367.5 (82,620)	306	204.6 (46,000)
3. LR-105 DERATED, $\triangle 1$	262.0 (58,900)	300	57.8 (13,000)
4. LR-99 + 2 LR-11 NH <sub>3</sub> FUEL FOR BOOST AND CRUISE	351.9 (79,100)	279	9.3 (2,100)*
5. LR-105 + 12 LR-101's FOR CRUISE ONLY	367.5 (82,620)	306	2.7 (600)
6. LR-105 + 12 LR-101's FOR BOOST AND CRUISE	442.6 (99,500)	288	2.7 (600)
7. LR-105 ALC FUELED + 2 LR-11's FOR CRUISE	298.9 (67,200)	289	9.3 (2,100)*
8. LR-105 ALC FUELED + 2 LR-11's FOR BOOST AND CRUISE	373.7 (84,000)	277	9.3 (2,100)*

$\triangle 1$  THROTTLEABLE

$\triangle 2$  21336 METER  
(70,000 FEET)

$\triangle 3$  27432 METER  
(90,000 FEET)

\* = INCREMENTS

Structural Systems - Three structural concepts were anticipated for the two categories of passive TPS: (1) high temperature metal, and (2) nonmetallics established for the study. The high temperature metal candidate used a substructure compatible with Lockalloy/beryllium paneling. The nonmetallic concept evolved around an aluminum substructure on which LI-900 RSI or Ablator TPS could be attached to the skin as an insulator. While the two nonmetallic TPS substructures were essentially the same, the panel stiffness required by the LI-900 did produce a structure somewhat heavier than that required for the Ablator TPS.

## TECHNICAL APPROACH

A systematic trade-off analysis was conducted on each of the candidate configuration concepts in sufficient depth to verify and support the final results. The Phase I study was subdivided into four main tasks:

- Task I - Developed mission profiles and maximum zero fuel mass for each of the propulsion concepts. This was done by determining that portion of 25855 kg launch mass that would be used as fuel to accomplish the mission.
- Task II - Developed realistic design and mass data for each configuration concept. The concept designs were carried to sufficient depth to permit valid comparisons between the spectrum of approaches. On concepts found to be lighter in mass than the zero fuel mass the excess was reflected as an increase in the research payload capacity.
- Task III - Evaluated the research capability of each of the candidate concepts, this involved primarily payload, speed, and time considerations, and included adaptability of each of the concepts to the research requirements.
- Task IV - Vehicle cost and program risks were evaluated. Costs were developed on detail design and mass for each concept.

The risk analysis took into account:

- Mission
- Cost
- Maintenance

Based on data developed at this point, recommendations were made relative to the selection of the concepts showing sufficient promise to be pursued further in the next phase of the study.

## MISSION PROFILES

Mission profiles were developed to allow performance comparison of the various propulsion concepts and to define aerodynamic heating data for evaluation

of the three thermal protection systems described in the 'Thermal Analysis' herein. These profiles also entered into the conceptual design of various vehicle components and systems required for development of realistic vehicle designs, mass and costs. Mission requirements, used in developing the mission profiles, were established by NASA and defined under 'BASIS FOR DESIGN TRADES' herein, include a 40 second cruise at Mach 6 and a dynamic pressure of 47.9 kPa on rocket power.

The boost phase varied for the different propulsion concepts requiring maximizing performance within the common requirements defined by NASA and delineated under 'BASIS FOR DESIGN TRADES' herein. Cruise, deceleration and descent were kept the same except for mass effects. A minimum heat input, high  $\alpha$ , deceleration was used.

The following paragraphs present the basic input data, methods and philosophy used and the resulting time histories.

### Flight Path Analysis

Aerodynamic Data - The configuration was established by NASA and defined under 'BASIS FOR DESIGN TRADES' herein. The 3 module scramjet module is intended for scramjet flight development and as such is nonthrusting.

A maximum usable angle of attack of  $20^\circ$  was found desirable and estimated to be attainable for the pullup during boost and during deceleration. This required an extrapolation of the LRC data from  $\alpha = 16^\circ$  to  $20^\circ$ . The trimmed lift characteristic used in this study as shown in Figure 1 is a function of Mach number at constant angle of attack.

The drag characteristics are shown in Figures 2 and 3 in the form used in this study. The data received from LRC was reworked to the form zero lift drag and drag due to lift. The scramjet drag increment is also shown in Figure 2. An overview of the lift/drag characteristics with the 3 scramjet modules is shown in Figure 4 in terms of drag polars, L/D max, and

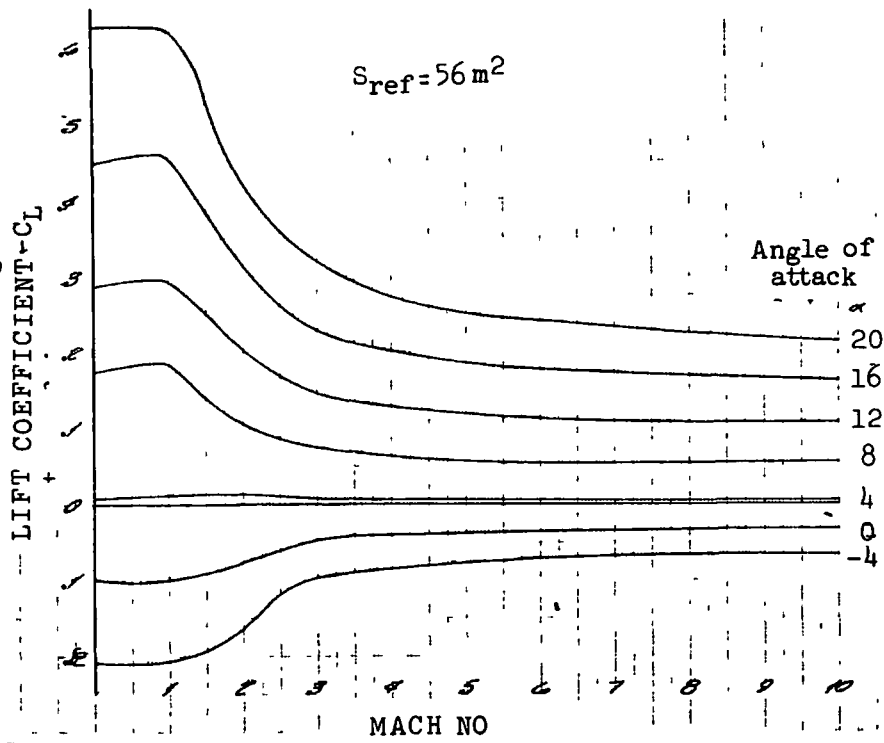


Figure 1 - Trim Lift Characteristics

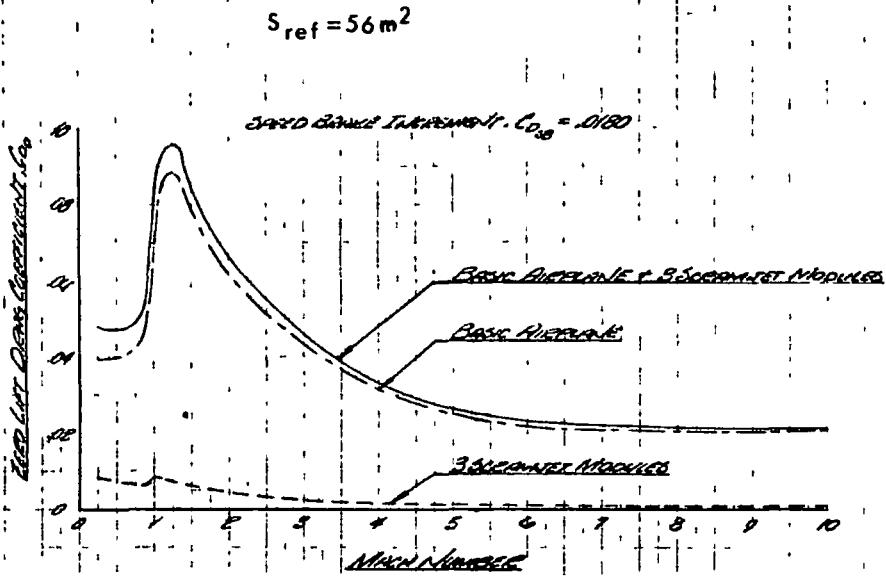


Figure 2 - Zero Lift Drag

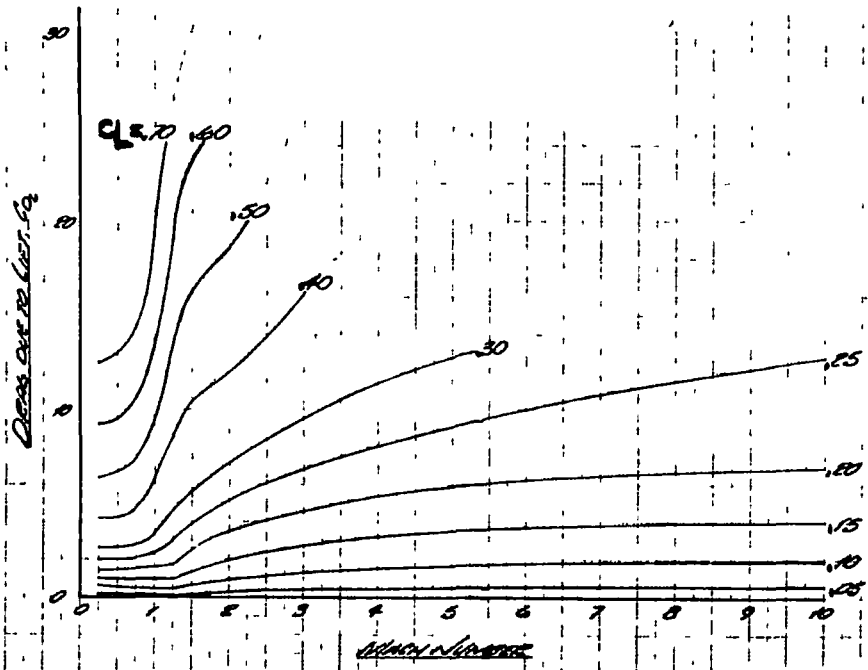


Figure 3 - Drag Due to Lift



angle of attack for L/D max versus Mach number. Of note is the L/D max of over 4 subsonically and 2.5 at  $M = 6.0$  with angle of attack for L/D max being 16 and 13 degrees; respectively. These data were the result of early analysis by NASA Langley Research Center. Subsequent wind tunnel data analysis indicate that these values are highly optimistic through the subsonic and transonic speeds and slightly pessimistic at moderate supersonic speeds ( $2 < M < 5$ ). The net result could be a slight loss in performance over that predicted in this study.

Propulsion Data - The statement of work, Appendix A, defined three propulsion concepts for the design trades: LR-99 -- extended nozzle, LR-105 -- throttleable, and LR-105 + Atlas verniers. Other engines were reviewed to assure that other potential contenders were not being overlooked. Also, a quick look at the cruise requirement indicated that more needed to be done in that area.

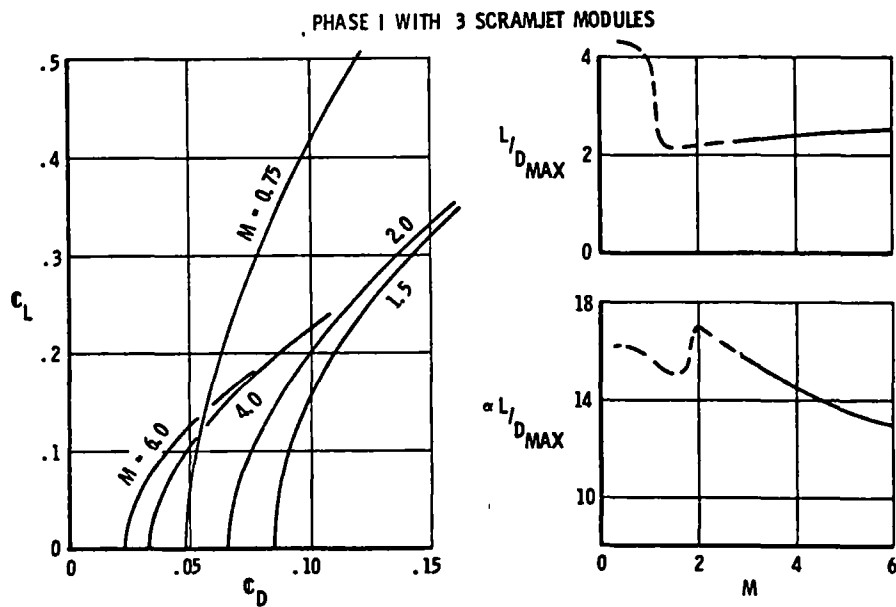


Figure 4 - Lift/Drag Characteristics with Scramjets

As far as the basic thrust engine and vehicle performance are concerned, the LR-91, Titan 2nd stage, and LR-105, Stlas sustainer, are essentially the same. The LR-81 Agena engines were ruled out because of the highly toxic IRFNA oxidizer. The LR-99 was specified for study because it is man rated, throttleable, and available. Due to the limited throttling capability of the basic LR-99 and LR-105 (132.6 kN and 204.6 kN, respectively, compared to 71.2 kN required) other cruise modes needed consideration. Excess thrust during cruise is detrimental in two respects. Excess propellant is burned and the speed brake requirements add considerable vehicle mass. A derated LR-105 was included with a throttling capability down to 57.8 kN.

Several cruise engine options were included. To allow flexibility between rocket cruise time and boosted Mach number, a common propellant is required. Therefore, two  $\text{NH}_3$  fueled LR-11's were considered as cruise engines with the LR-99. LR-101's are compatible with the LR-105 and, in fact, can utilize the LR-105 propellant pumping system. This gives a high degree of flexibility insofar as number of chambers used in combination with the potential throttling capability of the LR-105 pumps. The LR-101 thrust can vary from 2.74 to 6.23 kN per chamber. The presently qualified LR-11 is fueled with 75% ethyl alcohol. For propellant compatibility, an alcohol fueled LR-105 with two LR-11's was evaluated.

X-24C boost and cruise performance were evaluated for the above engines for preliminary review in the form of three throttleable and five cruise engine propulsion system concepts listed under 'CANDIDATE VEHICLES' herein. The engine performance used in this study is presented for each engine in Figures 5 through 10. This performance is based on data received from each of the engine manufacturers for application to the X-24C.

Basis for Mission Performance - The mission analysis required for the trade study included boost cruise, deceleration and descent. Launch and landing were assumed capabilities that affected all of the vehicle concepts equally.

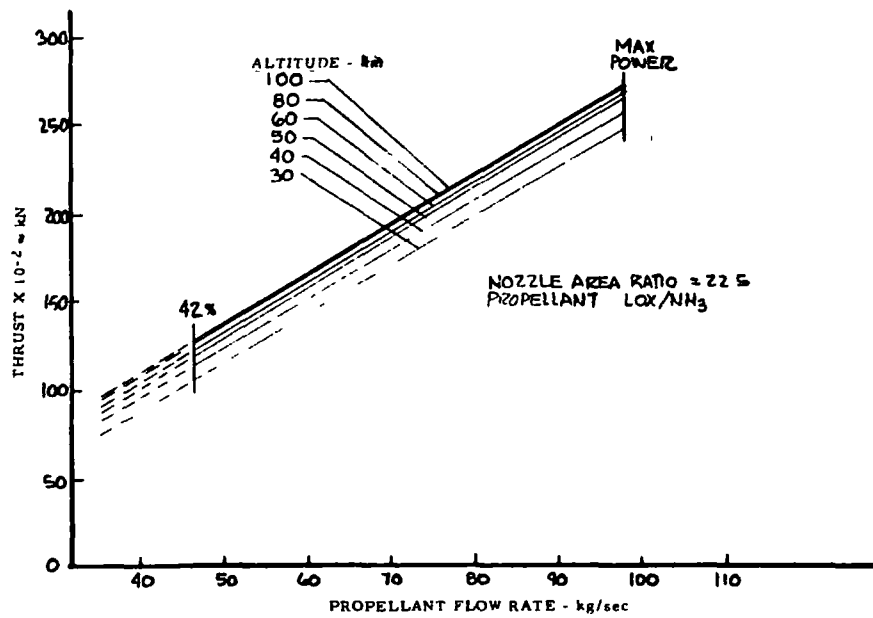


Figure 5 - LR-99 Throttled Performance

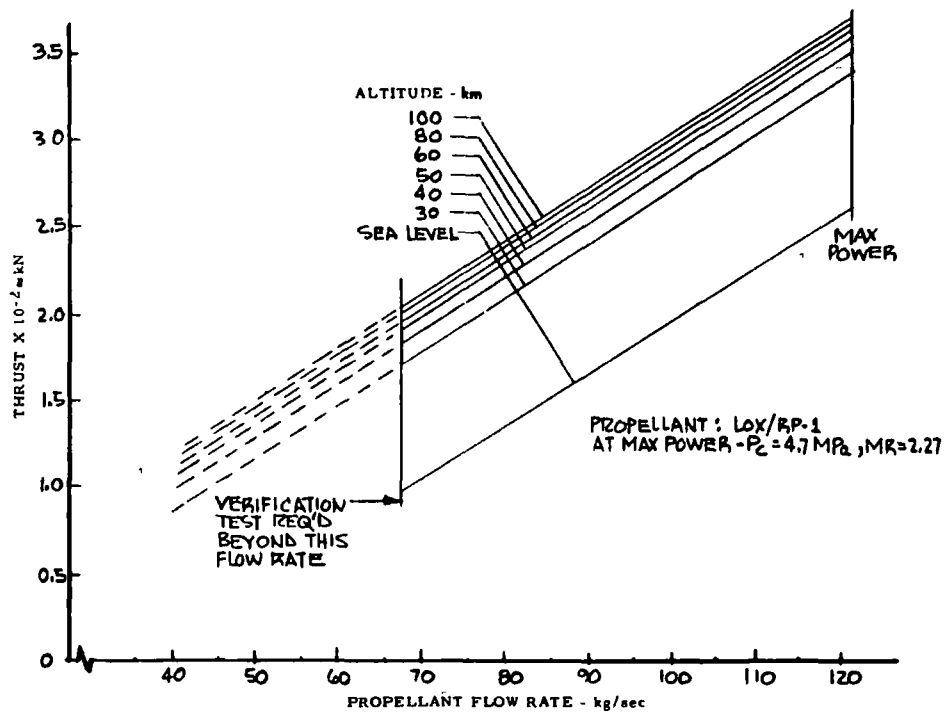


Figure 6 - LR-105 Throttled Performance

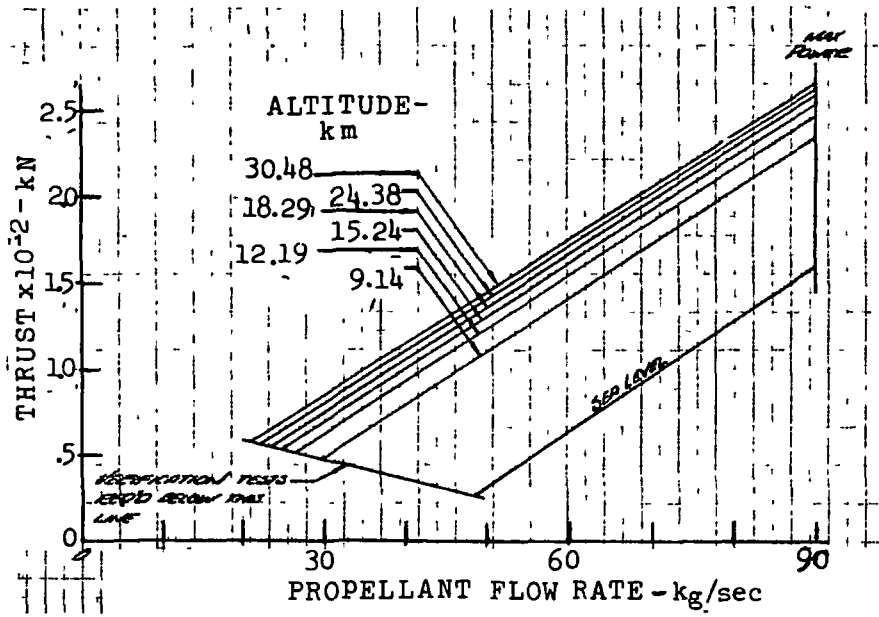


Figure 7 - LR-105 DT Derated Thrust Performance

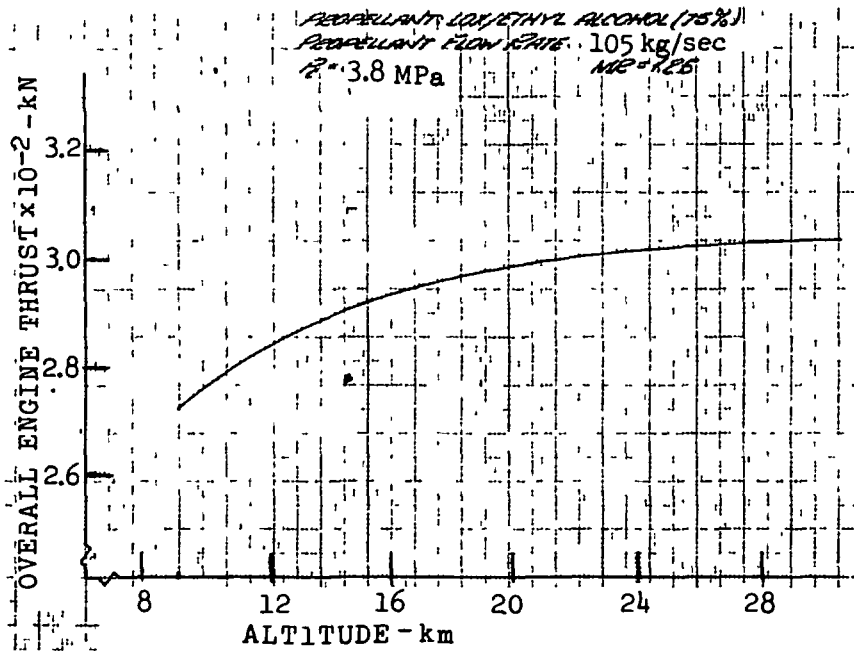


Figure 8 - LR-105 ALC Thrust

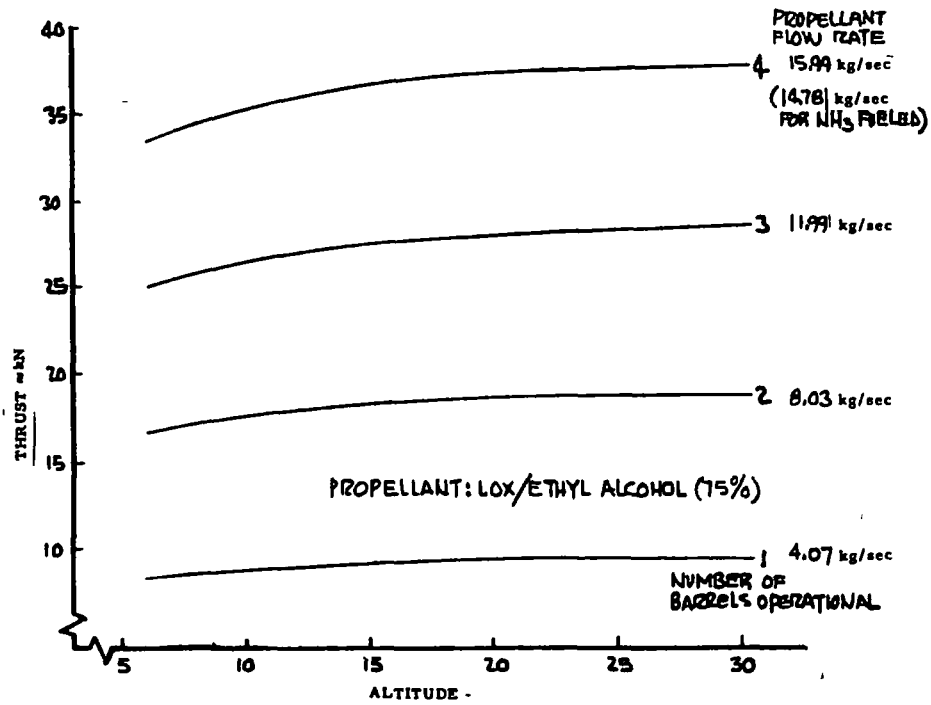


Figure 9 - LR-11 Thrust

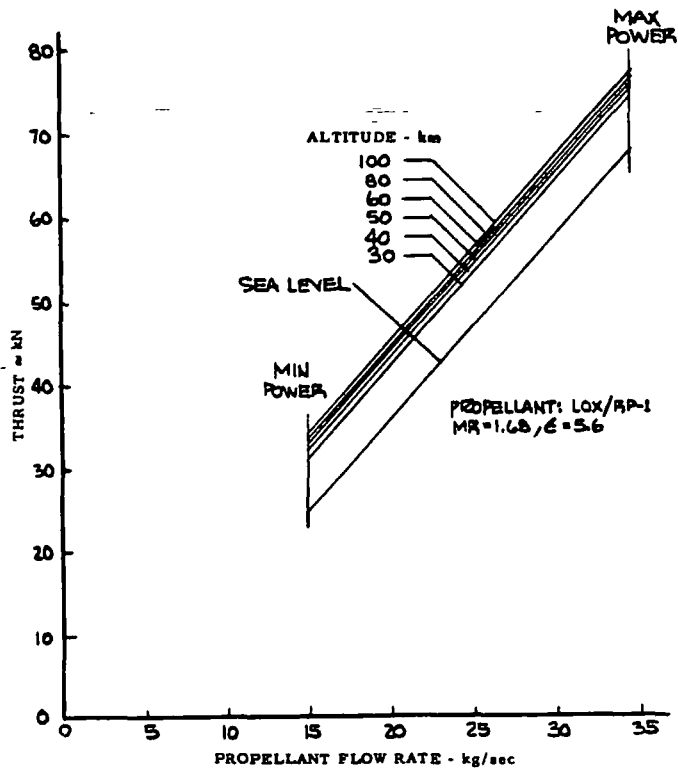


Figure 10 - LR-101 Throttled Performance

The mission constitutes a rather dynamic flight path with only the 40 second cruise portion amenable to accurate hand calculation. A point mass 3-dimension flight path computer program incorporating considerable flexibility as to control laws, vehicle limitations and nonlinearities was used. The 1962 U. S. Standard Atmosphere was used for the calculations.

Ground rules for vehicle concepts were established by NASA and are delineated in 'BASIS FOR DESIGN TRADES' herein. Maneuver load factors limits used include:

	<u>Mission</u>	<u>Structural Design</u>
Launch and pullup	0 - 2.0 g	-1.0 - 2.5 g
At high Mach	0 - 2.5	-1.0 - +3.0
Angle of attack limits 0 - 20 degrees		

The mission load factor limits were reduced from structural design limits to allow for real world accuracy and overshoot. Negative load factors were not allowed out of respect for the pilot.

Boost Analysis - The X-24C boost problem required that it (1) launch and clear the B-52, (2) pull-up to gain altitude and keep down the aerodynamic drag, and (3) push-over so it would be at zero flight path angle at  $M = 6.0$  and  $q = 47.9$  kPa.

With the high accelerations required to minimize drag and gravity losses, the optimum boost path is far from the path of instantaneous optimums, being compromised by the dynamic requirements.

Our experience has been that a relatively simple pitch attitude,  $\theta$ , schedule can be constructed that will yield a flight path very close to the minimum propellant path. The schedule used in this study was in basically two parts. For launch, separation and pullup,  $\theta$  was a function of time. This allows close control of separation and pullup where  $n_z$  and  $g$  are critical. To

capture cruise altitude,  $\theta$  was a function of ambient pressure,  $P_s$ . This gives a closed loop on the critical problem of capturing altitude. The  $\theta$  schedule is shown pictorially in Figure 11. For the first five seconds,  $\theta$  was held constant and a 91.4 m of separation from the B-52 was achieved. At five seconds, boost engine was started along with a linear increase in  $\theta$  with time.

The maximum increase in  $\theta$  with time, as limited by load factor, was found to minimize propellant. The  $\theta$  vs.  $P_s$  schedule was also linear in three segments. The commanded  $\theta$  was the smaller of the two  $\theta(t)$  or  $\theta(P_s)$ . For each engine/vehicle combination  $\theta(P_s)$  schedule was varied to minimize boost propellant. An example of the effect on the boost profile is shown in Figure 12 for an alcohol fueled LR-105 boost. As the profile shows, the Mach altitude relationship can be controlled directly by the  $\theta$  vs. altitude schedule.

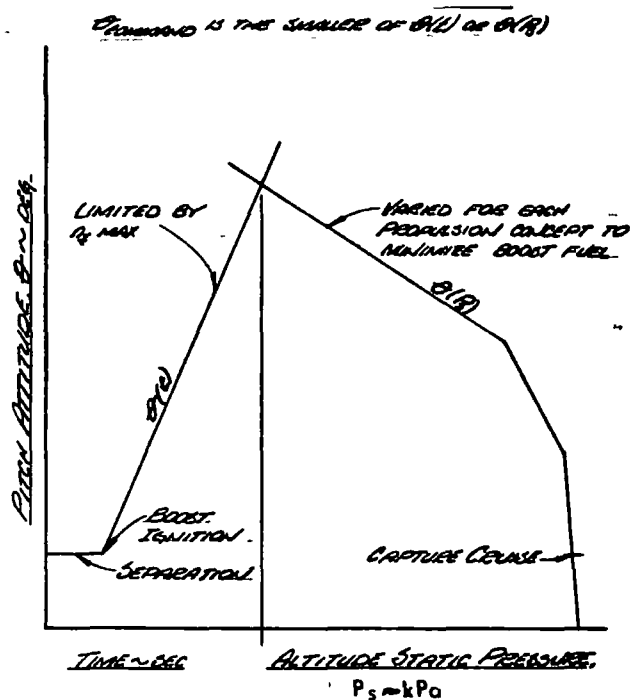


Figure 11 - Launch/Boost Control by Pitch Attitude Schedule

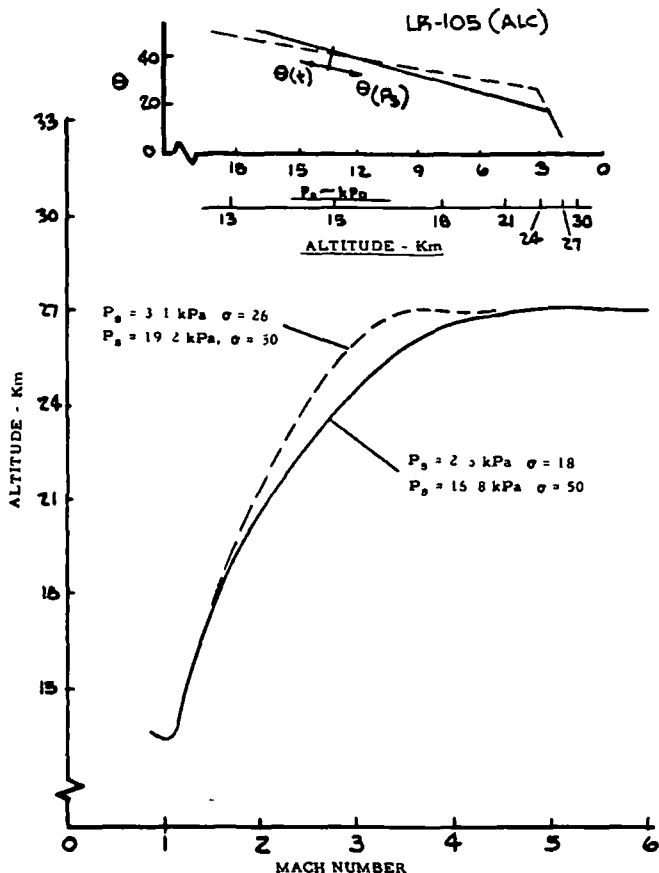


Figure 12 - Typical Boost Profile

Cruise Analysis - Cruise at  $M = 6.0$  requires approximately 71.2 kN of thrust. At  $q = 47.9 \text{ kPa}$  the effect of mass on thrust required is small. A problem develops as discussed in 'PROPULSION DATA' herein that the throttled booster's minimum thrust is excessive. This causes excessive propellant usage for cruise as well as design and mass problems to dissipate the excess thrust with speed brakes.

For the LR-99, the excess thrust is 60.1 kN and is 133.4 kN for the LR-105T both at  $q = 47.9 \text{ kPa}$ . It is a very serious speed brake design problem to handle the excess thrust of the LR-99 plus what is needed for speed control. For the LR-105T, it is prohibitive. Scramjet thrusting, other engine tests, and cruising at lower  $q$ 's where vehicle drag decreases while minimum rocket thrust increases slightly all make the speed brake design problem worse.



A basic speed brake requirement of 1/2-g at 47.9 kPa was used in the vehicle design. Even for this basic requirement, aerodynamic heating considerations will design the speed brake system (see elevon and rudder thermal analysis).

Deceleration and Descent Analysis - The deceleration to Mach 2.0 is primarily concerned with minimizing heating. The remaining deceleration and descent is available for flight path control to landing. Deceleration or the dissipation of kinetic energy of the X-24C is accomplished by aerodynamic drag. Achieving this drag in the form of pressure drag and minimizing friction drag in general minimizes the vehicle total heat absorbed. This is important for both the insulator and heat sink method of thermal protection. Increasing angle of attack increases the proportion of pressure drag.

Five deceleration paths at a mass of 9525 kg were investigated to verify and/or find the best technique. The techniques covered the available range of angles of attack and dynamic pressure. The maximum, 20° angle of attack as expected yielded the least total heat input with the savings primarily on the top surfaces.

For the initial deceleration, while at high dynamic pressure, angle of attack is limited by normal load factor limit of 2.5 g's. If this is done with wings level, the vehicle zooms to high altitude with loss of aerodynamic control and stretches the flight path down range. By holding a 60° bank angle, the vehicle climbs to approximately 30480 m and maintains sufficient dynamic pressure for control. Consistent with a minimum heat input is a short deceleration time and distance. Alternative descent modes must be studied in the event that 2.5g maneuvers become impractical due to abort conditions or research requirements.

The  $60^\circ$  bank can be used for cross-range maneuvering as shown in Figure 13 or alternated three times to stay within 19 km of track as shown in Figure 14. Figure 14 also shows that the descent from  $M = 2.0$  can be used for maneuvering to yield a terminal guidance foot print of approximately  $130 \times 130$  km.

Mission Profiles - Mission profiles were defined for three propulsion concepts to be used in vehicle design, thermal protection system design and vehicle system design. The three propulsion concepts are the throttleable LR-99, the LR-105 with LR-101's for cruise, and the alcohol fueled LR-105 with two LR-11's for both cruise and boost. The mission profiles are shown in the form of time histories, altitudes vs. Mach and altitude vs. distance. With the exception of the altitude vs. distance figure, all of the profiles end at  $M = 2.0$ . Figure 15 shows the time history of altitude and Mach number. During boost, it is noted, the final acceleration is at cruise altitude, 26930 m. During the deceleration the peak altitude is just over 30480 m and the altitude at  $M = 2.0$  is between 24380 and 27430 m. As the vehicle approaches  $M = 6.0$ , the longitudinal acceleration is between 3.0 and 3.5 g's. The deceleration from  $M = 6.0$  to  $M = 2.0$  is high taking less than 140 seconds.

Dynamic pressure, ( $q$ ), normal load factor ( $n_z$ ), and angle of attack, ( $\alpha$ ) are shown in Figure 16. During boost the  $q$  stays below 19.2 kPa until near the end when it climbs rapidly to the design point of 47.9 kPa. During deceleration it drops fairly linearly until below  $M = 3.0$ . Load factor,  $n_z$ , is seen to be initially near zero for separation then climb to the 2 g's for the pull-up. The remainder of the boost is pushing over at less than 1 g until capturing cruise. High load factor is used during deceleration.

The  $\alpha$  time history shows that the  $20^\circ$  capability is used during pull-up as well as deceleration.

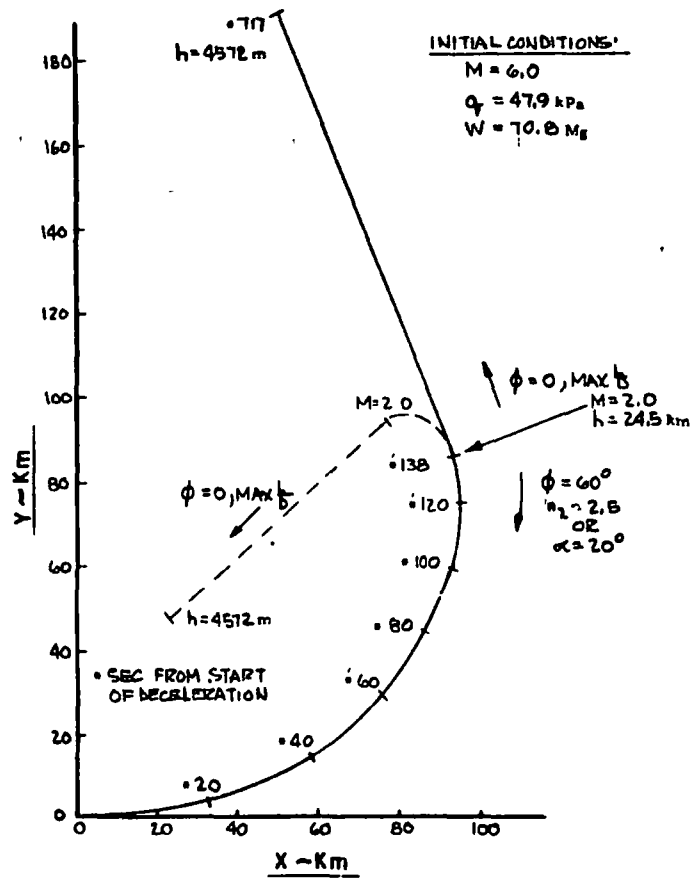


Figure 13 - Deceleration and Descent Path for Cross-Range

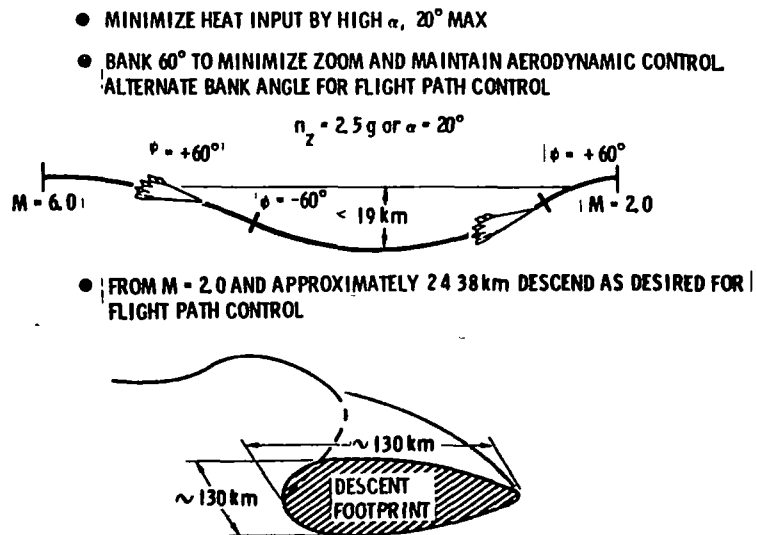


Figure 14 - Deceleration Control

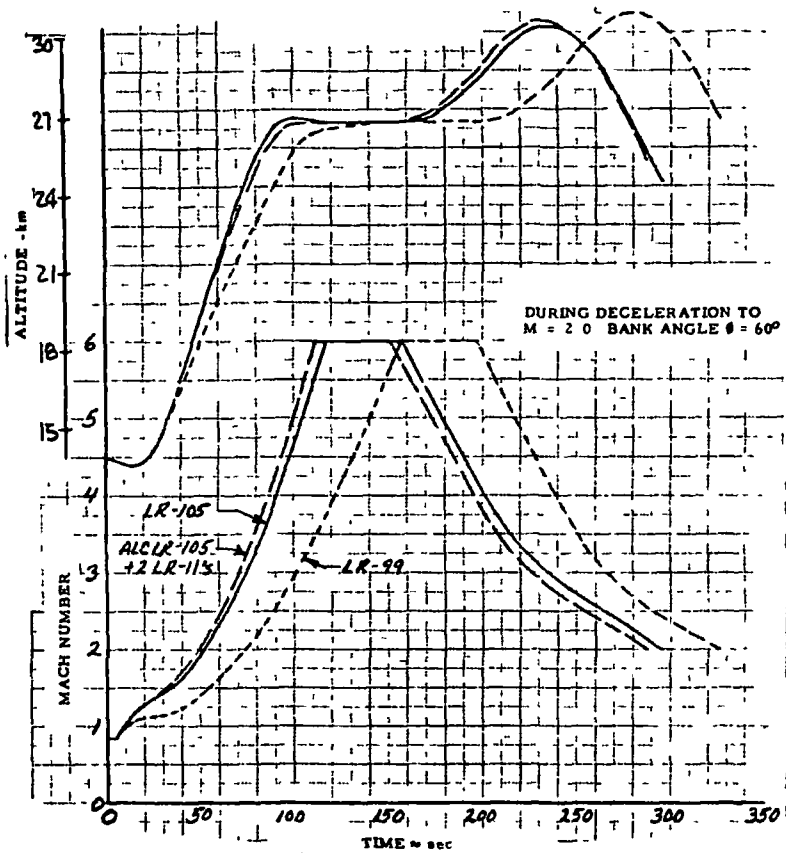


Figure 15 - Mission Profiles - Altitude/  
Mach vs Time

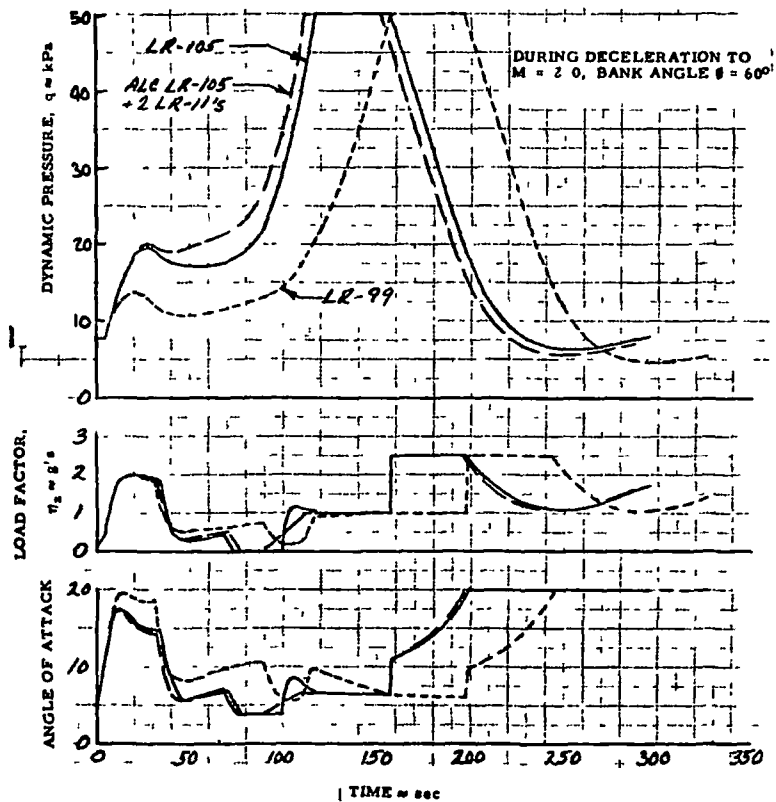


Figure 16 - Mission Profile -  $Q$ ,  $N_2$ ,  $\alpha$  vs. Time

Altitude vs. Mach number and vs. distance are shown in Figures 17 and 18. The boost, cruise and deceleration to  $M = 2.0$  takes approximately 315 km. The deceleration can be lengthened by using less than  $60^\circ$  bank and conversely shortened by using more  $\alpha$  with small effect on aerodynamic heat load. A maximum distance descent is shown in Figure 18 to illustrate maneuvering capability following the aerodynamic heating period.

Maximum Allowable Zero Propellant Mass - The eight (8) propellant concepts discussed under 'Propulsion Data' were analyzed to determine propellant required for boost and cruise. For each propulsion concept the boost path was varied to find the minimum propellant path with the constraints discussed under 'Boost Analysis' above, Table 1 summarizes the performance of the eight concepts.

For all propulsion concepts the launch mass was held constant at 25855 kg, propellant for boost and cruise are subtracted leaving a mass at end of cruise. Since there are no further propellant requirements the mass at the end of cruise is the Maximum Allowable Zero Propellant Mass. This represents the mass allowance available for vehicle/TPS, systems and payload. The larger the better.

In Table 1 the eight propulsion concepts are listed in descending order of zero propellant mass. The LR-105 plus cruise engines being first at 10759 kg as a result of the LR-105's high Isp and thrust. The throttleable LR-99 being last at 8876 kg due to its low Isp, thrust and high cruise propellant consumption.

Burning the cruise engine with the LR-105 during boost caused increased propellant usage. The Low Isp of the LR-101's was more detrimental than the saving boost time with the high thrust. The derated LR-105 suffers from the large reduction in thrust along with a 2% reduction in Isp. Burning the LR-11's during boost with both the LR-99 and alcohol fueled LR-105 reduced the boost propellant. The throttleable LR-105 is next to last due to the high propellant usage during cruise.

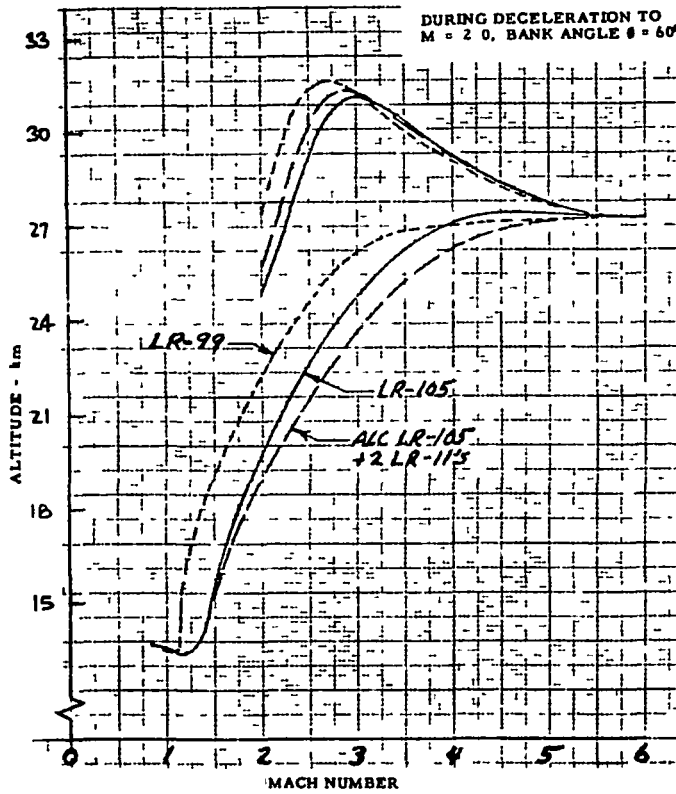


Figure 17 - Mission Profiles -  
Mach vs Altitude

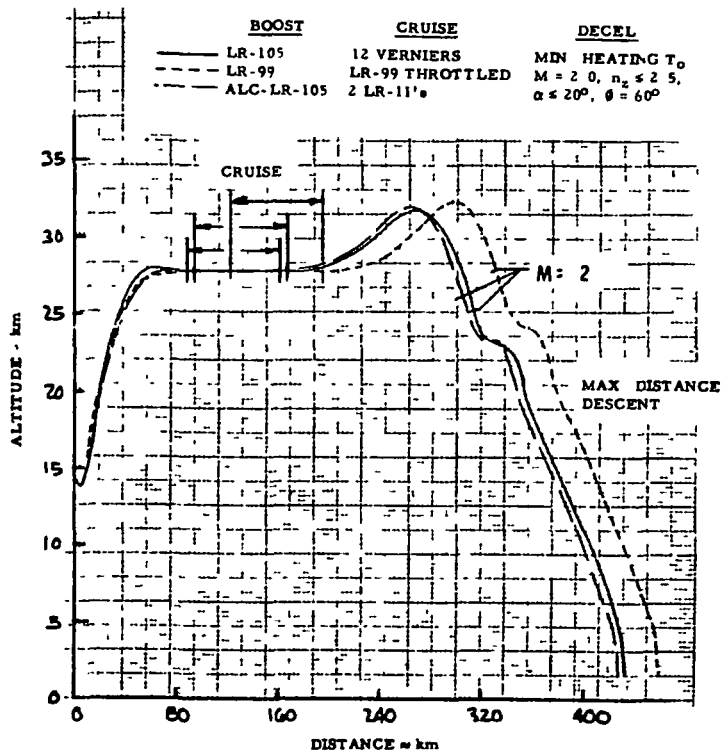


Figure 18 - Mission Profiles -  
Altitude vs Distance

CONCEPT	1	2	3	4	5	6	7	8
Average Boost Thrust @ 21340 M, kN (70 000') (Lb)	365.9 (82, 000)	442.6 (99, 500)	262.0 (58, 000)	351.8 (79, 100)	373.6 (84, 000)	298.9 (67, 200)	367.5 (82, 620)	277.1 (62, 300)
Average Boost Specific Impulse @ 21340 M, sec (70, 000')	306	288	300	279	277	289	306	285
Boost Propellant - kg (Lb)	13770 (30, 357)	14053 (30, 981)	14750 (32, 535)	14694 (32, 395)	14639 (32, 273)	14716 (32, 442)	13770 (30, 357)	15072 (33, 227)
Mass at End of Cruise - kg (Lb)	12085 (26, 643)	11802 (26, 019)	11097 (24, 465)	11161 (24, 605)	11216 (24, 727)	11140 (24, 558)	12085 (26, 643)	10783 (23, 773)
Cruise Propellant - kg (Lb)	1326 (2, 924)	1326 (2, 924)	1061 (2, 340)	1139 (2, 511)	1236 (2, 725)	1236 (2, 725)	2703 (5, 960)	1907 (4, 205)
Mass at End of Cruise or Max. Allowable Zero Propellant Mass - kg (Lb)	10759 (23, 719)	10476 (23, 095)	10036 (22, 125)	10022 (22, 094)	9980 (22, 002)	9903 (21, 833)	9382 (20, 683)	8876 (19, 568)
Total Propellant - kg (Lb)	15096 (33, 281)	15379 (33, 905)	15819 (34, 875)	15833 (34, 906)	15875 (34, 998)	15952 (35, 167)	16473 (36, 317)	16979 (37, 432)
Fuel Volume - M <sup>3</sup> (Ft <sup>3</sup> )	5.86 (207)			10.4 (368)	8.35 (295)			11.1 (392)
Oxidizer Vol. - M <sup>3</sup> (Ft <sup>3</sup> )	9.08 (321)			7.41 (262)	7.61 (269)			7.98 (282)
Total Vol. - M <sup>3</sup> (Ft <sup>3</sup> )	14.9 (528)			17.8 (630)	16.0 (564)			19.1 (674)

- |   |  |   |   |
|---|--|---|---|
| 1 | LR-105 + 12 LR-101's (Cruise)                        | 5 | LR-105 ALC + 2 LR-11's (Boost and Cruise) |
| 2 | LR-105 + 12 LR-101's (Boost and Cruise)              | 6 | Like 5 (Cruise)                           |
| 3 | LR-105 DT  | 7 | LR-105 Throttleable                       |
| 4 | LR-99 + 2 LR-11's NH <sub>3</sub> (Boost and Cruise) | 8 | LR-99 Throttleable                        |

Table 1 - Performance of Propulsion System -  
Launch Mass ≈ 25.85 Mg

The three propulsion concepts carried into design evaluation were: (1) LR-105 plus 12 LR-101 cruise engines, (2) the alcohol fueled LR-105 plus 2 LR-11 boost and cruise engines, and (3) the throttleable LR-99.

The LR-99 plus 2 NH<sub>3</sub> fueled LR-11 boost and cruise engines is a close substitute to the alcohol LR-105 plus 2 LR-11 combination requiring 12% more propellant volume. The LR-105 + 12 LR-101 combination not only gives the largest allowable zero propellant mass, it also requires the least propellant volume.

It is noted that the vehicle physical size and the vehicle aerodynamics remained constant for all cases studied.

## REALISTIC DESIGNS

The study objective to develop sound technical basis for the candidate vehicle concepts was achieved through a systematic program involving the interactions between the technical disciplines shown in Figure 19 in conjunction with results of the other tasks delineated in the Technical Approach section.

The primary purpose of the design study was to provide the basis for accurate cost and mass estimates on vehicle configurations meeting the NASA requirements. The study could not explore the details of all the structural concepts involved recognizing that further work would be required to finalize the detail design before hardware could be produced. Additionally, it is anticipated that the design phase will involve a number of structural tests which would assist in making the choice between design alternatives.

Using the results of the Mission Profiles and Maximum Fuel Loading Analysis, based on the technical constants defined in the 'BASIS FOR DESIGN' and 'CANDIDATE VEHICLES' sections, analysis on propellant tankage volumes and vehicle fuel cell placement was initiated. This initial activity was used as the starting point for each of the analysis investigations delineated in Figure 19. As



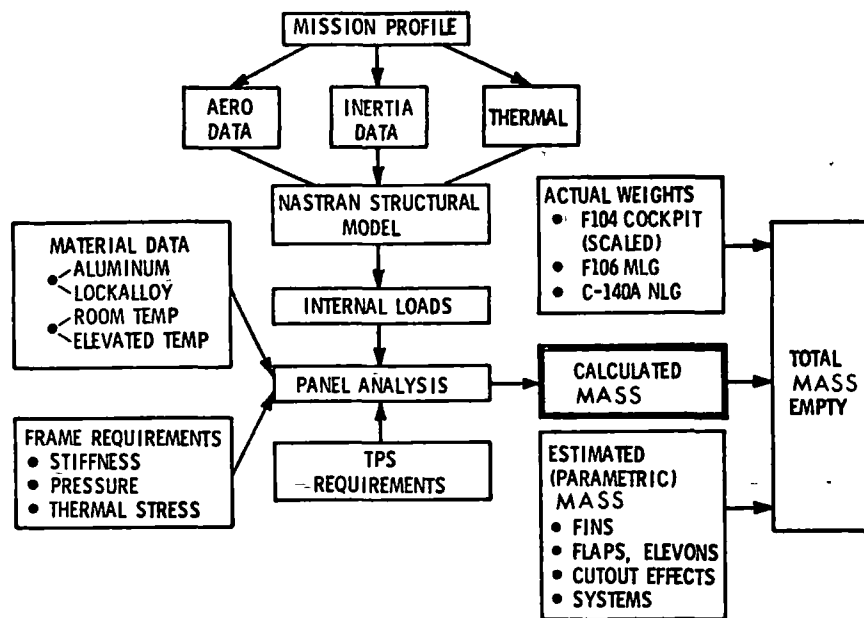


Figure 19 - Analysis Program

results of these on-going analysis were developed, trade-off decisions were possible leading to vehicle detail design finalization. Mass, Maintenance and Cost analysis contributed heavily in trade-off selection by defining those design concepts which would produce the results intended by the study.

### Load Analysis

Criteria - Of the load conditions defined in Appendix A for the X-24C the following conditions were found to be critical:

- $n_z = 2.0$  g B-52 Taxi, X-24C attached
- $n_z = -1.0$  g after launch
- $n_z = 2.5$  g after launch
- $n_z = 3.0$  g cruise
- Landing 3.0 m/s
- $n_z = -1.0$  g cruise

Airload Determination - Airloads for structural load analysis were based on the Lockheed VORLAX program, Reference 1, for both subsonic and low-supersonic conditions. For hypersonic conditions the "Hypersonic Arbitrary-Body Aerodynamic Computer Program," Reference 2 was used. These two programs produced the surface pressures used in the load analysis.

Inertia Data - Mass used in the loads analysis were consistent with the vehicle mission profile and the 25855 kg launch mass. Initial pushover and pull-up were calculated for a GW = 24040 kg, representing a 1814 kg fuel burn-off required to obtain sufficient airspeed for maneuvers. Cruise at maximum airspeed was calculated for a GW = 11204 kg.

Loads Program - Loads were applied at 74 point locations, see Figures 26 and 29 on the in-house NASTRAN model. Inertia is determined at each of the 74 points utilizing a boundary system. The loads program during this phase is a

"by hand" transformation due to the difference in grids between the air loads and NASTRAN.

Landing Loads - The basis for the loads determined and applied to the NASTRAN model are as follows: The landing condition is based on a gross mass of 10396 kg and a sink rate of 3.0 m/s. For design purposes the F-106 main landing gear has been used. (However, an extensive analysis on landing gear selection was conducted and reflected in the Landing Gear Selection analysis herein.) Utilizing 0.300 m of stroke a landing load factor of 1.85 g's has been calculated.

Elevon Loads for Trimming High Drag Configurations - Since the LR-99 is throttleable to only 132.6 kN, scramjets produce 40.03 kN of thrust and the drag of the baseline vehicle is 71.17 kN at cruise, approximately 101.4 kN of additional drag must be developed by drag brakes to maintain a steady  $M = 6.0$  cruise portion of the flight. Assuming the drag brakes on the vertical fin can develop this much drag, the elevon angle to trim at  $n = 1.0$  is  $+15^\circ$  (trailing edge down). This elevon position at a  $q = 47.9$  kPa produces 41.81 kN of elevon load (upward acting) and -23900 Newton-meter of hinge moment (nose down). These are total loads, for both sides. In the LR-105 with 12 LR-101 engine configurations, approximately 44.48 kN of additional drag is required by the drag brakes.

Critical Load Conditions - Net vehicle loads, based on the vehicle configuration and mission profile, were determined for application to the structural model. Using these external loads and the structural model, NASTRAN static solutions were obtained to define the internal axial loads, shear flows and stresses on the airframe.

The magnitudes of these loads and stresses defined the critical load conditions for each region of the airplane. At a given point in the structure, one condition may result in high axial loads and low shear flows, and another condition may give the reverse. When the critical condition in this situation is not obvious by inspection, the structure is analyzed for both conditions to determine the more critical condition.

A total of six load conditions were investigated; they included:

- B-52 2 g taxi (with  $\pm 0.25$  g  $n_x$  load factors)
- Pull-up after B-52 launch,  $n_z = 2.5$  g
- Negative load factor after launch,  $n_z = -1.0$  g
- Maneuver at maximum Mach,  $n_z = 3.0$  g
- Descent,  $M = 3.0$ ,  $n_z = 2.5$  g
- Two-wheel landing

For the Lockalloy design an additional condition corresponding to the time in flight when the maximum temperature differentials exist was included in the internal loads analysis.

Wing Critical Load Conditions - The external loads for each of the preceding load conditions were determined and applied to the applicable structural model to define the internal forces/stresses and deflections acting on the wing structure.

For the aluminum design, the most critical design condition for the wing upper surface was the pull-up after B-52 launch condition. The corresponding design condition for the wing lower surface was the negative  $n_z$  subsonic flight condition. A comparison of the wing load intensities for all of the load conditions is shown in Table 2. This table presents the ultimate inplane loads for the upper and lower surface panels at an inboard region in the vicinity of the rear beam.

Figures 20 and 21 display the wing surface load intensities on a spanwise strip for the two critical design conditions. This strip is located adjacent to the rear beam and spans from wing tip to root chord. The maximum compressive load intensities ( $n_y$ ) for the upper surface occurs during the pull-up after launch conditions, Figure 20, with loads approximately 19261 kN/m indicated at the root chord.

ITEM	WING UPPER SURFACE LOAD INTENSITIES - kN/m						WING LOWER SURFACE LOAD INTENSITIES - kN/m					
	LOAD CONDITIONS						LOAD CONDITIONS					
	①(A)	①(B)	②	③	④	⑤	①(A)	①(B)	②	③	④	⑤
N <sub>x</sub>	-5.1	-5.4	-44.8	-13.7	4.7	-3.9	-4.6	-4.9	42.7	15.8	-5.3	-5.3
N <sub>y</sub>	-2.5	-3.0	-159.0	-24.0	31.9	-0.5	-11.0	-10.3	177.0	30.0	-34.1	-14.4
N <sub>xy</sub>	8.2	8.2	97.7	35.2	4.9	8.4	3.7	3.2	92.1	40.3	2.5	4.7

LOAD CONDITIONS:

- ① B-52 TAXI @ 27.2 Mg  
(A) POSITIVE N<sub>x</sub>  
(B) NEGATIVE N<sub>x</sub>
- ② PULL-UP AFTER LAUNCH
- ③ PULL-UP AT MAX MACH NO.
- ④ SUBSONIC FLIGHT (NEGATIVE N<sub>z</sub>)
- ⑤ 2 WHEEL LANDING

Table 2 - Comparison Wing Inplane Load Intensities - Aluminum Design

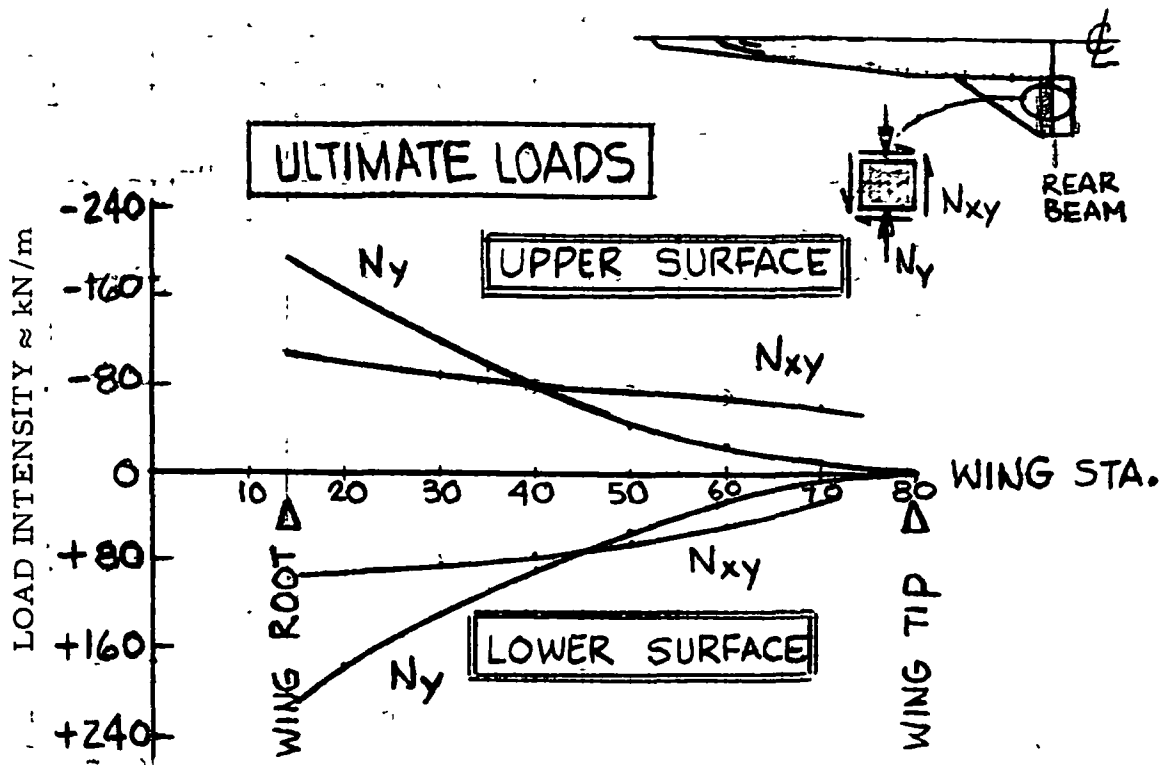


Figure 20 - Wing Spanwise Load Intensities - Pullup After B-52 Launch (Aluminum Design)

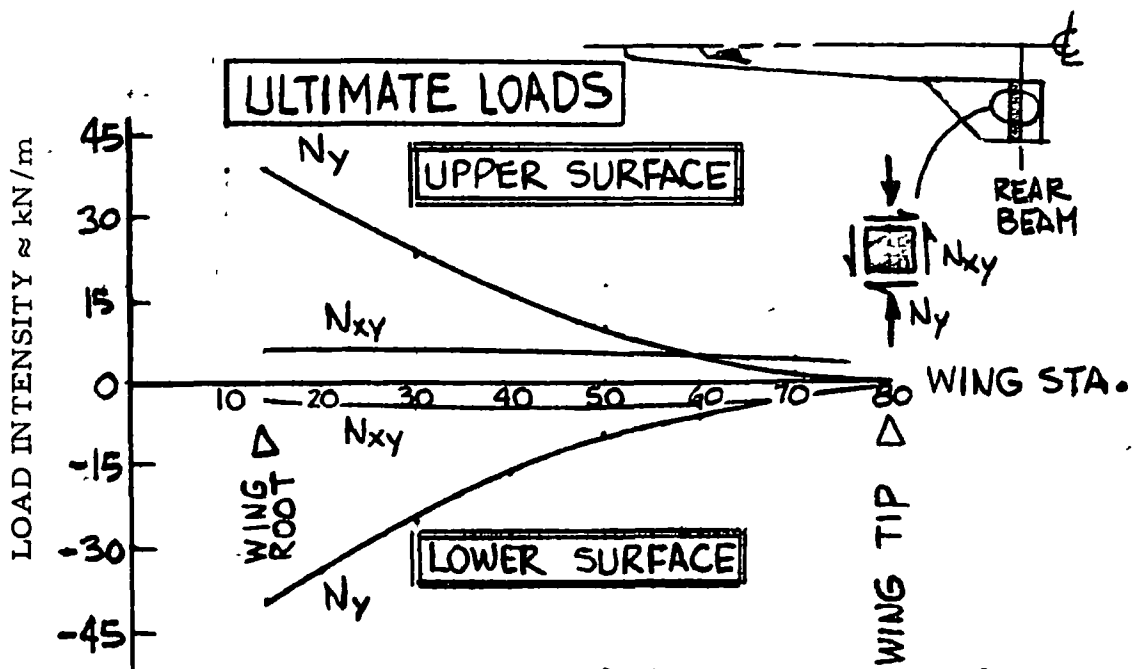


Figure 21 - Wing Spanwise Load Intensities - Subsonic Flight Negative One G (Aluminum Design)

Similarly, Figure 21 shows a maximum compressive load on the same spanwise wing strip of approximately 3940 kN/m on the wing lower surface for the negative  $n_z$  subsonic flight condition.

The critical load conditions for the Lockalloy design are the pull-up after launch and the maximum temperature gradient conditions. Generally, the wing upper surface is designed by the loads during the pull-up condition, the exception being those regions adjacent to the leading edge which are designed by the heat sink requirement and the maximum temperature differential condition. For comparison purposes, Table 3 presents the upper and lower wing surface load intensities for the complete set of load conditions investigated for the Lockalloy design. These loads exist on an inboard wing region adjacent to the rear beam and clearly illustrate the critical design conditions.

More definitive maps of the wing load intensities are shown in Figures 22 and 23 for the critical design conditions for the Lockalloy design. Figure 22 depicts the upper and lower surface load intensities for the pull-up condition; whereas, Figure 23 shows the lower surface load intensities for the maximum temperature gradient condition.

A comparison of the upper wing surface load intensities for the aluminum and Lockalloy design is presented in Figure 24. This figure displays the variations in chordwise load ( $n_x$ ) and spanwise load ( $n_y$ ) intensities for the two designs during the pull-up after launch load condition. The Lockalloy design has the highest chordwise loads and conversely the aluminum design has the highest spanwise loads.

### Structural Analysis Models

Finite element structural analysis models were used for the evaluation of the candidate structural design concepts. These models were coded in NASTRAN, (Ref. 3) and used to provide the internal loads/stresses and displacements for the stress analysis, and the stiffness matrices for the vibration and flutter analyses.

ITEM	WING UPPER SURFACE * LOAD INTENSITIES (kN/m <sup>2</sup> )						WING LOWER SURFACE * LOAD INTENSITIES (kN/m <sup>2</sup> )										
	LOAD CONDITIONS						LOAD CONDITIONS										
	①	A	①	B	②	③	④	⑤	⑥	①	A	①	B	②	③	④	⑤
N <sub>x</sub>	-4.0	-4.7	-60.6	-16.5	10.5	-0.9	28.2	28.2	-11.6	-11.9	45.5	17.2	-6.8	-8.2	-111.0		
N <sub>y</sub>	0.5	-0.8	-91.1	-3.5	28.9	5.8	-44.8	-44.8	-7.9	-0.7	137.0	15.9	-37.3	-10.7	-69.7		
N <sub>xy</sub>	8.9	8.8	93.2	27.7	5.4	7.2	50.8	50.8	7.7	7.7	69.5	28.9	4.2	4.5	3.2		

LOAD CONDITIONS: \* -ALL LOADS ARE ULT. VALUES, EXCEPT FOR COND. ⑥ = LIMIT

① B-52 TAXI  
 (A) POSITIVE N<sub>x</sub>  
 (B) NEGATIVE N<sub>x</sub>  
 ② PULL-UP AFTER LAUNCH  
 ③ PULL-UP AT MAX MACH NO.  
 ④ SUBSONIC FLIGHT (NEGATIVE N<sub>z</sub>)  
 ⑤ WHEEL LANDING  
 ⑥ MAX TEMP. DIFFERENTIALS

Table 3 - Comparison Wing Inplane Load Intensities - Lockalloy Design



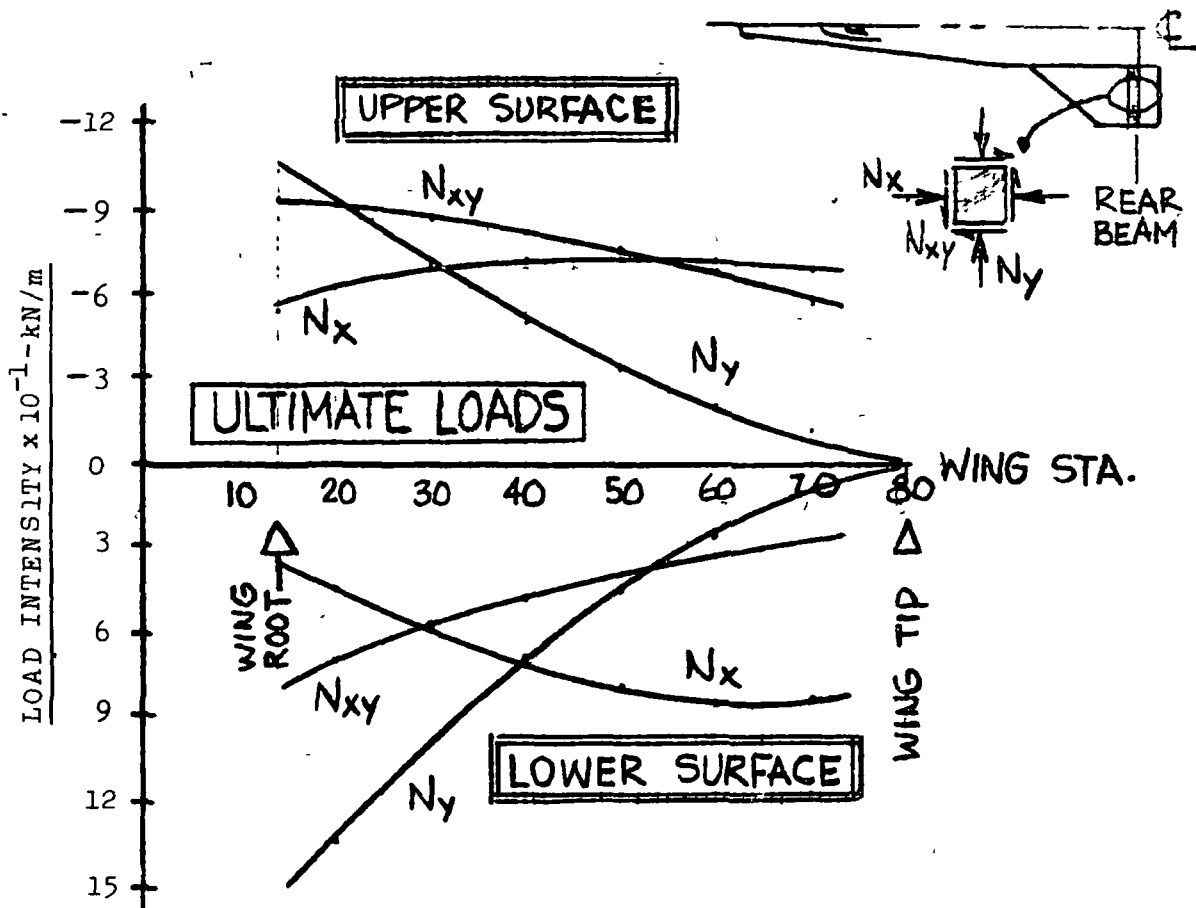


Figure 22 - Wing Surface Load Intensities - Pullup After B-52 Launch (Lockalloy Design)

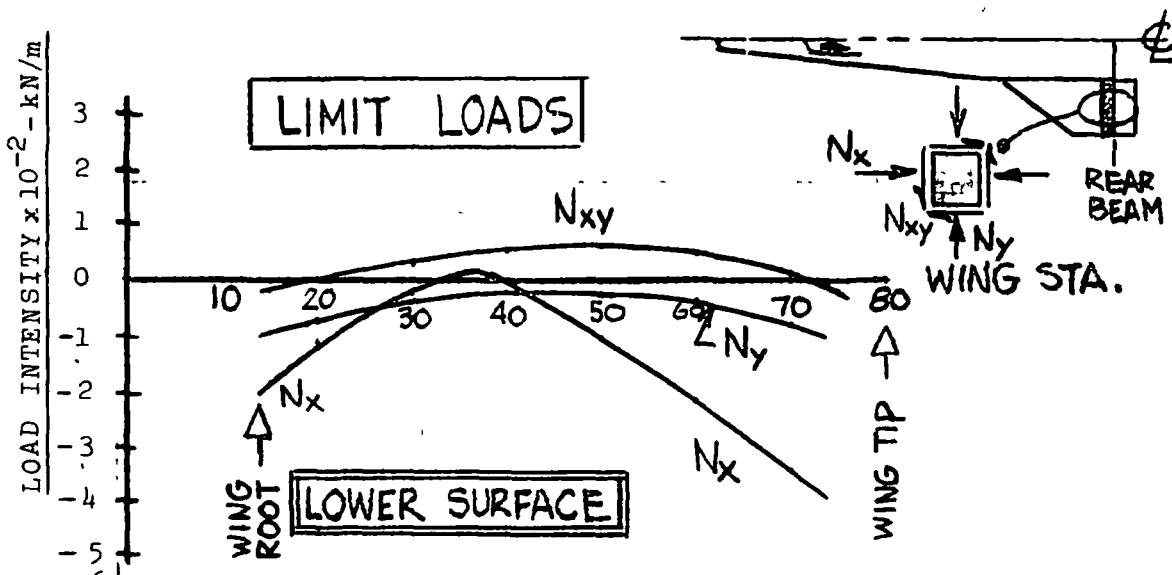


Figure 23 - Wing Surface Load Intensities - Maximum Temperature Gradients (Lockalloy Design)

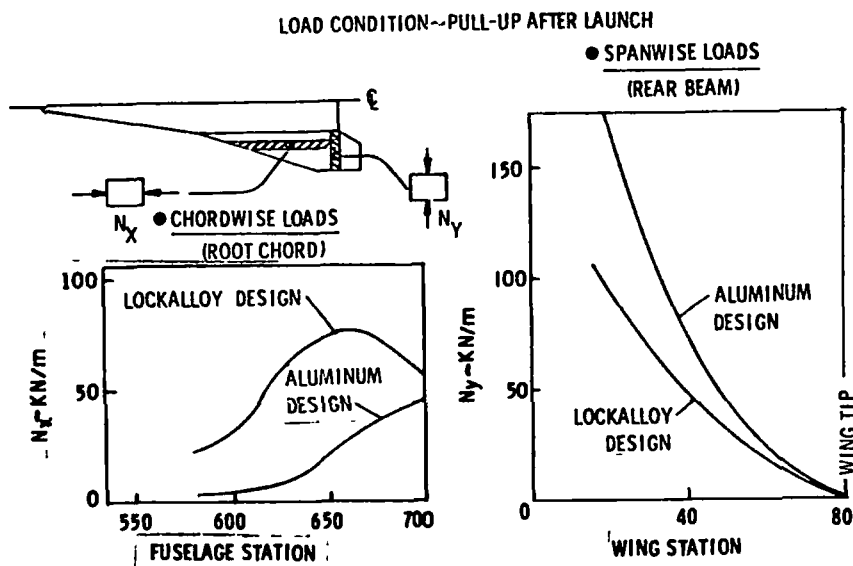


Figure 24 - Wing Surface Load Intensities - Comparison

The structural model is presented in Figure 25 and includes some pertinent model size statistics and the external load conditions applied to the model.

Two basic airframes were modeled for this investigation, which were characterized by their primary load carrying structural arrangement, and included:

- An Aluminum airframe design which incorporates a frame supported uniaxially stiffened fuselage shell with a spanwise stiffened wing, and
- A Lockalloy design consisting of a frame supported monocoque shell with a wing constructed of unstiffened surface panels.

In addition to these basic airframe structural models, a detail sub-model of a typical fuselage frame-to-shell juncture of the Lockalloy design was constructed to evaluate the thermal stresses associated with the application of various material candidates.

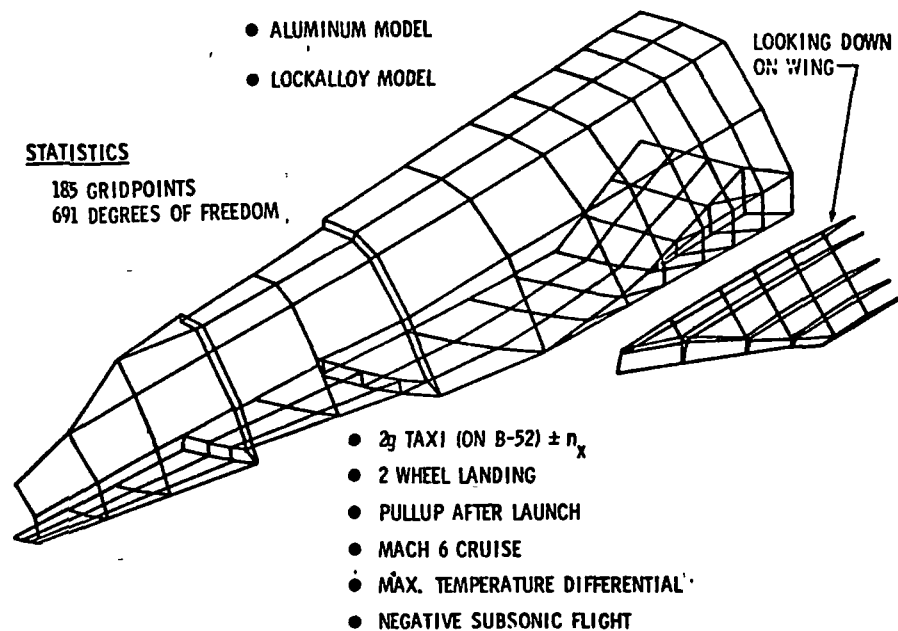


Figure 25 - NASTRAN Model

A summary table containing an annotated history of the NASTRAN runs conducted using the structural models is shown in Table 4.

Modeling Technique - Both Aluminum and Lockalloy general airframe structural models used the same grid system and coordinates with only the element properties and materials being varied to reflect the specific airframe under investigation. These three-dimensional structural models idealized the actual fuselage and wing structure using the rigid-format elements defined for NASTRAN. No attempt was made to include the strakes or vertical stabilizer in the basic airframe models. In addition, the airplane midplane of symmetry was assumed at the fuselage centerline, thus requiring only one-half of the airframe to be modeled.

The wing planform grid for the model is shown in Figure 26, and includes the grid and element identification numbers for the wing surface panels and

STRUCTURAL MODEL	RUN NO.	MODEL FLEXIBILITIES	LOAD/TEMP CONDITIONS	COMMENTS
ALUMINUM DESIGN	①	PRELIMINARY SET	INITIAL SET OF LOAD CONDITIONS	INITIAL DATA
	②	REVISED STIFFNESSES	5 LOAD CONDITIONS	INPUT STIFFNESSES REFLECT RESULTS OF PREVIOUS RUN
	③	SAME AS RUN ②	AN ADDITIONAL COND. ADDED.	SUBSONIC MANEUVER CONDITION ADDED
LOCKALLOY DESIGN	①	PRELIMINARY SET	5 LOAD CONDITIONS AND INITIAL TEMP SET.	INITIAL PANEL THK. BASED ON HEAT SINK REQUIREMENT - NO TEMP. GRADIENT MATCHING
	②	REVISED STIFF TO REDUCE TEMP GRADIENTS	SAME AIRLOAD COND, REVISE TEMP COND	REPLACED WING AND FUSELAGE RODS AND SHEAR PANELS WITH MEMBRANE ELEMENTS.
	③	REVISED STIFF TO REDUCE TEMP GRADIENTS	ADDED AIRLOAD COND, REVISE TEMP COND.	SUBSONIC MANEUVER CONDITION ADDED
	④	SAME STIFF. AS RUN ③	SAME AIRLOADS & TEMP. AS ③	REPLACED FUSELAGE MEMBRANE PANELS WITH RODS AND SHEAR PANELS
	⑤	REVISED WING L.I.E. (ERROR)	SAME AS RUN ④	REVISED WING LEADING EDGE STIFFNESS AND MATERIAL

Table 4 - History of NASTRAN Internal Load Runs

substructure. In general, the defined grid system proportioned the surface panels into aspect ratios of 2 or less, i. e., ratio of spar to rib spacing.

The fuselage is idealized using 13 frame stations with approximately 8 to 10 nodes describing the half-circumference. Typical frame model drawings depicting fuselage stations 498 and 553 are shown in Figures 27 and 28, and define the numbering system employed in the identification of the bending elements. The bending elements are at the local skin temperature, thus thermal stresses caused by the temperature gradient through the frame depth are not determined in the fuselage model. The complete fuselage shell model is shown in Figure 29 with axial load carrying rods and shear panels identified. In addition, the special frames at the forward and aft ends of the payload bay are shown at the right-hand side of this figure. Figures 27, 28 and 29 apply to both the aluminum and Lockalloy structure.

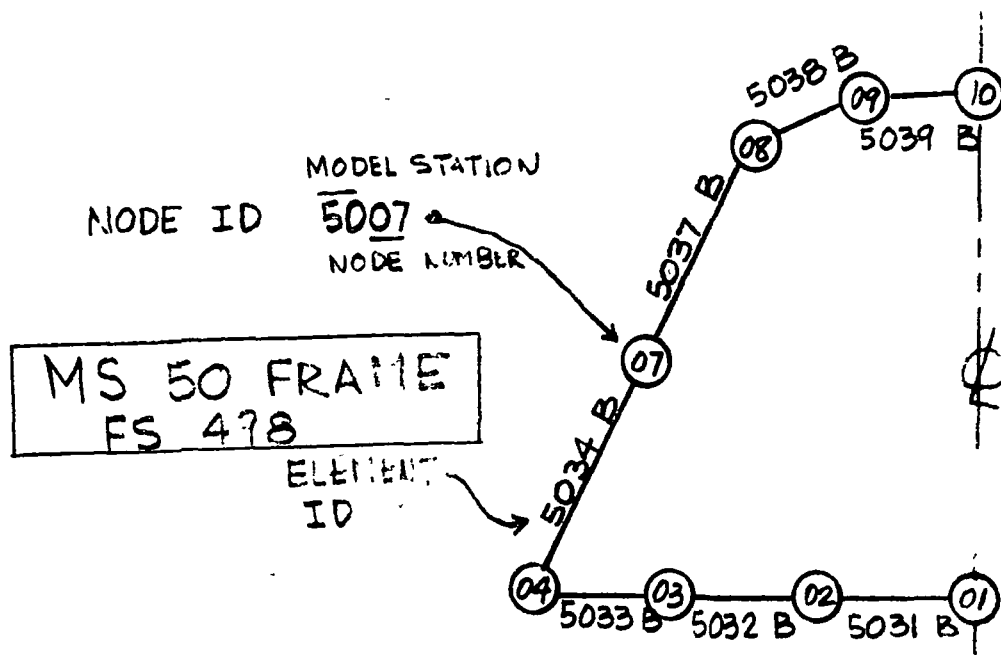


Figure 27 - NASTRAN Frame Model, F.S. 498

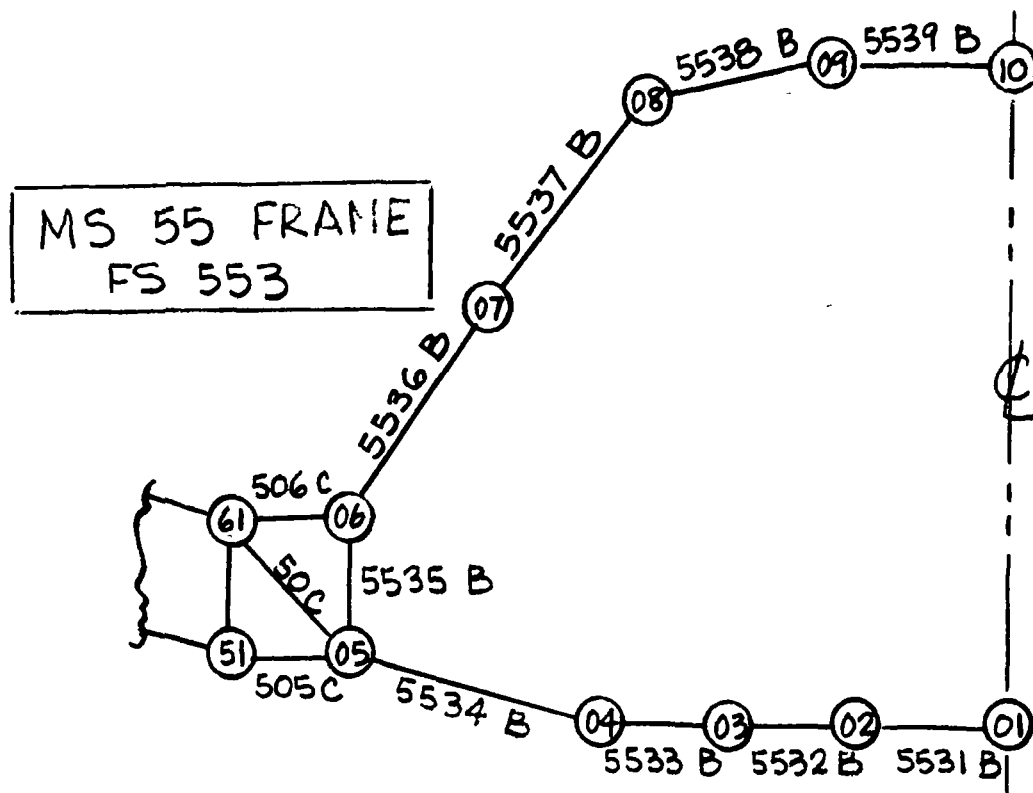
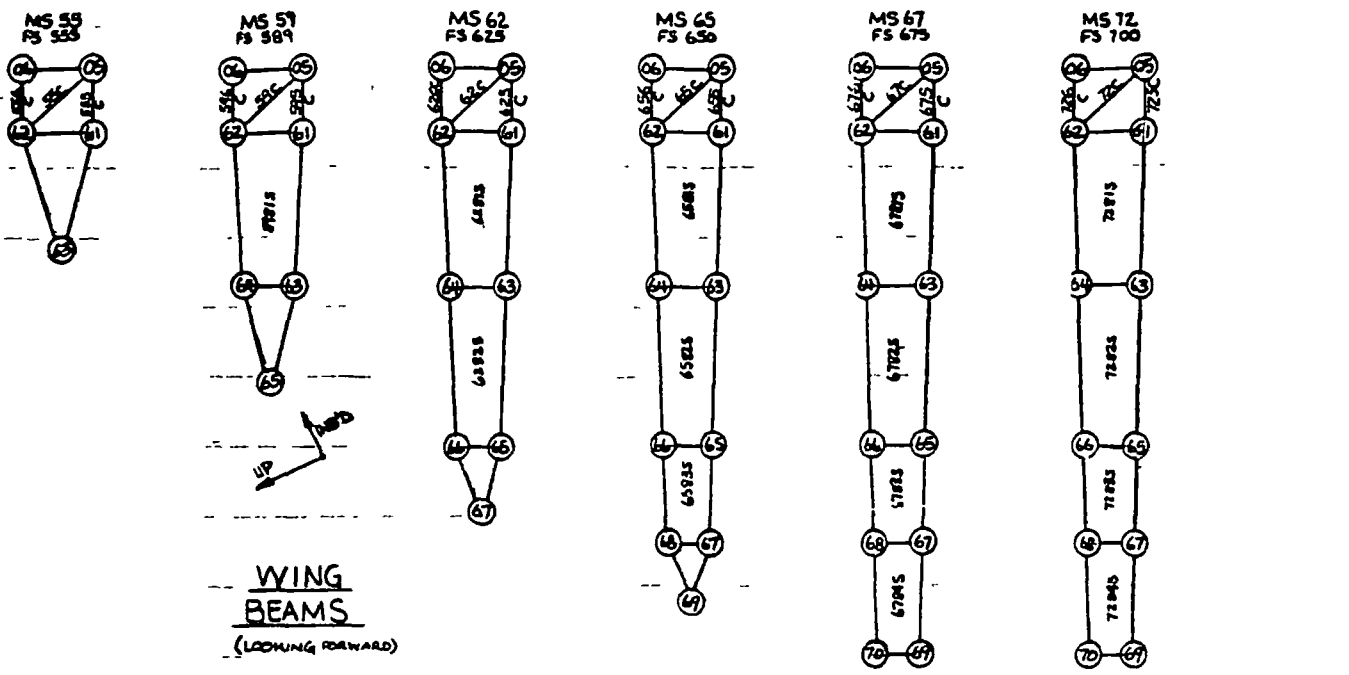
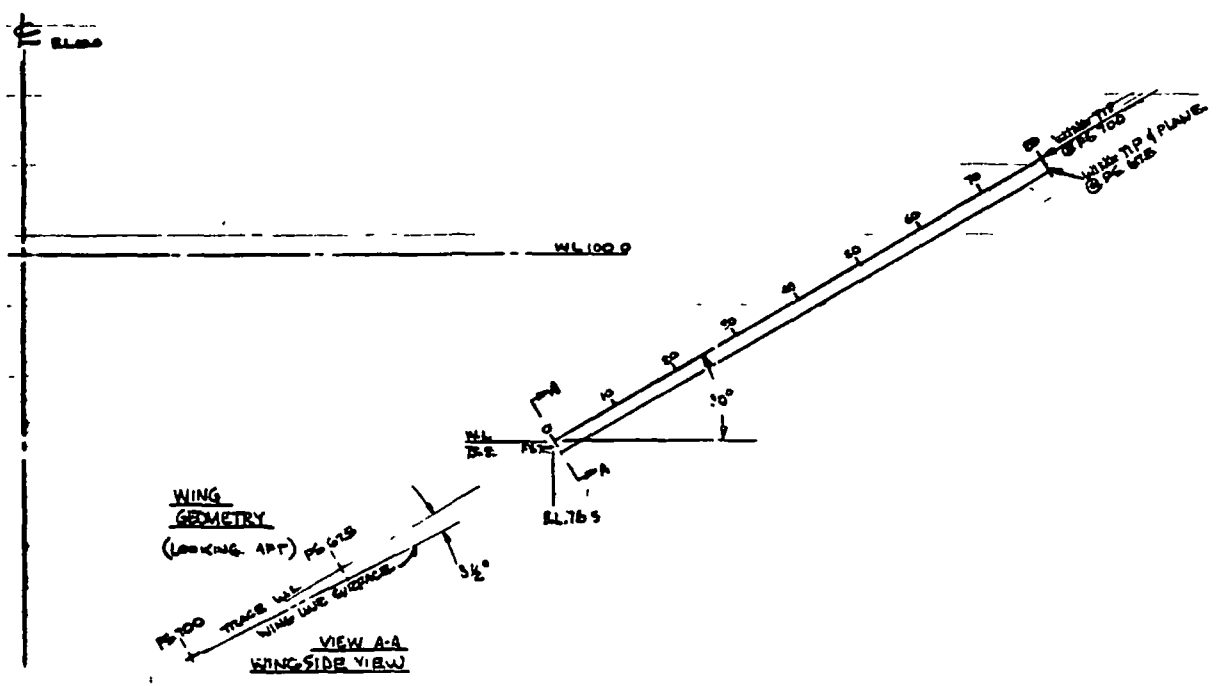
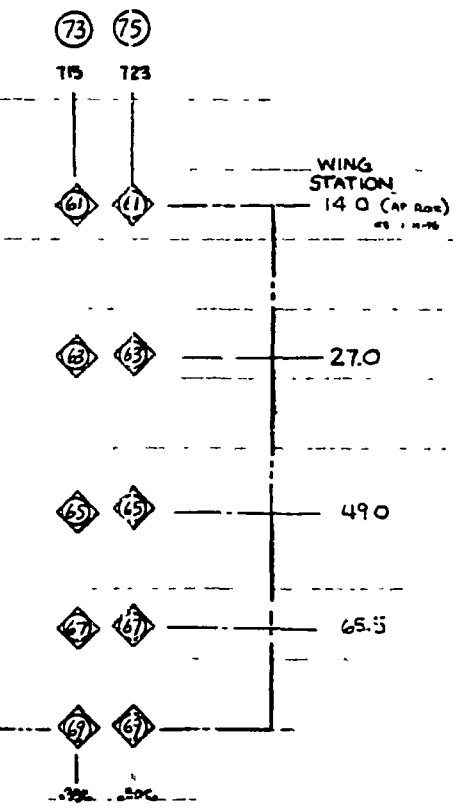
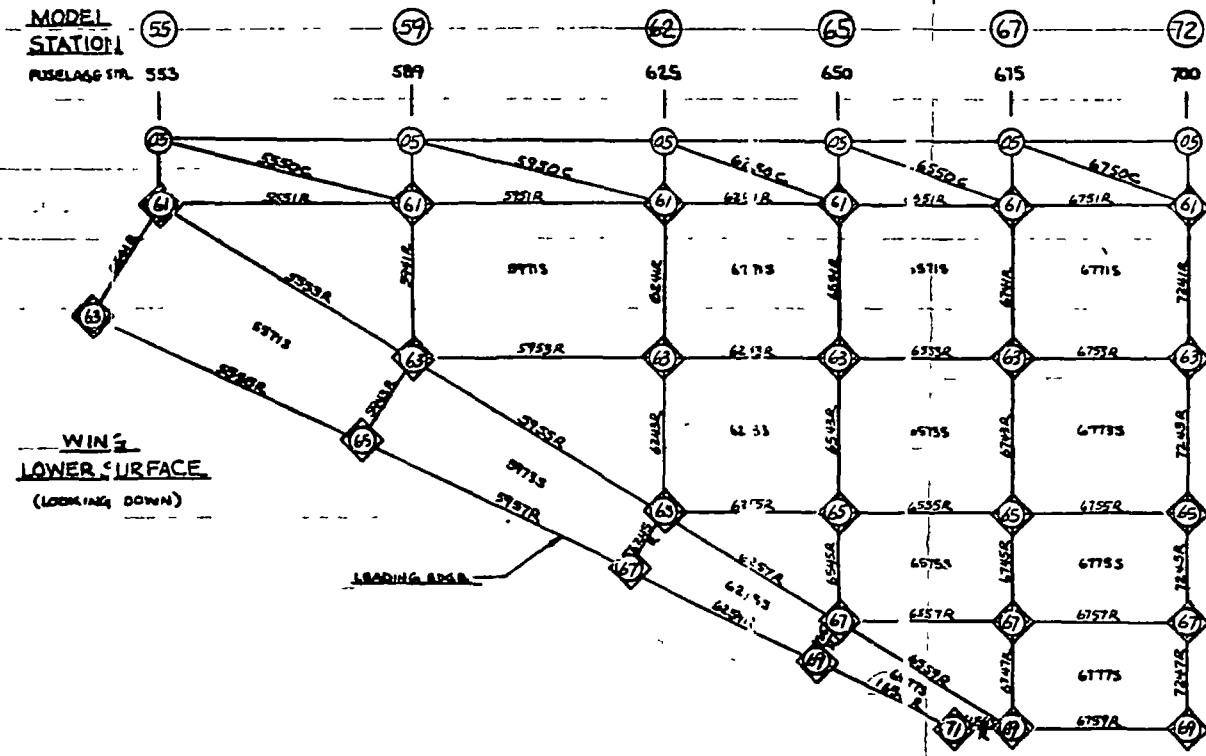
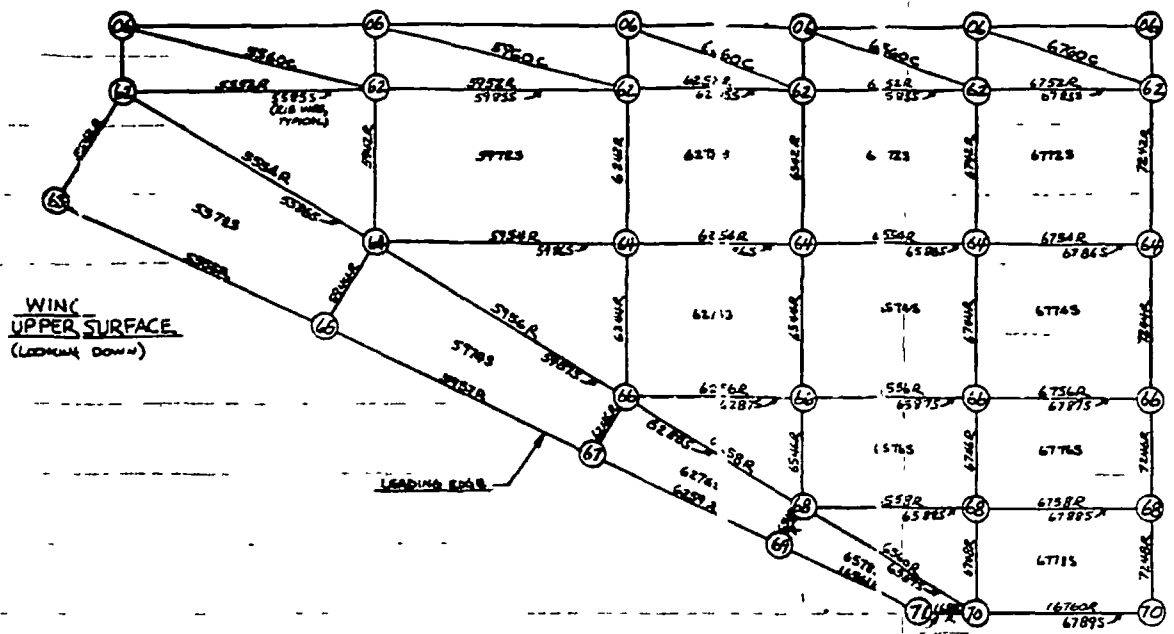


Figure 28 - NASTRAN Frame Model, F.S. 553



WING BEAMS  
(LOOKING FORWARD)

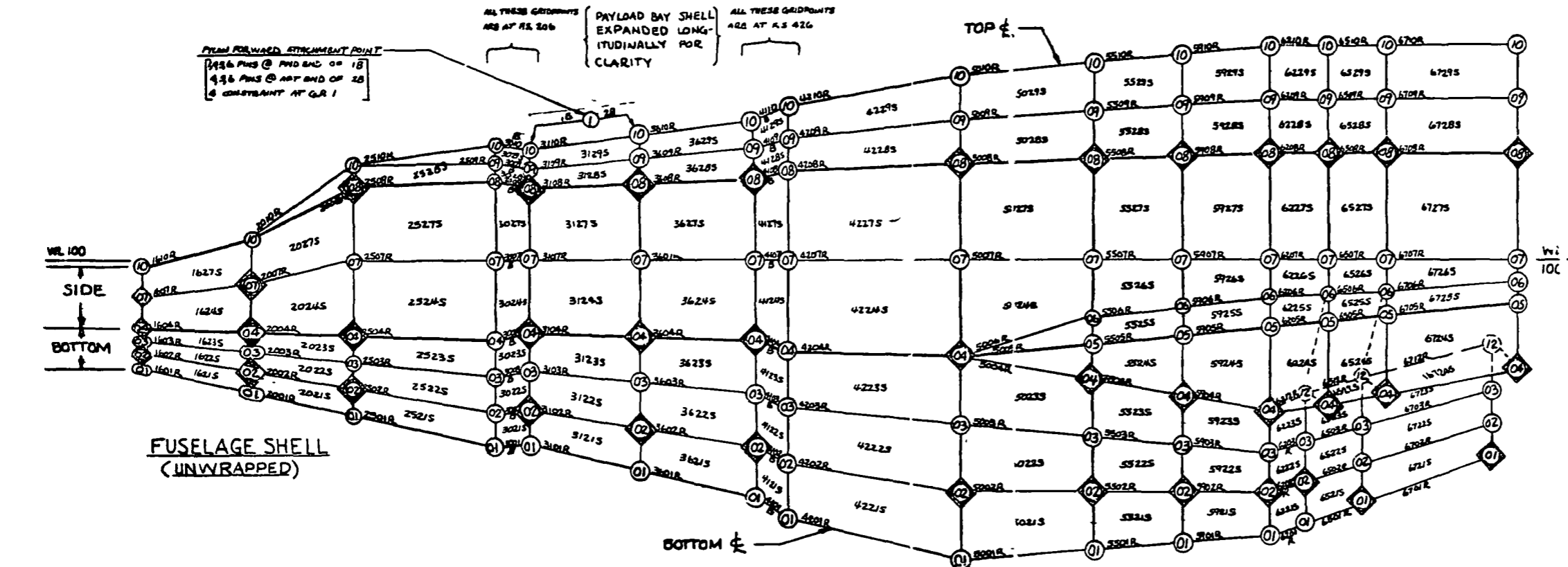


3. LOAD APPLIED

2. GRIDPOINTS ARE 4 DIGIT NUMBERS. MS (X)

NOTES: 1. APPROXIMATELY 1/10 SCALE

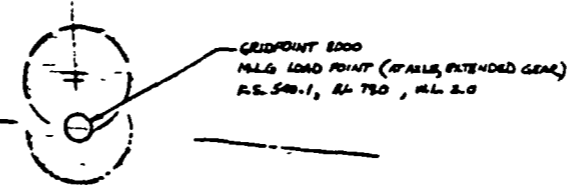
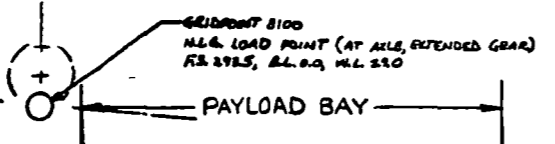
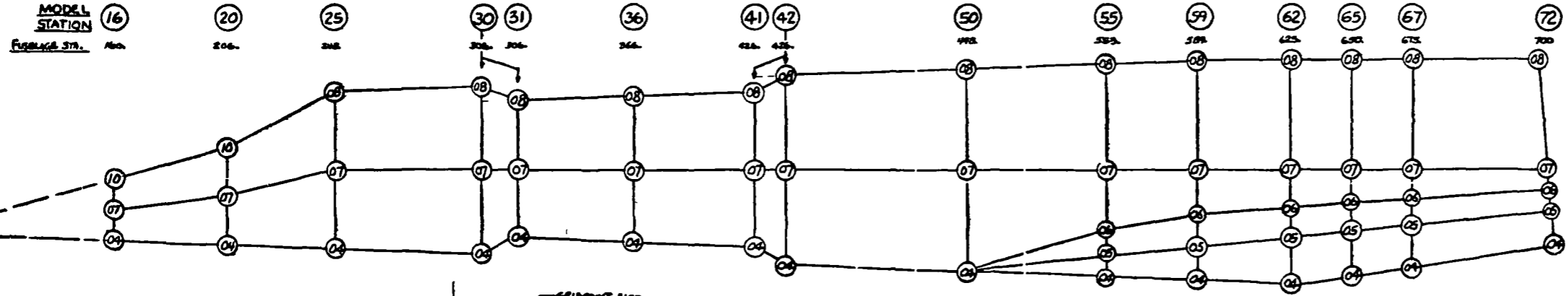
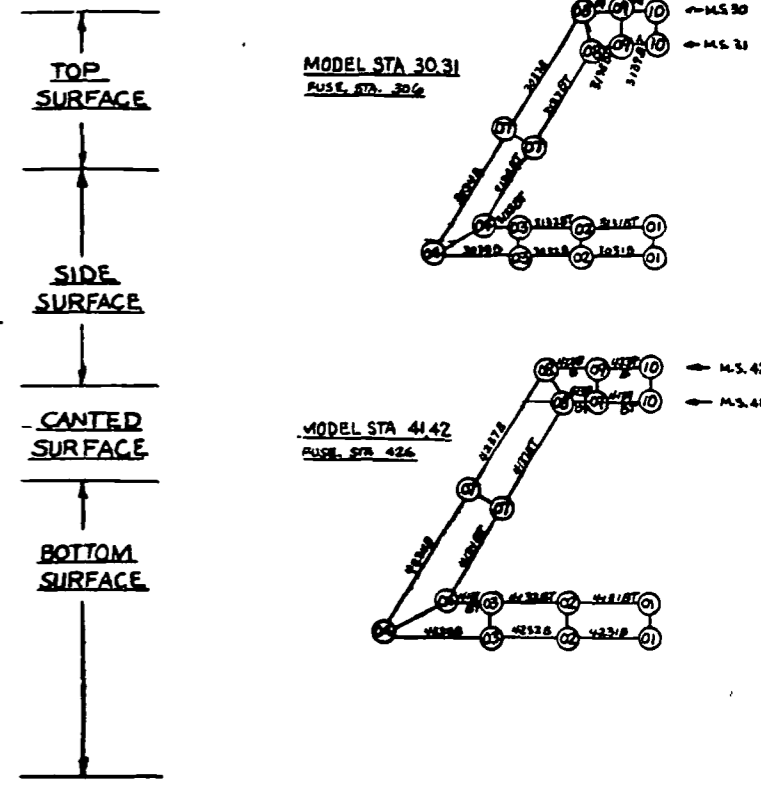
Figure 26 - NASTRAN Structural Model - Wing



FROM FORWARD STRUTMENT POINT  
 1436 PMS @ MID END OF 18  
 436 PMS @ AFT END OF 28  
 6 CONSTRAINT AT GR 1

ALL THESE GRIDPOINTS ARE AT RS 306  
 ALL THESE GRIDPOINTS ARE AT RS 426

- REV A - 11-27-73 C.S.  
 1. CHANGE EL 720 TO TOP  
 2. CHANGE EL 1 TO BOTTOM  
 3. CHANGE EL 2 TO SIDE  
 4. CHANGE EL 3 TO BOTTOM  
 5. CHANGE EL 4 TO BOTTOM
- REV B - 11-27-73  
 1. ADD G.R. 1, FROM MID/STRE. PT.  
 2. ADD G.R. 2, FROM AFT END EL.  
 3. CHANGE EL 1, 2, 3, 4, 5
- REV C - 1-7-75  
 1. EXPAND LOWER AFT STRUCTURE, EL 123-TOP  
 2. ADD AND CHANGE GRIDPOINTS



5. LOAD APPLIED
4. SHEAR PANEL SIGN CONVENTION.
3. GRID POINTS ARE 4 DIGIT NUMBERS:  
 MS(S)

2. R = ROW  
 S = SHELL  
 B = BOTTOM  
 T = TOP  
 M.S. = MODEL STATION
1. NOT TO SCALE, APPROXIMATELY 1/50 SCALE

NOTES:

Figure 29 - NASTRAN Structural Model - Fuselage

The detail frame structural model used in the thermal investigation of the Lockalloy design is shown in Figure 30 and depicts the shell and frame contour at F.S. 496. This model does not enable determination of thermal stress in the fuselage caused by the temperature gradient in the frames combined with hinge bends in the Lockalloy fuselage shell. A fuselage model consisting of the shell as shown in Figure 29 including the rings of the type shown in Figure 30 is required to evaluate thermal stress.

External loads for the taxi flight, and landing conditions, ref. Critical Loads section, were applied to the structural model at selective fuselage and wing grid points. These load points included at least three grid points at each fuselage station and the entire set of lower surface nodes for the wing. A combination of these load points is presented in Table 5.

Aluminum Structural Model - The Aluminum structural model uses the basic model grid system as defined on Figures 27 through 29. The structural arrangement for this design, which is idealized in the structural model, is summarized in Figure 31 and depicts the primary load-carrying structure for both the wing and fuselage. Bending, extensional, and shear stiffnesses corresponding to this structural arrangement are input into the structural model element properties cards, e. g., the frame extensional and bending stiffnesses are input using NAS-TRAN PBAR cards.

Figures 32 and 33 present maps of the fuselage shell and wing surface extensional thicknesses ( $\bar{t}$ ) and equivalent shear thicknesses ( $t_s$ ).

A description of the external load conditions used on the structural model was previously discussed. In review, a total of six conditions were input on the aluminum design structural model which consisted of three ground conditions (taxi and landing conditions) and three flight conditions covering both subsonic and supersonic maneuvers.



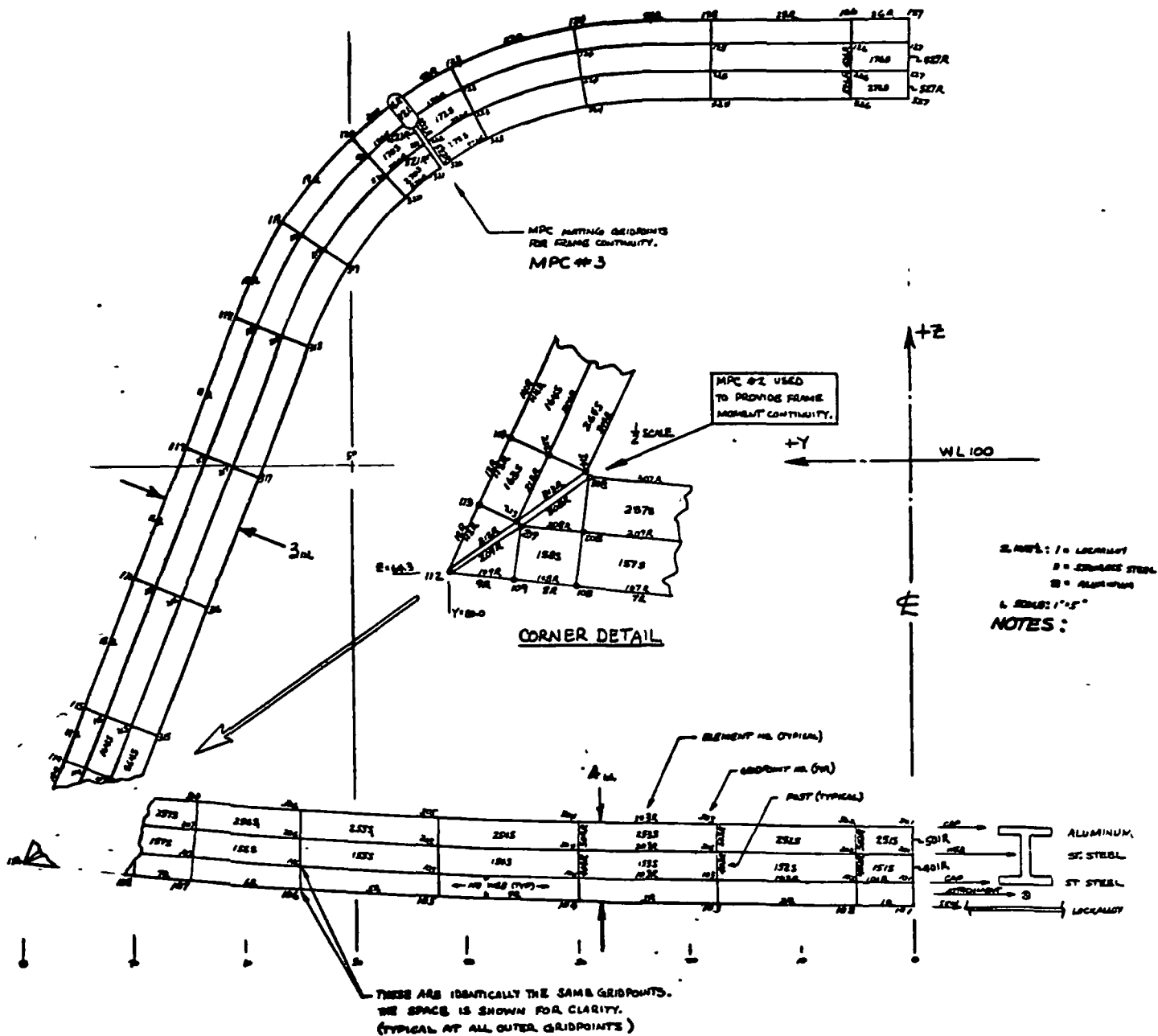


Figure 30 - NASTRAN Structural Model, F.S. 496 (Lockalloy Design)

NODE	X	Y	Z	NODE	X	Y	Z
1602	160.0	4.5	71.8	6261	625.0	89.8	75.5
1604	160.0	14.1	80.1	6263	↓	27.0	0.0
1607	160.0	11.0	84.3	6265	625.0	49.0	0.0
2002	206.0	7.5	70.0	6267	620.0	57.0	0.0
2004	206.0	22.6	71.0	6502	650.0	17.6	61.0
2007	206.0	16.9	88.2	6504	↓	53.8	56.8
2502	248.0	10.2	68.0	6508	↓	46.8	139.8
2504	248.0	31.0	69.8	6561	↓	89.3	77.0
2508	248.0	10.2	114.8	6563	↓	27.0	0.0
3102	306.0	14.0	71.8	6565	↓	49.0	0.0
3104	↓	27.0	72.5	6567	650.0	65.5	0.0
3108	↓	36.0	74.0	6569	647.0	69.0	0.0
3602	366.0	18.25	69.3	6701	675.0	0.0	70.2
3604	↓	48.50	72.5	6704	↓	56.3	60.0
3608	↓	21.50	121.0	6708	↓	47.6	140.8
4102	426.0	22.50	66.8	6761	↓	89.1	78.6
4104	↓	61.00	71.0	6763	↓	27.0	0.0
4108	↓	29.00	125.0	6765	↓	49.0	0.0
5002	498.0	27.00	57.8	6767	↓	65.5	0.0
5004	↓	79.80	65.5	6769	675.0	80.0	0.0
5008	↓	37.80	131.8	6771	666.0	80.0	0.0
5502	553.0	23.80	54.5	7201	700.0	0.0	81.0
5504	↓	71.10	60.0	7204	↓	59.2	63.6
5508	↓	42.60	135.6	7208	↓	48.3	142.0
5561	↓	40.80	71.3	7261	↓	88.9	80.2
5563	↓	21.00	0.0	7263	↓	27.0	0.0
5902	589.0	6.00	53.9	7265	↓	49.0	0.0
5904	↓	62.00	57.0	7267	↓	65.0	0.0
5908	↓	44.40	137.3	7269	700.0	80.0	0.0
5961	↓	90.20	73.2	* 8000	540.1	79.0	2.0
5963	589.0	27.00	0.0	* 8100	293.5	0.0	29.0
5965	582.0	39.00	0.0				
6202	625.0	18.80	52.2	* 8000 - MAIN LDG GEAR			
6204	↓	55.30	55.5	8100 - NOSE LDG GEAR			
6208	↓	45.80	138.8				

NODE	X	Y	Z
7361	715.0	14.0	0.0
7363	↓	27.0	0.0
7365	↓	49.0	0.0
7367	↓	65.5	0.0
7369	↓	80.0	0.0
7561	723.0	14.0	0.0
7563	↓	27.0	0.0
7565	↓	49.0	0.0
7567	↓	65.5	0.0
7569	↓	80.0	0.0

Table 5 - Model Load Inputs

The results of the NASTRAN static solution, using the previously discussed airframe stiffnesses and external loads, consisted of a definition of the airframe displacements and internal forces. A plot of the wing rear beam vertical displacement for the maximum up-bending flight condition, Pull-up after Launch, is shown on Figure 34 and indicates a wing tip displacement of approximately 0.06 meters. The corresponding displacements for the fuselage are shown on Figure 35 with a maximum vertical displacement of 0.02 meters noted at the nose.

The wing internal forces, presented as load intensities, for the Pull-up after Launch and the maximum down-bending conditions are shown in Figures 36 and 37, respectively. Similarly, the fuselage load intensities for the Pull-up after Launch conditions are presented in Figure 38. All wing and fuselage loads

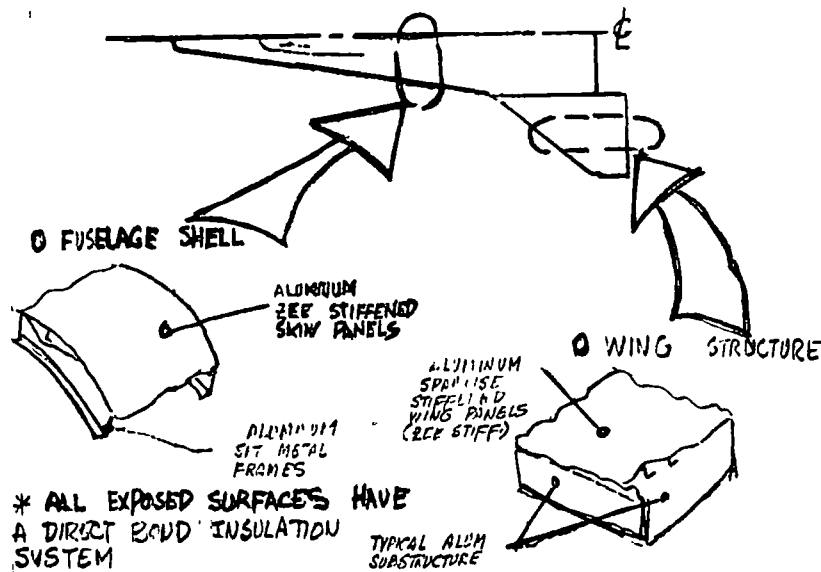


Figure 31 - Airframe Structural Arrangement - Aluminum

shown in the aforementioned figures are average ultimate mid-panel values calculated using the internal force/stress results of the NASTRAN static solution.

Lockalloy Structural Model - This structural model uses the basic model drawings shown in Figures 26 and 29 with the element property data reflecting the materials and structural arrangement of the Lockalloy airframe. The annotated history of the NASTRAN runs conducted using this model was previously shown in Table 4.

The fuselage shell and wing surface extensional and shear thicknesses are shown in Figures 39 and 40, superimposed on their respective structural model drawing. The fuselage stiffness data, Figure 39, reflects the input values used on the last NASTRAN run which had shell thicknesses ranging from a maximum thickness of 0.007 meters on the lower surface of the forebody to a minimum thickness of 0.003 meters on the upper surface of the fuselage aft body.

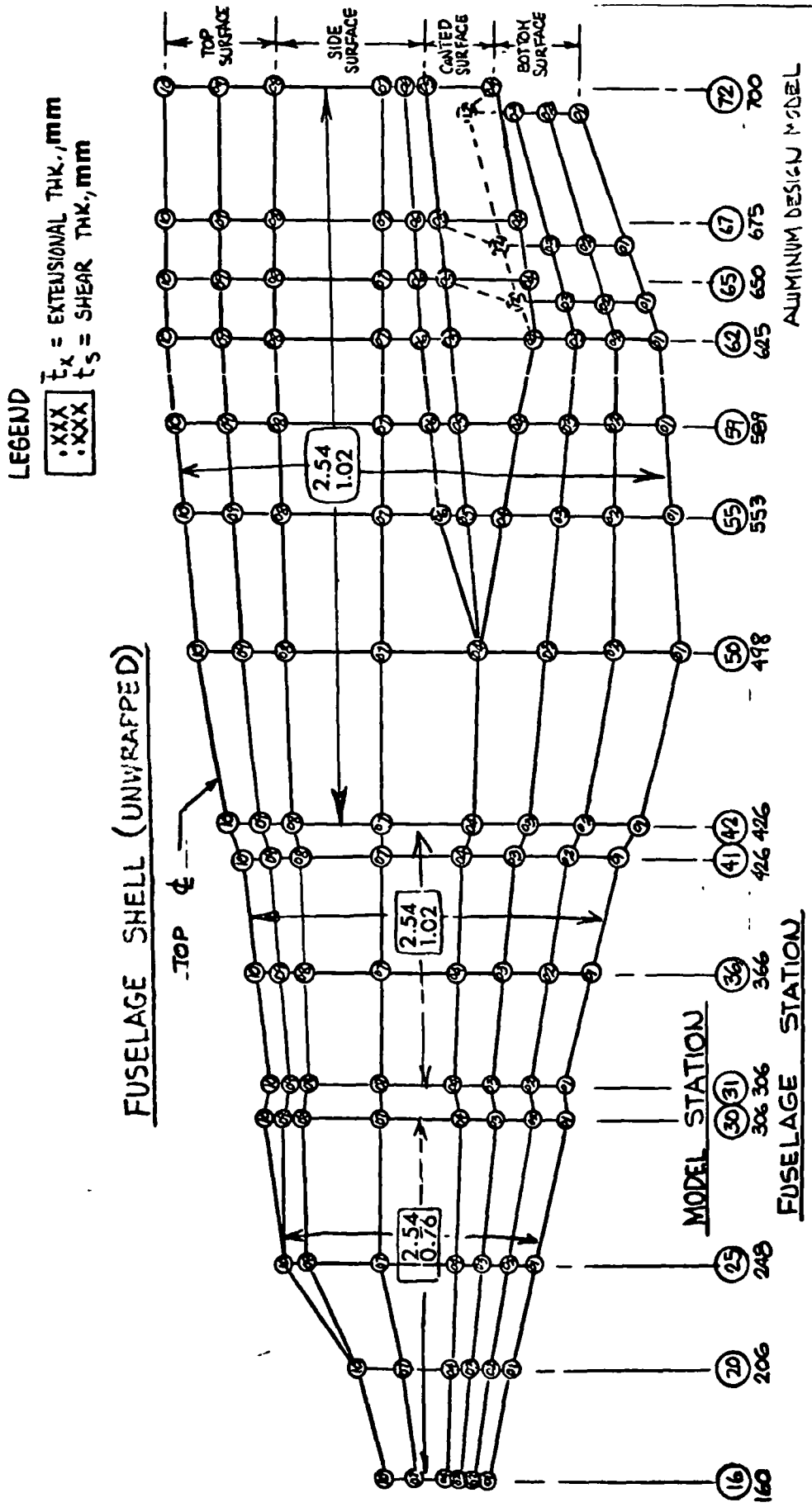


Figure 32 - Fuselage Extensional and Shear Thicknesses  
 Input into the Aluminum Design Structural Model

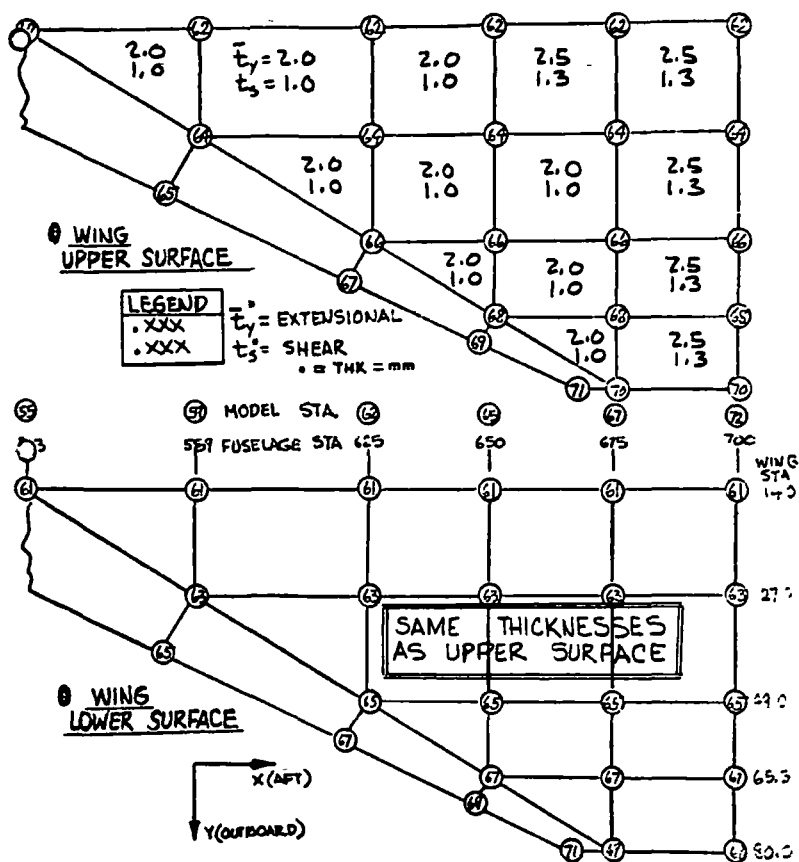


Figure 33 - Wing Surface Ext. and Shear Thicknesses - Aluminum

The wing stiffness data, Figure 40, indicates the lower surface panel thicknesses ranged from a thickness of 0.004 meters on the basic wing to 0.004<sup>+</sup>meters for the leading edge and adjacent panels. The wing upper surface thicknesses varied from a maximum thickness of 0.005 meters to a minimum thickness of 0.004 meters.

The load conditions used on the aluminum design were also used for the Lockalloy design. In addition to these load conditions, the Lockalloy design was evaluated for another flight condition where the maximum temperature gradients exist on the airframe.

Examples of the wing and fuselage deflection for the Lockalloy design during the Pull-up after Launch condition are compared to those of the aluminum design on the aforementioned Figures 34 and 35. From a review of Figure 34, it can be

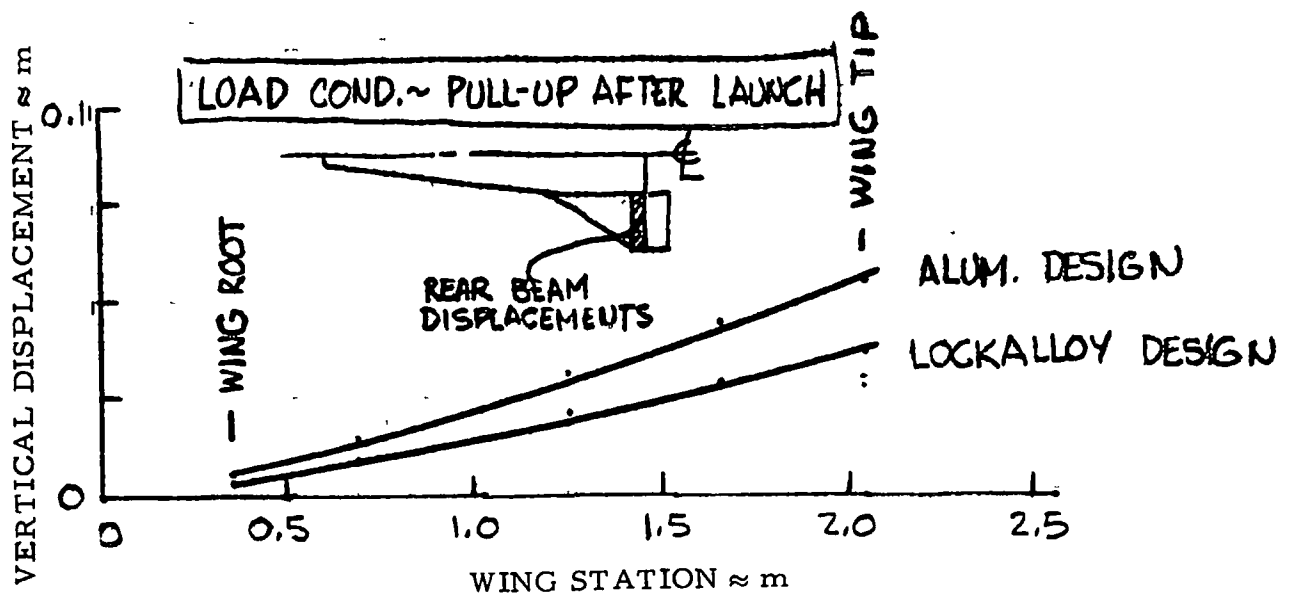


Figure 34 - Wing Rear Beam Vertical Displacement

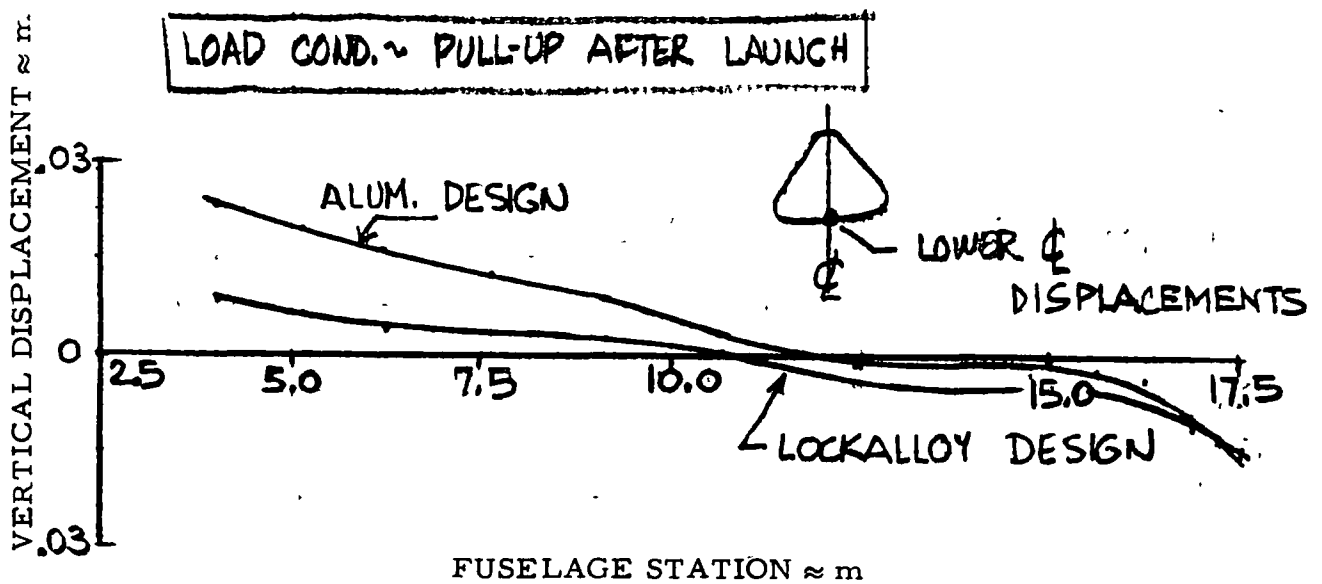


Figure 35 - Fuselage Lower Centerline Vertical Displacement

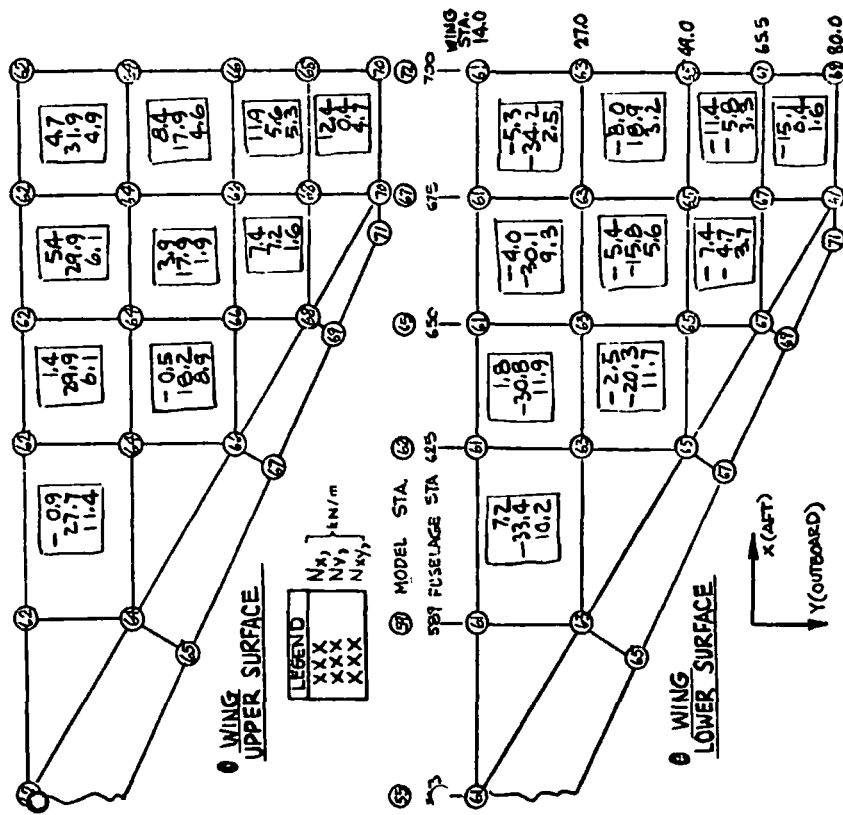


Figure 37 - Wing Surface Load Intensities - Subsonic

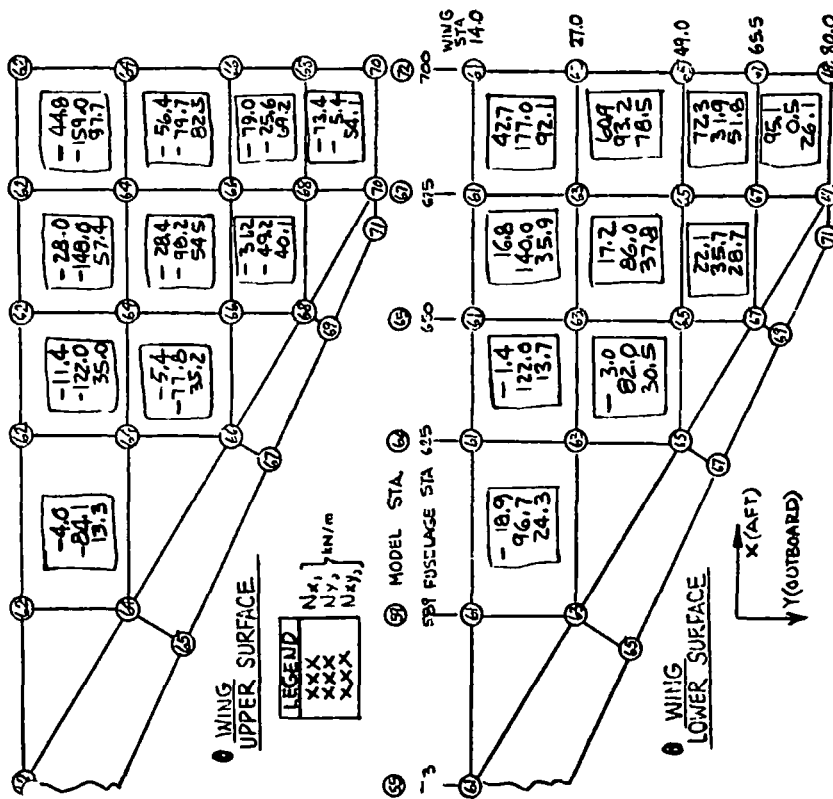


Figure 36 - Wing Surface Load Intensities - Pullup

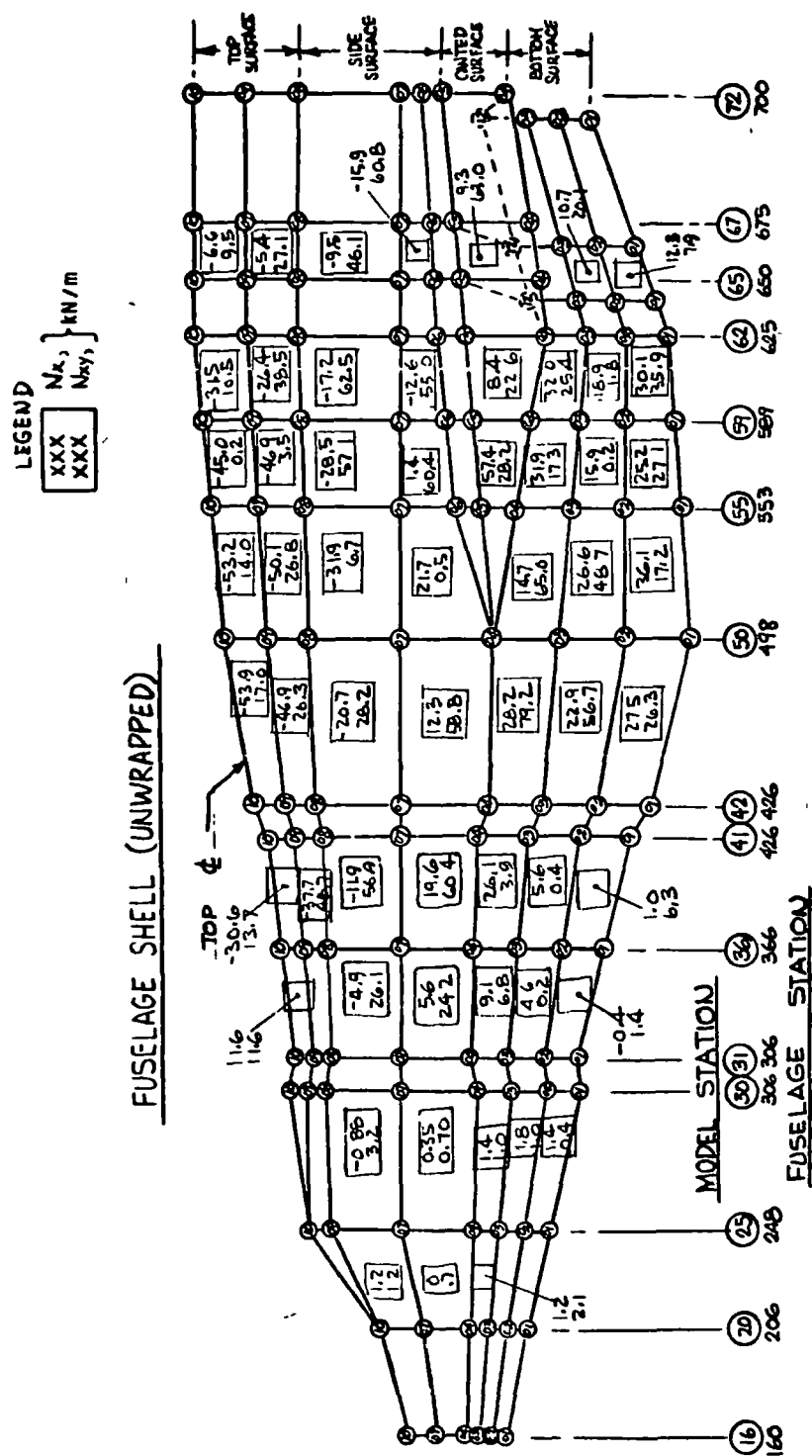


Figure 38 - Fuselage Load Intensities for Pull-up After Launch



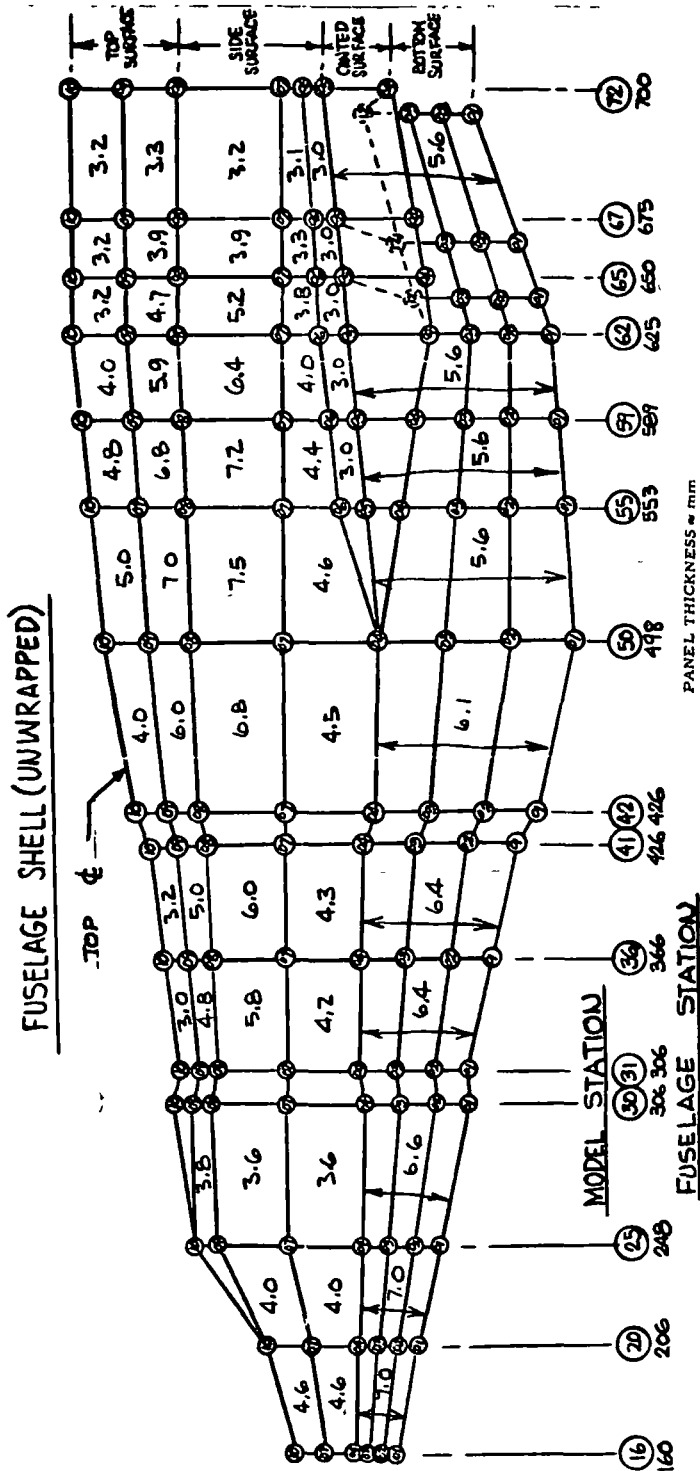


Figure 39 - Fuselage Panel Thicknesses Input - Lockalloy

seen that the Lockalloy design wing is approximately 65 percent stiffer than the corresponding aluminum design wing. Similar trends are noted on Figure 35 for the fuselage, e. g., the fuselage forebody of the Lockalloy design has approximately twice the stiffness (half the deflection) as the aluminum design.

The results of the NASTRAN static solution indicate the fuselage internal forces for the Lockalloy design are approximately equal to those of the aluminum design; hence, the load intensities previously shown in Figure 38 are also appropriate for the Lockalloy design. The wing surface inplane load states for the Pull-up after Launch, Maneuver at Max MACH, and the Maximum Temperature Gradient conditions are displayed in Figures 41, 42 and 43 respectively. The latter two conditions are combined in the stress analysis to form the total load/temperature state for the maximum Mach flight condition.

An example of the temperature-gradient matching aspects employed using the Lockalloy structural model are shown in Figure 44. This figure displays the fuselage shell configuration, temperature gradients, shell thickness, and resultant thermal stresses on a fuselage cross section at F.S. 462. Designs (A) and (B) represent two variations in the fuselage design evaluated during the NASTRAN thermal stress analysis. Design (A) is an earlier design which reflected a very abrupt circumferential temperature gradient between the upper and lower surfaces of the fuselage. Extremely high thermal stresses are noted for this design in the region of the upper surface of the shell, e. g., a tensile stress of 137.9 MPa occurs at the upper centerline. Design (B) indicates the mass penalty, added shell thickness required, associated with smoothing out this temperature gradient and reducing the stresses to a more realistic level, e. g., a tensile stress of 34.5 MPa occurs at the upper centerline. In design (A) the upper panels were thickened over the thickness required for heat sink purposes to avoid skin buckling. Consequently the temperature of the upper panels is lower than that of the side and lower panels, which were sized for 589 K heat-sink requirement. Either beading or adding stiffeners to the upper panels at a  $\bar{t}$  equal

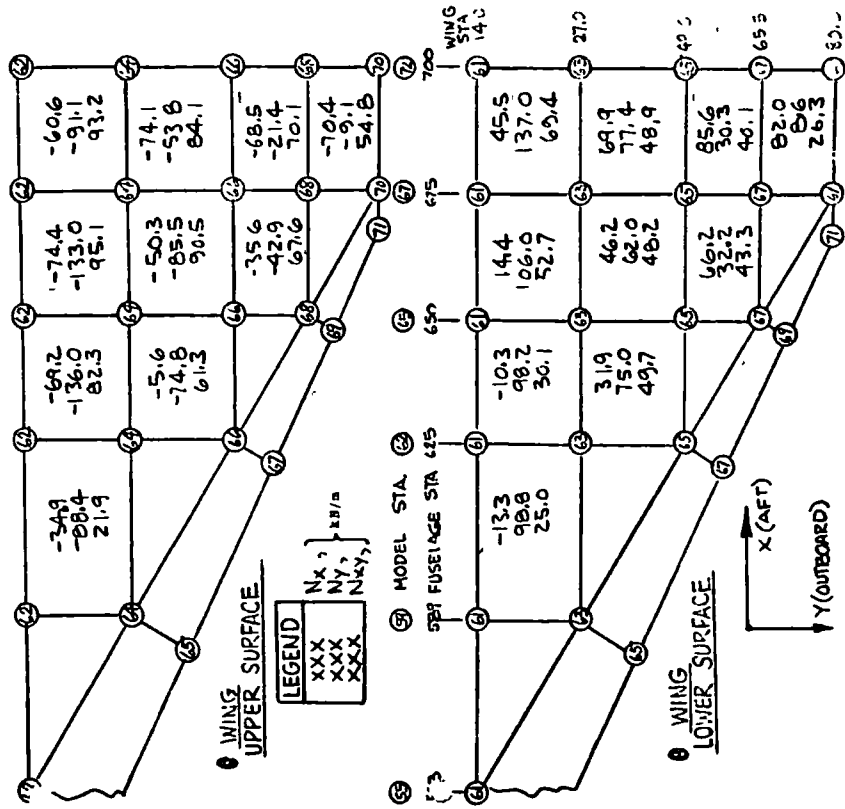


Figure 41 - Wing Surface Load Intensities, Pullup - Lockalloy Design

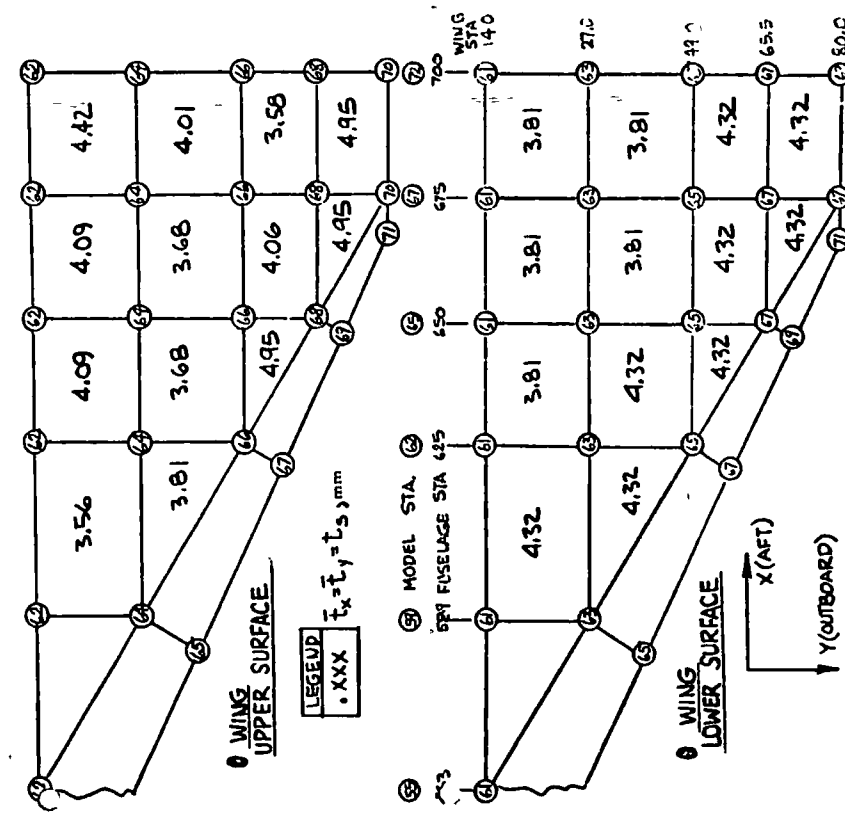


Figure 40 - Wing Surface Extensional and Shear Thicknesses - Lockalloy Design

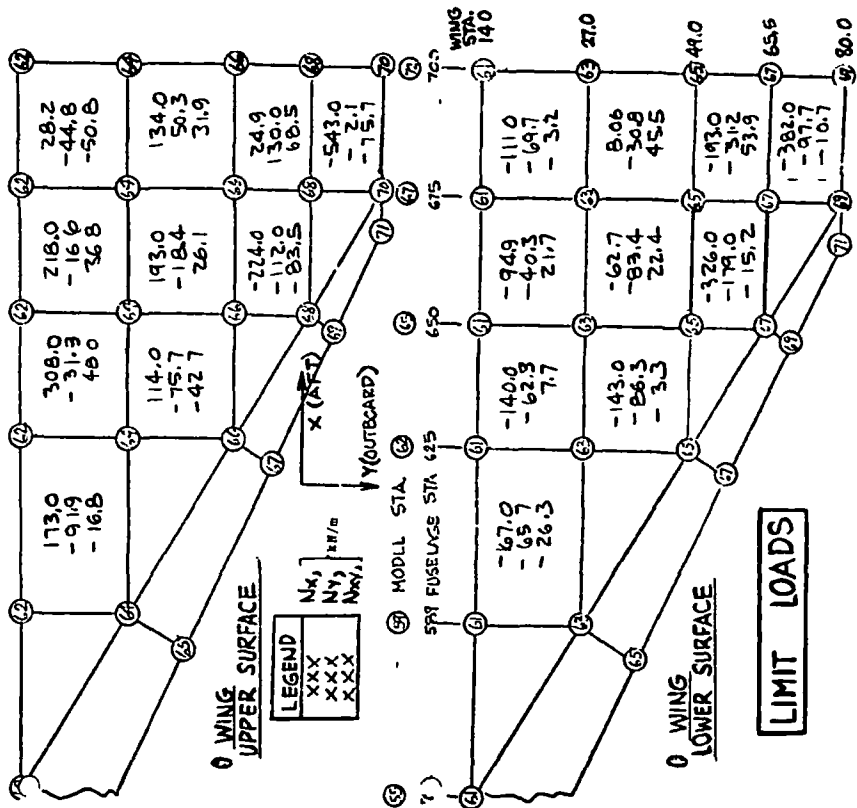


Figure 42 - Wing Surface Load Intensities, Maximum Maneuver - Lockalloy Design

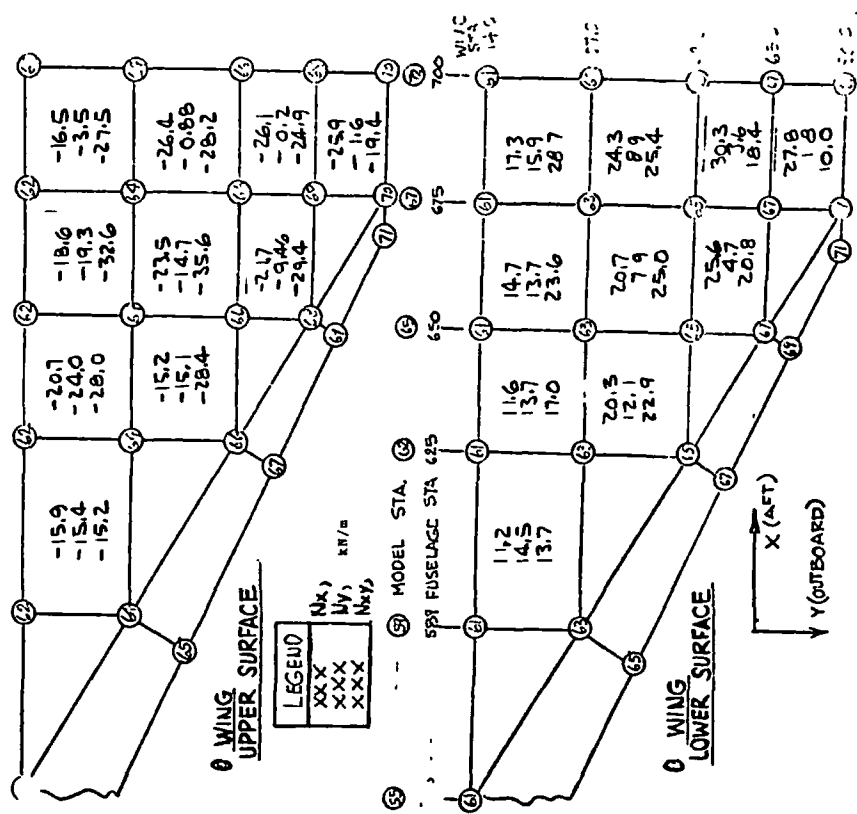


Figure 43 - Wing Surface Load Intensities, Maximum Temperature Gradient Condition - Lockalloy Design

F.S. 462 - LONGITUDINAL STRESS

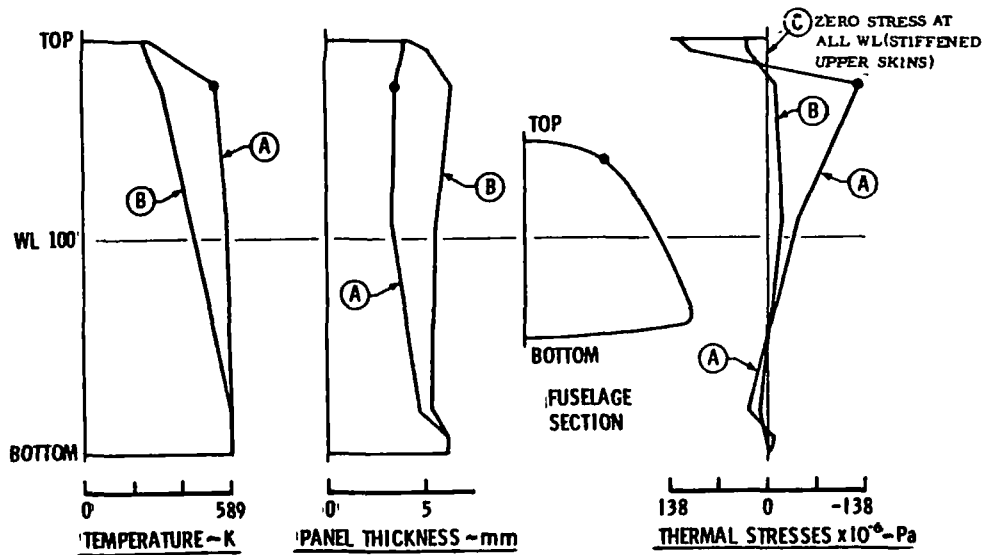


Figure 44 - Fuselage Thermal Stress

to heat-sink requirements, design (C), to avoid buckling would result in upper panel temperatures of 589 K, thus eliminating the thermal stress problem. Moreover, the mass of both upper and side panels would be less for design (C) than for design (B). In design (C) the beads or stiffeners are prefabricated in each panel. The stiffeners do not extend through the frames, thus the ease of access by separate panel removal is retained by panel edge bolts like the unstiffened panel designs of (A) and (B).

Wing Analysis

Detailed stress analyses were conducted to assess the mass of the wing primary load-carrying structure for each of the basic airframe designs. These analyses encompassed sizing the wing structural concepts for the internal forces obtained using the NASTRAN structural model and the structural design criteria specified in

the statement of work. Appropriate analytical methods were employed for this mass/strength evaluation. The wing analyses conducted during this phase can be categorized into two basic tasks, which are:

- A parametric mass/strength analysis to ascertain the wing rib/spar spacing for minimum mass design, and
- A more detailed stress analysis using the minimum mass panel proportions, to size a sufficient amount of the wing primary load-carrying structure to forecast a total wing mass.

Structural Design Criteria - Evaluation of the primary-structure for each concept was based on Appendix A.

Exceptions were noted in the design of the two aluminum concepts. For the aluminum design incorporating the direct-bond LI-900 insulation, the skin limit load stresses on the primary load-carrying panels were not allowed to exceed the skin initial buckling allowables. Similarly, for the panels with the Ablator system the skin was analyzed to be non-buckled at 80 percent limit loads. The limitations on the surface stress level for the LI-900 design was improved to preclude skin buckles from popping off the insulation tiles. The Ablator system is considered somewhat flexible and tolerant of a small amount of skin buckling, therefore, the non-buckled at 80 percent of limit load criterion was chosen. However, the possibility of cracking and losing pyrolyzed material with limit buckling is a possibility and will require substantial testing.

Typical design mechanical properties for the three basic materials, 2024-T81 Aluminum Alloy, Lockalloy, and 6Al-4V Titanium Alloy are shown in Table 6.

Wing Structural Arrangements - The structural concepts were divided into two major concepts as characterized by their thermal protection system. First, concepts which utilize a direct-bond insulation system to absorb the heat flow and allow the primary load-carrying structure to be constructed of conventional aluminum materials, and second, a heat sink design which combines the load-carrying

MATERIAL	LOCKALLOY(LX62)	2024 ALUM	6AL-4V Ti		
FORM	SHEET	SHT. PLATE	EXTR BAR		
SPECIFICATION	NONE	QQ-A-250/4	MIL-T-8155G		
CONDITION	ANNEALED	T-81	ANNEALED		
THICKNESS, mm	1.02 - 6.32	0.25 - 6.32	≤ 51.0		
BASIS	(b)	A	A		
TEMPERATURE (K)	ROOM	589	ROOM		
<u>MECHANICAL PROPERTIES:</u>					
$F_{tu}$ , MPa	L	345	193	462	896
	LT	345	193	462	896
$F_{ty}$ , "	L	241	172	407	827
	LT	241	172	400	827
$F_{cy}$ , "	L	228	152	407	883
	LT	228	152	400	883
$F_{su}$ , "		179	103	276	579
$F_{bru}$ , "	(e/D = 1.5)	-	-	689	1489
	(e/D = 2.0)	648	379	876	1848
$F_{bry}$ , MPa	(e/D = 1.5)	-	-	572	1255
	(e/D = 2.0)	441	276	648	1489
e, percent	L	7.0	7.8	-	-
	LT	7.0	7.8	5.0	10.0
E, GPa		193	183	72.4	110.0
$E_c$ , GPa		193	183	73.8	113.0
G, GPa		86.2	80.7	27.6	42.7
$\mu$		.14	.14	0.33	0.31
<u>PHYSICAL PROPERTIES:</u> (b)					
$\rho$ , kg/m <sup>3</sup>		2090	2090	2770	4430
C, J/g·K		1.65	2.29	0.88	0.52
K, W/m·K		212.7	153.9	138.3	7.3
$\alpha$ m/m/K	(c)	-	17.6	22.8	8.7

- NOTES: (a) Values shown are applicable after exposure to temperatures indicated for up to 100 hours.  
(b) Values to be substantiated by tests.  
(c) Values shown are the mean coefficient between room temperature and the temperature indicated.

Table 6 - Mechanical and Physical Properties -  
Candidate Structural Materials

and thermal protection functions. Lockalloy material was used for the heat sink design for this study effort.

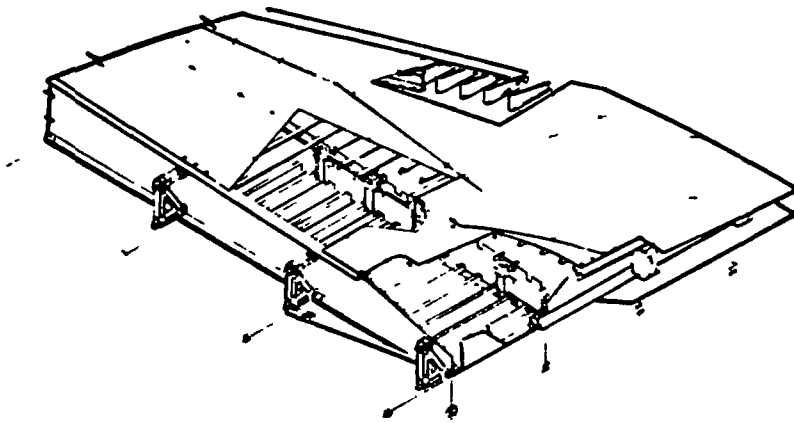
Two direct-bond insulation TPS's were investigated for application to an aluminum primary structure; they were the LI-900 block insulation and the Ablator systems. Each of these designs incorporated a common primary load-carrying structural arrangement which is displayed in Figure 45. This structural arrangement consists of 2024-T81 aluminum alloy surface panels fabricated with zee-stiffeners orientated in the spanwise direction. Conventional aluminum substructure composed of extruded spar and rib caps and flat-plate webs is utilized for this design. The spar caps are continuous; whereas, the rib caps are submerged to allow for continuation of the panel stiffeners. However, Shuttle experience indicates machined integrally stiffened skins may be required for areas where LI-900 is applied to avoid local skin buckling and loss of tiles. Cost estimates are needed to assess this type of panel for the X-24C.

The heat sink wing design is depicted in Figure 46. Flat sheets of Lockalloy, chem-milled to satisfy the variable material thickness requirements for applied loads and to eliminate any mismatch between panels, are mechanically fastened to the wing substructure. Currently, titanium alloy extrusions are used for the spar and rib cap designs with aluminum alloy webs. Caps of 301-1/2H stainless steel, similar to the fuselage frames, Figure 30, and use of beaded skin webs would reduce thermal stress from that of Figure 46 design.

Wing Point Design Environment - The environment imposed on the X-24C aircraft during its flight schedule was defined and used as the basis for evaluating each design concept. The procedure used for specifying this environment was as follows:

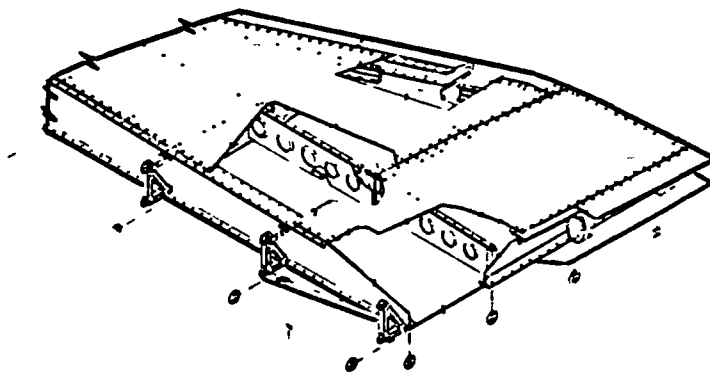
- 1) Specific regions of the wing were selected to use as point design regions for conducting the detail stress analysis.





**WING BOX  
STRUCTURE**

Figure 45 - Wing Arrangement - Aluminum



**WING BOX  
STRUCTURE**

Figure 46 - Wing Arrangement - Lockalloy

- 2) Load intensities and thermal stresses were defined for these regions using the results of NASTRAN static solution.
- 3) The normal loads acting on these regions were specified, considering both aerodynamic and venting pressures.
- 4) Average temperatures and gradients associated with the Lockalloy design were compiled using the results of the aerodynamic-heating analysis, and
- 5) The results of the above analysis were combined to specify the complete load environment at each point design region.

Representative structure was specified at selected wing regions to determine the load-temperature environment. The locations of the wing point design regions are shown in Figure 47 and include the three regions which are displayed on the wing planform of the structural model and are identified by the panel element numbers. Representative structure was specified at each of these locations and included a definition of the upper and lower surface panels, and typical rib and spar structure.

Wing Internal Loads (Airloads) - The wing internal loads and displacements for the flight and ground conditions were determined using the NASTRAN redundant-structure analysis solution. These solutions were performed for both the aluminum and Lockalloy structural models, with samples of these results shown in Figures 48 and 49. These figures display the wing surface load intensities for the aluminum and Lockalloy structural models for the Pull-up after Launch flight condition.

Wing Internal Loads (Thermal) - For the Lockalloy design a NASTRAN solution determined the thermal stresses and deflections due to the thermal expansion of the model elements. Figure 50 shows the wing surface panel load intensities for the maximum temperature gradient condition described under Critical Load conditions. Thermal loads were not determined for the aluminum structure. However, since the thin skin between stiffeners has a low buckling stress for large compression,

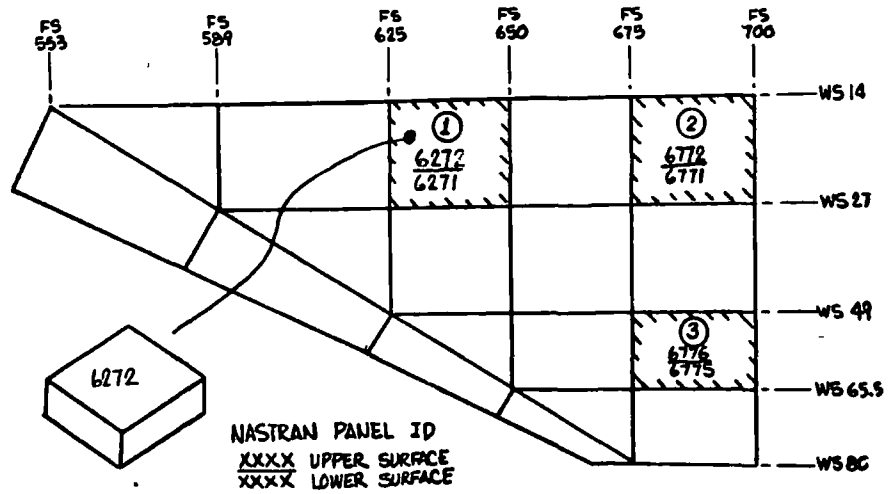


Figure 47 - Wing Point Design Region

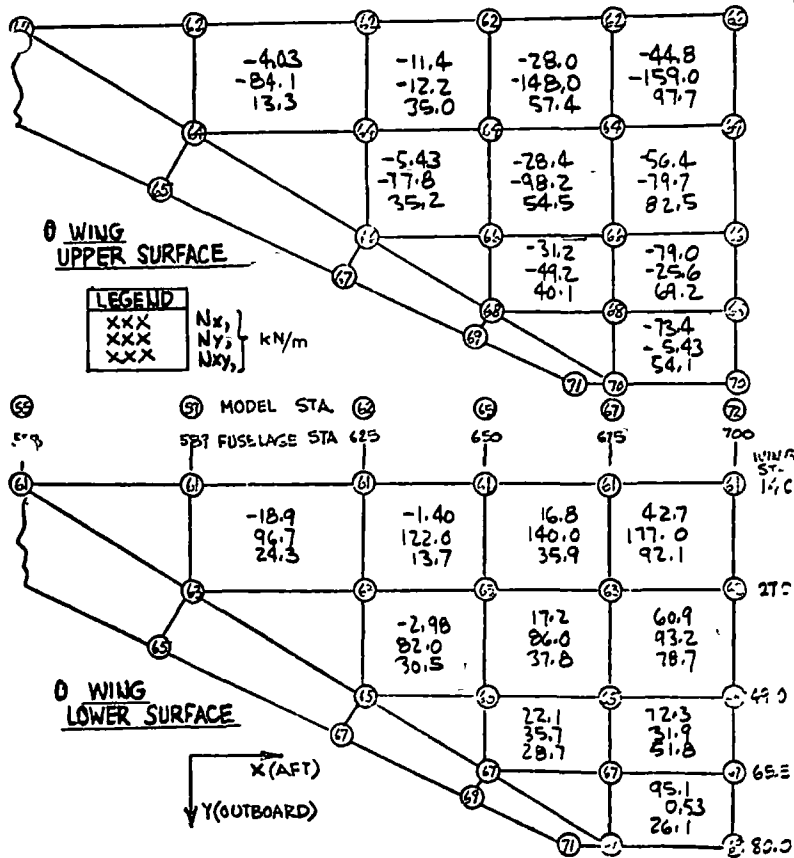


Figure 48 - Wing Surface Load Intensities, Pullup - Aluminum Design

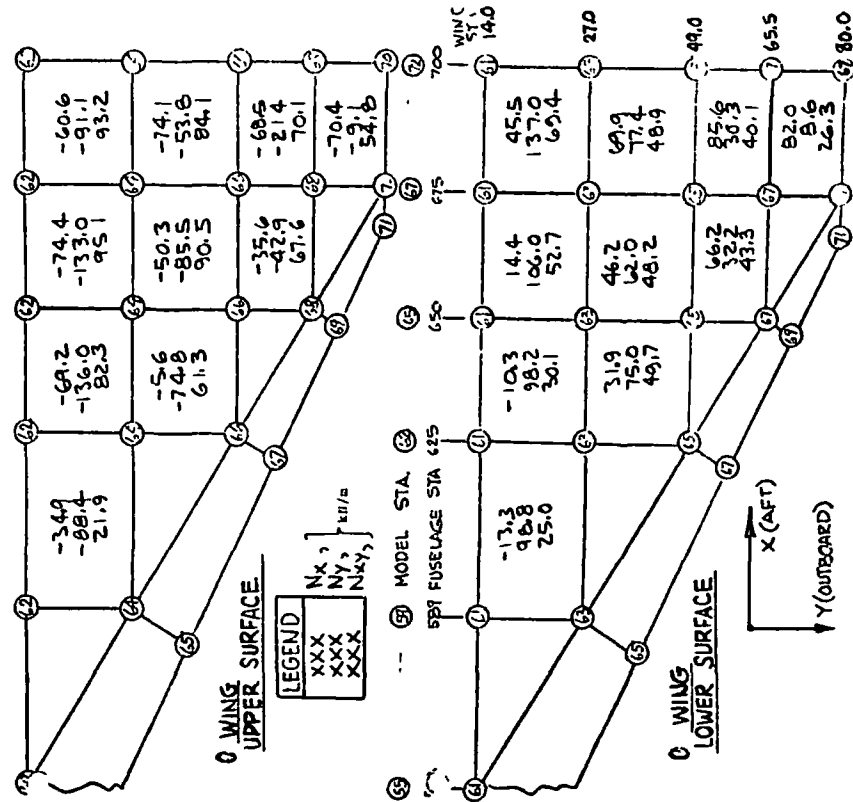


Figure 49 - Wing Surface Load Intensities, Pullup - Lockalloy Design

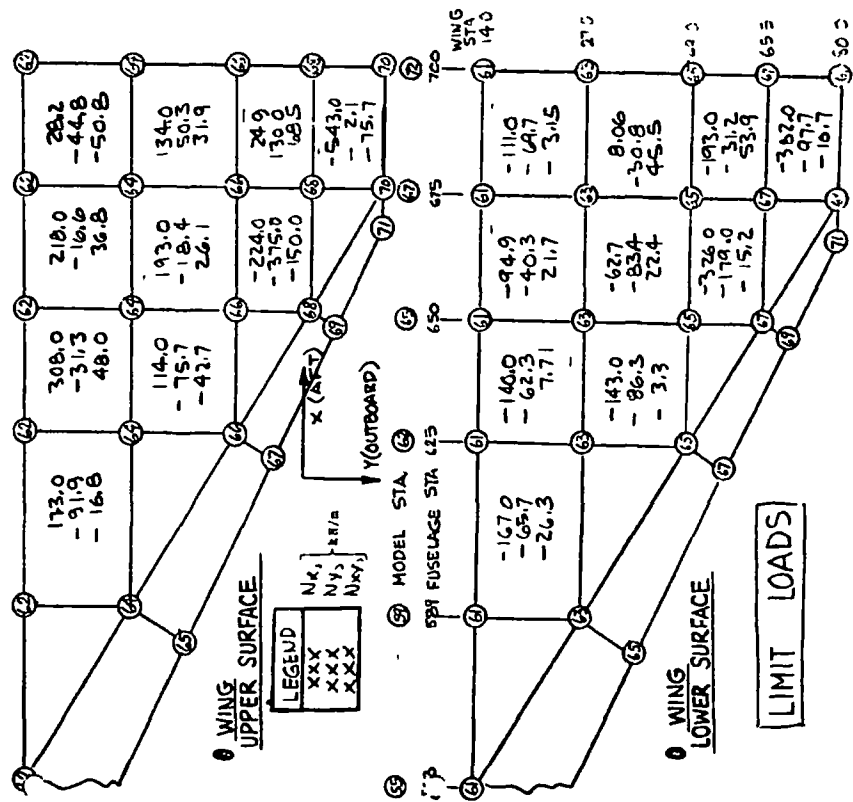


Figure 50 - Wing Surface Load Intensities, Maximum Temperature Gradient Condition - Lockalloy Design

even a low thermal stress may be enough to cause skin buckling and therefore violate the non-buckle skin criteria. Or the skin may have to be thickened requiring a thermal stress analysis of the aluminum structure.

Wing Aerodynamic Pressures - Surface pressure data were calculated using Lockheed's VORLAX program for the subsonic speed regime and the Hypersonic Arbitrary-Body Program (Gentry) for Mach 6.0 flight. Table 7 contains the aerodynamic pressures acting on the three point design regions for selective flight conditions.

Commensurate with the structural criteria in Appendix A, a limit load pressure difference of  $\pm 6.89$  kPa was applied to vented cavities.

CONDITION	AERODYNAMIC PRESSURE (kPa)					
	6272/6271		6772/6771		6776/6775	
	UPPER	LOWER	UPPER	LOWER	UPPER	LOWER
SUBSONIC FLIGHT ( $n_z = -1$ )	1.4	-2.2	0.3	-0.7	0.3	-0.5
MACH 6 • ( $n_z = 3$ )	-1.0	1.7	-1.4	2.1	-1.0	2.1
• ( $n_z = -1$ )	1.9	-0.9	0.7	-1.5	2.1	-1.5
PULL-UP AFTER LAUNCH	-5.2	5.2	-2.8	2.8	-2.8	2.8

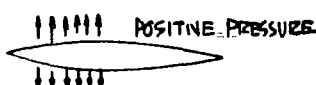
SIGN CONVENTION:  


Table 7 - Wing Aerodynamic Pressure

Wing Combined Loads - The wing combined loads and temperatures were defined for the wing point design regions. These point design environments were defined for each wing design and include the complete inplane load and normal load state. In addition, for the applicable flight conditions the thermal loads were included.

The point design environment for the aluminum structural arrangements for the Pull-up after Launch and negative  $n_z$  subsonic flight conditions are shown in Tables 8 and 9. For the Lockalloy design the point design environment are shown in Tables 10 and 11 for the Pull-up after Launch and the maneuver at maximum Mach light conditions.

ITEM	REGION ①		REGION ②		REGION ③	
	UPPER	LOWER	UPPER	LOWER	UPPER	LOWER
	6272	6271	6772	6771	6776	6775
AIR LOADS, kN/m						
N <sub>x</sub>	-11.4	-1.4	-44.8	42.7	-79.0	72.3
N <sub>y</sub>	-121.0	122.0	-159.0	177.0	-25.6	31.9
N <sub>xy</sub>	35.0	13.7	97.7	92.1	69.2	51.8
THERMAL LDS, kN/m						
N <sub>x</sub>	-	-	-	-	-	-
N <sub>y</sub>	-	-	-	-	-	-
N <sub>xy</sub>	-	-	-	-	-	-
PRESSURE (kPa)	15.1	15.1	14.5	14.5	14.5	14.5
TEMP. (K)	RT	RT	RT	RT	RT	RT

RT = ROOM TEMP = 294 K

Table 8 - Wing Point Design Load/  
Temperature Environment -  
Aluminum Design, Pull-up

ITEM	REGION ①		REGION ②		REGION ③	
	UPPER	LOWER	UPPER	LOWER	UPPER	LOWER
	6272	6271	6772	6771	6776	6775
AIR LOADS, kN/m						
N <sub>x</sub>	1.4	1.8	4.7	-5.3	11.9	-11.4
N <sub>y</sub>	27.9	30.8	31.9	-34.1	5.6	-5.8
N <sub>xy</sub>	5.1	11.9	4.9	2.5	5.3	3.3
THERMAL LDS, kN/m						
N <sub>x</sub>	-	-	-	-	-	-
N <sub>y</sub>	-	-	-	-	-	-
N <sub>xy</sub>	-	-	-	-	-	-
PRESSURE (kPa)	12.5	13.7	10.9	11.4	10.8	11.1
TEMP. (K)	RT	RT	RT	RT	RT	RT

RT = ROOM TEMP = 294 K

Table 9 - Wing Point Design Load/  
Temperature Environment -  
Aluminum Design, Subsonic

ITEM	REGION ①		REGION ②		REGION ③	
	UPPER	LOWER	UPPER	LOWER	UPPER	LOWER
	6272	6271	6772	6771	6776	6775
AIR LOADS, kN/m						
N <sub>x</sub>	-67.2	-10.3	-60.6	45.5	-68.5	85.6
N <sub>y</sub>	-136.0	98.2	-94.1	137.0	-21.4	30.3
N <sub>xy</sub>	82.5	30.1	93.2	69.4	70.1	40.1
THERMAL LDS, kN/m						
N <sub>x</sub>	-	-	-	-	-	-
N <sub>y</sub>	-	-	-	-	-	-
N <sub>xy</sub>	-	-	-	-	-	-
PRESSURE (kPa)	18.1	18.1	14.5	14.5	14.5	14.5
TEMP. (K)	RT	RT	RT	RT	RT	RT

RT = ROOM TEMP = 294 K

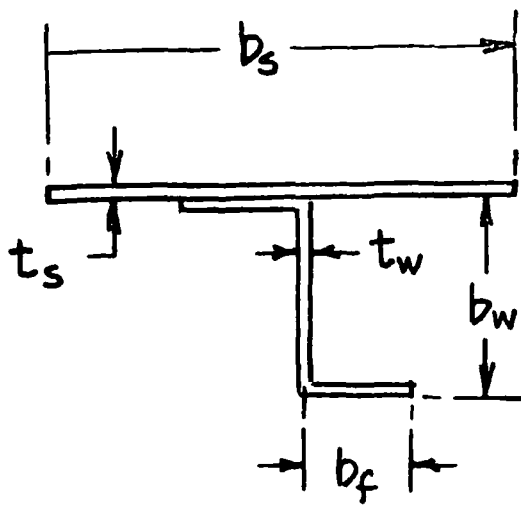
Table 10 - Wing Point Design Load/  
Temperature Environment -  
Lockalloy, Pull-up

ITEM	REGION ①		REGION ②		REGION ③	
	UPPER	LOWER	UPPER	LOWER	UPPER	LOWER
	6272	6271	6772	6771	6776	6775
AIR LOADS, kN/m						
N <sub>x</sub>	-26.7	11.6	-16.5	-7.3	-26.1	30.3
N <sub>y</sub>	-24.0	13.7	-3.5	5.9	-0.2	3.68
N <sub>xy</sub>	-28.6	17.0	-27.5	28.7	-24.9	18.4
THERMAL LDS, kN/m						
[LIMIT LOADS] N <sub>x</sub>	306.0	-140.0	28.2	-111.0	24.9	-193.0
[LIMIT LOADS] N <sub>y</sub>	31.3	-62.3	-44.8	-9.7	130.0	-31.1
[LIMIT LOADS] N <sub>xy</sub>	48.0	7.7	-50.8	3.2	68.5	53.9
PRESSURE (kPa)	11.8	12.9	12.4	13.6	11.8	13.6
TEMP. (K)	589	589	589	589	589	589

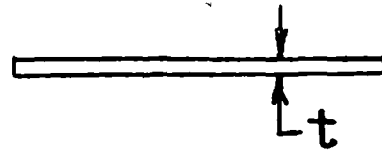
Table 11 - Wing Point Design Load/  
Temperature Environment -  
Lockalloy, Max. Maneuver

Analytical Methods - The stress analysis methods used to determine the minimum mass designs for the wing concepts of the aluminum designs and the Lockalloy design, Figure 51, used the direct search method and included:

- Panel loading - The total inplane stress resultants acting on the panels, Figure 52, are:



ALUMINUM DESIGN



LOCKALLOY DESIGN

Figure 51 - Cross-Sectional Geometry of Surface Panel Concepts

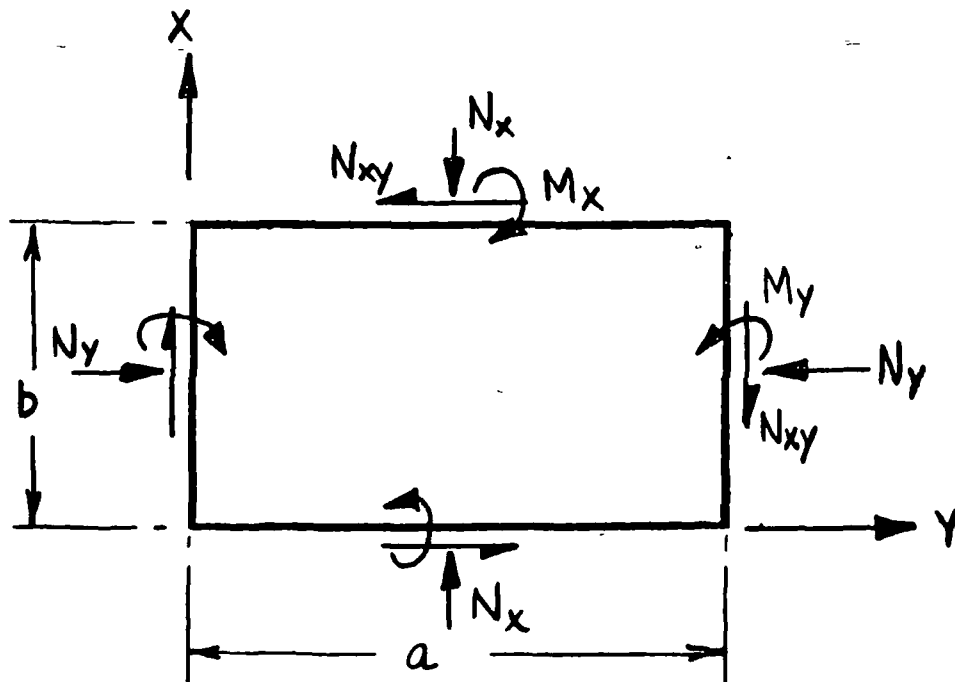


Figure 52 - Notation of Panel Dimension and Loading

$$N_x = N_x' + N_x''$$

$$N_y = N_y' + N_y''$$

$$N_{xy} = N_{xy}' + N_{xy}''$$

Where  $N_x'$ ,  $N_y'$ , and  $N_{xy}'$  are the loading components without thermal effects, and  $N_x''$ ,  $N_y''$ , and  $N_{xy}''$  are the thermal loads obtained from the structural model. The approximations for the bending moments at the center of the panel are:

$$M_x = M_x' / (1 - U_{GI})$$

$$M_y = M_y' / (1 - U_{GI})$$

For the Lockalloy design,  $M_x'$  and  $M_y'$  are the maximum mid-panel moments acting on a simply supported plate loaded with normal pressure, Reference 4, Page 117.

For the aluminum designs, an infinitely wide panel was assumed; hence, the bending moments are:

$$M_x' = 0$$

and

$$M_y' = \frac{pL^2}{8}$$

where  $p$  denotes the uniform normal pressure.

The utilization factor  $U_{GI}$  was based on the interaction equation:

$$R_c + R_s^2 = 1$$



and is defined as:

$$U_{GI} = \frac{R_c + \left( R_c^2 + 4 R_s^2 \right)^{1/2}}{2}$$

in which:

$$R_c = N_y / N_{y, cr}$$

$$R_s = N_{xy} / N_{xy, cr}$$

for the aluminum designs, wide column theory was used considering simply supported panels:

$$N_{y, cr} = \frac{\pi^2 D_2}{L^2}$$

where the stiffness  $D_2$  is defined in the Section Properties.

The shear buckling load intensities for the aluminum designs is expressed with simply supported, orthotropic plate theory as:

$$N_{xy, cr} = 32.6 (D_1 D_2^3)^{1/4} / L^2$$

For the Lockalloy design, the compressive buckling load for a biaxially-compressed, simply supported flat plate is used, Reference 5.

$$N_{I, cr} = K_c \pi^2 D_I / b^2$$

where

$$K_c = \left\{ \frac{\left[ 2 \left( \frac{a}{b} \right)^2 + m^2 \right] m^2 + \left( \frac{a}{b} \right)^4}{\left[ m + \left( \frac{a}{b} \right)^2 \left( \frac{N_x}{N_y} \right) \right]} \right\} \left( \frac{b}{a} \right)^2$$

and the shear buckling load of the plate as:

$$N_{xy, cr} = \frac{K_s \pi^2 E}{12 (1 - \nu^2)} \left( \frac{t^3}{b^2} \right)$$

- Stress analysis - The stresses at the centroid of the cross section are:

$$f_x = N_x / \bar{t}$$

$$f_y = N_y / \bar{t}$$

$$f_{xy} = N_{xy} / t_s$$

and the bending stresses are:

$$f_{x, b} = M_x Z / I_x$$

$$f_{y, b} = M_y Z / I_y$$

where the quantities  $\bar{t}$ ,  $t_s$ ,  $Z$ ,  $I_x$ , and  $I_y$  are defined for each design in the section entitled Section Properties.

The maximum biaxial stress state is:

$$f_x' = f_x + f_{x, b} \text{ (Lockalloy)} \quad f_y' = 0 \text{ (Aluminum)}$$

$$f'_y = f_y + f_{y, b}$$

and

$$f_{xy}$$

- Analysis of local buckling - For the aluminum designs, the initial buckling stresses of the skin due to compression and shear are:

$$f_{c, cr} = \frac{4 \pi^2 E}{12 (1 - \nu^2)} \left( \frac{t_s}{b_s} \right)^2$$

and

$$f_{s, cr} = \frac{5.35 \pi^2 E}{12 (1 - \nu^2)} \left( \frac{t_s}{b_s} \right)$$

the following interaction equation was used for combining the skin stresses for the aluminum designs:

$$r_c + r_s^2 = 1$$

in which

$$r_c = \frac{f_y + f_{y, b}}{f_{c, cr}}$$

$$r_s = \frac{f_{xy}}{f_{s, cr}}$$

For the Lockalloy design, the equivalent uniaxial stress is calculated using the Octahedral Shear Stress theory, Reference 63, which is:

$$\bar{f} = \left[ f_x'^2 + f_y'^2 - f_x' f_y' + 3 f_{xy}'^2 \right]^{1/2}$$

The applicable tension or compressive material allowable is compared to the above uniaxial stress to define the margin of safety.

● Section properties and stiffnesses - Section properties include:

For the aluminum design, Figure 51, the section properties and stiffnesses can be defined as:

$$D_1 = \frac{\eta_{sec} E}{(1 - \nu^2)} \bar{I}_{yy}$$

$$D_2 = \eta_{sec} E \bar{I}_{xx}$$

where:

$$\bar{I}_{yy} = \frac{t_s^3}{12} \quad (\text{mm}^4/\text{mm})$$

$$\bar{I}_{xx} = \left( \gamma - \frac{\beta^2}{\alpha} \right) b_s^2 t_s$$

$$\alpha = 1 + 1.6 \left( \frac{b_w}{b_s} \right) \left( \frac{t_w}{t_s} \right)$$

$$\beta = 0.80 \left( \frac{b_w}{b_s} \right)^2 \left( \frac{t_w}{t_s} \right)$$

$$\gamma = 0.633 \left( \frac{b_w}{b_s} \right)^3 \left( \frac{t_w}{t_s} \right)$$

Additional properties, which are required:

$$\bar{t} = \alpha t_s$$

$$Z_{\text{SKIN}} = \left(\frac{\beta}{\alpha}\right) b_s$$

$$Z_{\text{STR.}} = b_w - Z_{\text{SKIN}}$$

For the Lockalloy design, flat plate, the bending stiffnesses:

$$D_1 = D_2 = \frac{\eta E \bar{I}}{(1 - \nu^2)}$$

Where:

$$\bar{I} = \frac{t_s^3}{12}$$

and the skin thickness  $t_s$

$$t_s = \bar{t} = 2z$$

Mass/Strength Parametric Studies - The wing structural concepts were evaluated to define the rib and spar spacings commensurate with minimum mass design. These analyses were conducted at point design region 2 (inboard region adjacent to the rear beam), Figure 47, and considered the upper and lower surface panels, rib and spar caps, vertical webs, TPS, and vertical posts.

The mass for these components were determined using a constant spar spacing of 0.635 meter for the aluminum designs and 0.457 meter for the Lockalloy design. These spacings agree with the fuselage minimum mass frame spacings.

Aluminum Design/LI-900 TPS - Using the point design environment as specified in Tables 8 and 9 and the analytical methods previously described, a unit wing box at point design region 2 was sized for variable rib spacings of 0.25, 0.50, and 0.76 m with a constant spar spacing of 0.635 meters.

A summary of the panel geometry for this design is presented in Table 12 for the point design region, shown in Figure 47, located inboard and adjacent to the rear beam.

Time-temperature histories for the LI-900 RSI for typical upper and lower wing surface panels are shown in Figures 53 and 54. Since these insulation thicknesses are a function of the surface panel thickness, the insulation thickness varied with the rib spacings investigated. Figure 55 presents a cross-plot of the data shown in Figure 54. Table 13 contains a summary of the insulation thicknesses and corresponding unit mass of the LI-900 insulation for the various rib spacing investigated. The spars and ribs were sized using the internal forces from the aluminum structural model.

Using the constant 0.635 m spar spacing, the component and total box unit mass were defined as a function of rib spacing. These results, which are for point design region 2, are shown graphically in Figure 56 and in a tabular format in Table 14.

Aluminum Design/Ablator TPS - The design utilized the same point design environment and spar spacing as the previous aluminum design. For consistency, the same point design region and rib spacings were used for the mass/strength parametric evaluation of this concept.

The geometries, effective thicknesses, and unit mass for the surface panels are shown in Table 15. A maximum  $\bar{t}$  of 0.002 meters is noted on the wing upper surface for the 0.762 m rib spacing and conversely, a minimum thickness of 0.001 meter is indicated for the wing lower surface panel at a rib spacing of 0.254 meter.

SURFACE PANEL	L <sup>(1)</sup> m	$\bar{t}$ mm	b <sub>s</sub> mm	b <sub>w</sub> mm	b <sub>f</sub> <sup>(2)</sup> mm	t <sub>s</sub> mm	t <sub>w</sub> mm	w <sup>(3)</sup> kg/m <sup>2</sup>
UPPER SURFACE (6772)	0.254	2.03	76.2	31.8	9.5	1.3	1.6	5.7
	.508	2.35		30.5	9.1	1.3	1.7	6.6
	.762	2.80		28.2	8.5	1.6	2.0	7.8
LOWER SURFACE (6771)	0.254	1.42	76.2	19.1	5.7	1.0	1.0	4.0
	.508	1.73		26.7	8.0	1.0	1.3	4.8
	.762	2.13		34.3	10.3	1.0	1.5	6.0

NOTES:

(1) L = RIB SPACING, m

(2) b<sub>f</sub> = .30 b<sub>w</sub>

(3) w (kg/m<sup>2</sup>) = ρ × t̄  
FOR ALUM  
= 2800 × t̄

GEOMETRY

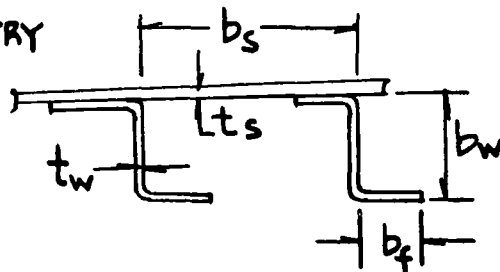


Table 12 - Wing Panel Requirement - Aluminum/LI-900 Design

SURFACE PANEL	RIB SPACING m	$\bar{t}$ PANEL mm	t <sup>(1)</sup> INSUL <sup>(3)</sup> mm	UNIT MASS <sup>(2)</sup> kg/m <sup>2</sup>
UPPER	0.254	2.0	5.1	0.73
	.508	2.4	5.1	.73
	.762	2.8	5.1	.73
	0.254	1.4	7.1	1.02
	.508	1.7	6.1	.88
	.762	2.1	5.1	.73

(1) INSULATION THK. PER PANELS 106 AND 132 OF FIGURES  
(2) UNIT MASS = ρt = 144 × t<sub>INSUL</sub> (kg/m<sup>2</sup>)  
(3) MIN. INSUL THK = 5mm

Table 13 - Insulation Requirement for Aluminum/LI-900 Design

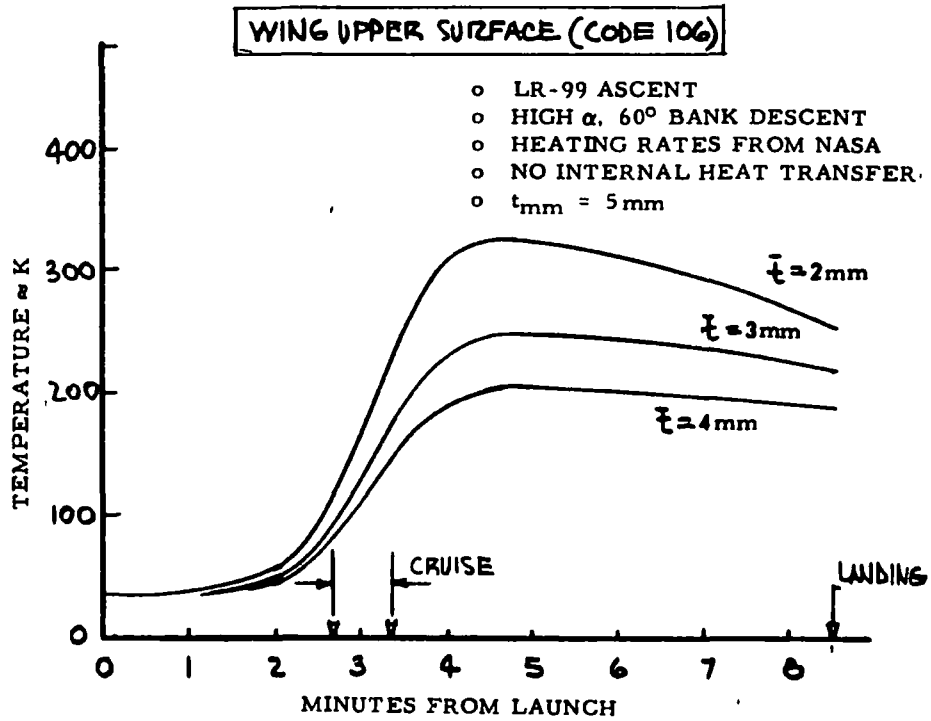


Figure 53 - Temperature History - Aluminum/LI-900 Design

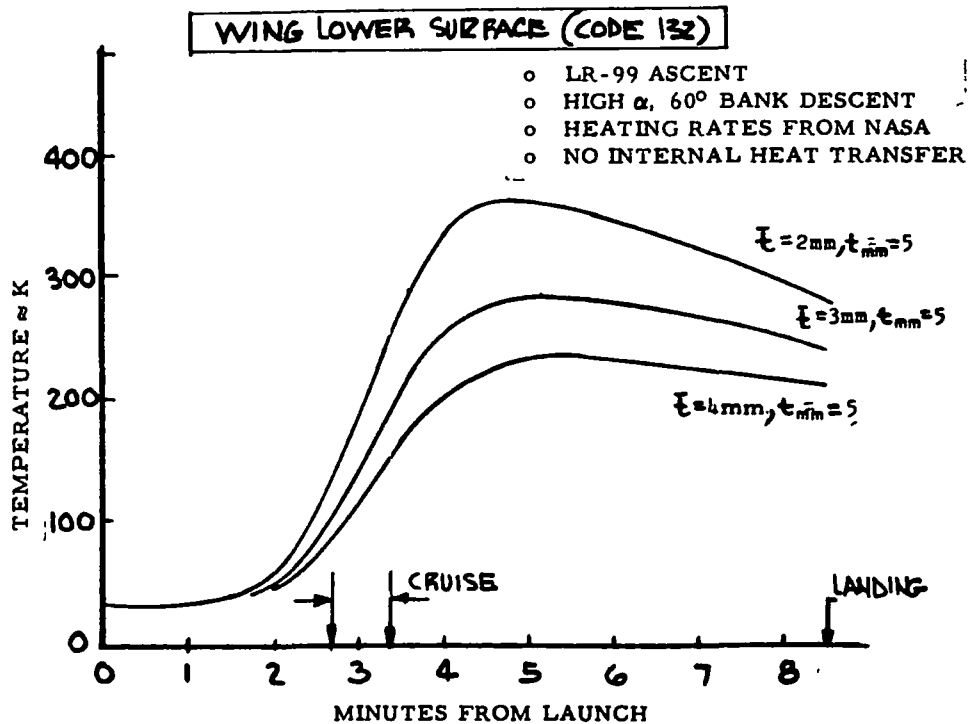


Figure 54 - Temperature History - Aluminum/LI-900 Design



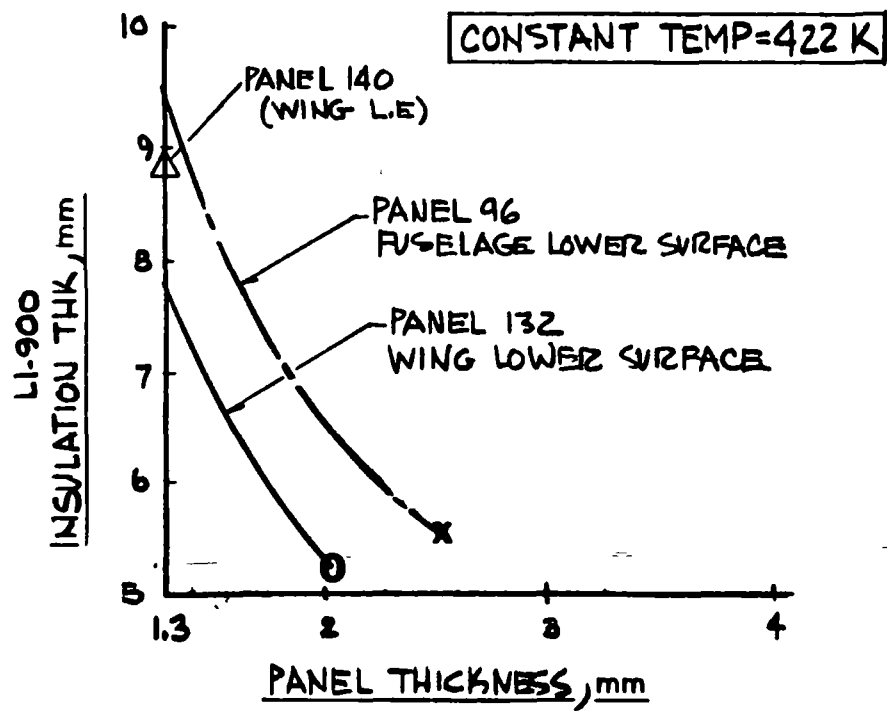


Figure 55 - Insulation Thickness - LI-900 as Function of Temperature

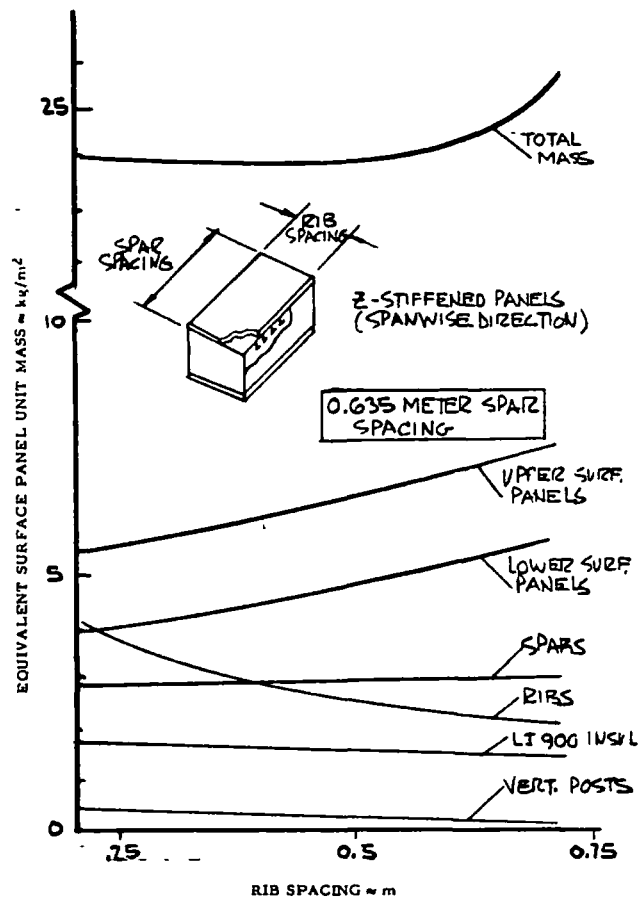


Figure 56 - Wing Box Unit Mass, Point Design Region 2

SPAR SPACING } m RIB SPACING } m	0.635 .254	0.635 .508	0.635 .732
o SURFACE PANELS •	(9.65)	(11.40)	(13.78)
UPPER	5.68	6.57	7.82
LOWER	3.97	4.83	5.96
o LI 900 INSVL. •	(1.76)	(1.61)	(1.46)
UPPER	0.73	0.73	0.73
LOWER	1.03	0.88	0.73
o RIBS •	(4.30)	(2.73)	(2.15)
CAPS	1.76	1.12	0.93
WEBS	2.54	1.61	1.22
o SPARS •	(2.89)	(3.02)	(3.07)
CAPS	0.95	0.95	0.95
WEBS	1.94	2.07	2.12
o VERTICAL POST •	(0.44)	(0.22)	(0.15)
TOTAL Σ	19.04	18.98	20.61

• kg/m²

Table 14 - Detail Mass Breakdown, Point Design Aluminum/LI-900 Design

The Ablator thickness requirements as a function of back-face structural temperature are shown on Figure 57 with the resultant insulation thicknesses for the variable rib spacings shown in Table 16. For ease in interpretation the data presented in Figure 57 was replotted in a different format and shown in Figure 58. A maximum insulation thickness of 0.006 meter is noted for the upper surface designs and 0.011 meter for the lower surface with 0.254 m rib spacing.

The results of the rib spacing study for the aluminum design with the Ablator TPS are shown in Figure 59. This figure displays the component and total mass of a unit wing box at point design region 2. The total mass curve is relatively flat for the range of rib spacing spacings between 0.254 meter and 0.635 meter with a unit mass of approximately  $20 \text{ kg/m}^2$ . Table 17 contains the detail mass breakdown of this design for the various rib spacings.

Lockalloy Design - The rib spacing parametric study conducted on this design was evaluated for the critical load conditions. In general, these conditions were the Pull-up after Launch condition for the upper inboard region and the maximum MACH condition with its high thermal stresses. Tables 9 and 10 in the point design environment section covers the inplane and normal loads for these conditions.

As with the two aluminum designs, the rib spacing study was conducted on point design region 2, for a constant spar spacing of 0.457 meter and variable rib spacings of 0.25, 0.50 and 0.76 meters.

The results of the panel sizing at the selected point design region are shown in Table 18. The panel thicknesses ranged from a minimum of 0.003 meter to a maximum of 0.005 meter, the upper and lower panels with 0.25 m rib spacings and the lower surface panel design at 0.762 m spacing, respectively.

The panel thicknesses at this region were dictated by the strength requirements, not the heat sink requirement, to maintain a structural temperature of 589 K. Figures 60 and 61 present plots of the panel thicknesses required to maintain structural temperatures of 589 K and 544 K. These temperature plots are

SURFACE PANEL	L <sup>(1)</sup> m	$\bar{t}$ mm	$b_s$ mm	$b_w$ mm	$b_f$ <sup>(2)</sup> mm	$t_s$ mm	$t_w$ mm	$w$ <sup>(3)</sup> kg/m <sup>2</sup>
UPPER SURFACE (6772)	0.254	1.8	76.2	19.1	5.7	1.3	1.3	5.0
	.508	2.2		26.7	8.1	1.3	1.6	6.2
	.762	2.5		30.5	9.1	1.3	1.9	7.0
LOWER SURFACE (6771)	0.254	1.4	76.2	19.1	5.7	1.0	1.0	4.0
	.508	1.6		22.9	6.9	1.0	1.3	4.5
	.762	1.8		30.5	9.1	1.0	1.3	5.0

(1) RIB SPACING, m  
(2)  $b_f = .30 \times b_w$   
(3) UNIT MASS ( $w$ ) =  $\rho \cdot \bar{t} = 2800$

GEOMETRY:

Table 15 - Wing Surface Geometry - Aluminum/Ablator Design

SURFACE PANEL	RIB SPACING m	$\bar{t}$ PANEL mm	$t$ <sup>(1)</sup> INSUL. <sup>(3)</sup> mm	UNIT <sup>(2)</sup> MASS kg/m <sup>2</sup>
UPPER	0.254	1.8	6.1	1.43
	.508	2.2	5.1	1.19
	.762	2.5	5.1	1.19
LOWER	0.254	1.4	8.9	2.08
	.508	1.6	8.6	2.01
	.762	1.8	8.1	1.90

(1) INSUL. THK PER PANEL 106 AND 132 OF FIGURE  
(2) UNIT MASS =  $\rho t = 234 t$  INSUL  
(3) MIN. INSULATION THK = 5.1 mm

Table 16 - Insulation Requirement - Aluminum/Ablator Design

- MAT'L : ABLATOR-SLA 220
- RADIATION VIEW FACTOR FOR PT 96 IS 1.00, FOR PT. 106 IT IS 0.40

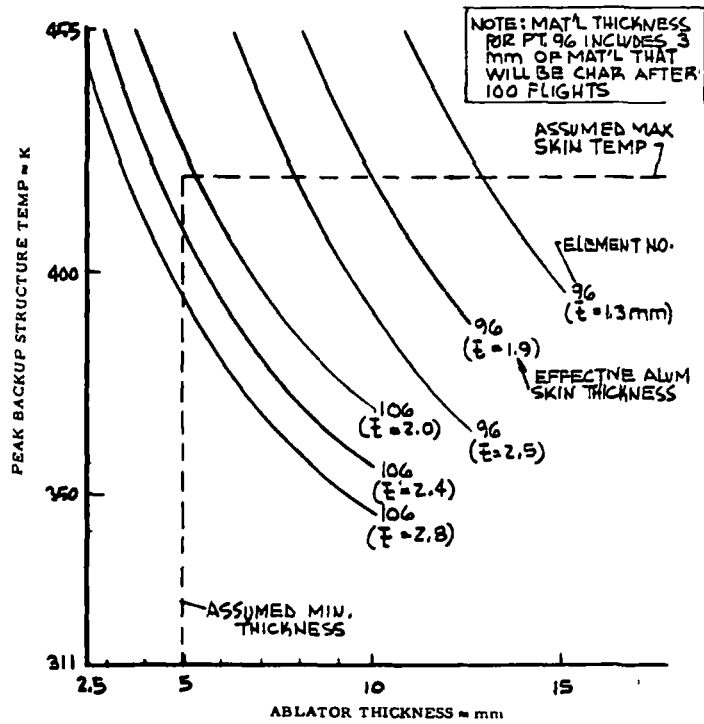


Figure 57 - Estimated Ablator Thicknesses

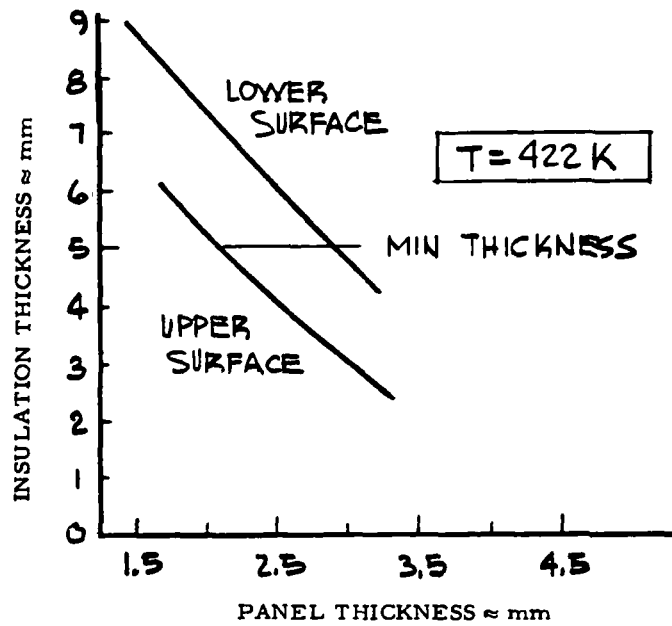


Figure 58 - Ablator Thicknesses as Function of Panel Thickness

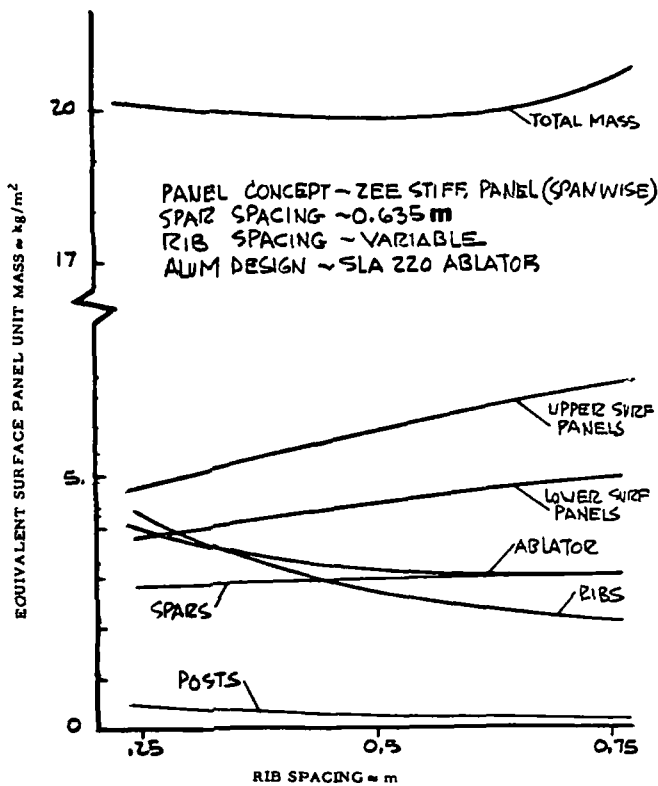


Figure 59 - Wing Box Unit Mass, Point Design - Aluminum/Ablator Design

Table 17 - Detail Mass Breakdown, Point Design - Aluminum/Ablator Design

SPAR SPACING	(3) 0.635	0.635	0.635
RIB SPACING	(3) 0.254	0.508	0.762
SURFACE PANEL	(1) (8.93)	(10.54)	(12.10)
UPPER	4.98	6.05	6.98
LOWER	3.95	4.54	5.12
ABLATOR	(1) (3.52)	(3.17)	(3.07)
UPPER	1.42	1.17	1.17
LOWER	2.10	2.00	1.90
RIBS	(1) (4.30)	(2.73)	(2.15)
CAPS (2)	1.76	1.12	0.93
WEBS (2)	2.54	1.61	1.22
SPARS	(1) (2.93)	(3.03)	(3.13)
CAPS (2)	0.98	0.98	0.98
WEBS (2)	1.95	2.05	2.15
VERT. POSTS (2)	(1) (0.44)	(0.24)	(0.15)
TOTAL Σ (1)	20.12	19.76	20.60

- (1) ALL PANELS ARE EQUIV. SURFACE PANEL MASS - kg/m<sup>2</sup>
- (2) SAME AS ALUM DESIGN WITH LI-900.
- (3) SPACING - m

WING SURFACE	SPAR SPACING m	RIB SPACING m	PANEL t mm	UNIT (1) MASS kg/m <sup>2</sup>
UPPER	0.457	0.254	3.3	6.8
		.457	4.0	8.4
		.762	4.5	9.4
LOWER	0.457	.254	3.3	6.8
		.457	4.3	9.0
		.762	5.2	10.8

(1) UNIT MASS = 2093 x t

Table 18 - Wing Panel Thickness - Lockalloy Design

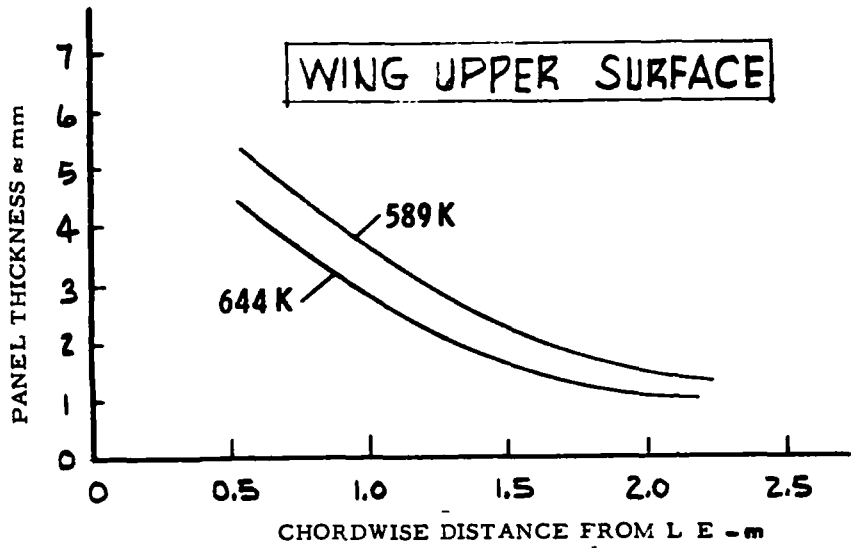


Figure 60 - Wing Upper Surface Panel Thicknesses

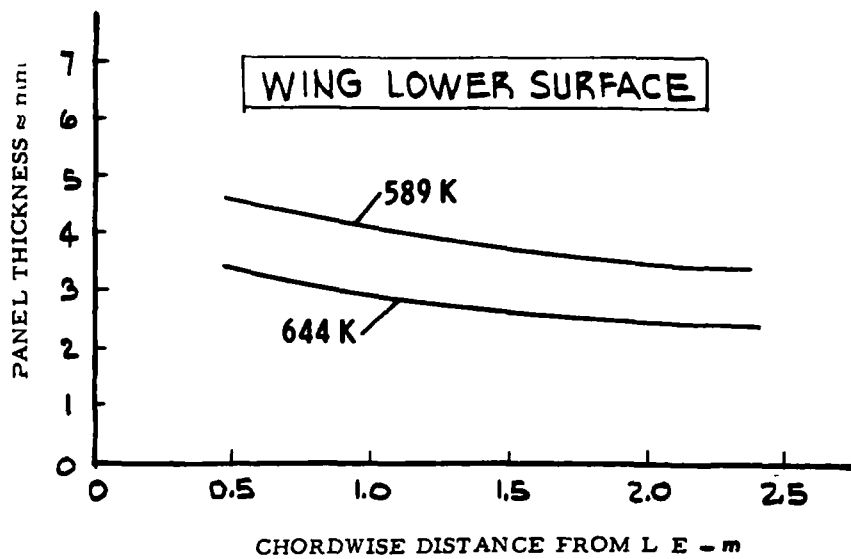


Figure 61 - Wing Lower Surface Panel Thicknesses

presented as a function of the chordwise distance from the leading edge. Point design region 2 is approximately 3.048 meters aft of the leading edge and it can be seen by comparing the strength size thicknesses (Table 18) and the heat sink thicknesses (Figures 60 and 61) that the strength sized thicknesses are greater than those required by the heat sink function.

The results of the rib spacing study on the Lockalloy design are shown in Figure 62. As with the other designs this data reflects the component and total mass for a unit wing box at point design region 2. No discernable minimum mass rib spacing is encountered for those rib spacings investigated. For a 0.457 m rib spacing, a unit box mass of approximately  $25.0 \text{ kg/m}^2$  is noted. The data shown on Figure 62 is shown in tabular form in Table 19.

Total Wing Results - Additional analysis were conducted on the two spanwise-stiffened aluminum wing designs to define the surface panel thicknesses for the entire wing. For both designs, aluminum structure with the LI-900 TPS and the aluminum structure with the Ablator TPS, the critical flight conditions were invariant and the load intensities were defined from the NASTRAN static solution using the aluminum structured model. Figure 63 displays the critical design conditions for the wing upper and lower surfaces for the aluminum designs.

The final rib/spar spacing for the wing is shown in Figure 64. These rib/spar proportions are identical for both aluminum designs and reflect the results of the wing and fuselage parametric spacing studies. A constant rib spacing of 0.457 m is indicated with a spar spacing of approximately 0.635 meter. For the lightly loaded forward wing box region a wider spar spacing of approximately 0.889 meter was used.

Maps of the wing panel effective thicknesses for the aluminum designs are presented in Figures 65 and 66. For the aluminum design with the LI-900 TPS, Figure 65, a maximum effective thicknesses of 0.002 m and 0.0017 m are indicated for the wing upper and lower surface panels, respectively. Figure 66 contains the corresponding thicknesses for the aluminum design with the Ablator TPS. The



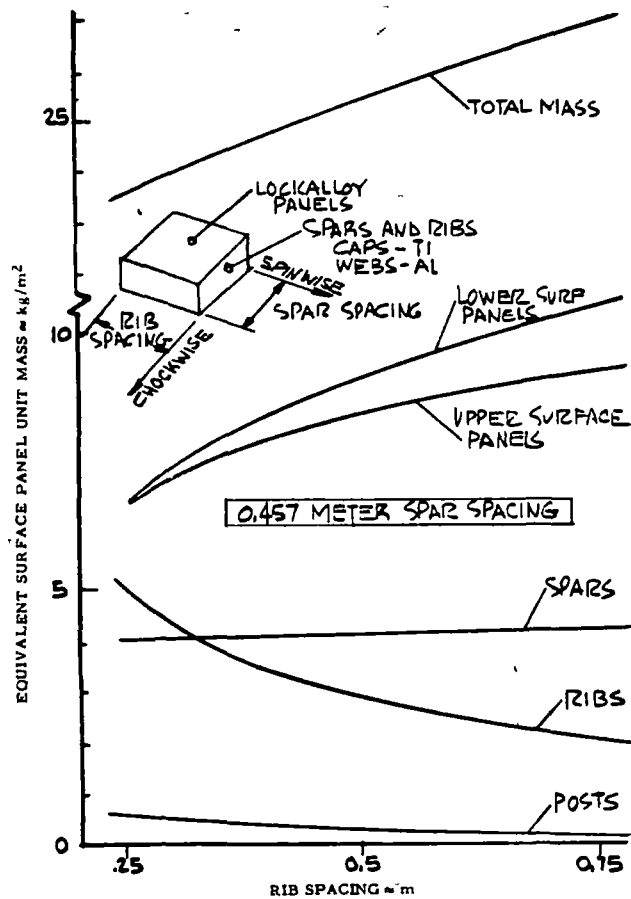


Figure 62 - Detail Mass Breakdown Point Design - Lockalloy Design

◦ SPACING, m			
SPAR	0.457	0.457	0.457
RIB	0.254	0.457	0.762
◦ SURFACE PANELS •	(13.56)	(17.43)	(20.21)
UPPER } Lockalloy	6.78	8.40	9.42
LOWER }	6.78	9.03	10.79
◦ INSULATION (NONE)	-	-	-
◦ RIBS	(5.08)	(2.88)	(2.05)
CAPS (Ti)	2.54	1.27	0.83
WEBS (Al)	2.54	1.61	1.22
◦ SPARS	(4.10)	(4.20)	(4.24)
CAPS (Ti)	1.90	1.90	1.90
WEBS (Al)	2.20	2.30	2.34
◦ VERTICAL POSTS •	(0.54)	(0.29)	(0.20)
(Al)			
TOTAL, kg/m²	23.28	24.80	26.70

• = kg/m²

Table 19 - Detail Mass Breakdown Point Design - Lockalloy Design

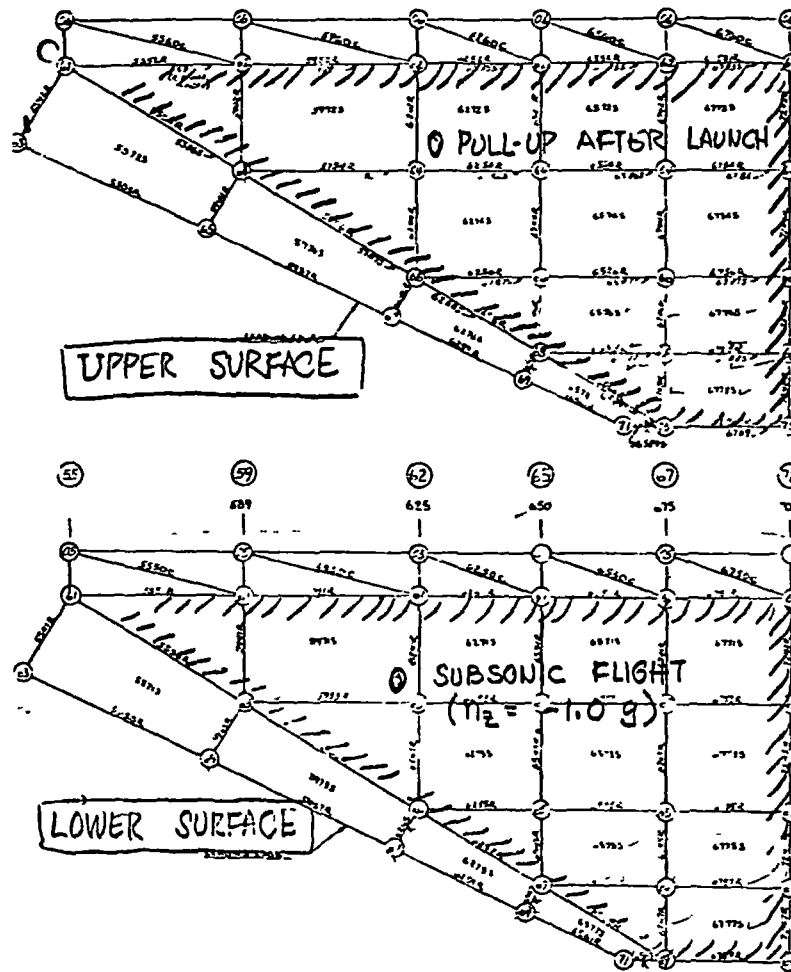


Figure 63 - Aluminum Design Critical Design Regions

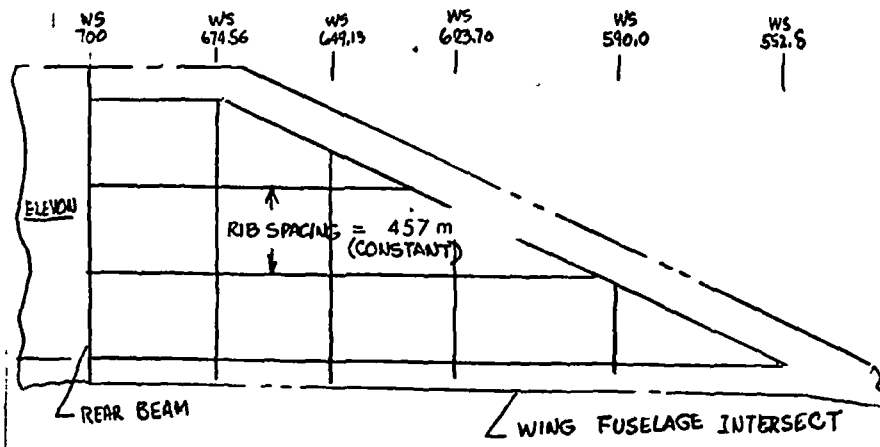


Figure 64 - Wing Rib/Spar Spacing - Aluminum Designs

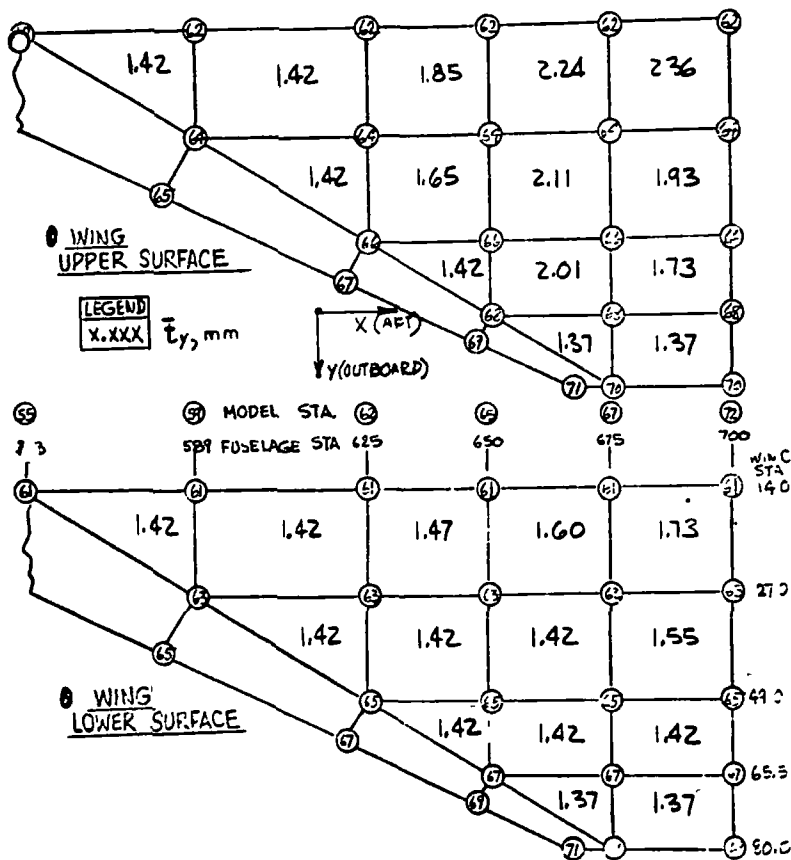


Figure 65 - Wing Surface Effective Thickness Map - Aluminum/LI-900 Design

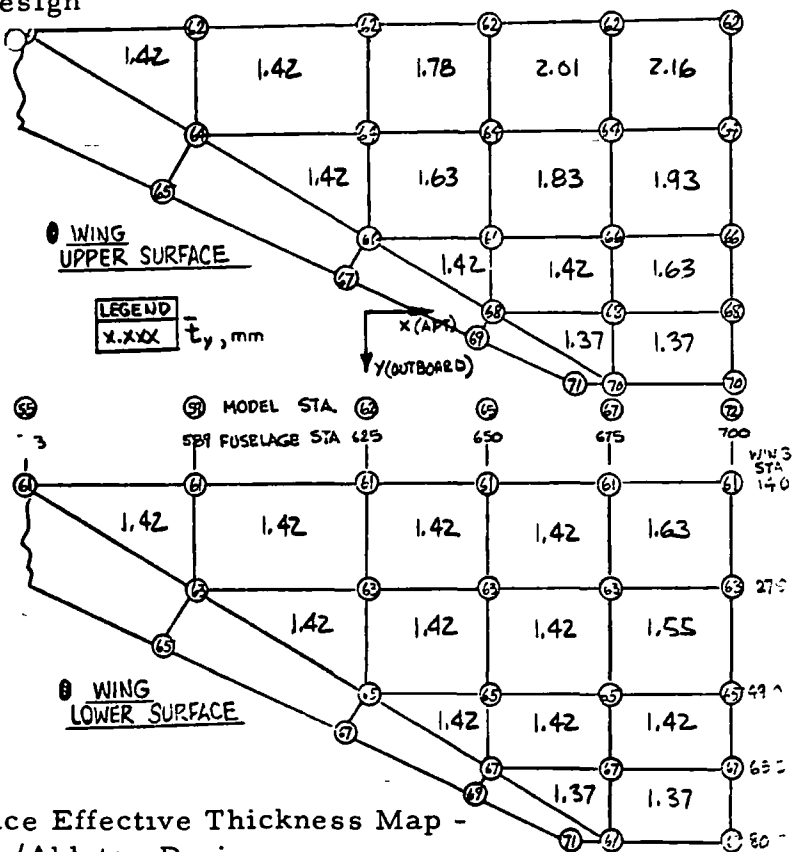


Figure 66 - Wing Surface Effective Thickness Map - Aluminum/Ablator Design

maximum thicknesses for this design are 0.0022 m and 0.0016 m for the upper and lower wing surfaces, respectively.

For the Lockalloy design, the critical design conditions for the wing are shown in Figure 67. As to be expected, these conditions are more varied than those for the aluminum designs with areas being designed by heat sink, thermal stresses, and airload requirements. In general, the majority of the wing upper panels are designed by the Pull-up after Launch condition and the lower surface by the thermal stresses caused by the maximum temperature gradient condition.

The wing rib/spar spacing for the Lockalloy design is shown in Figure 68. A constant rib spacing of 0.457 meter was combined with a spar spacing of approximately 0.48 meter.

The panel thicknesses for this design are shown on Figure 69 with maximum thicknesses of approximately 0.006 meter indicated for both surfaces.

### Fuselage Analysis

The fuselage of the X-24C, Figure 70, is of a nearly flat-bottomed shape in keeping with the lifting body concept. The cross section is of a generally triangular shape in the forward section evolving into a trapezoidal shape which progressively widens, moving toward the aft end. The surfaces generally have a large radius of curvature to aid in carrying longitudinal axial loads in the Lockalloy monocoque shell concept. The lower surface radius of curvature is 10 meters constant, while the top and sides in general vary in the 7.62 to 15 meter radius range.

Two major categories of structural concepts are investigated; an aluminum airframe of conventional skin-stringer construction and a Lockalloy heat sink structure of relatively thick monocoque shell construction.

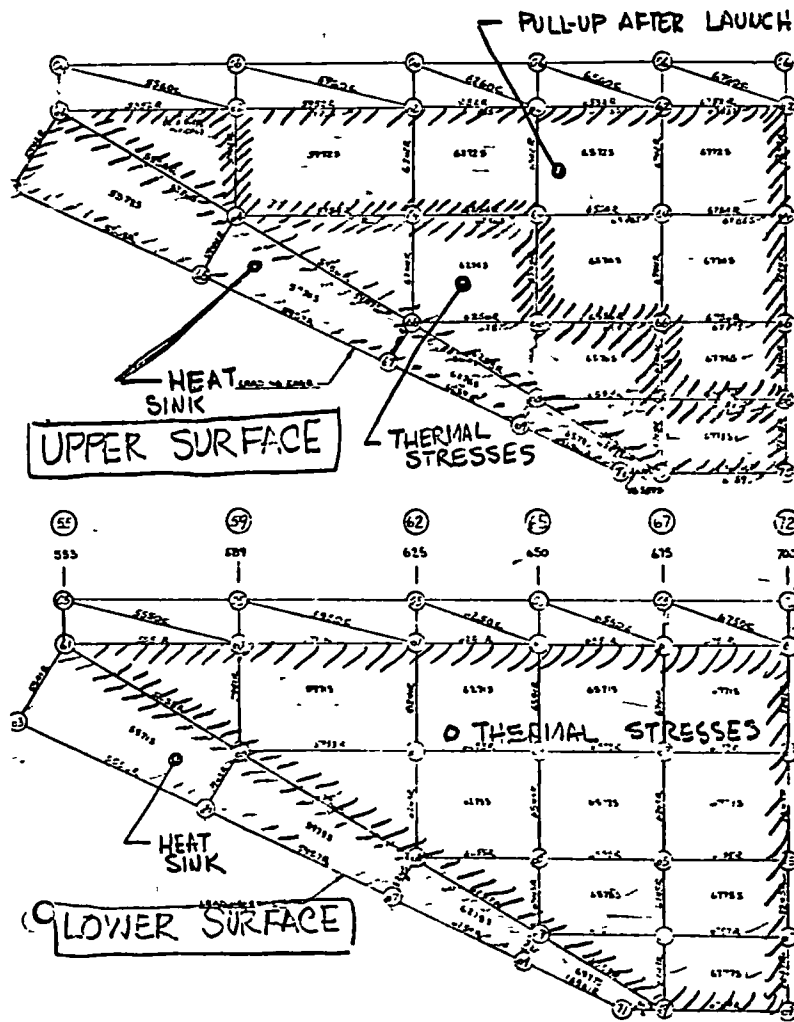


Figure 67 - Critical Design Regions - Lockalloy Design

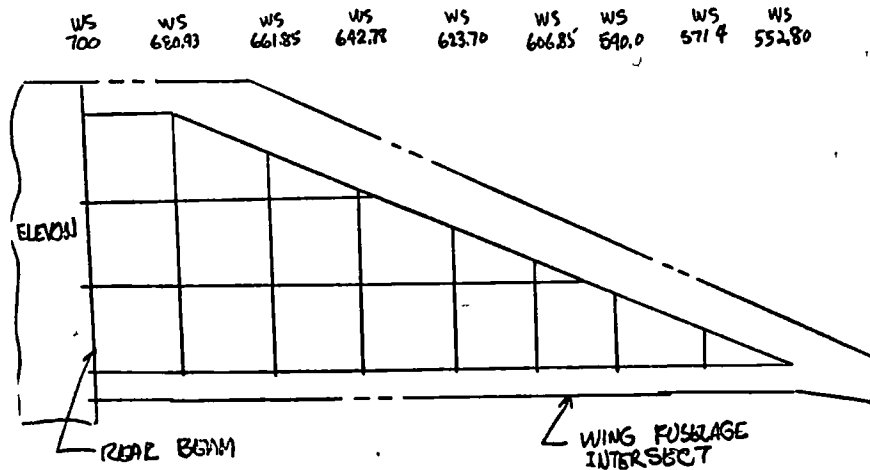


Figure 68 - Wing Rib/Spar Spacing - Lockalloy Design

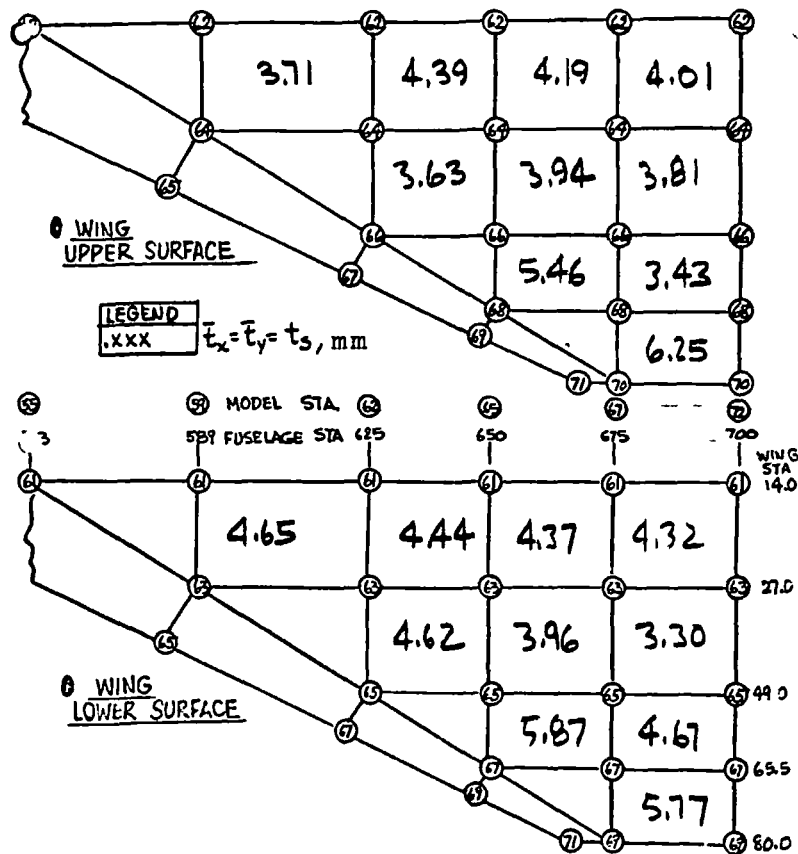


Figure 69 - Wing Surface Thickness Map - Lockalloy Design

The aluminum structure employs light, shallow stringers spaced at approximately 0.762 m c. c. with frames spaced at 0.609 m. The frame outer cap is located inside the stiffener depth with stiffener-to-frame clips provided and with frame-to-skin shear transfer clips provided as required. A typical fuselage section of this construction is shown on Figure 71.

The Lockalloy structure consists of thick, load-carrying skin supported by frames at 0.457 m spacing. The skin panels are spliced together with screws, and screws are used to fasten the surfaces to the substructure. This enables the removal of many of the fuselage surface panels, providing access to the

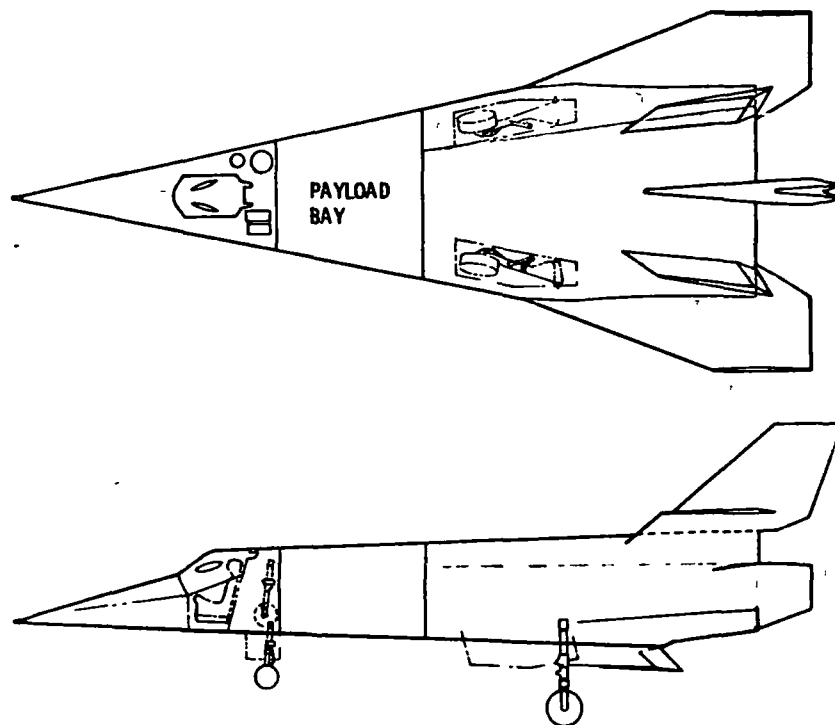


Figure 70 - X-24C General Arrangement

interior. A typical frame and Lockalloy assembly are shown on Figure 72. The Lockalloy surfaces are designed to reach a maximum temperature of 489 K during the high Mach phase of the trajectory. Since many of the skin thicknesses are sized by structural requirements as well as by minimum gauge cutoff, the resultant temperature distribution causes high thermal stresses. Accordingly, the skin thicknesses are tailored to provide close to a linear temperature gradient between the upper and lower surfaces of the fuselage. This results in a mass penalty, but is necessary to minimize the thermal stresses for unstiffened skins.

The critical design conditions for the aluminum fuselage are shown on Figure 73 and for the Lockalloy fuselage on Figure 74. The fuselage internal loads from the NASTRAN program are used in conjunction with internal pressurization and external aerodynamic pressures to analyze the structure and determine which condition designs the various portions of the fuselage shell.

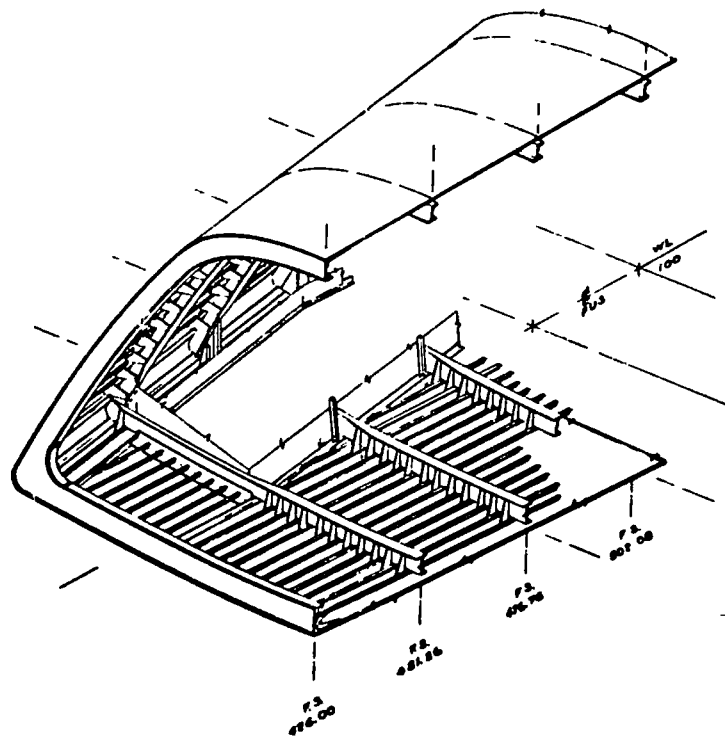


Figure 71 - Fuselage Section - Aluminum Design

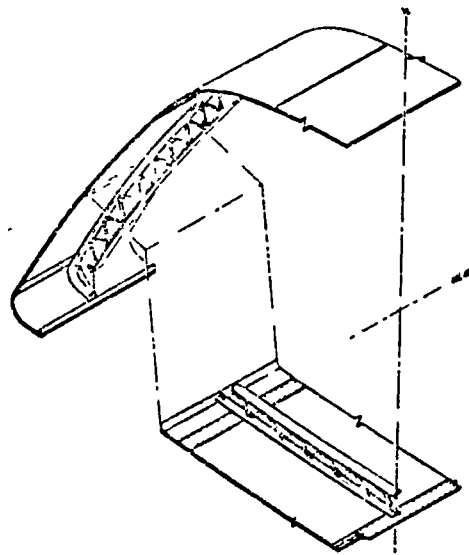


Figure 72 - Fuselage Frame - Lockalloy Design



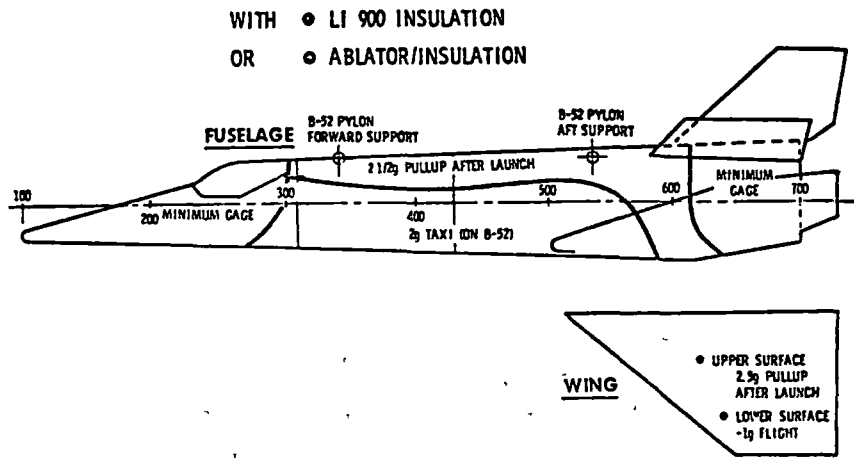


Figure 73 - Critical Design Conditions - Aluminum Design

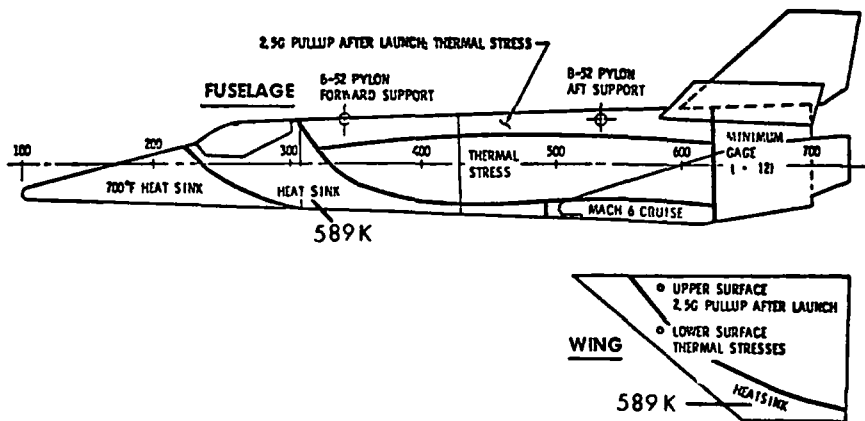


Figure 74 - Critical Design Conditions - Lockalloy Design

Aluminum Surfaces - The surfaces of the aluminum concept are analyzed by techniques which account for the shell internal axial loads, Figure 75, the panel shear loads, and the surface pressure loads, Figures 76, 77 and 78. Surface pressure loads are imposed for internal pressurization and combined with air load pressures. Where internal pressures are relieving they are not applied and the design is based on aerodynamic pressures.

The surfaces are basically a simple skin-stringer design with stringer spacing of 76.2 mm to preclude skin buckling at limit load for the LI-900 TPS. For the ablator TPS the stringer spacing is opened up slightly to 83.8 mm, so as to allow skin buckling at 80% of limit loads.

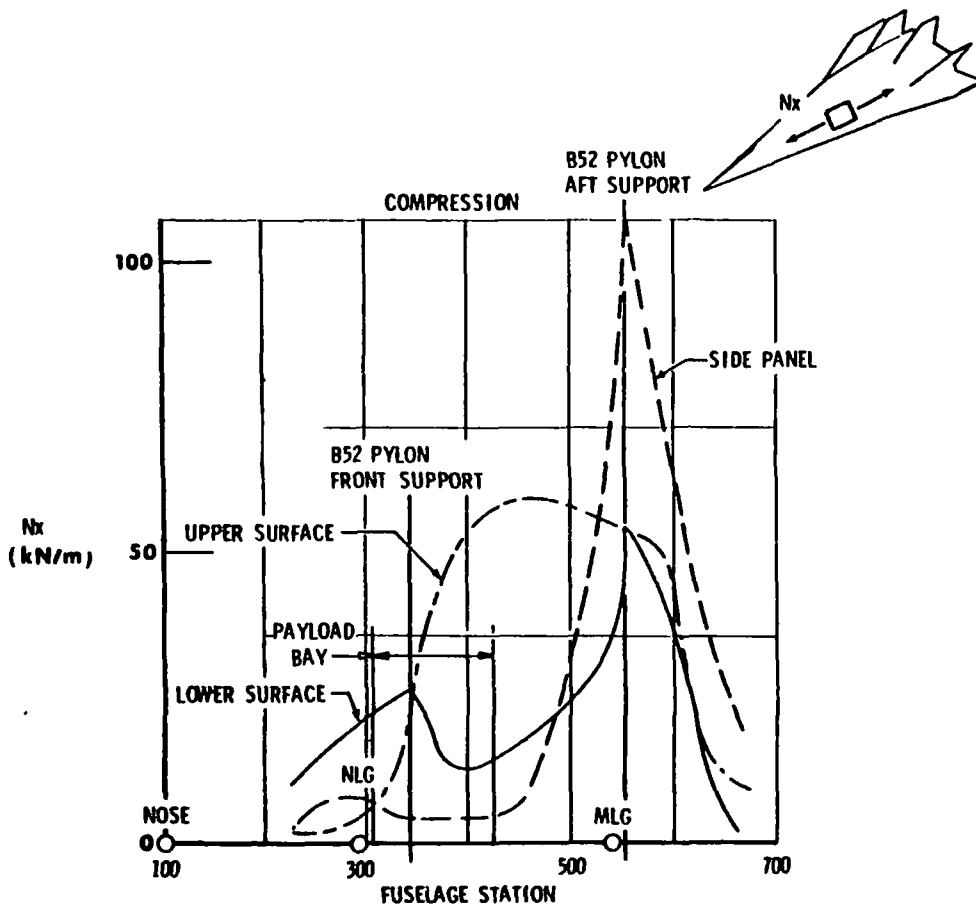
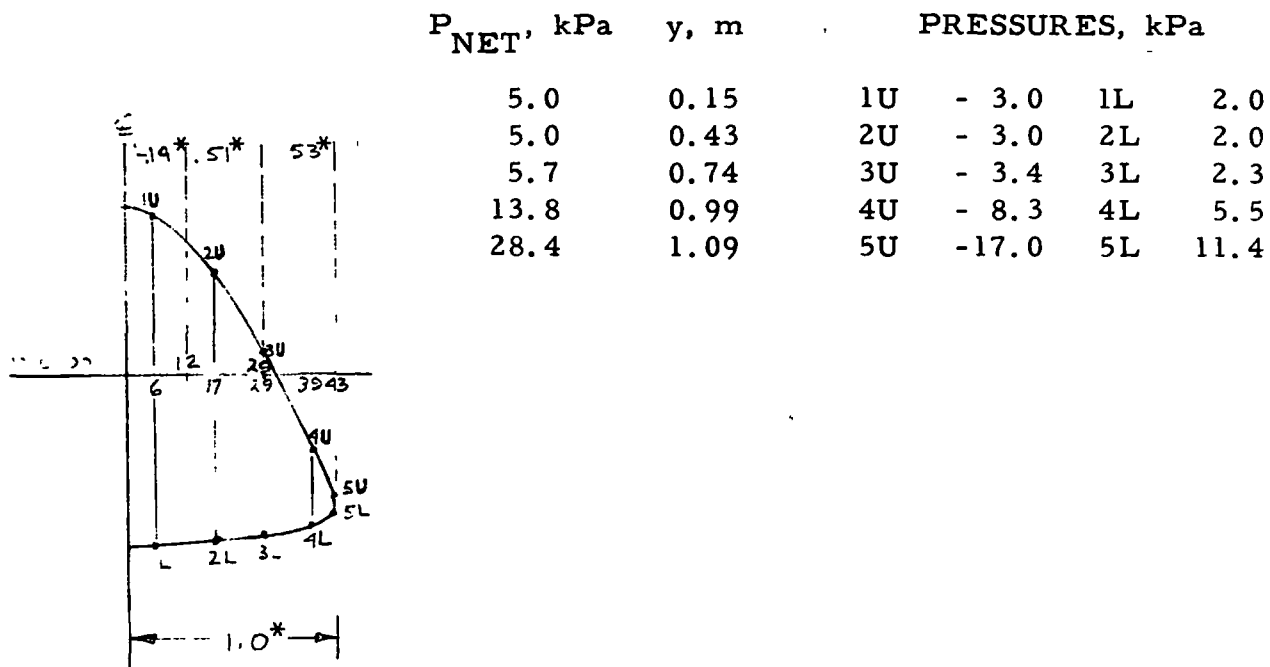
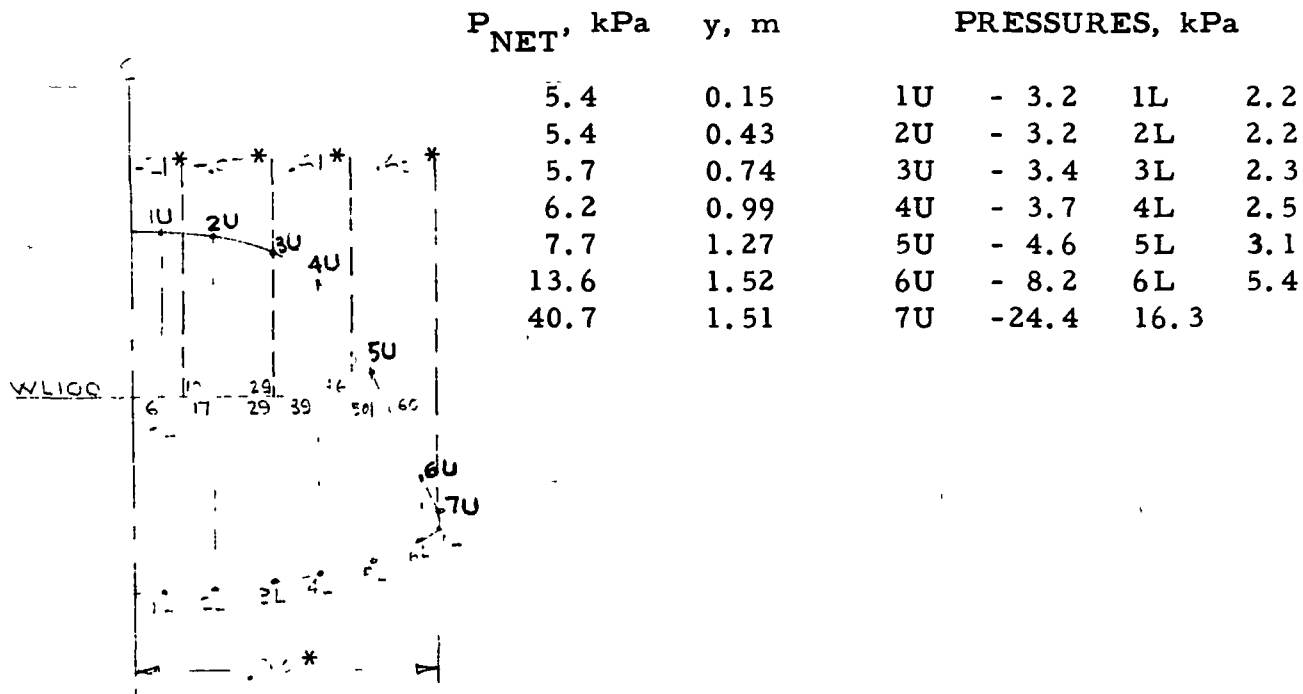


Figure 75 - Fuselage Surface Design Loads



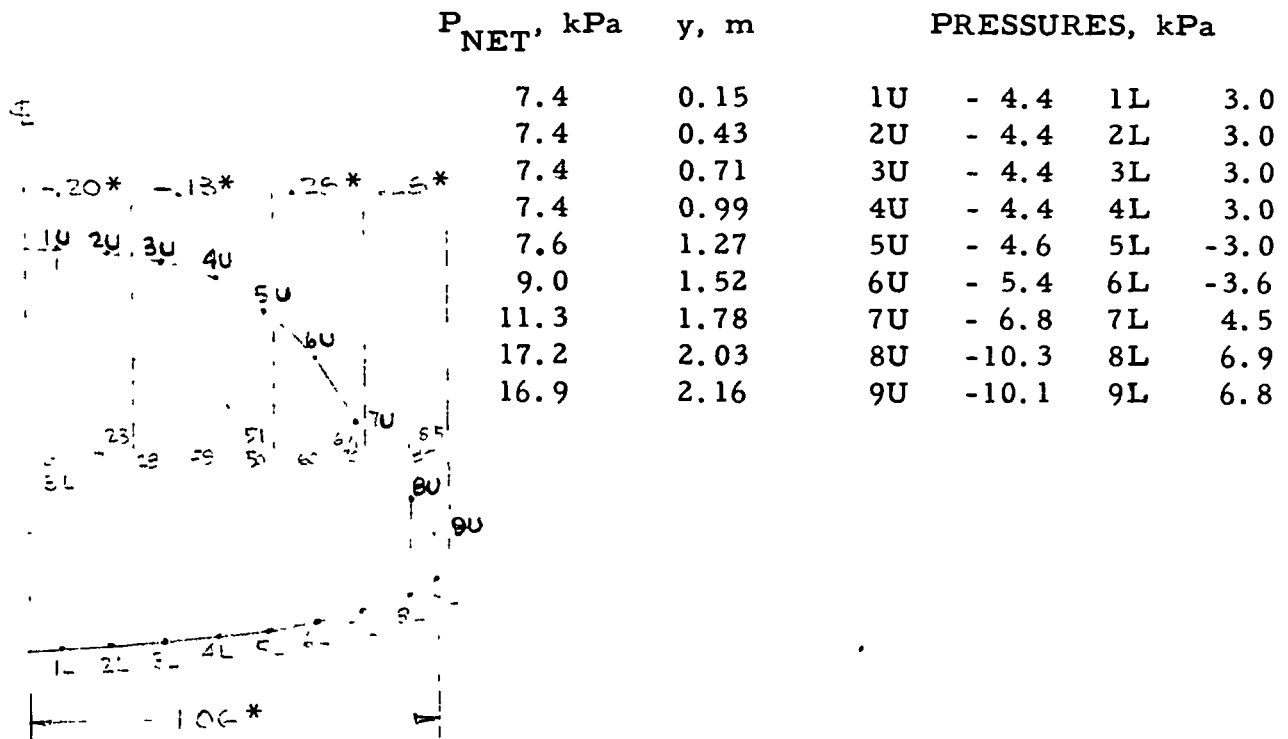
**NOTES:** + = POS. PRESS.; - = SUCTION; ALL PRESSURES LIMIT;  
 n = 2.5 MANEUVER SUBSONIC COND.; \*n = 3.0, M = 6.0 MANEUVER

Figure 76 - Fuselage Surface Pressures - FS 300



**NOTES:** + = POS. PRESS.; - = SUCTION; ALL PRESSURES LIMIT;  
 n = 2.5 MANEUVER SUBSONIC COND.; \*n = 3.0, M = 6.0 MANEUVER

Figure 77 - Fuselage Surface Pressures - FS 400



**NOTES:** + = POS. PRESS.; - = SUCTION; ALL PRESSURES LIMIT  
 n = 2.5 MANEUVER SUBSONIC COND.; \*n = 3.0, M = 6.0 MANEUVER

Figure 78 - Fuselage Surface Pressures - FS 525

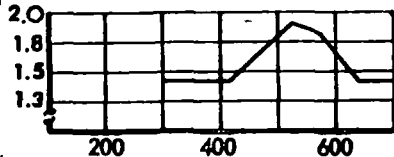
The skin-stringer combination is designed as a beam column for maximum compression unit loading and pressure loading. Panel shear interaction is included in the analysis. Frame spacing was chosen as a tradeoff balance between beam column mass and frame mass.

The skin-stringer combination is also analyzed for general instability involving axial and shear loadings. A minimum practical sheet metal thickness of 0.813 mm is established as a lower cutoff and this results in a lumped effective thickness of 1.435 mm. Effective thicknesses are plotted versus fuselage station on Figures 79 and 80.

t, mm  
 EFFECTIVE THICKNESS  
 OF ALUMINUM SURFACES

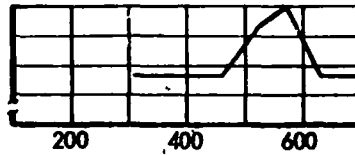
## ALUMINUM

### UPPER SURFACE



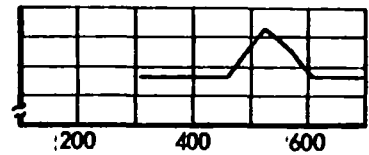
FUSELAGE STA.

### SIDE PANELS



FUSELAGE STA.

### LOWER SURFACE



FUSELAGE STA.

Figure 79 - Fuselage Shell Thickness

- THICKNESSES ARE BASED ON COMBINATION OF THERMAL HEAT SINK AND STRUCTURAL REQUIREMENTS
- THICKNESSES SHOWN IN INCHES

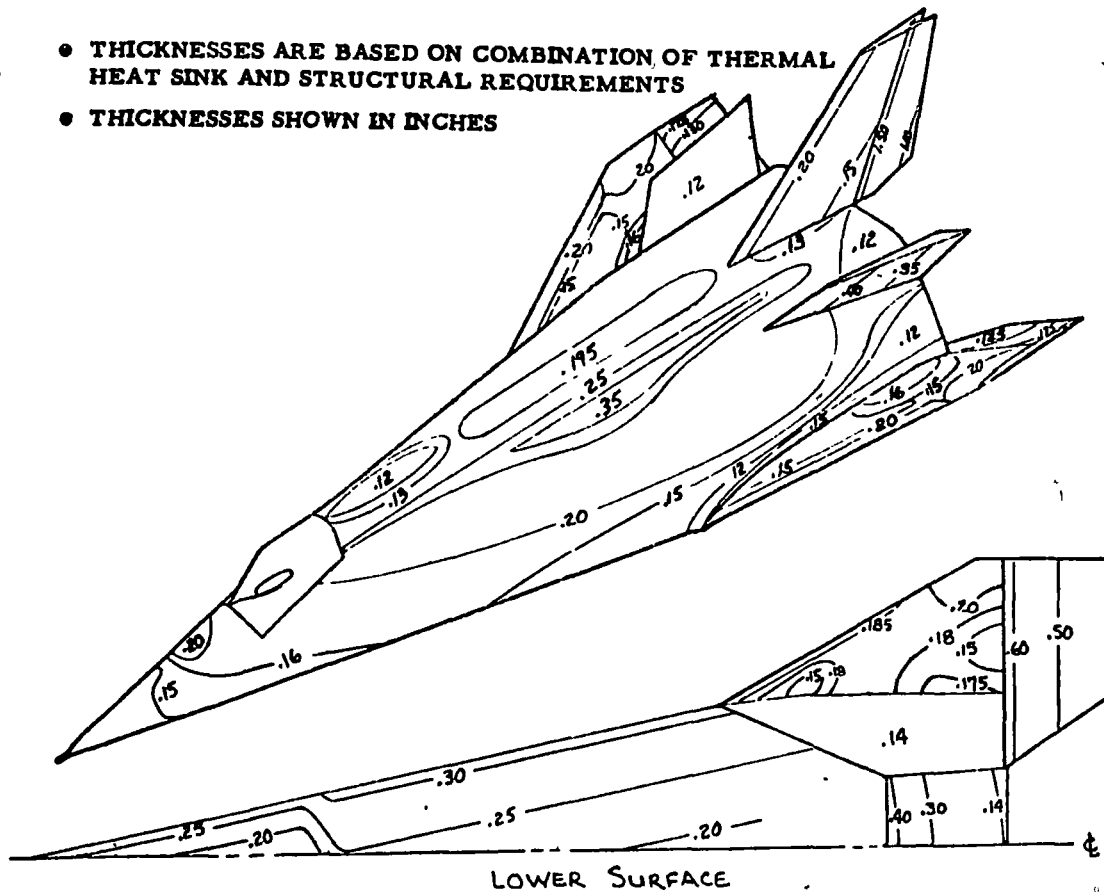


Figure 80 - Fuselage Shell Thickness - LR-99 Mission

Analysis Method - The following calculations demonstrate the methods used to establish the surface skin-stringer combinations required for the aluminum air-frame. A 25 mm deep 0.8 mm zee stringer spaced at 0.08 m is established as a manufacturing minimum. A typical section at F.S. 607 upper surface is checked:

For the 2.50 g pullup after launch condition:

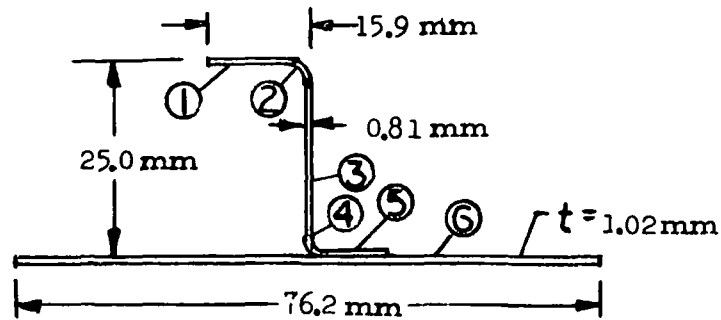
$$N_x = -79.7 \text{ kN/m (rod element 5909) (Appendix B)}$$

$$g = 38.5 \text{ kN/m (shear panel 5928)}$$

There is 6.9 kPa (limit) internal pressurization and 4.4 kPa (limit) aerodynamic suction pressure on the upper surface. (Reference Loads Analysis.)

$$P_{\text{tot}} = (6.9 + 4.4) \times 1.5 = 17.0 \text{ kPa (ultimate)}$$

Surface Properties:



<u>EL.</u>	<u>A, (mm<sup>2</sup>)</u>	<u>Z, mm</u>	<u>I<sub>o</sub>, mm<sup>4</sup></u>
①	10.4	26	
②	3.5	25.1	
③	15.6	13.7	479
④	3.5	2.79	
⑤	10.4	1.42	
⑥	<u>77.4</u>	0.51	

$$\Sigma AZ = 636.5 \text{ mm}^3$$

$$\bar{Z} = 5.27 \text{ mm}$$

$$\Sigma AZ^2 = 12246 \text{ mm}^4$$

$$I = 12246 + 47 - 636.5 \times 5.273$$

$$I = 9369 \text{ mm}^4$$

$$\rho = \sqrt{\frac{936.9}{120.8}} = 8.81 \text{ mm}$$

$$\bar{t} = \frac{120.8}{76} = 1.59 \text{ mm}$$

For a.61 m frame spacing:

$$L/\rho = 0.61/0.009 = 69$$

$$F_{\text{col}} = 136 \text{ MPa}$$

$$R_c = \frac{7.97 \times 10^4}{(1.36 \times 10^8) \cdot (0.00159)} = 0.370$$

### Panel Buckling Check

$$\text{Compression} \quad \sqrt{k} = 1.9$$

$$\text{Shear} \quad \sqrt{k} = 2.6$$

$$\text{Compression} \quad (b/t)_e = 76/(1.02 \times 1.9) = 40$$

$$\text{Shear} \quad (b/t)_e = 76/(1.02 \times 2.6) = 29$$

$$\text{Compression} \quad F_{\text{ccr}} = 45.5 \text{ MPa}$$

$$\text{Shear} \quad F_{\text{scr}} = 82.7 \text{ MPa}$$

$$f_c = \frac{7.97 \times 10^4}{0.00159 \times 1.5} = 33.42 \text{ MPa (Limit)}$$

$$R_c = \frac{33.42}{45.5} = 0.735$$

$$f_s = \frac{3.85 \times 10^4}{0.00102 \times 1.5} = 25.16 \text{ MPa (Limit)}$$

$$R_s = \frac{25.16}{82.7} = 0.306$$

$$R_c + R_s^2 = 1$$

$$\text{M.S. (Buckling)} = 0.19$$

A check for general instability and beam-column stresses using L.R. 14709, "Margins of Safety for Integrally Stiffened Sheet Wing Surfaces."

For shear:

$$Q_{cr} = \frac{32}{L^2} (EI_{SK.})^{1/4} (EI_{PANEL})^{3/4}$$

$$(EI_{SK.})^{1/4} = \left( 7.29 \times 10^{10} \times \frac{0.0254 \times 0.00102^3}{0.30} \right) = 1.600$$

$$(EI_{PANEL})^{3/4} = \left( 7.29 \times 10^{10} \times \frac{9.369 \times 10^{-9}}{0.076} \right) = 923.0$$

$$Q_{cr} = \frac{32}{0.61^2} (1.600) (923) = 127 \text{ kN/m}$$

$$R_s = \frac{38.5}{127} = 0.307$$

$$R_c = 0.370$$

$$R_c + R_s^2 = 1$$

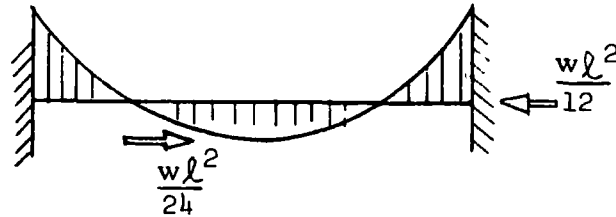
$$\text{M.S.} = 0.84$$



$$U^* = 1/1.84 = 0.54$$

$$\beta M = 0.80$$

Beam-column:



Check bending in center of span for compression on inside flange:

An initial bow of the stringer,  $A_f = \ell/200$ , is assumed. This is equivalent to a side loading of:

$$W' = \frac{P}{25\ell}$$

$$W_{TOT} = 17.0 \times 10^3 \times 0.076 + \frac{7.97 \times 10^4 \times 0.076}{25 \times 0.61} = 1.69 \times 10^3 \text{ N/m}$$

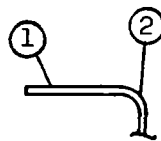
$$M = \frac{W\ell^2}{24} = \frac{1.69 \times 10^3 \times 0.61^2}{24} = 26.2 \text{ N.m}$$

$$f_c = \frac{nMc}{I} + \frac{P}{A}$$

$$n = 1/\beta M = 1/0.80 = 1.25$$

$$f_c = \frac{1.25 \times 26.2 \times 0.02113}{9.369 \times 10^{-9}} + \frac{7.97 \times 10^4}{0.00159} = 124 \text{ MPa}$$

Crippling stress of inner flange of z stiffener:



<u>ITEM</u>	<u>A, mm<sup>2</sup></u>	<u>b/t</u>	<u>F<sub>c</sub></u>	<u>F<sub>c</sub>A</u>
①	10.4	15.7	103 MPa	1.07 kN
②	3.5	3.3	441 MPa	1.54 kN
	<u>13.9</u>			<u>2.61 kN</u>

$$F_{cc} = \frac{2.61 \times 10^3}{1.39 \times 10^{-5}} = 188 \text{ MPa}$$

$$\text{M.S.} = \frac{188}{124} - 1 = \underline{\underline{0.52}}$$

Lockalloy Surfaces - The Lockalloy surfaces are largely designed by thermal considerations. The forebody and a portion of the lower surface are sized by the heat sink required to restrict maximum temperature to 589 K (644 K on the forebody). A great deal of the remaining surface is sized so as to produce a linear temperature gradient between the upper and lower surfaces during the period of maximum surface temperatures. This is necessary in order to minimize the thermal stresses in the surfaces. Figures 81, 82 and 83 show the skin thickness requirements for the Lockalloy fuselage shell. Included in these plots are the skin thickness requirements to sustain structural loads and to provide sufficient heat sink. Figure 84 shows the shell thickness distribution around the periphery of a typical fuselage station. Note that the previous plots of effective thickness vs. fuselage station are average values of the surfaces.

It is possible that the surface skin near the top centerline could be integrally stiffened so as to permit a higher working stress and a lower effective thickness. This would result in a higher upper surface temperature and a smaller gradient between the fuselage upper and lower surfaces. Further mass savings could then be effected because the additional Lockalloy heat sink required to linearize the temperature could be reduced.

The surfaces are analyzed for the load conditions and the thickness requirements shown. The method of analysis is basically a beam-column approach.

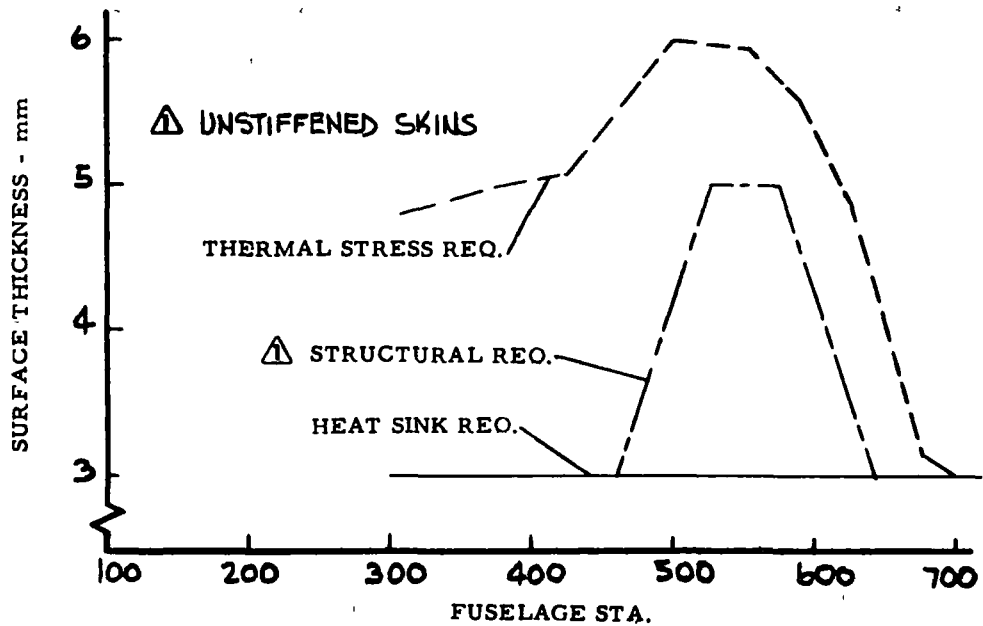


Figure 81 - Skin Thickness Requirements, Side Panels - Lockalloy Design

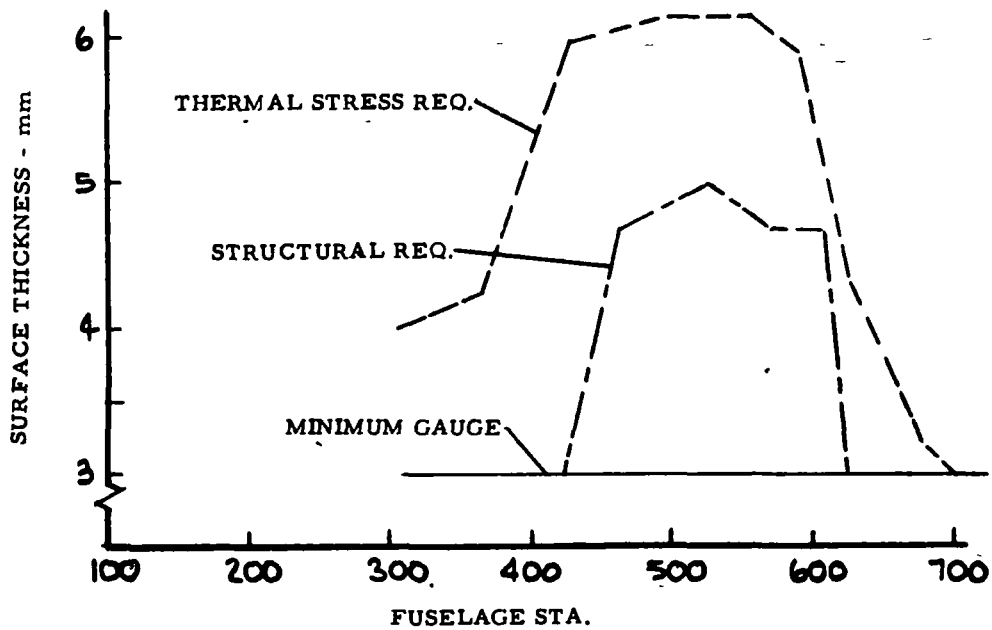


Figure 82 - Skin Thickness Requirements, Upper Surface - Lockalloy Design

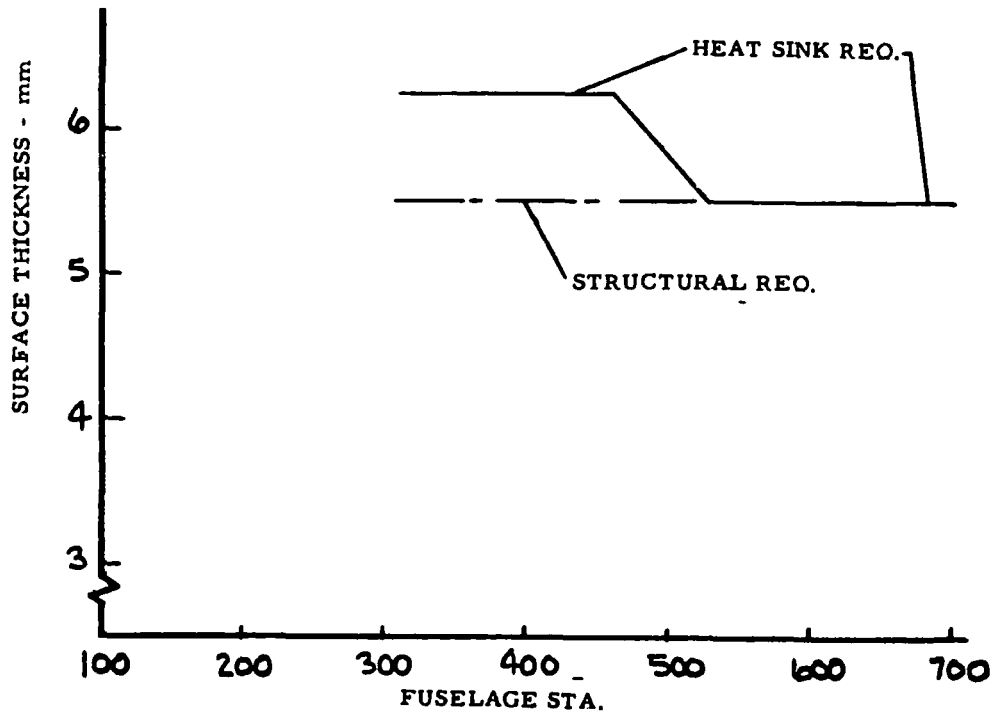


Figure 83 - Skin Thickness, 0.46 Meter Frames - Lockalloy Design

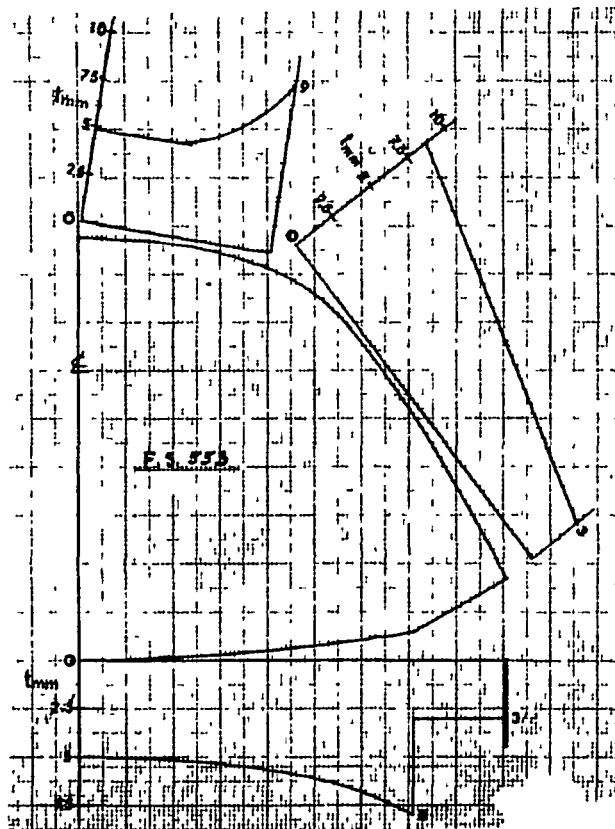


Figure 84 - Surface Thickness, Typical Station - Lockalloy Design

Axial compression allowable is calculated as the sum of two components; a simple column allowable plus the additional load-carrying capability due to surface curvature. Pressure loads are applied, these are either aerodynamic pressures or internal fuselage pressurization or both when they are additive. Bending moments are calculated from the beaming of pressure loads by the surface panels to the frames. A beam-column magnification factor is then applied to the bending moment and the bending and axial stresses are combined. A margin of safety is then calculated which includes shear interaction.

Where biaxial compression occurs the surfaces are analyzed accordingly. Peripheral compressive stresses can occur from pressure loads with the surface acting as the outer cap of the frame and from thermal effects. The method used for the biaxial loading case is based on a paper by W. H. Wittrick, Reference 5.

- Analysis Method - The following calculations demonstrate the method used to establish the Lockalloy surface thickness required to support the loads. A typical section at F.S. 571 upper surface is checked.

For the 2.5 g pullup after launch condition:

$$N_x = -88.4 \text{ kN/m (rod element 5508) (Appendix B)}$$

$$q = 57.1 \text{ kN/m (shear panel 5527)}$$

There is 6.89 kPa (Limit) internal pressurization and 4.4 kPa (Limit) aerodynamic suction pressure on the upper surface

$$P_{\text{tot}} = (6.89 + 4.41) \times 1.5 = 17.0 \text{ kPa (Ultimate)}$$

At F.S. 571 the top  $G_L$  surface thickness is 4 mm. Distance to next frame forward = 0.49 m. Upper surface radius at this station = 10.3 m.

Compression allowable load is a combination of flat column allowable and curved panel allowable.

$$F_c = \frac{\pi^2 E}{(L/p)^2} + F_{\text{curve}}$$

For the  $F_{\text{curve}}$  portion for large  $R/t$  values an empirical equation of the following form is used:

$$\frac{F_{\text{curve}}}{E} = 9 \left( \frac{t}{R} \right)^{1.6} + 0.16 \left( \frac{t}{L} \right)^{1.3} \quad \begin{array}{l} \text{(Ref. Airplane Structural} \\ \text{Analysis and Design,} \\ \text{Sechler and Dunn, p. 311)} \\ \text{(Ref. 51)} \end{array}$$

Assuming an  $L/R = 0.25$ :

$$F_{\text{curve}} = 0.688 \times 10^{-4} \times 193 \times 10^9 = 13.3 \text{ MPa}$$

$$F_{\text{col}} = \frac{\pi^2 \times 193 \times 10^9}{\left( \frac{0.493}{0.289 \times 0.00406} \right)^2} = 10.8 \text{ MPa}$$

$$F_c = 13.3 + 10.8 = 24.1 \text{ MPa}$$

$$R_c = \frac{8.84 \times 10^4}{24.1 \times 10^6 \times 0.00406} = 0.903$$

For Shear:

$$(b/t)_e = 0.493 / (0.00406 \times 2.6) = 47$$

$$F_{\text{scr}} = 72.4 \text{ MPa}$$

$$R_s = \frac{5.71 \times 10^4}{72.4 \times 10^6 \times 0.00406} = 0.194$$

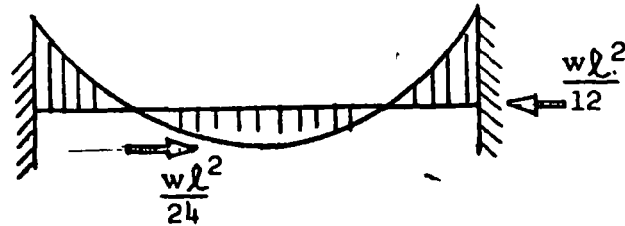
$$R_c + R_s^2 = 1$$

$$\text{M.S. (Buckling)} = \underline{\underline{0.06}}$$

$$U^* = 1/1.06 = 0.943$$

$$\beta_E = 0.62$$

Beam - column:



An initial bow of the surface  $A = \ell/400$  is assumed. This is equivalent to a side loading of  $W = P/50\ell$ .

$$W_{\text{tot}} = 17 \times 10^3 + \frac{8.84 \times 10^4}{50 \times 0.493} = 20.6 \text{ kPa}$$

At the supports:

$$M = \frac{W\ell^2}{12} = \frac{2.06 \times 10^4 \times (0.493)^2}{12} = 417 \text{ N}$$

$$f = \frac{nMc}{I} + \frac{P}{A}$$

$$n = 1/\beta_E = 1/0.62 = 1.613$$

$$f = \frac{1.613 \times 6 \times 417}{(0.00406)^2} + \frac{8.84 \times 10^4}{0.00406} = 267 \text{ MPa}$$

$$F_{\text{tu}} = 345 \text{ MPa}$$

$$F_{\text{su}} = 179 \text{ MPa}$$

$$M.S. (Shr., Comp., Bndg.) = \frac{1}{\sqrt{\left(\frac{267}{345}\right)^2 + \left(\frac{14.1}{179}\right)^2}} = -1 = \underline{\underline{0.27}}$$

The following calculations demonstrate the analysis method used to determine shell thickness for the lower surface under a thermal stress condition.  $M = 6.0$  cruise. There are thermal compressive stresses in the peripheral direction as well as longitudinal compressive stresses and pressure. Pressure acting inward on the surface causes bending of the Lockalloy as a longitudinal beam. In addition, the pressure acting on the frame, with the Lockalloy surface as the frame cap, causes peripheral compression in the surface panels. F.S. 571 is analyzed as typical.

The following numbers are used in the calculations:

$$T = 589 \text{ K (M = 6 Cruise)}$$

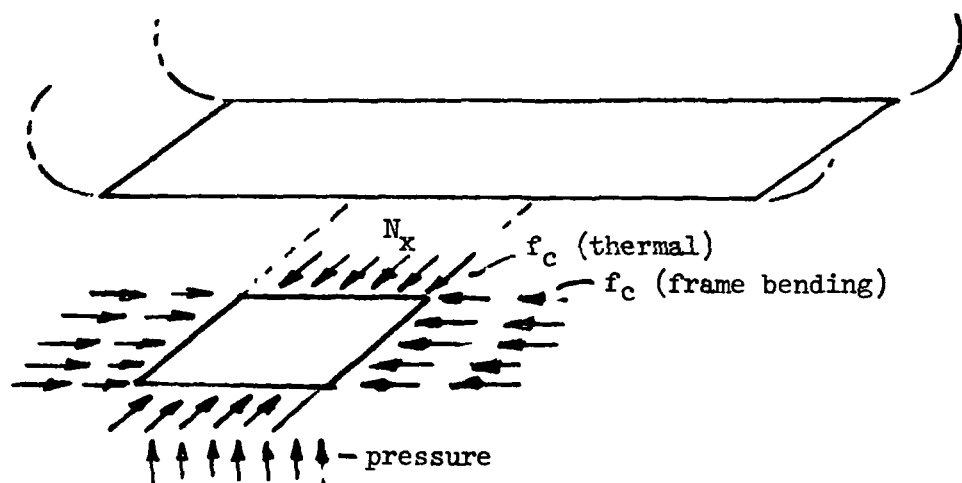
$$L = 0.493 \text{ m (Frame Spacing)}$$

$$t = 5.3 \text{ mm (Lockalloy Thickness)}$$

$$N_x = -39.4 \text{ kN/m} \quad (\text{M = 6 Cruise Condition Appendix B})$$

$$g = 13.8 \text{ kN/m}$$

$$P = 10.3 \text{ kPa (Ultimate) (Acting up on Fuselage)}$$





Thermal and frame bending stresses are modified slightly for difference between model skin thickness of 5 mm and the 5.3 mm thickness used herein. The frame modeled for NASTRAN is considered typical.

$$f_c = 6.14 \times 10^7 \times 0.0051/0.0053 = 59.1 \text{ MPa (Ref. Figure 90B)}$$

$$N_y = 5.84 \times 10^7 \times 0.0053 = 310 \text{ kN/m}$$

The following calculation determines the destabilizing effect of the  $N_x$  loading on the  $N_y$  buckling allowable. The method of W. H. Wittrick cited previously is used. The critical buckling unit load is expressed as:

$$N_{ycr} = \frac{K_c \pi^2 D}{b^2}$$

where  $K_c$  is expressed in the following form for isotropic plates:

$$K_c = \left\{ \frac{\left[ 2 \left( \frac{a}{b} \right)^2 + M^2 \right] M^2 + \left( \frac{a}{b} \right)^4}{M^2 + \left( \frac{a}{b} \right)^2 \frac{N_x}{N_y}} \right\} \left( \frac{b}{a} \right)^2$$

from "Structural Optimization of Six Different Types of Rectangular Plates Subjected to Combined Shear and Biaxial-Compressive Loading," L. R. 21662, Page 23 (Reference 51)

for

$$N_x/N_y = 39.4/310 = 0.126 \text{ iteration yields a minimum } K_c = 3.52.$$

$$N_{yce} = \frac{K_c \pi^2 t^3 E}{12 b^2}$$

$$@ 589 \text{ K } E = 179 \text{ GPa}$$

$$F_{tu} = 186 \text{ MPa}$$

$$N_{ycr} = \frac{3.52 \times \pi^2 \times (0.0053)^3 \times 179 \times 10^9}{12 \times (0.493)^2} = 322 \text{ kN/m}$$

$$\frac{N_y}{N_{ycr}} = \frac{310}{322} = 0.96$$

$$\beta_E = 0.58$$

Beam-column:

An initial bow of the surface  $A = \ell/400$  is assumed. This is equivalent to a side loading of  $W = P/50\ell$ .

$$W_{tot} = 10.3 \times 10^3 + \frac{39.4 \times 10^3}{50 \times 0.493} = 11.9 \text{ kPa}$$

$$M = \frac{W\ell^2}{12} = \frac{11.9 \times 10^3 \times (0.493)^2}{12} = 241 \text{ N}$$

$$f = \frac{nMc}{I} + \frac{P}{A}$$

$$n = 1/\beta_E = 1/0.58 = 1.724$$

$$f = \frac{1.724 \times 6 \times 241}{(0.0053)^2} + \frac{39.4 \times 10^3}{0.0053} = 96.1 \text{ MPa}$$

This is not critical-margin based on peripheral stresses is lower.

$$M.S. = 322/310 - 1 = \underline{\underline{0.04}}$$

Frames - The basic shell frames were analyzed to satisfy criteria:

- Frame loads were calculated for internal pressure and external airload.
- Moments of inertia required to stabilize the compression surfaces were determined.
- Thermal stresses were calculated for various frame materials and for various pin joint configurations.

The principal purpose of this frame analysis was to establish the preferred frame materials and the optimum frame spacing in terms of mass and cost. Primary frames, such as tank support, landing gear support, and engine support frames were not included in this analysis because their location and size are established by their individual support functions. Frames at each end of the payload bay were analyzed to determine the effects of the 0.10 to 0.15 m step in the surface axial loads at each end of the bay.

The frame analysis is based on the fuselage cross section at F.S. 496, Figure 85, the widest point on the fuselage, where the wing leading edge intersects the fuselage shell. Results from this analysis are extrapolated to other stations on the basis of load and fuselage width.

Although this frame is actually interrupted by the main landing gear cutout, it is analyzed as though continuous through the cutout for purposes of extrapolation to other stations. However, the effects of the cutout are accounted for over the length of the fuselage where the cutout actually exists.

The basic depth of the frames is 0.10 m on the bottom and 0.08 m on the top and sides, for both the Lockalloy and aluminum vehicles. The depth is a trade between frame strength requirements and fuel tank space requirements.

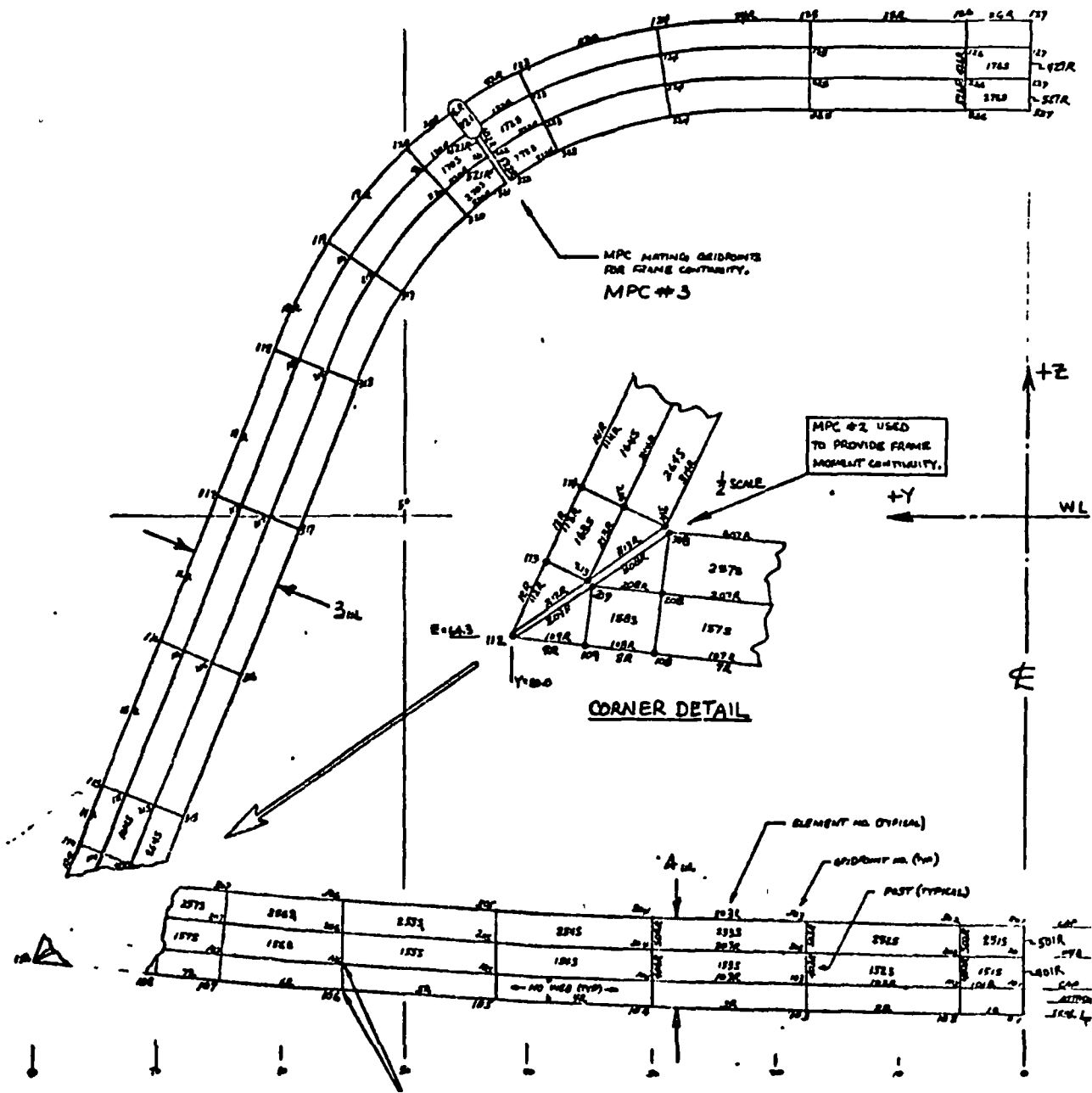
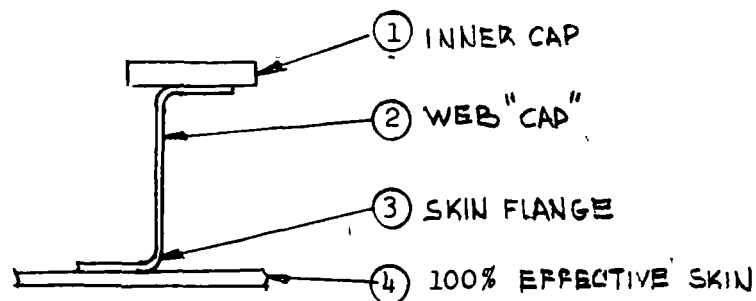


Figure 85 - NASTRAN Structural Model FS 496

The unbuckled Lockalloy skin is used as the frame outer cap on the Lockalloy concept, Figure 86. The aluminum skin is not considered effective on the aluminum version, and a separate outer cap, Figure 87, is included to complete the frame.

A NASTRAN model of the F.S. - 496 frame was assembled for use in computing internal loads due to pressures and due to thermal effects. This model is shown in Figure 84 and consists of four circumferential axial members and their associated shear webs:



Several frame configurations, in terms of frame continuity, were analyzed. This was accomplished through the use of pin joints at various locations. The applied loads and frame configurations are shown in Figure 88.

In addition, a simplified "model," Figure 89, was used to investigate the effects of various frame material combinations on thermal stress for the Lockalloy concept. This model consisted of a unit length of frame, constrained against rotation but unconstrained against translation. The results from this simplified model correlated adequately with the NASTRAN model analysis for the same material.

Pressure Analysis - Frame internal loads were determined for a unit up pressure applied to the lower surface of the frame. The vertical load was reacted by a  $VQ/I$  shear flow distribution around the frame. Internal loads were also calculated for a unit internal pressure, which is self-reacting. Four pin joint

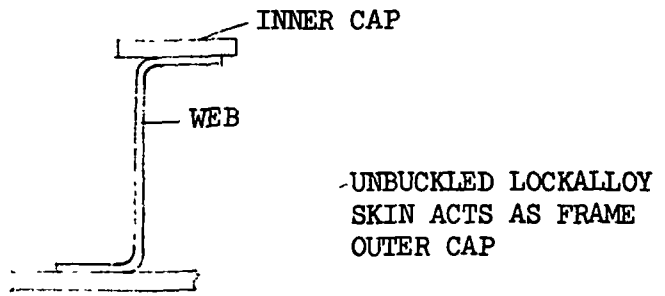


Figure 86 - Frame for Lockalloy Vehicle

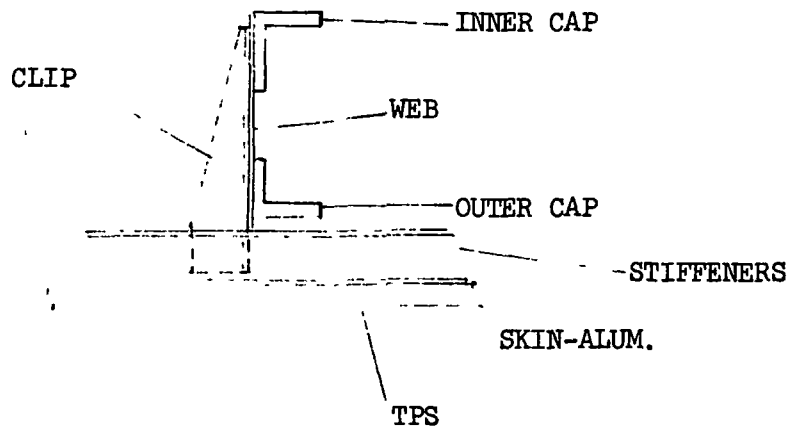
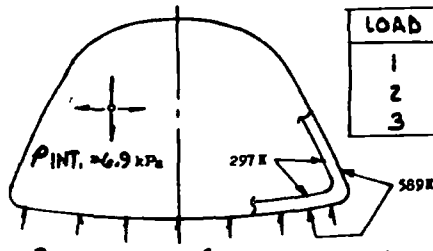


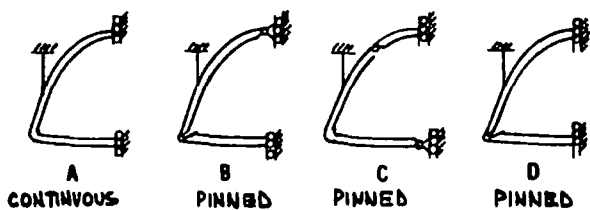
Figure 87 - Frame for Aluminum Vehicle

LOADS



LOAD	DESCRIPTION
1	Δ TEMPERATURE
2	6.9 kPa INT.
3	6.9 kPa LWR SURF.

CONSTRAINTS



LOAD/CONSTRAINT CASES

LOAD NO	CASE NO			
	SUPPORT			
	A	B	C	D
1	11	21	31	41
2	12	22	32	42
3	13	23	33	43

Figure 88 - Frame Load and Constraint Combination Configuration - FS 496

EVALUATION OF THERMAL STRESSES

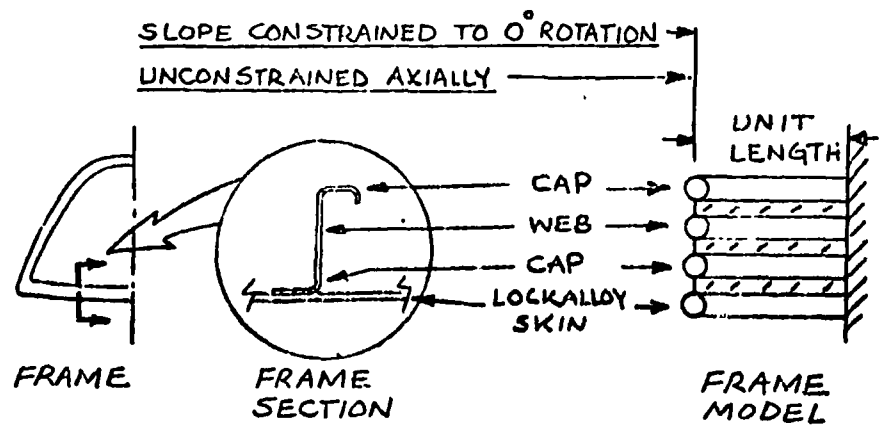


Figure 89 - Simplified Frame Model

configurations were investigated, as shown in Figure 88. 6.89 kPa (limit) negative internal pressure (suction) is combined with 3.45 kPa (limit) up pressure on the lower surface for frame analysis. Frame moments are shown in Figure 90 for a continuous frame with no pin joints. The effect of adding pins at the top centerline and at the bottom outer edges is also shown.

Frame area requirements for pressure loads are shown in Figures 91 through 94.

Stability Requirement - Frame moments of inertia required to stabilize the compression surfaces are determined using the equation

$$(EI)_{\text{REQUIRED}} = 4 \left( \frac{N}{a} \right) \left( \frac{L}{\pi} \right)^4 \quad (\text{Reference 52})$$

where

N is the surface axial compression load, N/M

a is the frame spacing, meters

L is the frame element length between supports, meters

L is assumed as shown in Figure 95.

Note that L is to the 4th power. The wide, flat bottom therefore requires significant frame EI even though the physical magnitude of the applied loads is low (n 175 kN/m).

The frame area requirements, based on 0.10 m deep frames on the bottom, and 0.08 m on the sides and top, are shown in Figure 91 for the aluminum shell and in Figures 92, 93 and 94 for the Lockalloy shell.

Thermal Analysis - Analysis on the aluminum shell with Ablator or LI-900 showed small temperature differences through the frame cross section, therefore no thermal stress analysis was conducted on the frames in the aluminum vehicles.



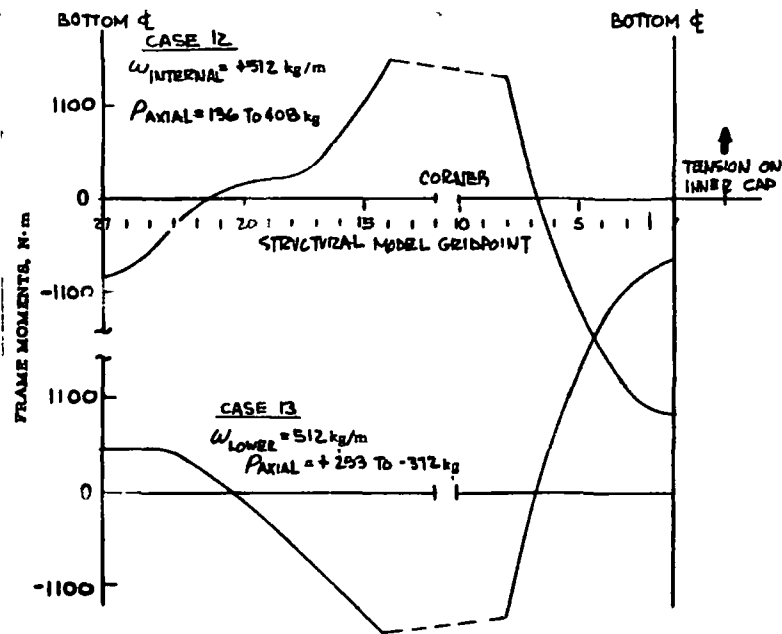


Figure 90 - Frame Moments - FS 496

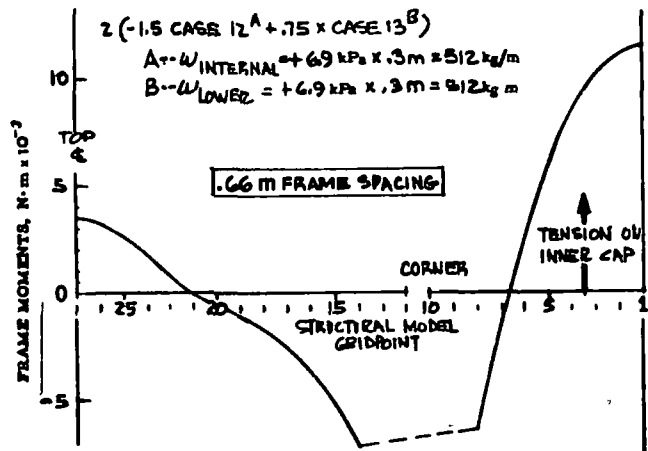


Figure 90A - Frame Moments - Continued

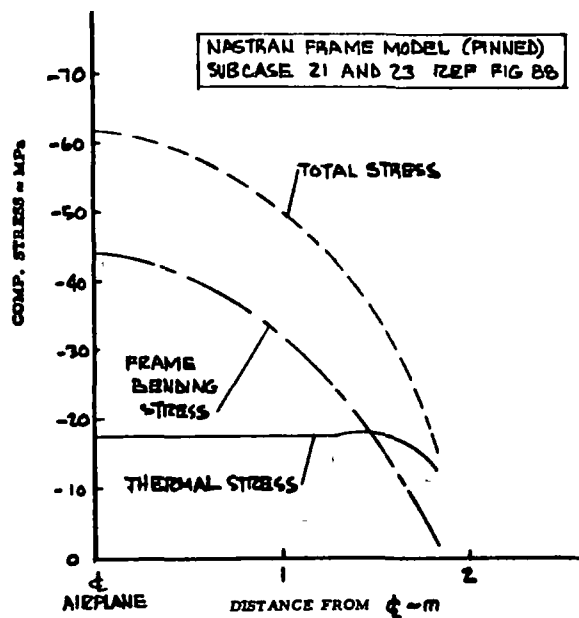


Figure 90B - Frame Moments - Continued

ALUM SHELL (0.6M FRAME SPACING)  
 EFFECT OF THERMAL STRESS NOT INCLUDED, BUT CONSIDERED  
 NEGLIGIBLE, FALL ~ 207 MPa

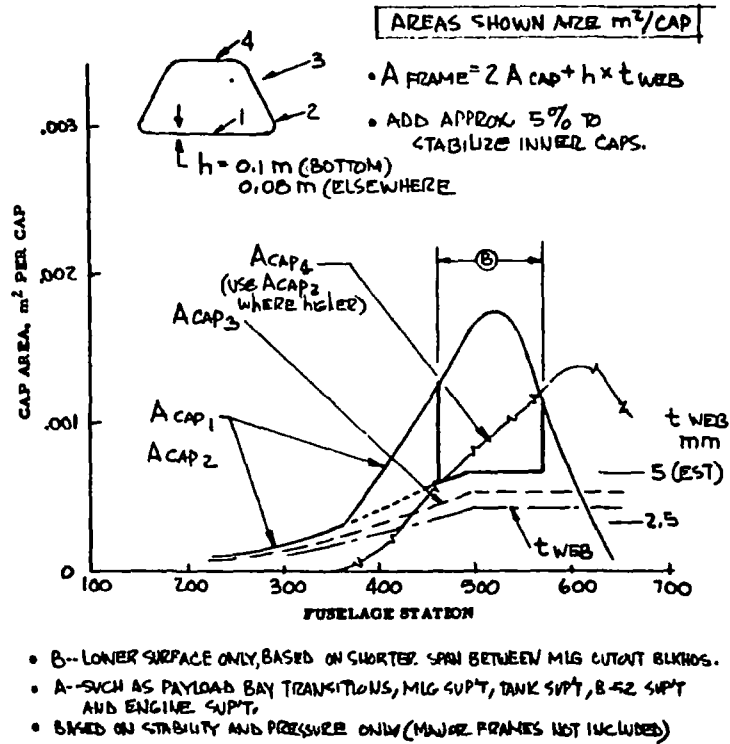


Figure 91 - Fuselage Frames - Area Requirement

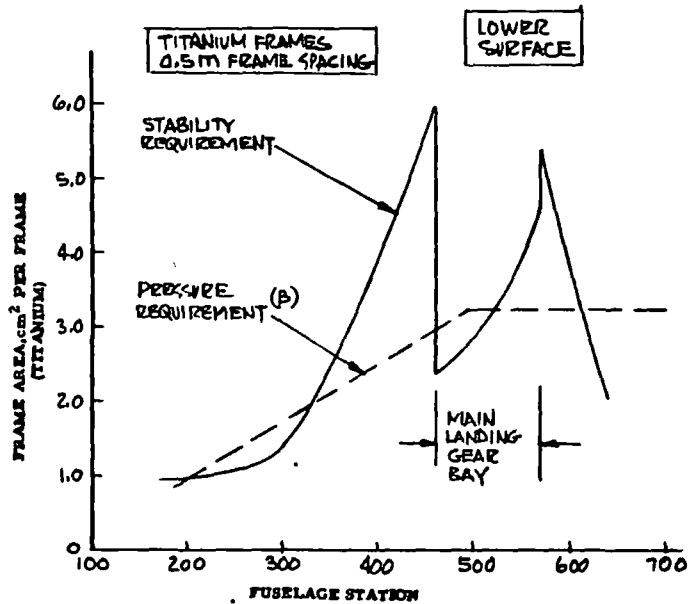


Figure 92 - Frame Area - Titanium Frames

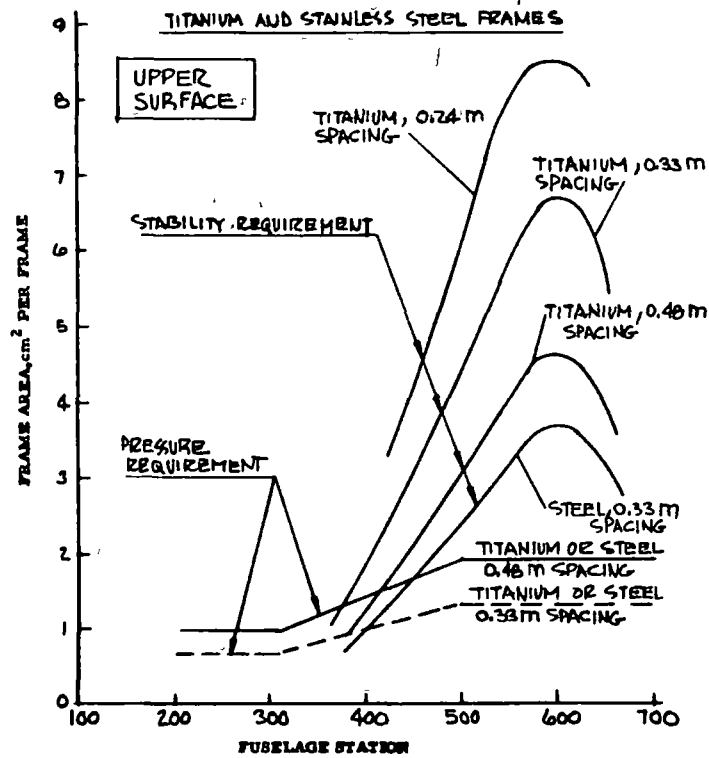


Figure 93 - Fuselage Frames, Area Requirement - Upper Surface

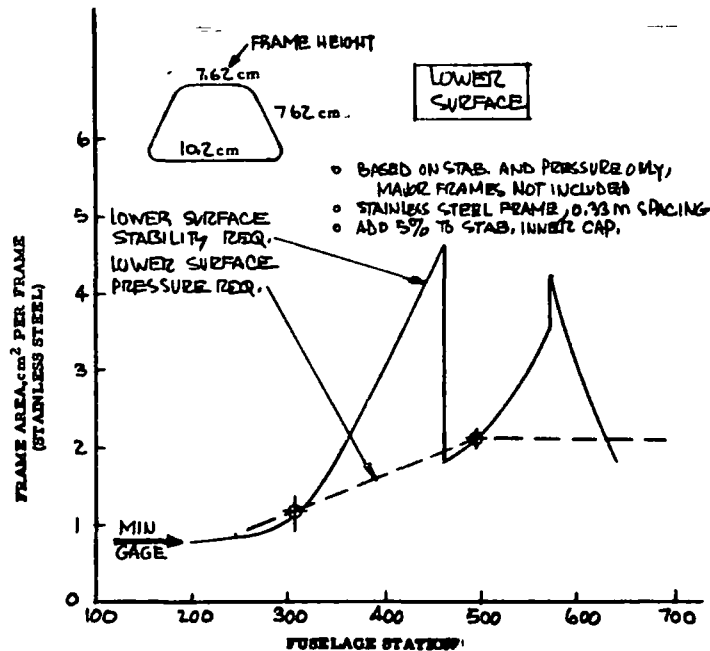


Figure 94 - Fuselage Frames, Area Requirement - Lower Surface

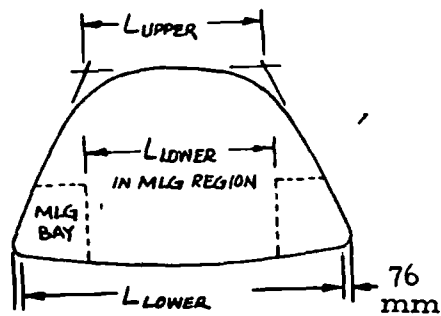


Figure 95 - Frame Length Between Supports for Frame - Stability Requirement

There would however be a problem with skin buckling in the peripheral direction due to thermal gradients across the aluminum frames. There are two possibilities associated with this thermal problem. The first is that the skin buckling might cause the Ablator or insulator to pop off of the skin surface. The second is that the Ablator/insulator would stabilize the skin sufficiently to prevent the compression buckles from forming. Tests would have to be performed to ascertain the skin panel behavior under these conditions.

Thermal stress analysis on the Lockalloy vehicle was conducted for various material combinations and for various pin joint configurations. The basic frame cross section that was analyzed is shown in Figure 96. Thermal stresses were calculated for the material, pin joint, and structural model configurations shown in Table 20.

The temperature profile for the 40-second mission is shown in Figure 97. The temperatures used for the frame thermal stress analysis are shown in Figure 96. The results of these thermal stress analyses are shown in Figure 98. The results are consistent between the various approaches, and show significant compression thermal stress on the Lockalloy skin regardless of the frame material, for continuous frames without pin joints. These stresses result more from the large temperature differential between the Lockalloy skin and cap (589 K to

Method	Figure 85	Figure 89	Reference 6
Stainless Steel	A, B, C	a , Fig. 98	X, Fig. 98
Titanium	---	b , Fig. 98	◇ Fig. 98
Aluminum	---	c , Fig. 98	
Lockalloy	---	d , Fig. 98	

A - Continuous Frame  
B - Pins at top  $\mathcal{C}$  and Bottom Outer Edges  
C - Pins at Bottom  $\mathcal{C}$  and Upper Outer Corners

Table 20 - Thermal Stress Analysis Configurations

room temperature) than from the difference in thermal elongation coefficient between materials. For example, Lockalloy frames with the Lockalloy skin still show -96.5 MPa stress on the skin, Figure 98. (Configuration d, Lockalloy skin). However, the skin stress drops dramatically if the frames are pinned at three places on each frame. This allows the frame to relieve itself almost entirely of thermally induced bending stresses. The Lockalloy skin stress is -17.2 MPa (compression) for Configuration b, Figure 98, which has pin joints at the top centerline and the bottom outer edges.

Transverse thermal stresses in the Lockalloy skin for continuous frames approach the skin compression buckling allowable, particularly for wider frame spacings. Panel allowables can be increased by reducing the frame spacing or increasing panel thickness, but these solutions cost mass. The solution chosen is to reduce the thermal stresses by using 3 pin joints in each frame. The details of the pin joints have not been established and further design and analysis are required in this area. If continuous frames were to be used, it is possible that intermediate frames could be employed to increase the panel allowable stress by cutting the panel width in half. These auxiliary frames could be shallow depth and designed to perform the panel support function only. Additionally, where the skin is thin it may be necessary to add frame cap material against the skin to prevent skin panel buckling.

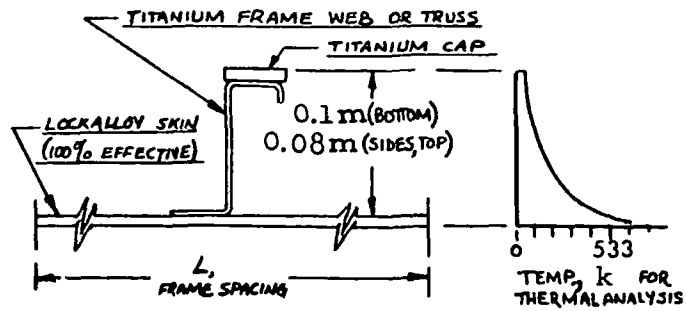


Figure 96 - Frame Construction - Lockalloy Design

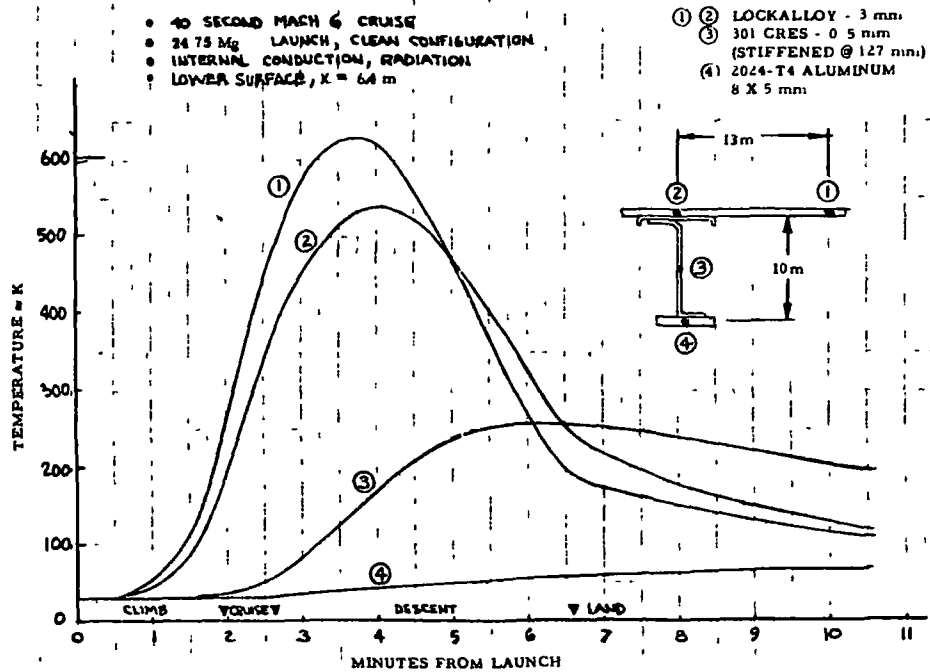


Figure 97 - Lockalloy Supports - Lower Surface

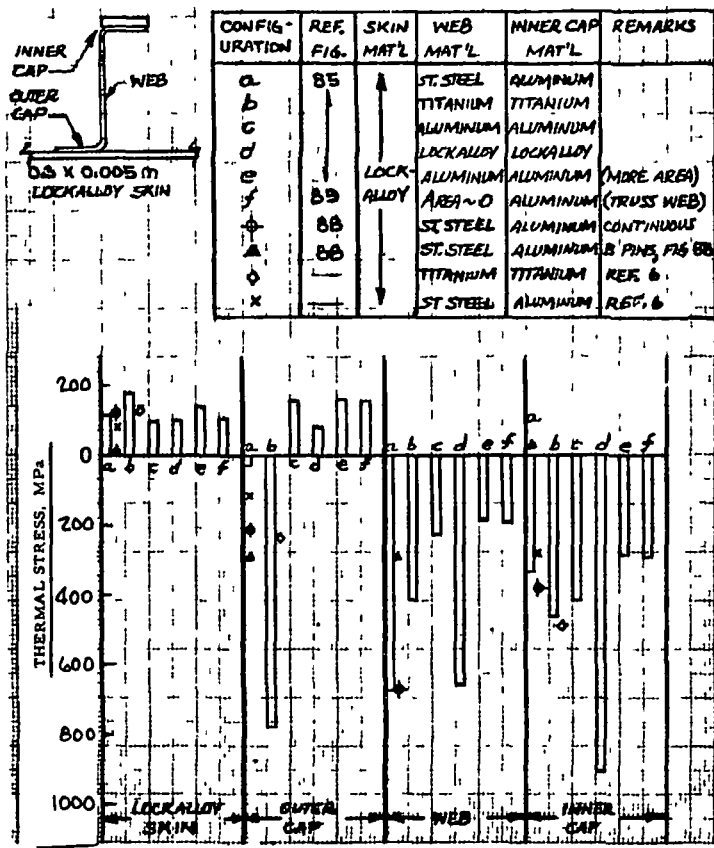


Figure 98 - Frame Thermal Stress vs Material

### Lockalloy Thermal Stresses Where Attached to Massive Substructure -

Thermal stresses are relieved in much of the Lockalloy structure by allowing the structure to rotate. Pin joints are used in fuselage frames, for example to allow the frame members to deflect rotationally to reduce thermal stress. There will inevitably be some cases, however, that this relief may not be available. Longerons supported over several frames, and bulkheads that are continuous either longitudinally (MLG support bulkheads) or transversely, are examples of webbed or continuous bulkhead that restrains the outer (Lockalloy) cap from rotating. The analysis that follows shows the potential stresses and strains in the Lockalloy as a function of the ratio of Lockalloy to substructure (titanium) area, and as a function of temperature.

The basis of the analysis is given in the equation below, which assumes that the sum of the load strains plus thermal strains in the Lockalloy are equal to those in the substructure, or,

$$\Delta \text{ Titanium} = \Delta \text{ Lockalloy}$$

$$\frac{f}{E} + \alpha \Delta T_{\text{Titanium}} = \frac{f}{E} + \alpha \Delta T_{\text{Lockalloy}}$$

$$f = \frac{P}{A}, P_{\text{Titanium}} = - P_{\text{Lockalloy}}$$

The titanium is assumed to be at a constant 297 K ( $T_{\text{Titanium}} = 0$ ), therefore, for  $R = A_{\text{Lockalloy}}/A_{\text{Titanium}}$ ,

$$f_{\text{Lockalloy}} = \frac{(\alpha \Delta T)_{\text{Lockalloy}}}{\frac{R}{E_{\text{Titanium}}} + \frac{1}{E_{\text{Lockalloy}}}}$$



This equation is plotted in Figure 99, and shows, for example, that for a Lockalloy surface area equal to the titanium substructure area ( $R = 1$ ), the Lockalloy stress at 477 K is -221 MPa (compression), slightly exceeding the Lockalloy compression yield. The titanium stress (in this case +221 MPa for  $R = 1$ ) is well within titanium material allowables.

The stresses and strains for Lockalloy heated to 589 K and cooled to 297 K are shown in Figure 100. This shows that for the conditions specified, the Lockalloy material strains well into the plastic region at 589 K, and retains a 134 MPa residual tension stress after cooling down.

The analysis represents a limiting case with no allowance for relief of any kind. In actual practice a detailed thermal analyzer solution would be made showing actual temperature distributions through the structure, which would undoubtedly result in a smaller temperature differential than the 589 K to 297 K temperatures used in this analysis. In addition, steps would be taken to make bulkhead webs less affective axially, for example, by using beads or corrugations in the webs to absorb thermal strains. Nevertheless, the analysis shows that thermal strains in regions where massive substructure ties directly to the outer Lockalloy skin must be determined and accounted for.

Creep Analysis - An investigation was conducted to assess the effects of creep on the X-24C vehicle during its service life of 100 flights. This investigation included defining the limit stresses due to thermal loads and air loads and comparing the resultant equivalent stress to the creep allowable for a maximum permanent deformation of 0.2%.

A time-temperature history plot for a typical Lockalloy surface panel on the fuselage is shown in Figure 101. This panel is located on the lower surface of the fuselage approximately 5.08 meters aft of the nose. This data is typical of the temperature response curves for most regions undisturbed by the influence of other surfaces.

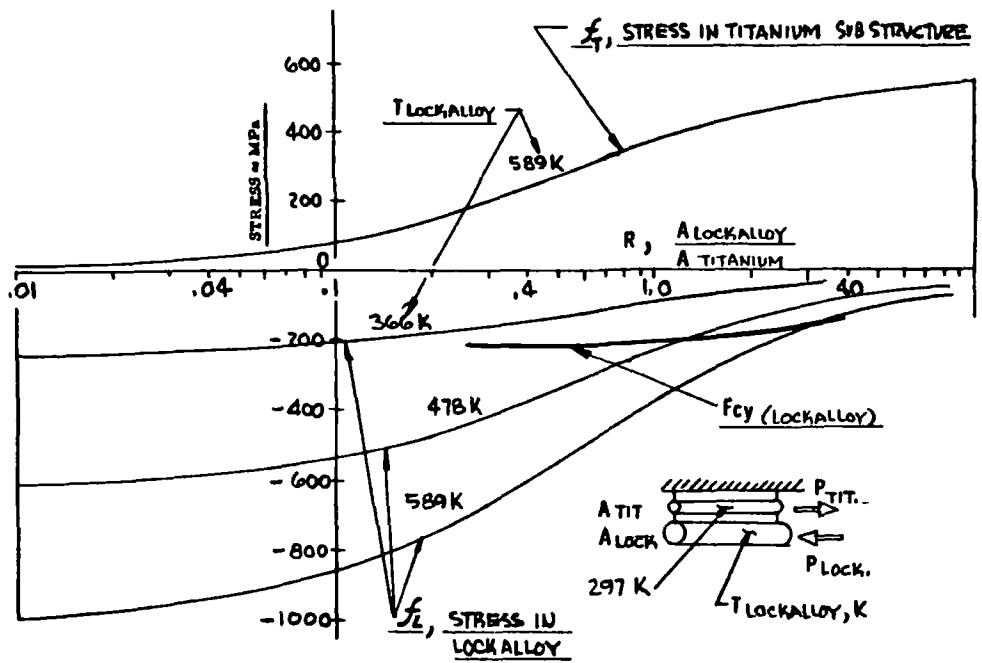


Figure 99 - Thermal Stress with Rotational Constraint

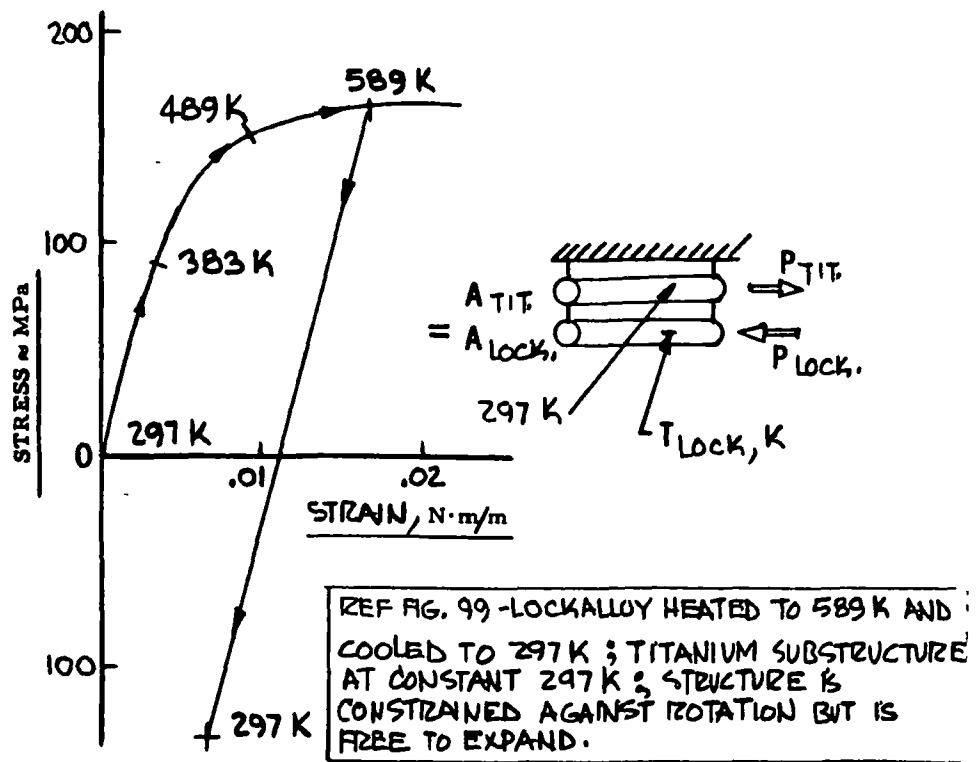


Figure 100 - Lockalloy Stresses and Strains During Heating and Cooling

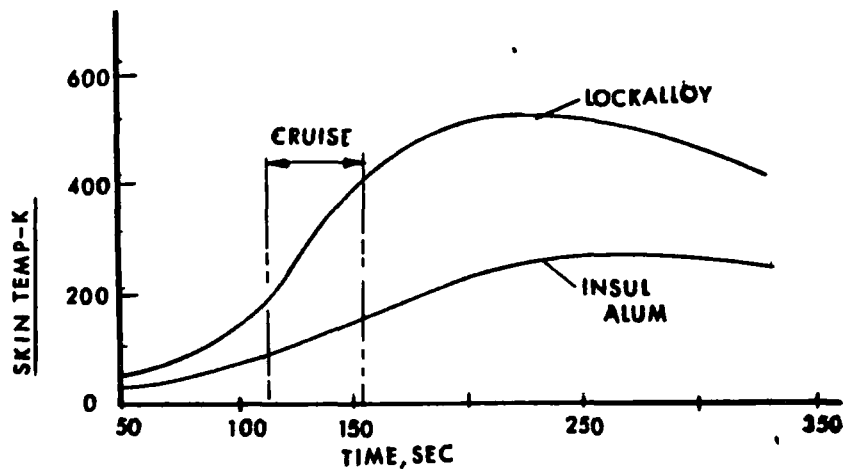


Figure 101 - Fuselage Skin Panel Time-Temperature History

The maximum temperature occurs shortly after cruise and is sustained for approximately 150 seconds during the descent portion of the mission. Since creep is predominately associated with the elevated temperature conditions a duration of 150 seconds per flight was used to define the creep design life for the 100 flight service life.

$$t = \frac{150 \times 100}{3600} = 4.17 \text{ Hrs.}$$

The corresponding limit stresses associated with this time period were conservatively assumed to be the maximum combination of airload and thermal stresses occurring within this time bracket of 150 seconds. For example, if the limit 1-g airload stresses were maximum at cruise these were combined with

the maximum thermal stresses which occurs approximately 70 seconds later in flight.

The stress analysis methods used to assess the effect of creep on the Lock-alloy design primary structure were as follows:

The applied stresses are defined as:

$$f_x = f_{x, \text{air}} + f_{x, \text{thermal}}$$

$$f_y = f_{y, \text{air}} + f_{y, \text{thermal}}$$

$$f_{xy} = f_{xy, \text{air}} + f_{xy, \text{thermal}}$$

Where  $f_{x, \text{air}}$ ,  $f_{y, \text{air}}$ , and  $f_{xy, \text{air}}$  are the stresses calculated using the maximum limit of 1-g airloads with the corresponding thermal loads being defined by the NASTRAN structural model run for the maximum temperature gradient condition.

The airload stresses reflect the combined mid-plane and bending stresses, e.g.,

$$f_{x, \text{air}} = \frac{N_x}{t} \pm \frac{6M}{t^2}$$

Where the maximum mid-panel bending moments are calculated using Reference 4. For a uniformly loaded simply-supported square plate with a Poisson's ratio of 0.14 the maximum bending moments are:

$$M_x = M_y = 0.042 \text{ pa}^2$$

The equivalent uniaxial stress state as defined by Octahedral Shear Stress Theory, Reference 4.

$$\bar{f} = \left[ f_x^2 + f_y^2 - f_x f_y + 3f_{xy}^2 \right]^{1/2}$$

This equivalent uniaxial stress is then compared to the allowable creep stress for 0.2% permanent deformation, or expressed in terms of a margin of safety:

$$MS = \frac{F_{0.2}}{\bar{f}} - 1$$

The creep allowables for Lockalloy at 589 K are shown in Figure 102 for various percentages of permanent deformation. For the creep design life of this vehicle, 4.2 hours, an allowable stress of 51.7 MPa for 0.20% permanent deformation is noted.

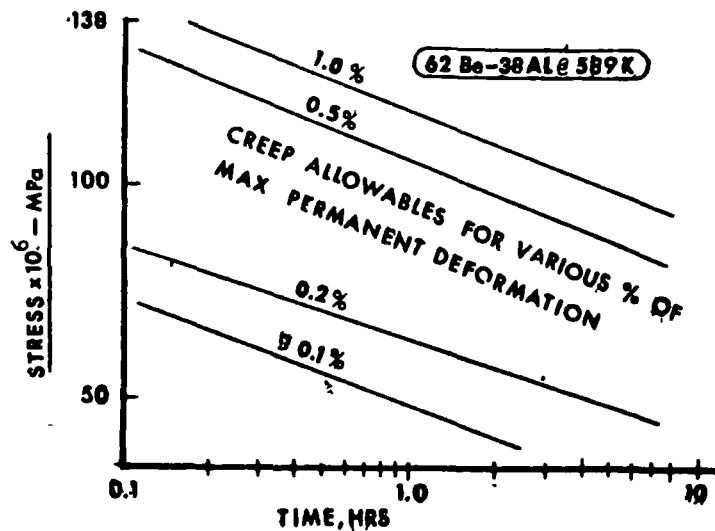


Figure 102 - Lockalloy Creep Allowances

As an example of the creep evaluation, the analyses conducted on the Lockalloy wing surface panels adjacent to the rear beam at the root chord, point design region 2, are presented in the following text.

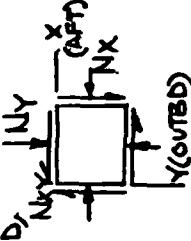
The total load state, both inplane loads and normal loads, are shown in Table 21. The maximum limit 1-g airloads for these panels occur during the Mach 3.0 descent condition; whereas, the thermal loads reflect the maximum temperature gradient condition.

A summary of the stress analysis conducted on these panels is presented in Table 22 and shows the panel geometry, airload stresses, thermal stress and combined stresses. In addition, the equivalent stress state and material allowable are presented, with positive margins of safety of 40 and 24 percent noted for the upper and lower surface panels, respectively.

A summary chart, Table 23, presents the results of the creep investigation conducted on the wing surface panels of the Lockalloy design. This table lists the panel proportions, panel thicknesses and combined airload and thermal stresses for the wing three point design regions. In addition, the equivalent stresses are shown with the allowable creep stresses and corresponding margins of safety for two percentages of permanent deformation, 0.2 and 0.5 percent. For the creep criteria as specified in the Work Statement, 0.20 percent permanent deformation, negative margins are noted for the upper surface panels at point design regions (1) and (3). In addition, a slightly negative margin of safety of 4 percent is indicated for the lower surface panel at design region (3). These panels were reanalyzed with increased thicknesses until positive margins were obtained. These incremental thicknesses were used to assess the mass penalty associated with creep.

The effect of the creep criterion on the structural mass is indicated by comparing the margins of safety calculated using the 0.2 percent maximum permanent deformation value as specified in the Work Statement with those using an 0.50 percent permanent deformation. The allowable stresses for the permanent

ITEM	WING SURFACE	
	UPPER	LOWER
AIRLOADS (1)		
$N_{x,AIR}$ *	+3.15	+3.85
$N_{y,AIR}$ *	-0.53	+3.15
$N_{xy,AIR}$ *	+0.35	-1.75
$P_z$ †	±6.9	±6.9
THERMAL LOADS (2)		
$N_{x,TH}$ *	+28.2	-11
$N_{y,TH}$ *	-44.8	-69.7
$N_{xy,TH}$ *	-50.8	-3.15

(1)  $M=3.0$  DESCENT COND, LIMIT 1-g LOADS 

(2) MAX TEMP GRADIENT COND, LIMIT LOADS

\* = KRF/IN.  
† = KPS

Table 21 - Limit Load State for Wing Surface Panels

PANEL LOCATION WING SURFACE PT. DESIGN REGION	UPPER (2)	LOWER (2)
PANEL GEOMETRY RIB SPACING, m SPAR SPACING, m THICKNESS, mm	0.457 0.457 4.01	0.457 0.457 4.32
AIRLOAD STRESSES $M_x = M_y = 0.42 P D^2 / N$ • $f_{x,AIR} = N_{x,AIR} \pm 6 M / Z$ • $f_{y,AIR} = N_{y,AIR} \pm 6 M / Z$ • $f_{xy,AIR} = N_{xy,AIR}$	±60.5 -21.8 -22.7 +0.09	±60.5 -20.3 -18.8 -0.41
THERMAL STRESSES, * $f_{x,THERM} = N_{x,TH} / t$ $f_{y,THERM} = N_{y,TH} / t$ $f_{xy,THERM} = N_{xy,TH}$	+7.03 -11.2 -12.7	-25.8 -16.1 -0.76
COMBINED STRESSES, * $f_x = f_{x,AIR} + f_{x,THERM}$ $f_y = f_{y,AIR} + f_{y,THERM}$ $f_{xy} = f_{xy,AIR} + f_{xy,THERM}$	-21.8 -33.9 -12.6	-46.1 -34.9 -1.17
EQUIVALENT STRESSES, * $f_z$	36.9	41.7
MATERIAL ALLOWABLE $t$ , hr $F_{0.2}$ *	4.2 51.7	4.2 51.7
MARGIN OF SAFETY $MS = (F_{0.2} / F) - 1$ * = MPa	0.40	0.24

Table 22 - Detail Creep Analysis - Lockalloy Design

POINT DESIGN REGIONS	WING SURFACE	PANEL PROPORTIONS		PANEL THK. mm	COMBINED STRESS			EQUIV. STRESS $\bar{f}$ MPa	F <sub>0.2</sub> MPa	MS <sub>0.2</sub>	F <sub>0.5</sub> MPa	MS <sub>0.5</sub>
		SPAR SPACING m	RIB SPACING m		f <sub>x</sub> MPa	f <sub>y</sub> MPa	f <sub>xy</sub> MPa					
①	UPPER	0.457	0.457	4.39	87.8	24.8	9.51	80.2	5.17	-0.35	89.6	0.12
	LOWER			4.44	-49.3	-31.9	2.62	43.5		0.19		1.06
②	UPPER			4.01	-21.8	-33.9	-12.7	36.9		0.40		1.43
	LOWER			4.32	-46.1	-34.9	-1.17	41.7		0.24		1.15
③	UPPER			3.43	36.4	68.7	18.3	67.5		-0.23		0.33
	LOWER	0.457	0.457	4.67	-23.1	-23.1	12.4	53.6	5.17	-0.04	89.6	0.67

(1) STRENGTH SIZED THICKNESS  
(2) EQUIVALENT UNIAXIAL STRESS  $(\bar{f}) = [f_x^2 + f_y^2 - f_x f_y + 3 f_{xy}]^{1/2}$   
(3) CREEP ALLOWABLE FOR 0.2% PERMANENT DEFORMATION & CORRESPONDING MARGIN OF SAFETY  
(4) CREEP ALLOWABLE FOR 0.5% PERMANENT DEFORMATION & CORRESPONDING MARGIN OF SAFETY



Table 23 - Summary of Creep Analysis, Wing Surface Panels - Lockalloy Design



deformations are 51.7 MPa and 89.6 MPa, respectively. This amounts to an increase of 73 percent in the allowable stress using the 0.50 percent deformation criteria for the same creep design life of 4.2 hours. Increasing the maximum permissible permanent strain affords positive margins on all panel designs shown in Table 23; thus, no added mass penalty would be required for these wing locations. However, the accumulative deflection of panels and structure such as the wing need to be assessed.

Lockalloy Crack Susceptibility - The following observations are made with regard to the potential problem of cracking of the Lockalloy structure:

- Machined beryllium surfaces exhibit microcracking or twinning damage which necessitates a 0.05 to 0.10 mm chemical etch to remove the affected surface. This tendency is not present in Lockalloy and thus the potential for crack initiation is not a problem as it is with pure beryllium, Reference 7.
- Lockalloy exhibits as good or better (i. e., slower) crack growth rates than aluminum or titanium alloys. This has been established by the tests of the Lockalloy characterization study, Reference 8.
- Stress levels are generally low for the Lockalloy structure (less than 69 MPa) which greatly reduces the possibility of any cracks occurring in the 100 flight life cycle of the vehicle. Fatigue tests conducted during the Lockalloy ventral fin program, Reference 8, indicate an endurance limit for  $K_t = 3$  of 103 MPa at room temperature and 69 MPa at 589 K.
- In the event a crack should occur during the life of the vehicle, the low operating stress levels makes the airframe much more damage tolerant. Additionally, almost all of the Lockalloy structure is external, making it available for visual inspection and maintenance.

## Thermal Analyses

Thermal analyses were performed primarily to size TPS requirements and provide structural temperatures for stress calculations. Studies to determine the effects of shock wave/boundary layer interactions and heating rate uncertainty factors on TPS designs and structural temperatures were also performed.

The TPS analyses were necessarily limited to representative locations over the aircraft, designation throughout the study as vehicle element locations. These elements are roughly defined by the numbers shown in Figure 103. They correspond to locations for which aerodynamic heating rates were computed by NASA/Langley. These heating rates were supplied for optional usage. They were checked in representative areas of the aircraft to see how they compared with heating rates computed with the Lockheed methods. Good agreement was achieved, and the NASA heating rates were used in much of the subsequent work.

Additional thermal analyses on tank insulation requirements and vehicle pressurization were also made. All analyses, plus the results of each, are described in the sections below.

Lockalloy Thickness Calculations - A general computer program was set up to compute the transient thermal response of a single nodal skin with aerodynamic heating, and radiation exchange with two arbitrary sinks. Multiple thicknesses of skin were analyzed simultaneously to provide information on the effect of thickness on peak temperature. Heating rates were obtained for the most part from the NASA supplied information as a function of Mach number, dynamic pressure, skin temperature, and vehicle angle of attack at each computing cycle of the analysis. The heating on the lower fuselage ramp was modified to reflect local one-dimensional flow effects from the Scramjet exhaust. Other special heating areas were treated separately. The thermal conductivity and specific heat of the Lockalloy were varied with temperature, and the external surface was assumed pointed ( $\epsilon = 0.85$ ). The boundary layer was determined to be laminar for all leading edge areas.

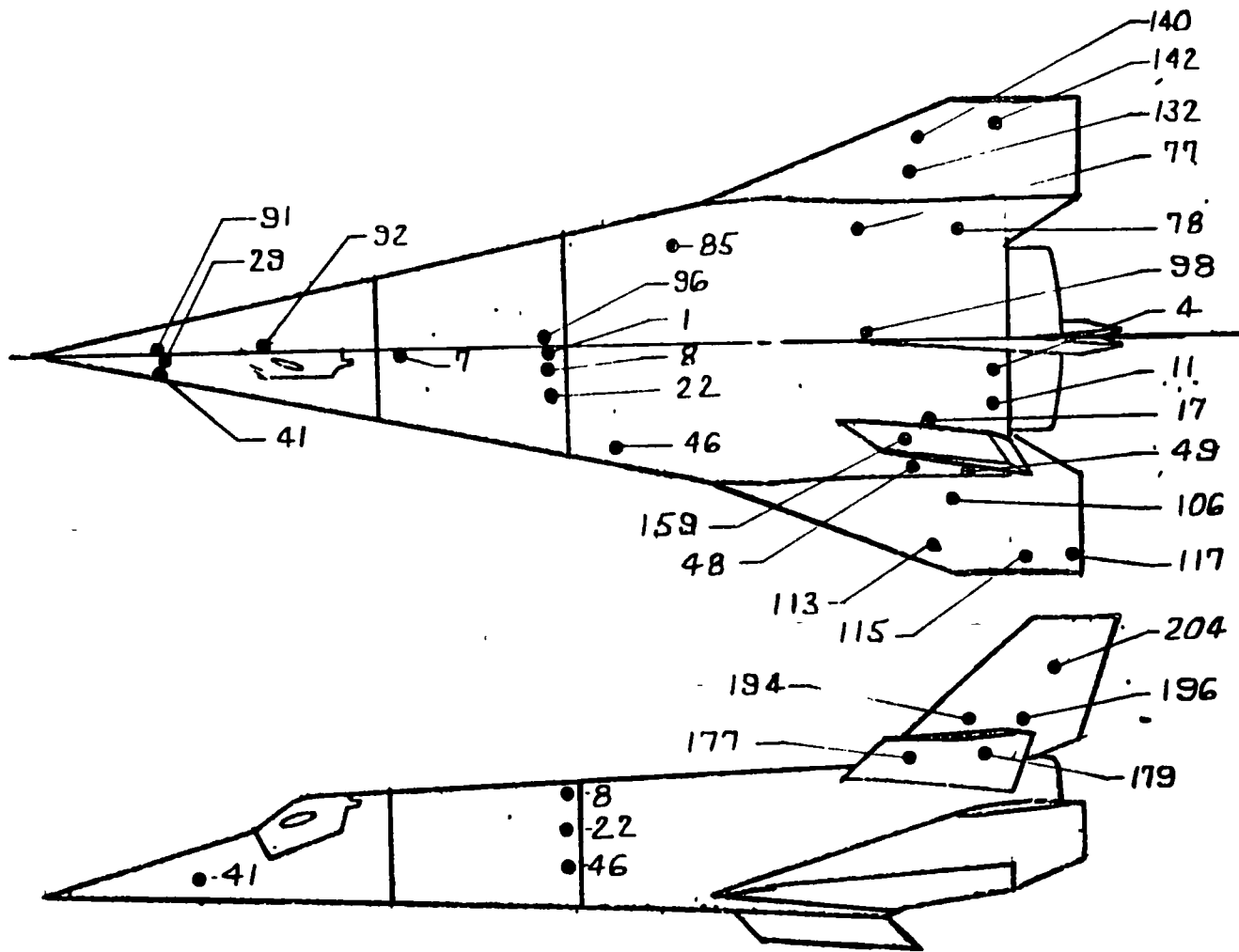


Figure 103 - Vehicle Heat Treat Element Numbers

Two extreme climbs, plus five optional descents were used in a preliminary analysis to determine the effect of various missions on the peak skin temperature. The two climbs yielded differences in peak skin temperature of approximately 269 K (depends on location), which represents a thickness difference of 0.25 mm. This small difference in design thickness did not justify the additional analyses required to analyze all vehicle locations for multiple climbs. Therefore, the slower climb (LR-99) yielding the higher total heating was used in all subsequent analyses.

The various descents analyzed yielded substantial differences in total heating to the vehicle. Since the actual descent profile flown could be tailored to minimize aerodynamic heating, the descent yielding minimum total heating was selected for all subsequent analyses (high  $\alpha$ , 60° bank).

Figures 104 and 105 present the results of the thickness analyses for various vehicle locations. These locations are identified by element numbers corresponding to aerodynamic heating locations supplied by NASA. Peak temperature during the mission is shown as a function of skin thickness.

Forebody Transition Analysis - Basic transition data correlations are available for sharp nose cones and wedges. The effect of bluntness and low turbulence (as in the atmosphere) is to delay transition, but the effect of manufacturing irregularities is to reduce the distance to transition characteristics of the boundary layer. The transition data correlation of prior Lockheed analysis was used. The empirically derived equations for transition Reynolds number on a cone are:

$$Re_{\text{BEGINNING OF TRANSITION}} = \left( \frac{Re/m}{3.28 \times 10^6} \right)^{0.70} \times 10^{(5.29 + 0.108 M)}$$

$$Re_{\text{END OF TRANSITION}} = \left( \frac{Re/m}{3.28 \times 10^6} \right)^{0.35} \times 10^{(6.19 + 0.061 M)}$$

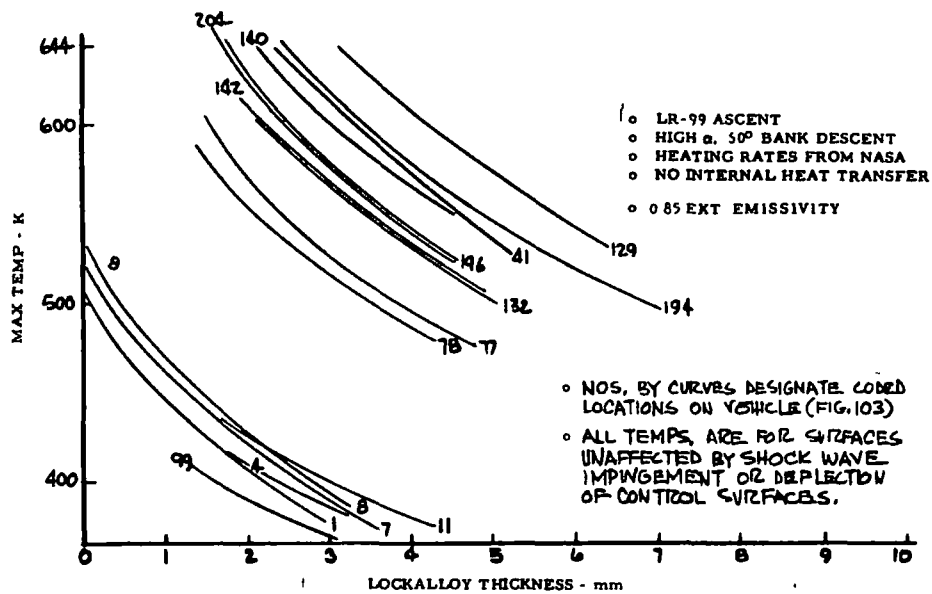


Figure 104 - Peak Temperature During Mission Vs Skin Thickness - Lockalloy Design

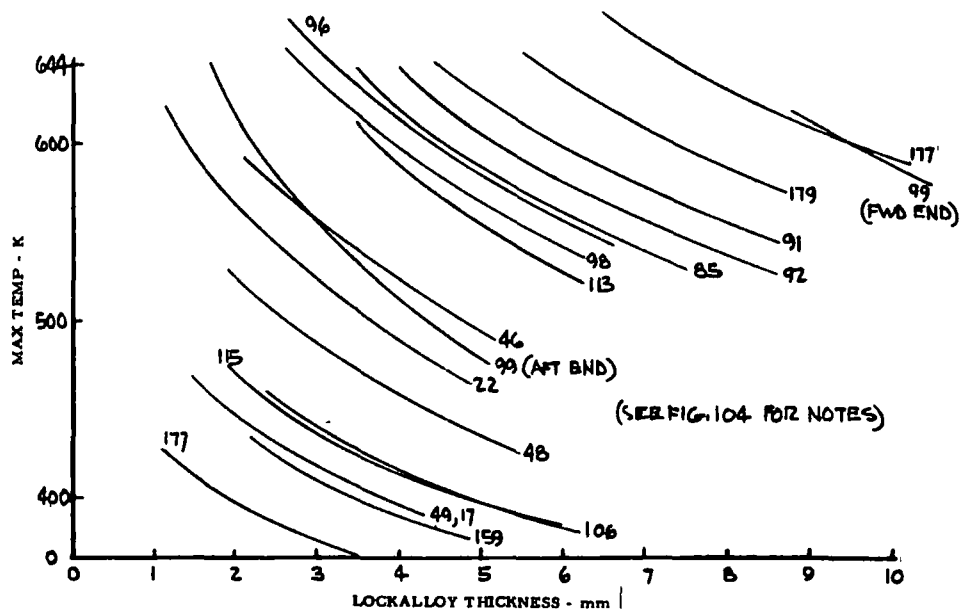


Figure 105 - Peak Temperature During Mission vs Skin Thickness - Lockalloy Design

Surface temperature was assumed to have negligible effect on transition Reynolds number.

The relationship between effective conical half angle and included angle of attack was estimated by use of the experimental and theoretical data of NASA reports, Reference 9. For each freestream MACH number and vehicle angle of attack, an equivalent conical axisymmetric flow was found which produced the same MACH number on the cone surface as that measured on predicted under the forebody near the Scramjet inlet station.

Results of these analyses are shown in Figures 106 through 109. The forebody equivalent conical half angle was defined by the curve in Figure 106. For example, when the X-24C aircraft is at 10.4 degrees angle of attack (i. e., the angle between the W. L. and the freestream direction is  $10.4^\circ$ ). The equivalent cone half angle is found from Figure 106 as follows:

$$\text{Angle between W. L. and lower surface of fuselage} = 2.8^\circ$$

$$\theta_1 = 10.4 + 2.8 = 13.2^\circ$$

$$\theta_{\text{cone}} - \theta_1 = -0.2^\circ$$

$$\theta_{\text{cone}} = 13.2 - 0.2 = 13.0^\circ$$

Transition distances summarized in Figures 107, 108 and 109 were obtained from the two equations noted above, using the equivalent conical flow correlation shown in Figure 106.

LI-900 Thickness Calculations - A general thermal network of externally insulated skin was generated for the calculation of aluminum skin thermal response with various insulation amounts. The aerodynamic heating rates and trajectory were obtained as described in the "Lockalloy thickness calculations" section.

The thermal properties of both the aluminum skin and the LI-900 were varied with temperature during the analyses. The effective aluminum skin

SYM	M <sub>0</sub>	REF	CROSS SEC.
○	10	NASA TMX TPT1	FORE BODY 1
□	10	" " "	" " 2
◇	10	" " "	" " 3
△	8	NASA TND 776B	MODEL 9
◊	8	NASA TMX 71971	FOREBODY 1
○	6	" " "	" " 1
◇	4	" " "	" " 1

$\theta_{\text{CONE}}$  = CONE HALF ANGLE IN AXISYMETRIC FLOW.  
 $\theta_1$  = ANGLE BETWEEN BOTTOM OF FUSELAGE & JULET STR AND FREESTREAM DIRECTION

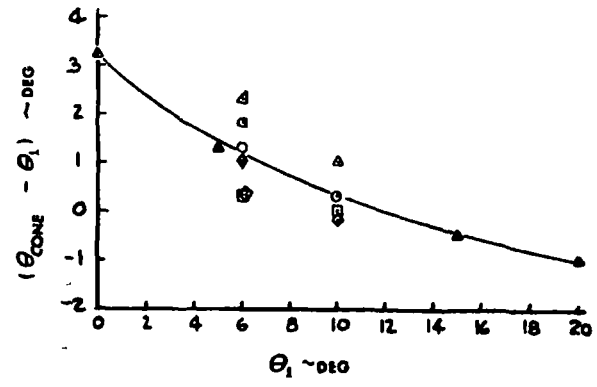


Figure 106 - Conical Half Angle

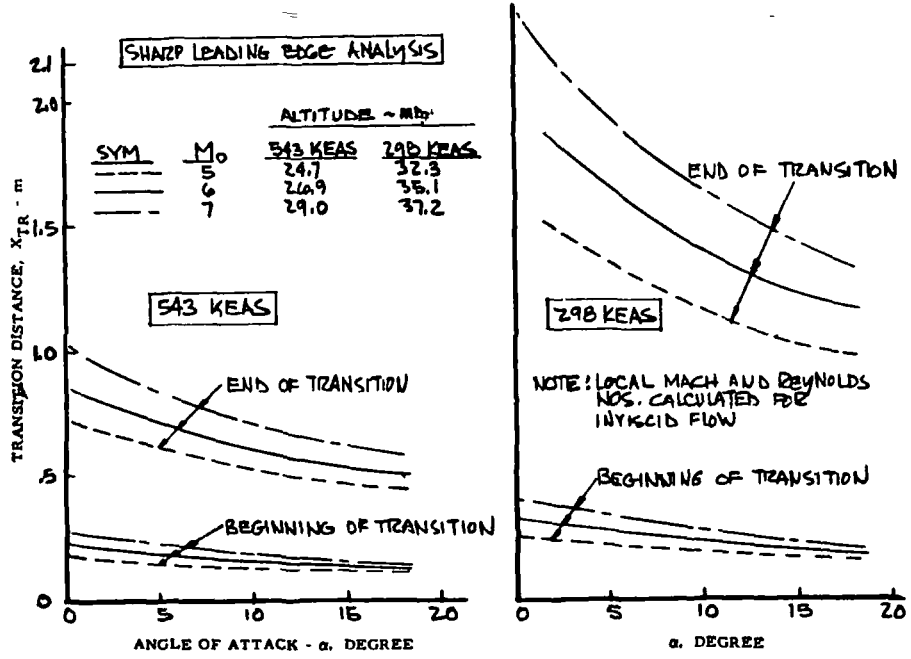


Figure 107 - Axial Distance to Transition Location

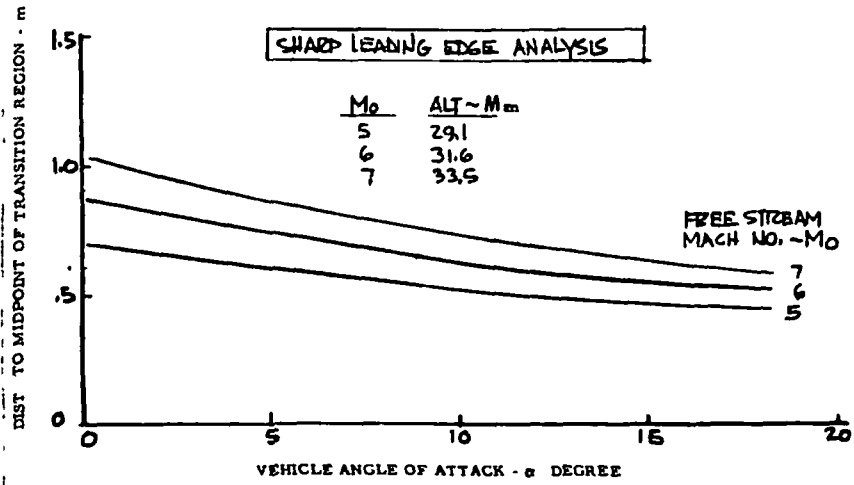


Figure 108 - Axial Distance to Midpoint of Transition - Nominal Flight

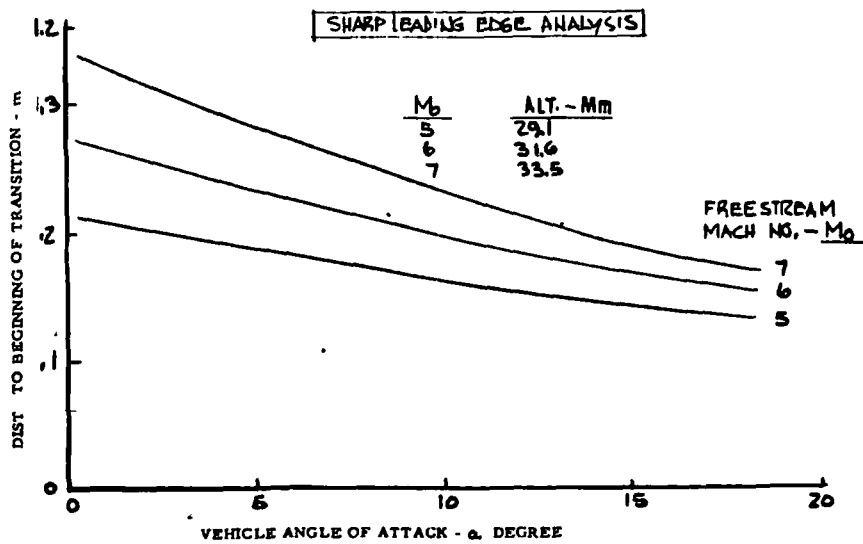


Figure 109 - Axial Distance to Beginning of Transition - Nominal Flight



thickness ( $\bar{t}$ ), which simulates the mass of actual skin plus substructure, was varied with location on the vehicle. No adhesive or other material was assumed under the LI-900, resulting in a slightly conservative estimate of insulation thickness.

Insulation thicknesses were not varied below 5.1 mm, since this is the minimum practical thickness, according to Rockwell International.

Table 24 shows the required LI-900 thickness to maintain a maximum aluminum temperature of 422 K. Also shown is the maximum aluminum temperature attained in areas where the minimum LI-900 thickness was required. At certain locations the analyses were made for multiple values of  $\bar{t}$  in order to evaluate its effect on the aluminum thermal response.

Figures 110 through 113 present the predicted temperature history of the aluminum skin for various locations.

Ablation Material Thickness Analysis - An analysis was undertaken to determine the optimum thickness of a lightweight elastomeric Ablator material considered for use as a thermal protection system (TPS) to ensure that the backup aluminum skin temperature is less than 422 K during the expected life of the X-24C vehicle. The study consisted of gathering physical and thermal properties of the elastomeric Ablator, calculating ablation and pyrolysis rate parameters, and using an ablation computer program to calculate the transient response of the Ablator and the backup aluminum skin. The results were cross-plotted to determine the required ablation material thicknesses for several locations on the vehicle for the maximum heating mission. The mission and heating rates used were similar to those described in the Lockalloy thickness section. The specific material analyzed was Martin Marietta SLA-220.

Representative thermal properties were required to accurately define the transient response and to determine the rate of pyrolysis (charring). The thermal properties used for SLA-220 were estimated from data presented in Reference 10.

Location (Element No)	$\bar{t}$ (in)	0.8" Min Thickness		0.4" Min Thickness	
		Insul. Thick. (in)	Atom. Thick. Temp. (°F)	Insul. Thick. (in)	Atom. Thick. Temp. (°F)
41	.05	.34	300	.40	265
22	.05	.26	300		240
46	.05	.30	300		240
	.075	.20	300		180
	.10	.20	250		155
159	.05	.21	300		195
17 (away from fin)	.08	.20	205		150
17 (near fin)	.08	.20	240		120
48 (away from fin)	.12	.20	195		120
" (near fin)	.12	.20	225		135
29	.05	.35	300		275
7	.05	.20	260		155
1	.05	.20	250		155
8	.05	.20	240		160
194 (near fin)	.05	.43	300	.43	300
194 (away from fin)	.05	.375	300	.40	285
196 (near fin)	.10	.22	300		200
196 (away from fin)	.10	.20	255		175
204	.10	.20	275		165
4	.07	.20	225		140
11	.07	.20	230		140
177 (near fin)	.05	.53	300	.53	300
177 (away from fin)	.05	.475	300	.475	300
99 (end of ramp)	.08	.40	300	.40	300
99 (left end of ramp)	.08	.30	290	.40	190

Location	$\bar{t}$ (in)	Insul. Thick. (in)	Atom. Thick. Temp. (°F)	Insul. Thick. (in)	Atom. Thick. Temp. (°F)
49	.07	.20	250	.40	160
106	.08	.20	270		175
	.12	.20	205		135
	.16	.20	170		120
113	.05	.36	300		280
115	.08	.20	230		150
117	.05	.20	240		165
92	.05	.39	300		295
85	.05	.38	300		285
96	.05	.375	300		285
	.075	.27	300		220
	.10	.23	300		185
91	.08	.24	300		210
	.12	.20	270		160
	.16	.20	230		135
99	.08	.20	170		120
77	.08	.20	280		150
78	.07	.20	300		190
132	.08	.21	300		190
	.12	.20	235		150
	.16	.20	195		120
140	.05	.55	300		270
91	.05	.41	320	.41	300
C142	.10	.20	265	.40	300
179	.05	.43	300	.43	300

\*Note: Thicknesses shown in inches.

Table 24 - LI-900 Insulation Thermal Results

- o LR-99 ASCENT
- o HIGH  $\alpha$ , 60° BANK DESCENT
- o HEATING RATES FROM NASA
- o NO INTERNAL HEAT TRANSFER
- o LI-900 BOND MAT'L IGNORED

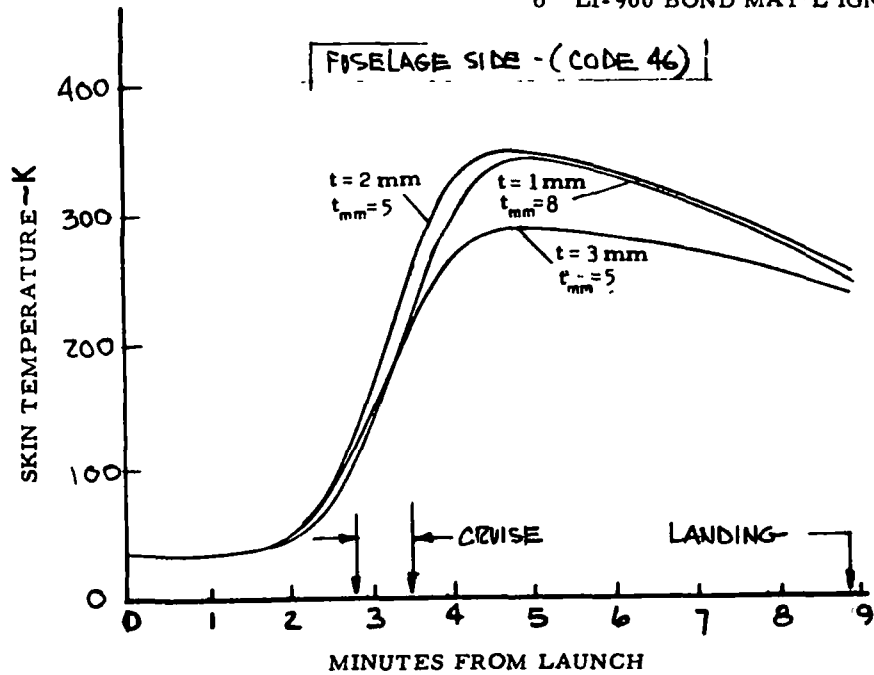


Figure 110 - Temperature History, Fuselage Side - Aluminum/LI-900 Design

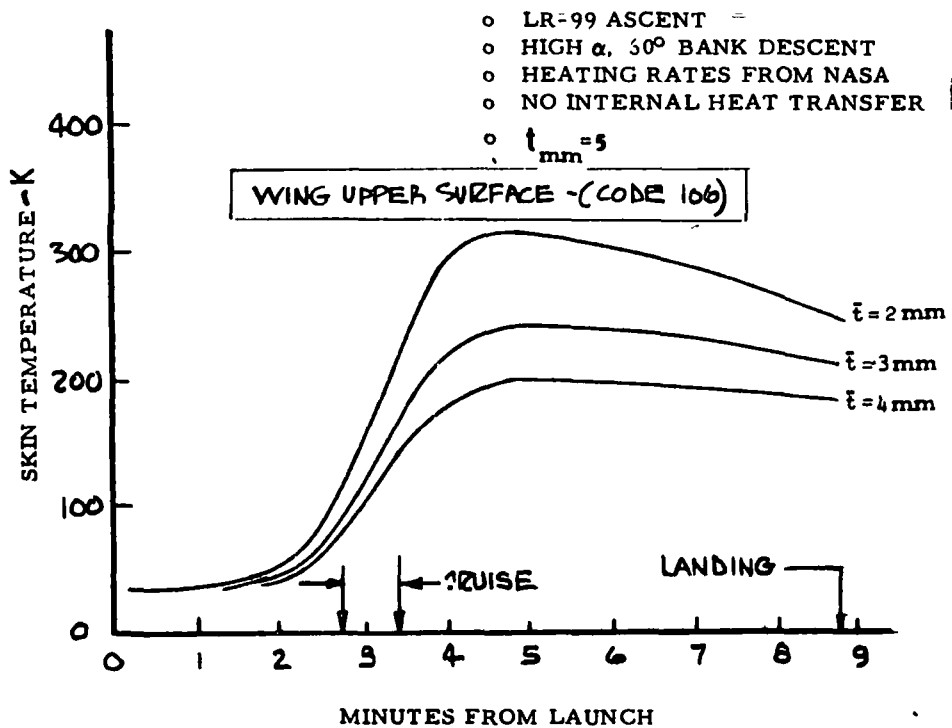


Figure 111 - Temperature History, Wing Upper Surface - Aluminum/LI-900 Design

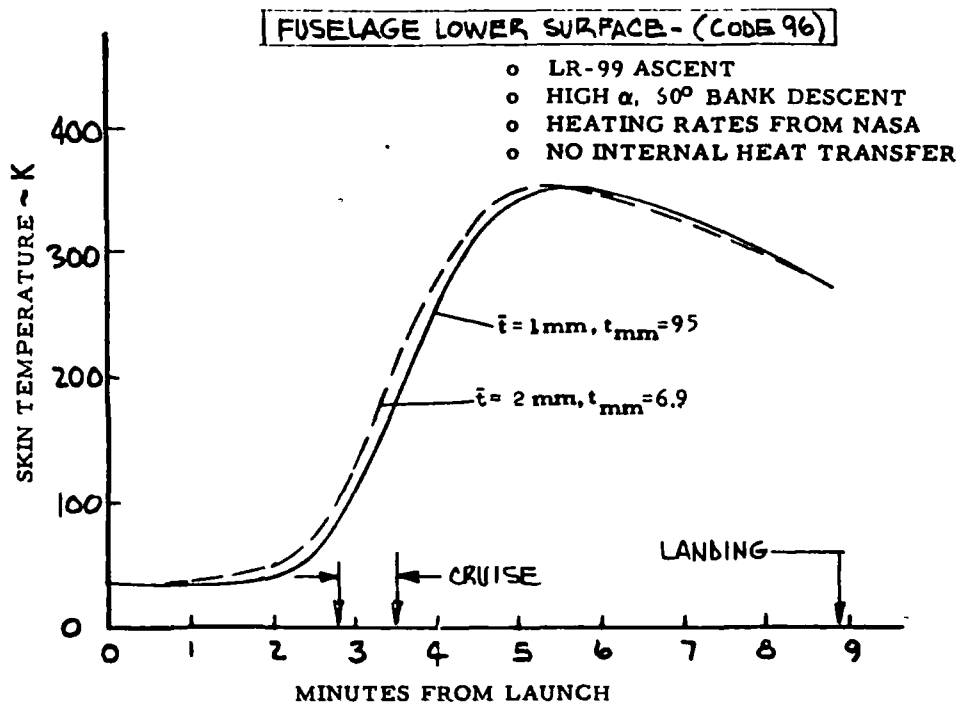


Figure 112 - Temperature History, Fuselage Underside - Aluminum/LI-900 Design

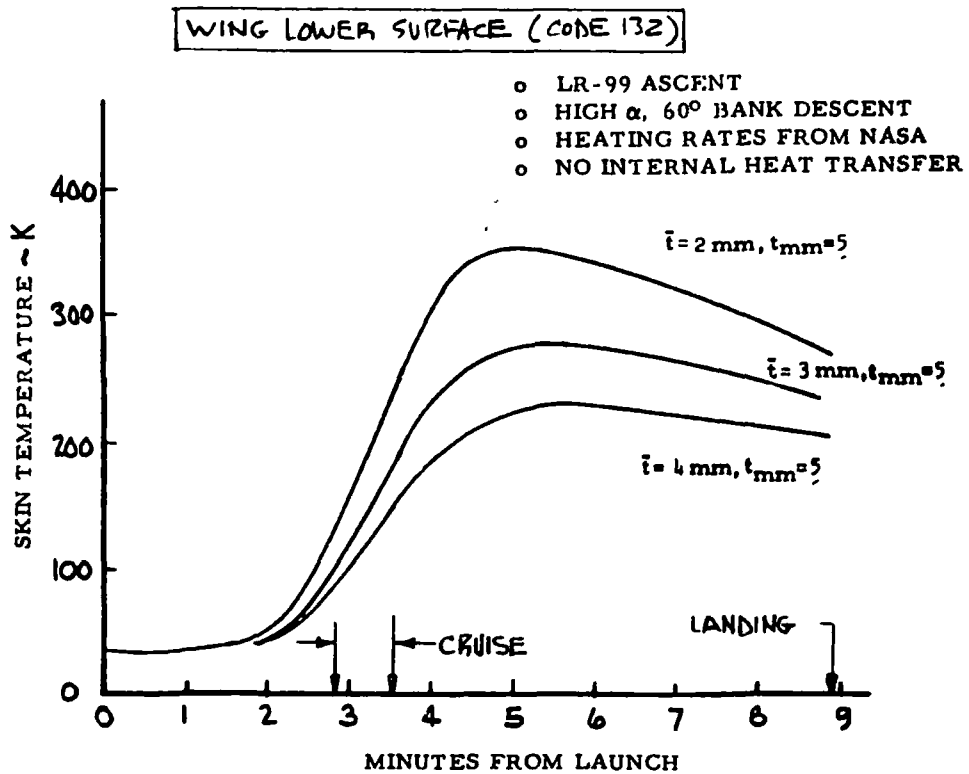


Figure 113 - Temperature History, Wing Lower Surface - Aluminum/LI-900 Design

The parameters necessary to calculate the rate at which the virgin material is converted into char material (rate of pyrolysis) were estimated from a thermogravimetric analysis (TGA). The TGA data was presented as a function of Ablator material temperature for a furnace heating rate of 3°C/minute. The pyrolysis parameters used were as follows:

$$N = 1.0, E/R = 25110 \text{ K}^{-1}, k_0 = 31.5 \text{ sec}^{-1}$$

Other pyrolysis variables required for the thermal analysis were not available and were treated as follows. The heat of pyrolysis as a function of temperature, the generated gas enthalpy as a function of temperature and pressure, and the effect of gas generated on local heat transfer rates were assumed to be zero. These variables reduce the surface heating rate slightly, and assuming them to be zero results in a conservative value for initial virgin material thickness. Also not available was the temperature at which char surface recession occurs (or when the char layer erodes from the material surface). It was assumed that no surface recession occurred at any location on the vehicle.

To compute the temperature response of the ablator-covered skin, a thermal model was set up. Inputs required to analyze the thermal model included: Effective aluminum skin thickness, initial ablator virgin and char material thicknesses, and heating rate data at the point being analyzed for the particular mission being considered. The points analyzed (referred to as vehicle element numbers) and the missions used were discussed in the Lockalloy thickness section. For the computer analysis, it was assumed that no bonding material was present between the ablation material and the aluminum skin.

The computer program utilized for calculating the thermal transients was obtained from LMSC and is called CHIRP IV. The program was modified for in-house use and is now referred as CHIRP V.

Several effective skin thicknesses and thermal radiation view factors were investigated at certain points. In areas of the vehicle where heating rates are

above approximately  $34000 \text{ W/m}^2$ , char material is formed by decomposition of virgin material. The amount of char produced during each flight is a function of the heating rate and amount of char produced on previous flights. The char material formed from previous flights acts as an insulator and tends to reduce the amount of new char material produced on subsequent flights.

To determine the amount of initial virgin material required at each point, the amount of char which will be produced over 100 flights must be found. Several heating rates and initial char material thicknesses were analyzed, and the results are presented on Figure 114. This curve shows that an increase in initial char thickness results in a lower rate of virgin material pyrolysis (char information) per flight. It was assumed for the study that after 100 flights the pyrolysis rate would decrease to approximately 0.1 percent per flight as a result of the increasing char material thickness. (Further analysis indicated that the 0.1 percent value used for the pyrolysis rate was good for more than 100 flights, so the initial char thicknesses assumed were slightly conservative.) The curve presents data to determine the amount of char material to be added to the virgin material, as a function of the maximum heating rate expected during the Mach 6.0 portion of the mission. For heating rates below  $34000 \text{ W/m}^2$ , an insignificant amount of char material was shown to be produced in 100 flights and was, therefore, neglected for the analysis.

Figure 115 shows the transient response of vehicle element number 96 for the first flight (no initial char) and the 100th flight (3.8 mm of initial char). To ensure that the maximum aluminum skin temperature is 422 K or less on the 100th flight, an initial virgin material thickness of 12.2 mm is required. This thickness results in a first flight maximum temperature of 394 K. This figure is typical of the comparison between first and last flight thermal response in areas where char material is formed as a result of aerodynamic heating.

It was assumed that the minimum thickness of elastomeric ablator on the vehicle surface would be 5.1 mm. This minimum thickness results in many areas

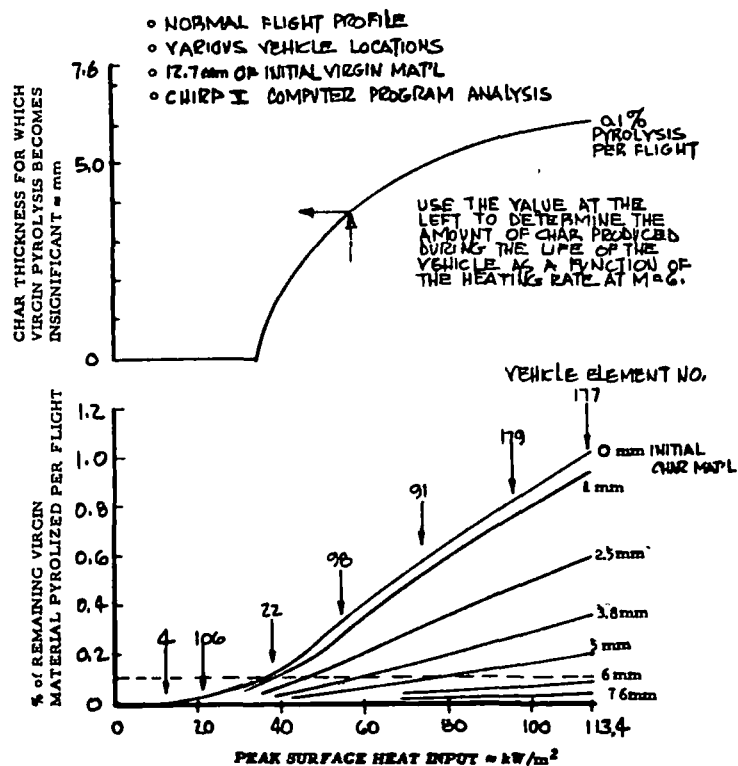


Figure 114 - Effects of Aerodynamic Heating on Ablator Charing Rate

where the maximum aluminum skin temperature is less than 422 K. Figure 116 shows the effect of the aluminum skin thickness on thermal response with 5.1 mm of ablator on the surface at vehicle element No. 106.

At each point, several ablator material thicknesses were analyzed, and the results were cross plotted to obtain a required ablator thickness to limit the aluminum skin to 422 K. Figure 117 shows typical cross plots, made to establish the ablator thickness required or to determine the actual maximum temperature for a given minimum ablator thickness.

**VEHICLE ELEMENT NO. 96**

- BOTTOM CENTERLINE, 7.9 METER AFT OF NOSE
- ALUM SKIN EFFECTIVE THICKNESS IS 14 MM
- SLA-220 TOTAL THICKNESS IS 12 MM.
- INITIAL CHAR REPRESENTS EFFECTS OF SEVERAL PREVIOUS FLIGHTS (100), UNTIL CHAR RATE IS LESS THAN 0.1% PER FLIGHT.
- RADIATION VIEW FACTOR TO OUTER SPACE IS 1.0
- BASED ON NASA PREDICTED HEATING RATES.

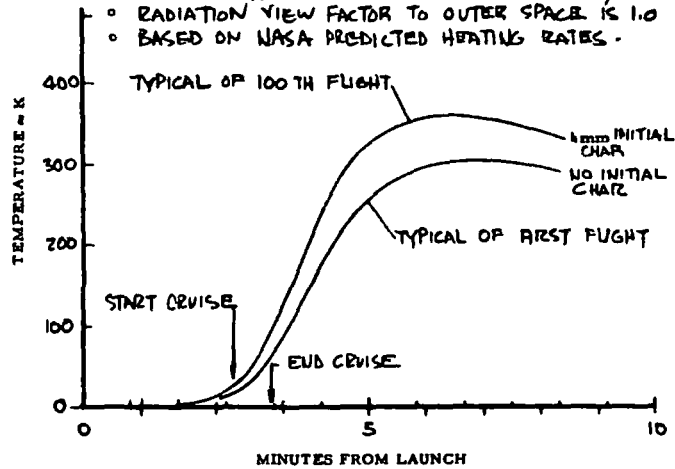


Figure 115 - Effects of Initial Char on Temperature - Aluminum/Ablator Design

**VEHICLE ELEMENT NO. 106**

- SLA-220 THICKNESS IS 5MM
- RADIATION VIEW FACTOR TO OUTER SPACE IS 0.9
- BASED ON NASA PREDICTED HEATING RATES
- NO CHAR FORMATION AT THIS POINT

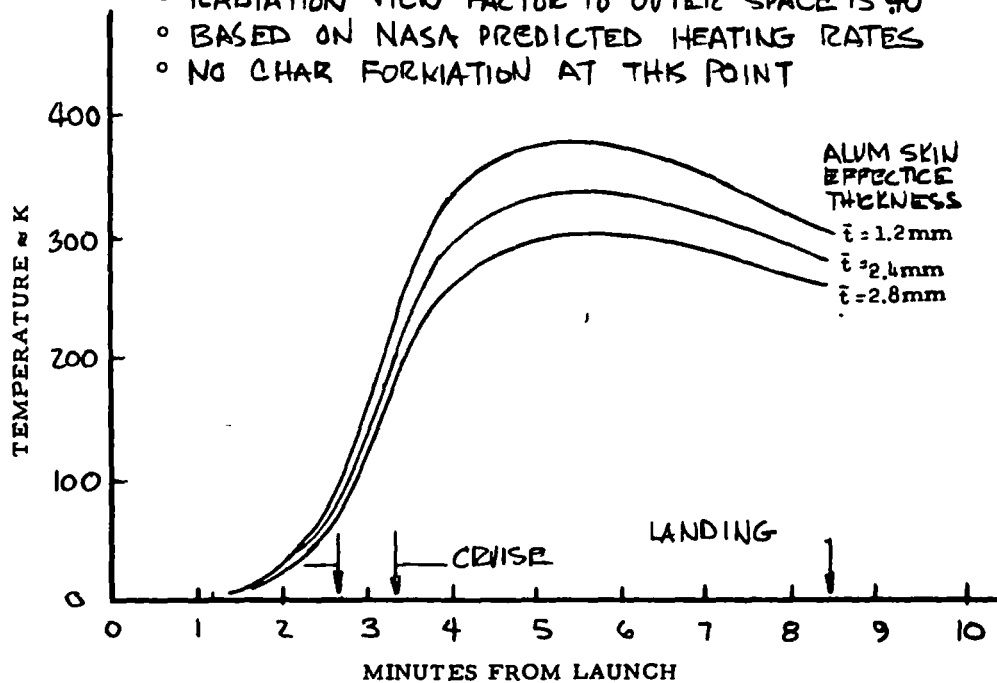


Figure 116 - Effects of Initial Char on Temperature - Aluminum/Ablator Design



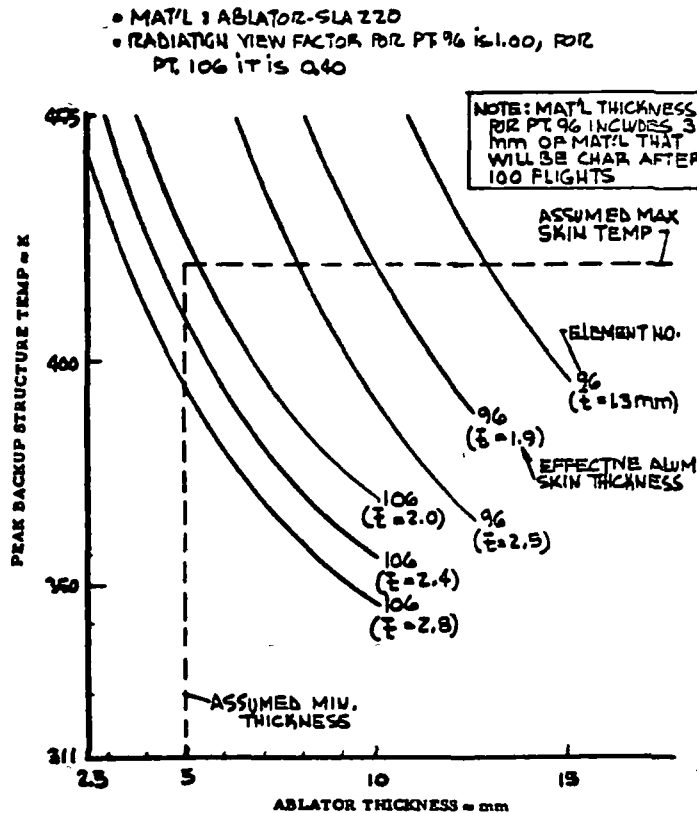


Figure 117 - Estimated Ablator Thickness - Elements 96 & 106

Table 25 presents the results of the ablation thickness analysis. The points are arranged in descending order by virtue of the maximum heating rate at Mach 6. The data is presented for minimum ablator thicknesses of both 5.1 mm and 10 mm.

Leading Edge Thermal Analyses - Leading edge temperatures were computed for both Lockalloy and insulated aluminum. Heating rates were determined by the method of Beckwith, Reference 11, for the stagnation line of a yawed cylinder. The heating distribution around the circumference was taken from Lees, Reference 12. Laminar flow was assumed for the entire proximity of the leading

REPORT NUMBER	LOCATION	SURF AREA SQ. INCHES	0.20" MIN.		0.40" MIN.	
			MAX TEMP °F	TEMP. DIFF. INCHES	MAX TEMP °F	TEMP. DIFF. INCHES
177	WAKE AFT FUSELAGE	0.05	300	0.72	300	0.72
179	"	"	300	0.67	300	0.67
91	"	0.05	300	0.61	300	0.61
29	"	0.05	300	0.57	300	0.57
42	"	0.05	300	0.53	300	0.53
113	"	0.05	300	0.55	300	0.55
85	"	0.05	300	0.52	300	0.52
41	"	0.05	300	0.52	300	0.52
46	"	0.05	300	0.49	300	0.49
"	"	0.05	300	0.51	300	0.51
98	"	0.05	300	0.49	300	0.49
"	"	0.05	300	0.32	300	0.32
"	"	0.05	300	0.37	300	0.37
"	"	0.05	300	0.27	300	0.27
"	"	0.05	300	0.21	300	0.21
194	"	0.05	300	0.57	300	0.57
"	"	0.05	300	0.63	300	0.63
204	"	0.05	300	0.28	300	0.28
140	"	0.05	300	0.47	300	0.47
196	"	0.05	300	0.34	300	0.34
"	"	0.05	300	0.30	300	0.30
46	"	0.05	300	0.42	300	0.42
"	"	0.05	300	0.32	300	0.32
"	"	0.05	300	0.25	300	0.25
22	"	0.05	300	0.38	300	0.38
132	"	0.05	300	0.42	300	0.42
"	"	0.05	300	0.31	300	0.31
142	"	0.05	300	0.34	300	0.34
77	"	0.05	300	0.24	300	0.24
48	"	0.05	300	0.23	300	0.23
"	"	0.05	300	0.29	300	0.29
78	"	0.05	300	0.25	300	0.25
29	"	0.05	300	0.29	300	0.29
"	"	0.05	287	0.20	287	0.20
"	"	0.05	300	0.22	300	0.22

REPORT NUMBER	LOCATION	SURF AREA SQ. INCHES	0.20" MIN.		0.40" MIN.	
			MAX TEMP °F	TEMP. DIFF. INCHES	MAX TEMP °F	TEMP. DIFF. INCHES
106	"	0.08	300	0.21	204	0.10
"	"	0.08	278	0.20	180	
115	"	0.08	250		162	
17	"	0.08	264		148	
"	"	0.08	234		144	
"	"	0.06	300	0.24	208	
"	"	0.07	244	0.20	181	
44	"	0.08	274	0.20	177	
"	"	0.07	300	0.21	199	
"	"	"	283	0.20	180	
8	"	0.05	300		191	
7	"	0.05	245		187	
159	"	0.05	300	0.23	202	
11	"	0.07	270	0.20	177	
"	"	"	250		160	
1	"	0.05	281		180	
3	"	0.072	300		135	
4	"	0.07	253		167	
"	"	0.057	289		190	
117	"	0.05	280		180	
99	"	0.08	190		127	
SLOPE INTERFERENCE AREAS						
48	"	0.07	300	0.43	300	0.43
24	"	0.07	300	0.36	273	0.40
24	"	0.06	300	0.34	261	
17	"	0.06	300	0.24	240	
3	"	0.072	300	0.21	141	
4	"	0.057	300	0.34	209	
SLOPE INTERFERENCE AREAS						
99	"	0.08	300	0.54	300	0.54
79	"	"	300	0.46	300	0.46
204	"	0.125	300	0.46	300	0.46

\*Note: Thicknesses shown in inches.

Table 25 - Ablator Insulation Thermal Results

edge structure, with the minimum heat transfer set at one-tenth the stagnation line value. This minimum value was used for computing the heating to the attached flat surface in the near vicinity of the leading edge. The same trajectory was used as was described in the "Lockalloy Thickness Calculations" section.

The results of these analyses are presented in Figures 118 and 119. The figures show that there would be no problem maintaining acceptable temperature levels with the Lockalloy or high density RSI ( $481 \text{ kg/m}^3$ ) covered leading edge designs, for this mission and the specified geometry. However, mass maybe reduced by use of beryllium segments operating to 922 K for the leading edges.

Possibility exists for the leading edge boundary layer to become turbulent as a result of end effects at the wing-body juncture. Aerodynamic tests will be required to determine these effects.

Substructure Thermal Analyses - An analysis was conducted for the transient heating of the Lockalloy internal frame linkage. Its purpose was to determine whether aluminum links could be used without the possibility of their operating at excessive temperature. A typical location on the vehicle (lower centerline,  $x = 13.7 \text{ m}$ ) was chosen for the analysis.

Figure 120 demonstrates the design of the attachment between the frame and the links, the link temperature should not exceed 350 K during the 40-second cruise mission.

Thermal analyses of various materials frame supports for Lockalloy skins were also conducted. Figures 121 through 126 are presented along with a description of pertinent assumptions.

Temperature analysis of frame supports was also conducted for Lockalloy skins to assess the thermal stress effects between hot exterior surface panels and relatively cooler interior support structure. Two frame concepts were analyzed: A combination stainless steel frame/aluminum cap design, and an

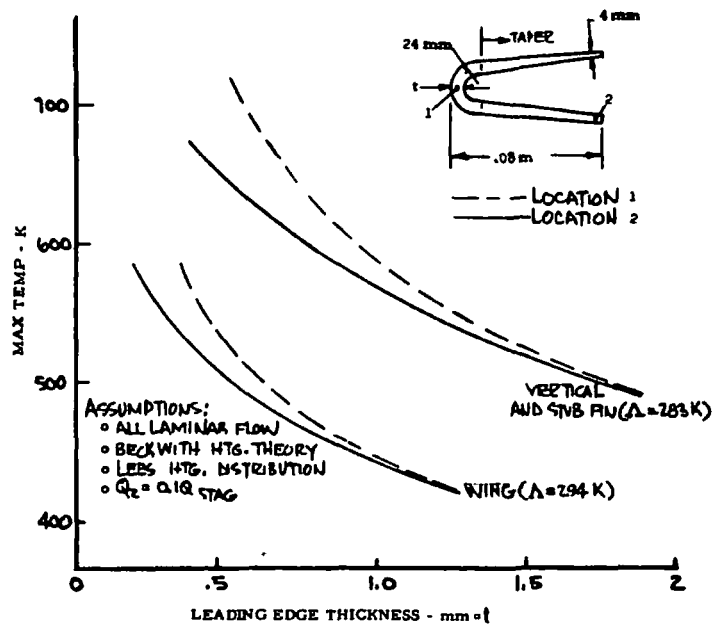
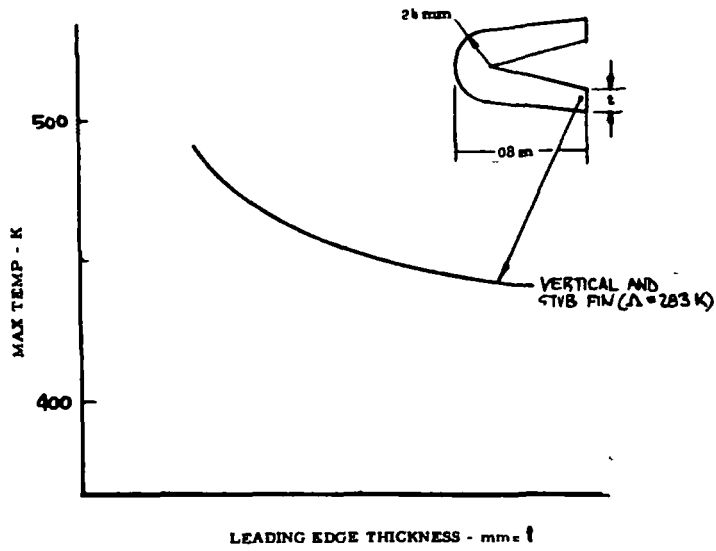


Figure 118 - Peak Temperatures of Lockalloy Leading Edges

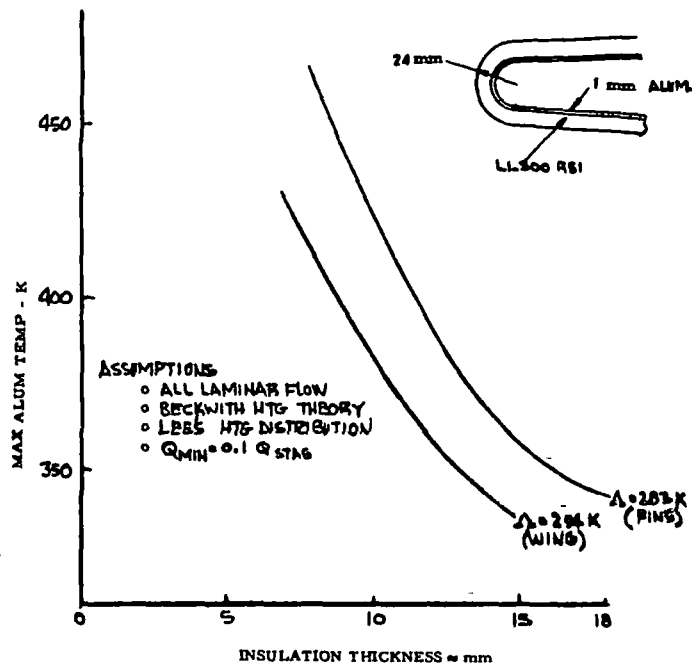


Figure 119 - Effect of Insulation on Aluminum Leading Edge

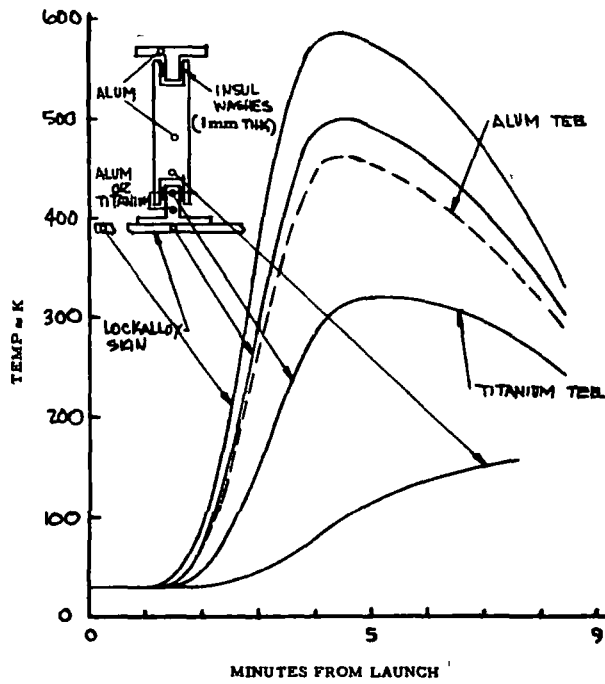


Figure 120 - Thermal Response - Linkage Assembly

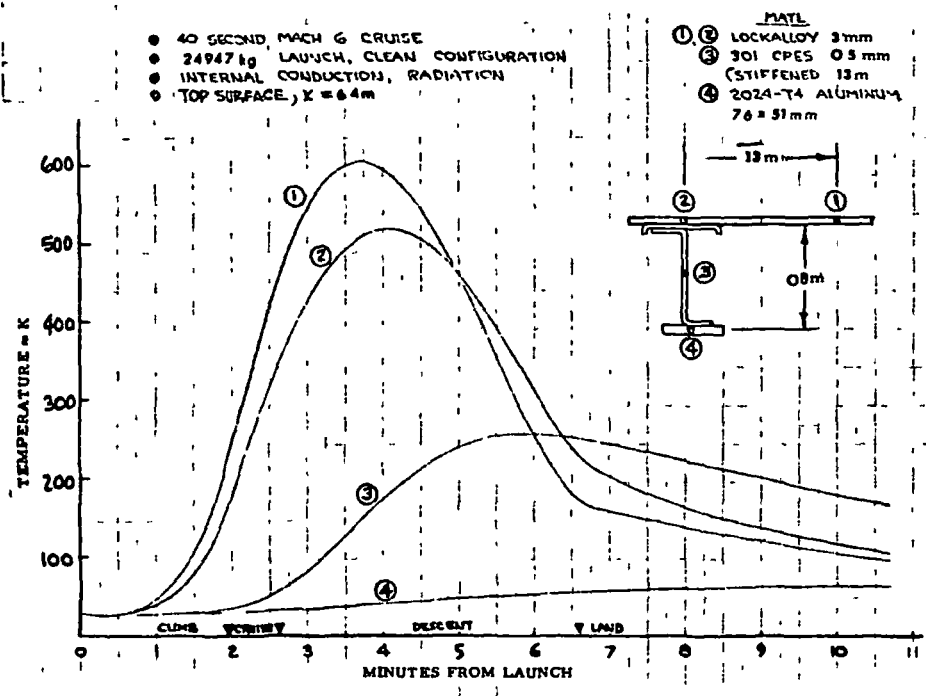


Figure 121 - Lockalloy Supports - Top Surface

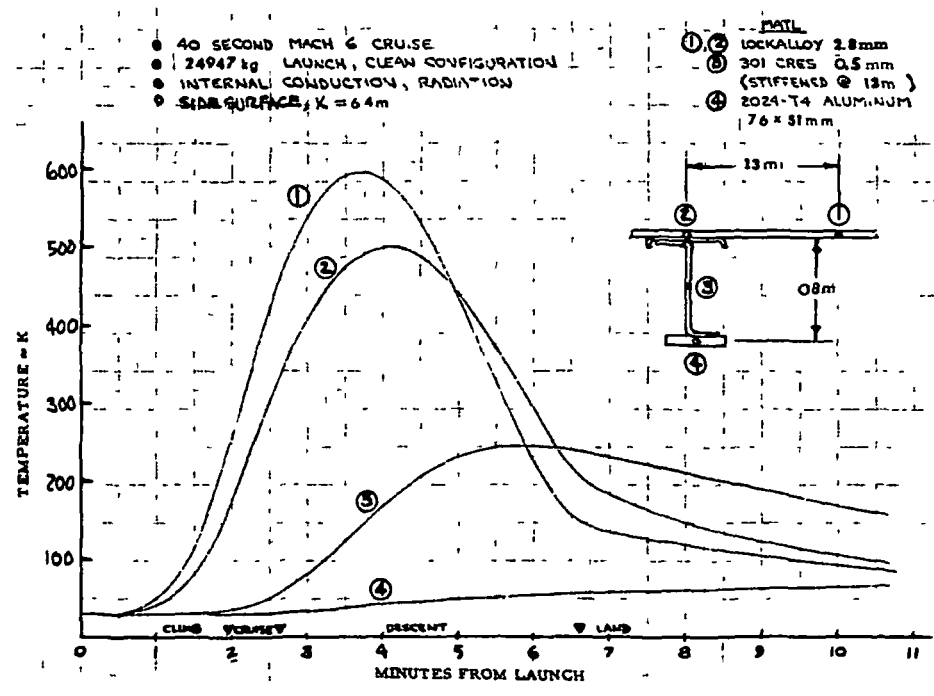


Figure 122 - Lockalloy Supports - Side Surface

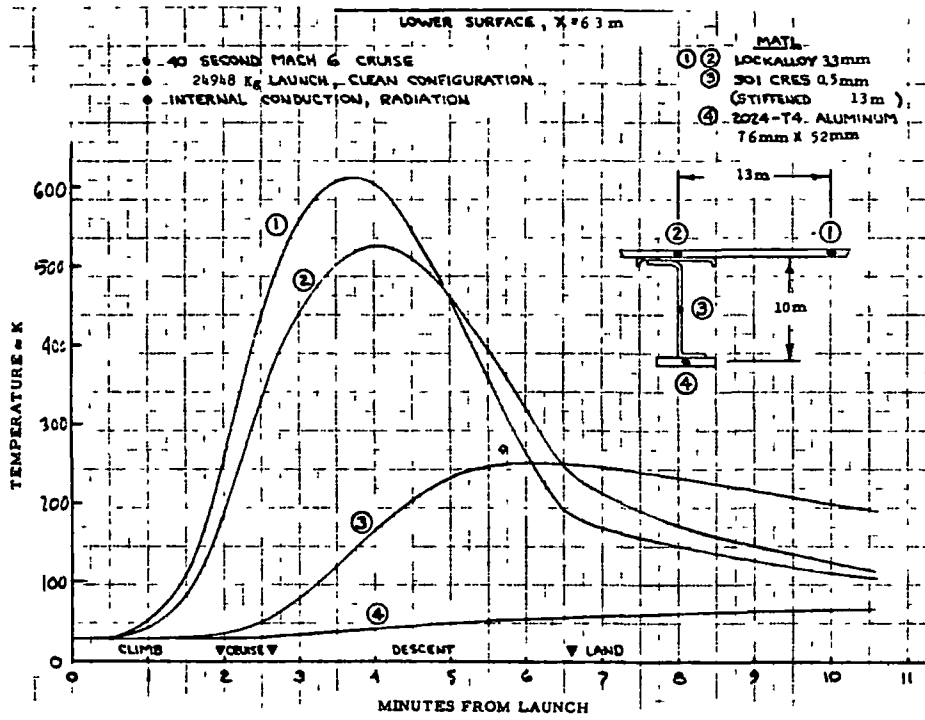


Figure 123 - Lockalloy Supports - Lower Surface

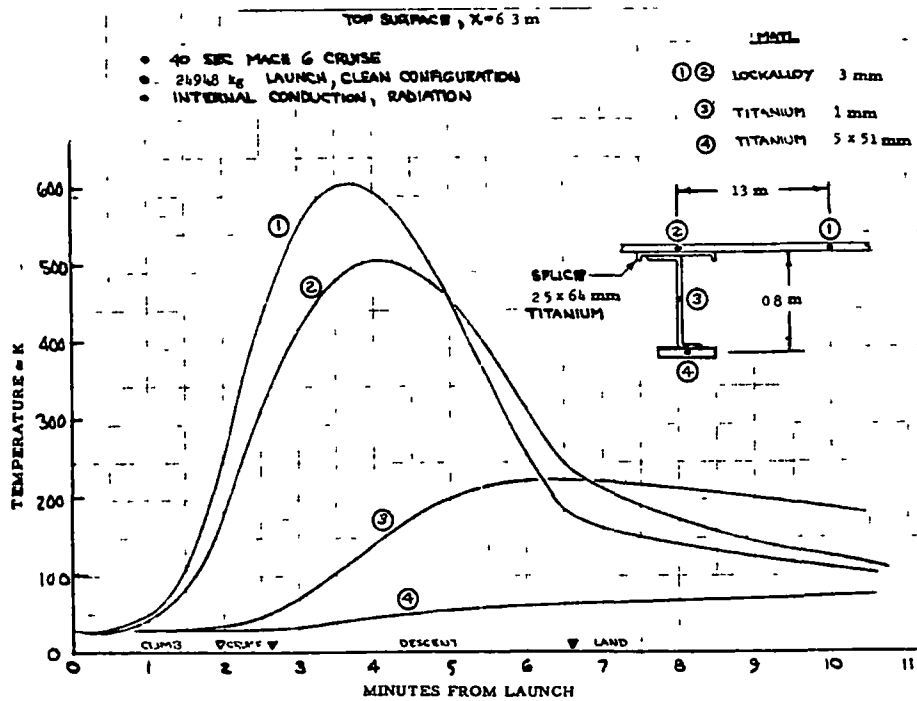


Figure 124 - Lockalloy Supports - Top Surface

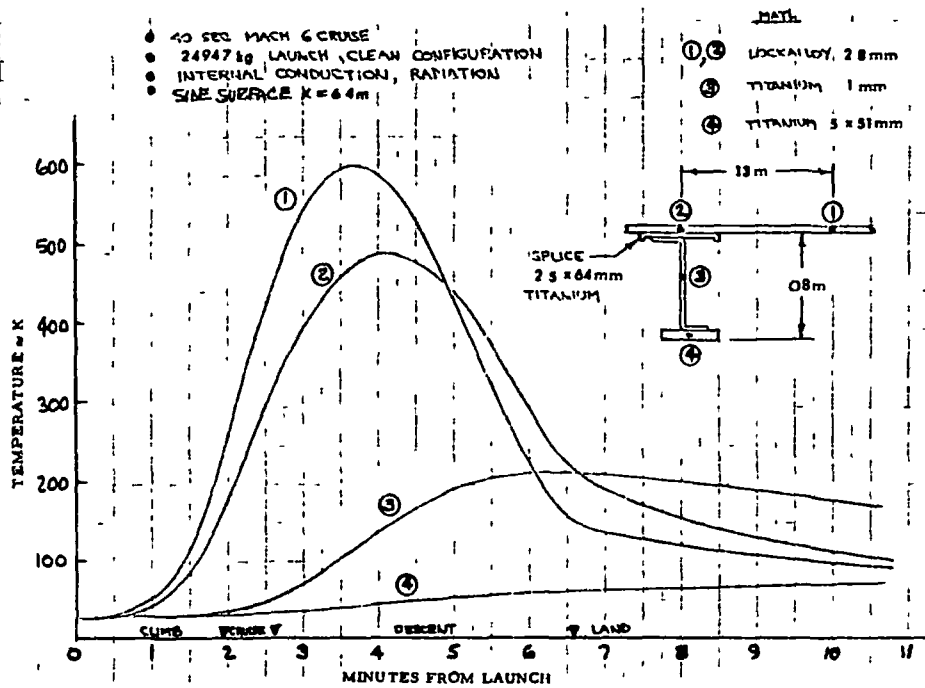


Figure 125 - Lockalloy/Titanium Frames - Side Surface

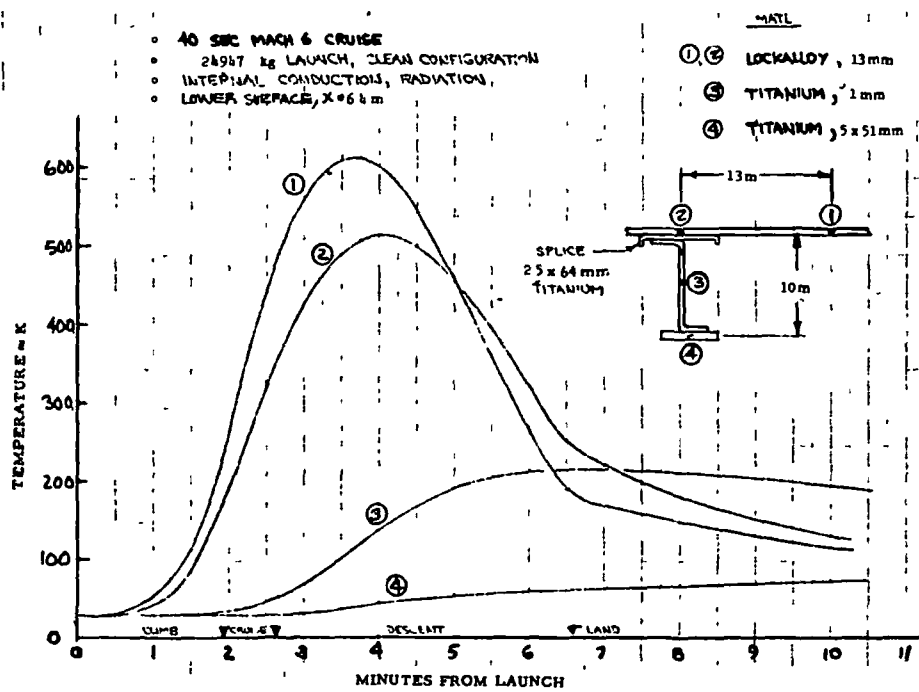


Figure 126 - Lockalloy/Titanium Frames - Lower Surface



all-titanium design. Locations on the top, side, and bottom surfaces of the vehicle, about 6.5 meters back from nose, were examined. A typical 40-second Mach 6 cruise profile was selected and the Lockalloy skin thicknesses were adjusted to yield an approximate 589 K peak temperature in the surface panels.

Figures 121 through 123 show temperature results for the stainless steel/aluminum configuration. Figures 124, 125 and 126 show the same for the titanium configuration. The weak conducting characteristic of both stainless steel and titanium isolates the interior frame cap rather effectively, so that the most interior part of the frame remains near room temperature. This results in a maximum gradient across the frame of about 225K (478 K) for either configuration. The maximum temperature difference between the frame interior cap and the middle of a surface panel is shown to be about 275K (533 K) for either frame configuration.

Shock Wave/Boundary Layer Interaction Around Fins - Analysis based on References 19 through 25. The following conclusions regarding the heating rate increase caused by the shock wave/boundary layer interaction in the vicinity of fins were developed:

- Mach number has little or no effect.
- The fin sweep angle has a strong effect on the heating rate increase; the greater the sweep, the less the heating increase.
- The ratio of boundary layer depth to fin leading edge diameter has a strong effect on the heating rate increase; the greater this ratio, the less the heating increase.
- The angle between the local airflow and side of the fin has a moderate effect on the heating rate increase; the greater this angle, the greater the local heating increase.

A quantitative assessment of the data in these references led to the following maximum values of heating rate increase in each area of shock/boundary layer interaction:

<u>Location</u>	$\frac{h_{\max}}{h_o}^*$
● Adjacent to wing	1.6
○ Forward of canted fin	2.2
● Below canted fin	1.3
● Above canted fin	1.3
● Forward of vertical fin	2.2
● Beside vertical fin	1.3
● Wing and fin surfaces	1.0 (all cases)

The effect that this increase has on the TPS design of each of these locations is reflected in Table 26.

Effects of Heating Rate Uncertainty Factor - Thermal analyses have been conducted to assess the effect of NASA recommended heating uncertainty factors for each TPS scheme. The factors recommended were 1.1 times the predicted heating in areas of laminar flow, 1.25 in areas of turbulent flow, and 1.50 in areas of shock wave/boundary layer interaction.

These factors were applied to the heating rate at example locations on the vehicle where the TPS had previously been sized without any uncertainty considered (basic heating rates from NASA data). Figures 127 through 132 show the effects of these heating factors on skin temperature for each TPS concept.

Since TPS sizing was done without consideration of heating uncertainties, these temperatures represent the maximum overheat values which would result from the specified heating uncertainties. These temperatures were derived without any consideration of relief from lateral conduction, which in certain areas (e. g., shock impingement areas) could appreciably reduce local temperature increases.

---

\*  $h_o$  is the local heat transfer coefficient without regard to any interaction effects.

<u>Location</u>	<u>Effect on Temperature or Design</u>		
	<u>Lockalloy</u>	<u>LI-900</u>	<u>Ablator</u>
o Adjacent to wing	Increases Lockalloy temperature to 589K with no change in thickness from minimum gauge	Increase insulation thickness from 5mm to 7mm near wing	Increase thickness from 7.3mm to 11mm near wing
o Forward of canted	Increases Lockalloy temperature to 600K with no change in thickness from minimum gauge	Increase insulation from 5mm to 7mm	Increase thickness from 5mm to 9mm
o Below canted fin	Increases Lockalloy temperature to 505K with no change in thickness from minimum gauge	Increases aluminum temperature to ~ 422K with no change in insulation thickness from 5mm minimum	Increase thickness from 7.3mm to 8.6mm
o Above canted fin	Same, but only 478K maximum	Same as above	Increase thickness from 6mm to 7.3mm
o Forward of vertical fin	Same, but only 533K maximum	Same as above	No effect
o Beside vertical fin	Same, but only 455K maximum	Same, but increases aluminum temperature to less than 422K	Increase thickness 5mm to 6mm
o Wing and fin surfaces	No effect	No effect	No effect

Table 26 - Shockwave and Boundary Layer Interaction

Vehicle Pressurization Analysis - A brief study was made to determine the feasibility of pressurizing the whole airplane to 6.9 kPa (gauge) to prevent air leakage into the airframe. Based on structural leakage test data obtained from an SR-71 program, it was assumed that an effective leakage area of 45 cm<sup>2</sup> was reasonable. An allowance of 8.6 kg of helium was made for this in the pressurization storage system. It was also assumed that the helium would only be used between M = 2.0 on acceleration and M = 2.0 on deceleration to conserve the amount of helium needed. Ram air could be used at the lower Mach numbers if required.

Oxygen Tank Insulation - An analysis was undertaken to determine the temperature of the structure, such as the inner frame caps, for two surface materials in the vicinity of the liquid oxygen tank. The temperatures were determined for external surface material configurations of 5.1 mm Lockalloy, 5.1 mm LI-900, and 7.6 mm LI-900 with various thicknesses of fiberglass-type insulation (from 0.0 to 51 mm) on the outside of the oxygen tank. In all cases

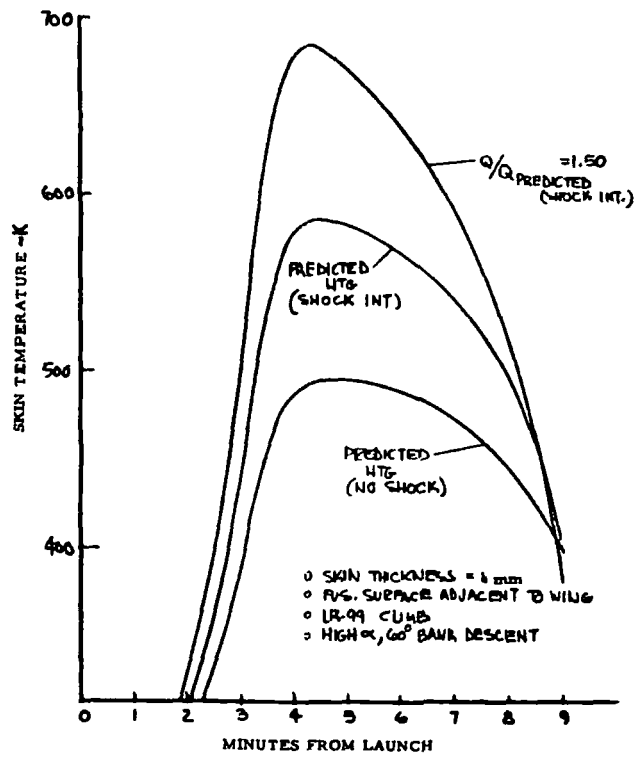


Figure 127 - Effects of Heating Rate Uncertainty Factor on Skin Temperature - Shock Interference Area (Lockalloy Design)

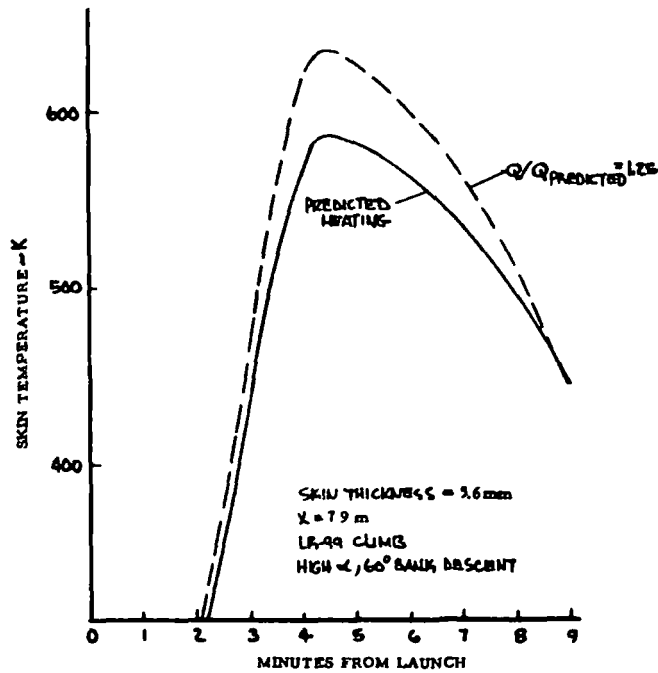


Figure 128 - Effect of Heating Rate Uncertainty Factor of Skin Temperature - Lower Centerline (Lockalloy Design)

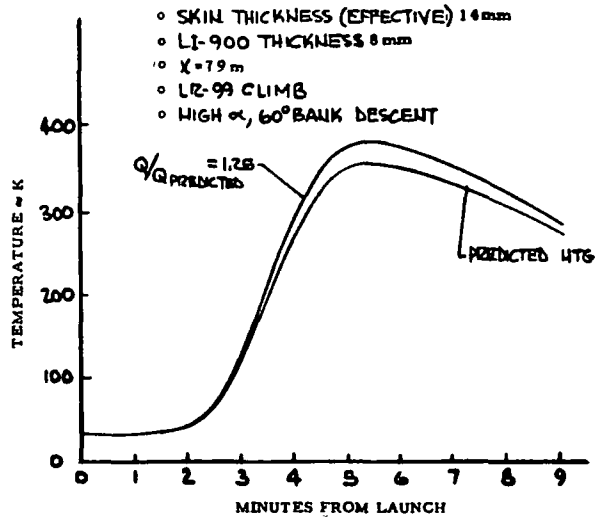


Figure 129 - Effect of Heating Rate Uncertainty Factor on Aluminum/LI-900 - Lower Centerline

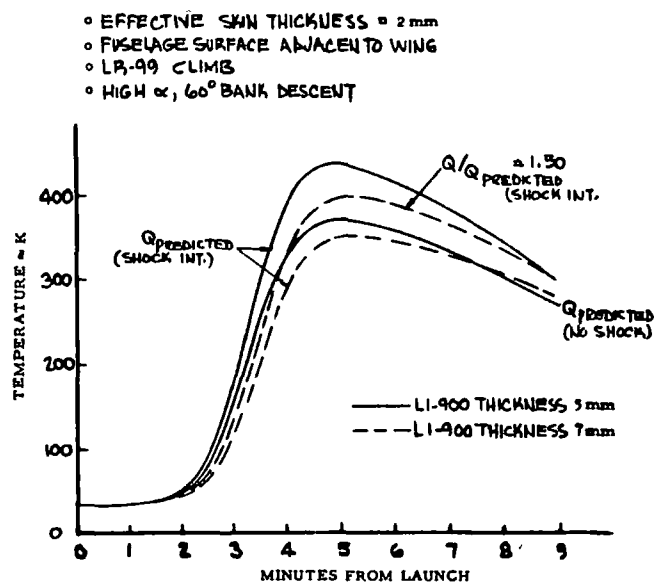


Figure 130 - Effect of Heating Rate Uncertainty Factor on Aluminum/LI-900 - Shock Interference Area

**VEHICLE ELEMENT NUMBER 96**

- BOTTOM CENTERLINE, 19 METERS AFT OF NOSE
- ALUM. SKIN EFFECTIVE THICKNESS IS 15mm
- SLA-220 TOTAL THICKNESS IS 12mm  
(3.5mm CHAR AND 8mm VIRGIN MATERIAL)
- INITIAL CHAR IS FROM EFFECTS OF SEVERAL PREVIOUS FLIGHTS, UNTIL CHAR RATE IS LESS THAN 0.1% PERZ FLIGHT
- RADIATION VIEW FACTOR TO OUTER SPACE IS 1.0

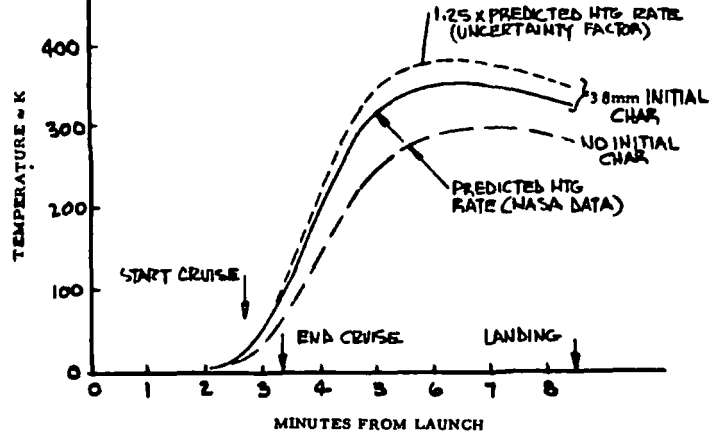


Figure 131 - Effect of Heating Rate Uncertainty Factor on Aluminum/Ablator

**VEHICLE ELEMENT NUMBER 48**

- FUSELAGE SURFACE ADJACENT TO WING
- ALUM. SKIN EFFECTIVE THICKNESS IS 2mm
- SLA-220 TOTAL THICKNESS IS 11mm  
(2.5mm CHAR AND 8mm VIRGIN MAT'L.)
- INITIAL CHAR IS FROM EFFECTS OF SEVERAL PREVIOUS FLIGHTS, UNTIL CHAR RATE IS LESS THAN 0.1% PERZ FLIGHT
- RADIATION VIEW FACTOR TO OUTER SPACE IS 0.50

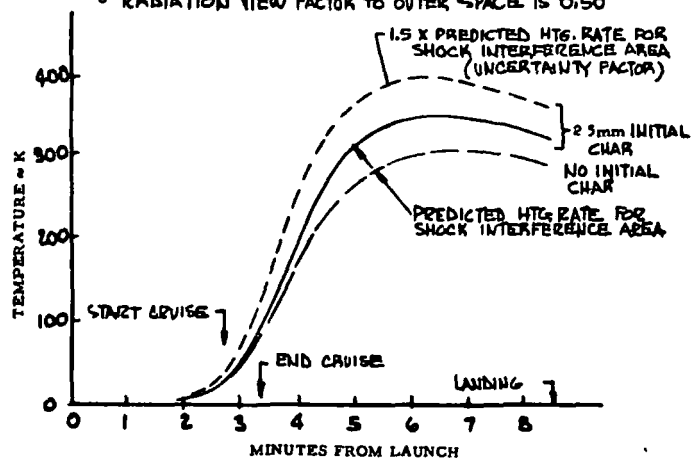


Figure 132 - Effect of Heating Rate Uncertainty Factor on Aluminum/Ablator - Shock Interference Area

the external surface is assumed to be a constant temperature of 244 K. Thus a temperature gradient is established through the wall and the temperature of structural elements between the outer surface and the lox depends on the amount of insulation on the tank.

The temperatures were calculated utilizing the Lockheed Thermal Analyzer computer program, based on the following assumptions:

- Steady-state temperatures during mated operation above 10970 meter (duration of carryout and heat sink potential of liquid oxygen would result in steady-state temperatures).
- External surface is always 244 K during mated operation above 10970 m for each wall construction.
- Free convection heat transfer coefficient between the inner surface of the outer structure and between the outer surface of the insulation on the oxygen tank surface is  $5.7 \text{ W/m}^2 \cdot \text{K}$ .
- Emissivity of internal surface of external skin is 0.30 (semi-clean alclad aluminum).
- Emissivity of the structure located between the outer skin and tank is 0.30.
- Emissivity of oxygen tank insulation surface is 0.10 (foil).
- Oxygen tank wall temperature is constant at 89 K.
- Lockalloy skin thermal conductivity is  $69 \text{ W/m} \cdot \text{K}$ .
- LI-900 insulation thermal conductivity is  $0.043 \text{ W/m} \cdot \text{K}$ .
- Fiberglass-type oxygen tank insulation thermal conductivity is  $0.026 \text{ W/m} \cdot \text{K}$  for 16 to  $32 \text{ kg/m}^3$  density at about 172 K.

Figures 133 and 134 indicate that increasing the oxygen tank surface insulation thickness increases the minimum temperature of structure located in the

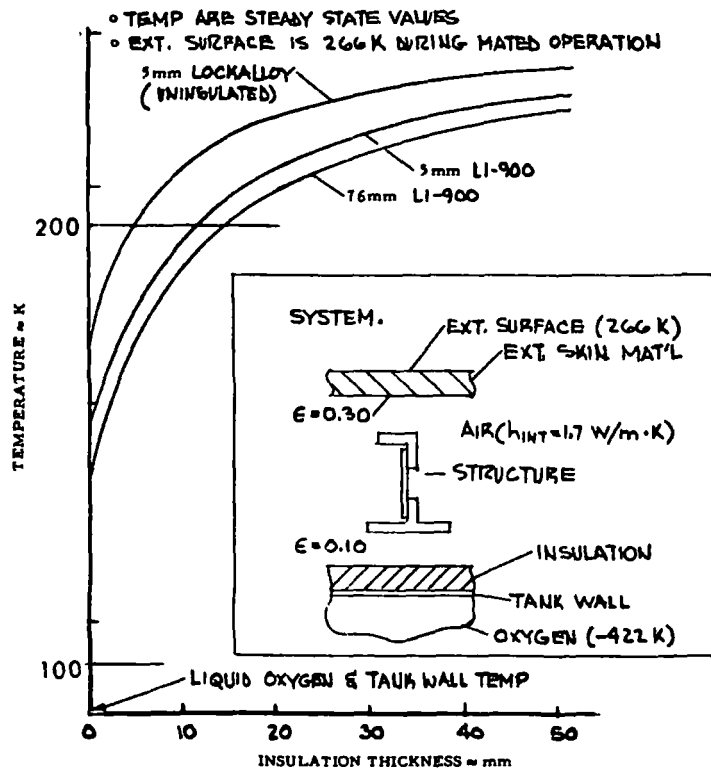


Figure 133 - Oxygen Tank Insulation Study

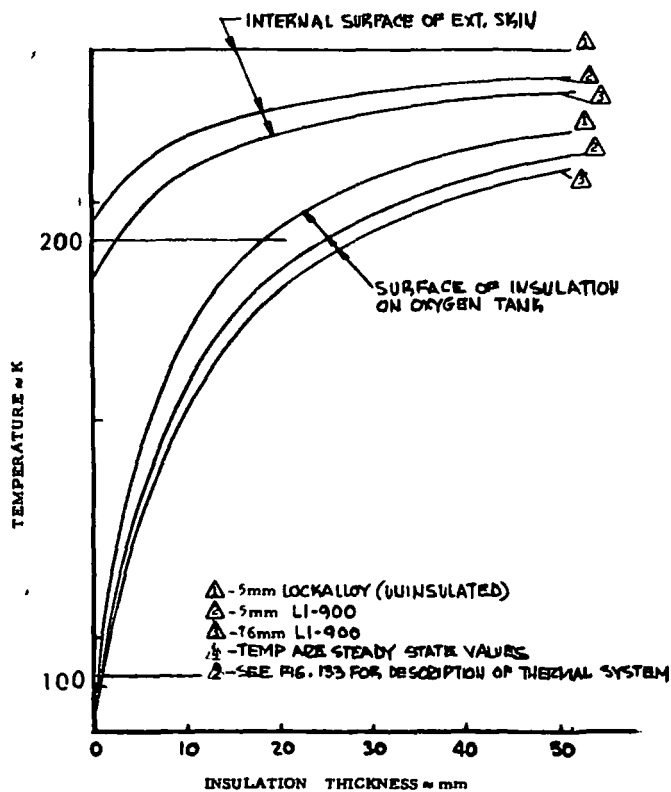


Figure 134 - Oxygen Tank Insulation Study



cavity. Using 33 mm of insulation assures that structure temperatures for members placed between the outer surface of the aircraft and the tank are close to or above 219 K in the vicinity of the oxygen tank.

Elevon and Rudder Thermal Analyses - Computations to determine the Lockalloy thickness requirements on control surfaces were made for the speed brake requirements. Calculations of the local flow conditions showed that none of the design conditions resulted in separation of the boundary layer, Reference 20, for the elevons. Heating rates were computed by the Spalding and Chi turbulent heating theory by using boundary layer edge properties from oblique shock theory and assuming that the boundary layer originated at the flap hinge line, Reference 21. Figure 135 presents the Lockalloy temperature as a function of its thickness for the elevon.

Local flow conditions for the rudders indicated that the boundary layer would separate at the flap. This results in high localized heating in the region of flow reattachment. Many literature sources on turbulent boundary layer separation indicate a relationship between peak heating and peak pressure of the form

$$\frac{h_{\text{peak}}}{h_o} = \frac{P_{\text{peak}}^n}{p_o}$$

where subscript "o" pertains to conditions just prior to separation. From Reference 21,  $n = 0.85$ , and this value was used in the analyses.

Extensive data collected at Mach 6 and 8, and ramp angles ranging from 5° to 30°, with the boundary layer separated, indicated that the peak pressure at reattachment closely matched the oblique shock value on the ramp, Reference 23, therefore the analysis was made with that assumption.

In order to ascertain the extend of surface over which the reattachment heating rate might be assumed to exist, a Lockheed analysis method was used to

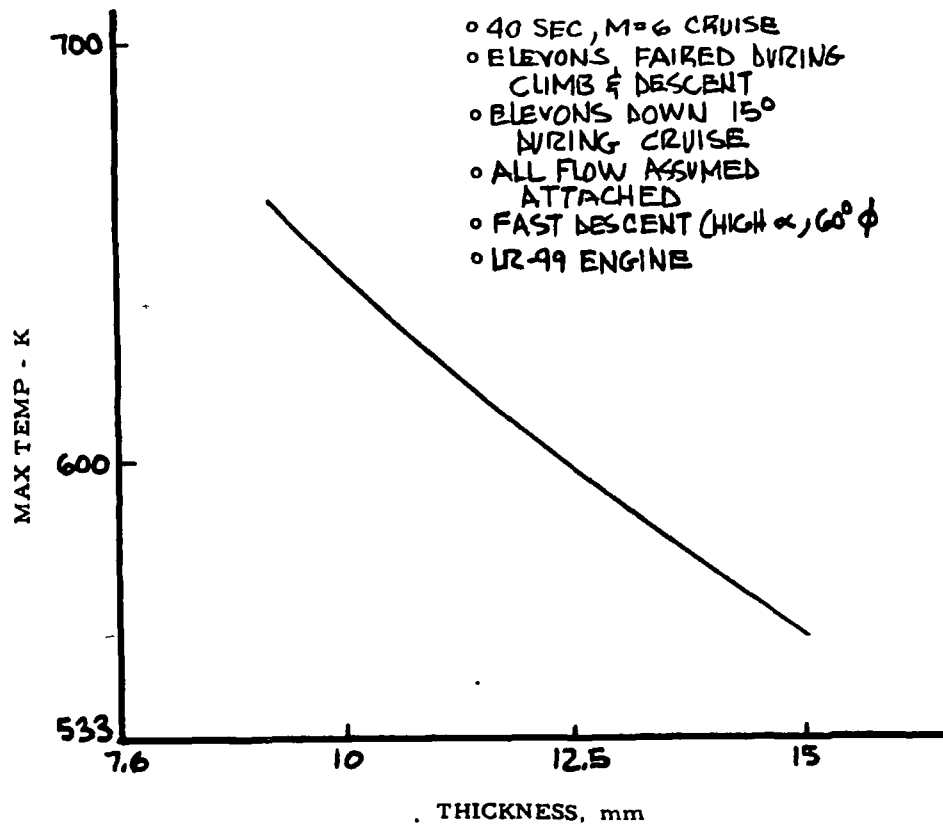


Figure 135 - Effects of Lockalloy Maximum Temperature on Windward Side of Elevon

approximate the length of the upstream and downstream interaction lengths. The calculations indicated a reattachment length of 0.38 m for a local flap angle of  $35^\circ$  during Mach 6 cruise. This means that the zone of high, reattachment heating is of sufficient size that local conduction away from the area should be neglected when sizing the TPS requirements.



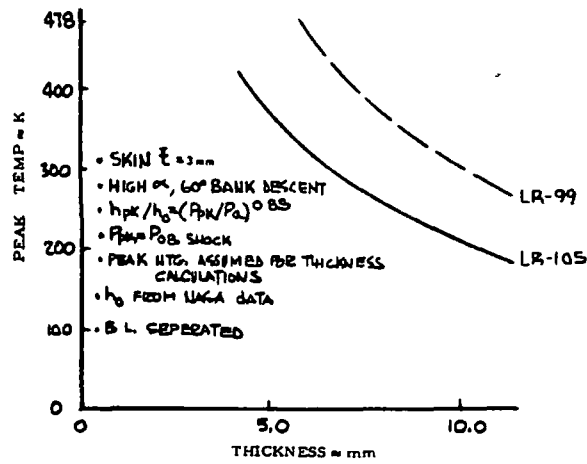


Figure 136 - Effect of LI-900 Thickness in Flow Reattachment Area of Rudder

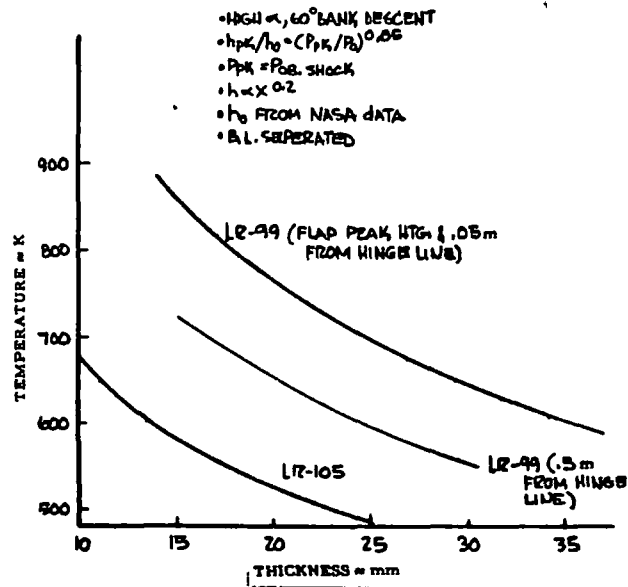


Figure 137 - Effect of Lockalloy Thickness in Flow Reattachment Area of Rudder

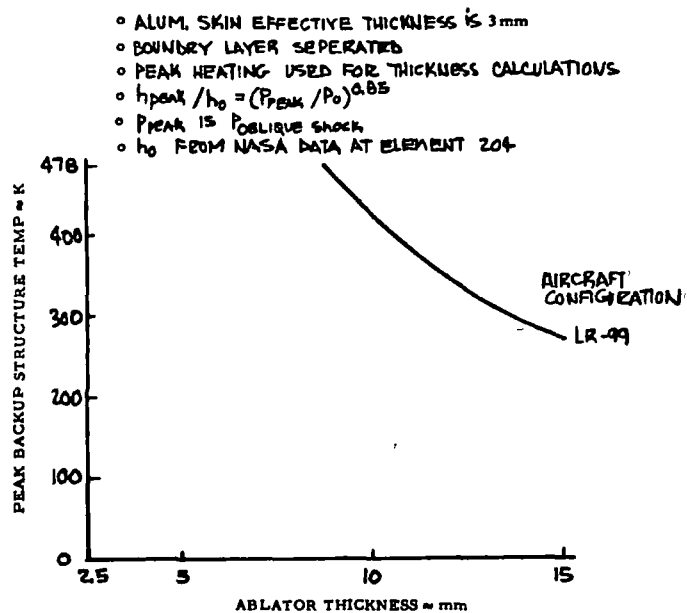


Figure 138 - Effect of Ablator Thickness in Flow Reattachment Area - Speed Brake

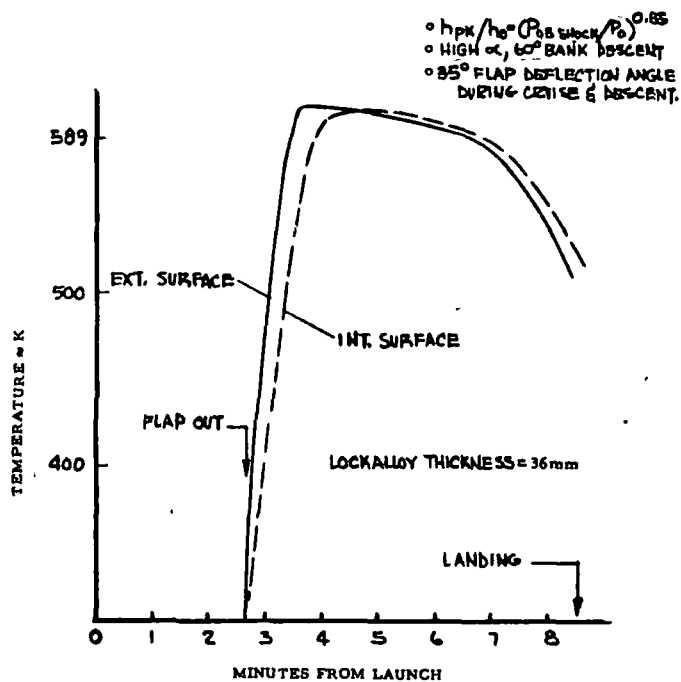


Figure 139 - Thermal Response of Lockalloy Rudder Flaps

- Touch-down attitude 15° nose up
- MLG length (desired) 1.65 - 1.98 m  $\phi$  trunnion to  $\phi$  axle
- MLG tire number single
- NLG length 1.29 m maximum  $\phi$  trunnion to  $\phi$  axle
- NLG tire number dual

Load Requirements - Load requirements for the MLG and NLG included:

- MLG energy/gear =  $\frac{10890}{2} \times (3.0)^2 / 2 = 24500 \text{ N} \cdot \text{m}$
- Assume 2 g average over stroke =  $\frac{24500}{\left(\frac{10890}{2}\right) \times 2 \times 9.81}$   
= 0.229 m stroke minimum
- MLG static air pressure @ 5.52 MPa =  $\frac{12000}{800} = 0.00968 \text{ m}^2$   
= 0.0555 m piston radius
- NLG static load =  $\frac{10890 \times 9.81 \times 0.58}{612} = 10100 \text{ N}$
- NLG sink rate (rotation) @ 3 seconds - 15° + 8° (nose down)  
= 23° rotation
- NLG 6.22 m rotation arm =  $2.44 \text{ m} \frac{\text{Vertical}}{3} = 0.813 \text{ m/s}$
- NLG design sink rate =  $\frac{10100 \times (3.0)^2}{2 \times 9.81} = 4630 \text{ N} \cdot \text{m}$
- 2 g average over stroke =  $\frac{4630}{2 \times 10100} = 0.229 \text{ m min. stroke}$
- NLG static air pressure @ 5.52 MPa =  $\frac{10100}{5.52 \times 10^6} = 0.00183 \text{ m}^2$   
= 0.024 m piston radius

Gear System Survey - A review of approximately 70 gear designs was made, many of which were rejected because (1) item was no longer available, (2) excessively over or understrength, and (2) unique design would not conveniently fit the requirements. From the remaining designs the following candidates were selected:

- | <u>NLG</u>           | <u>MLG</u>           |
|----------------------|----------------------|
| ● USAF C-140A        | ● USAF F-106         |
| ● Grumman Gulfstream | ● Grumman Gulfstream |
| ● USAF F-106         | ● USAF F-102         |
| ● USN F-4            | ● USN F-4            |

NLG Location Selection - Previous USAF studies on the growth potential of the X-24B research vehicle concept, References 10 and 44, depicted the NLG forward of the cockpit. Studies conducted herein, using existing NLG concepts indicated that NLG placement forward of the cockpit produced an unnecessary constraint to the X-24C. The design investigation revealed that in order to fit the gear within the aerodynamic envelope, established by NASA, and the structural/TPS concepts defined for this study, the NLG trunnion would have to be located within the minimum envelope of the cockpit. The solution would have required a shift rearward or upward of the cockpit envelope, resulting in a violation of the aerodynamic envelope.

To avoid an aerodynamic shape revision, the NLG was located between the aft wall of the cockpit and forward structural break of the payload bay, as depicted in Figure 141. This arrangement permits the NLG mount to share existing structural frames and thereby provides the lightest vehicle forebody construction. Also, the arrangement produces the minimum NLG door size requiring special TPS treatment and sealing along the door/opening edges.

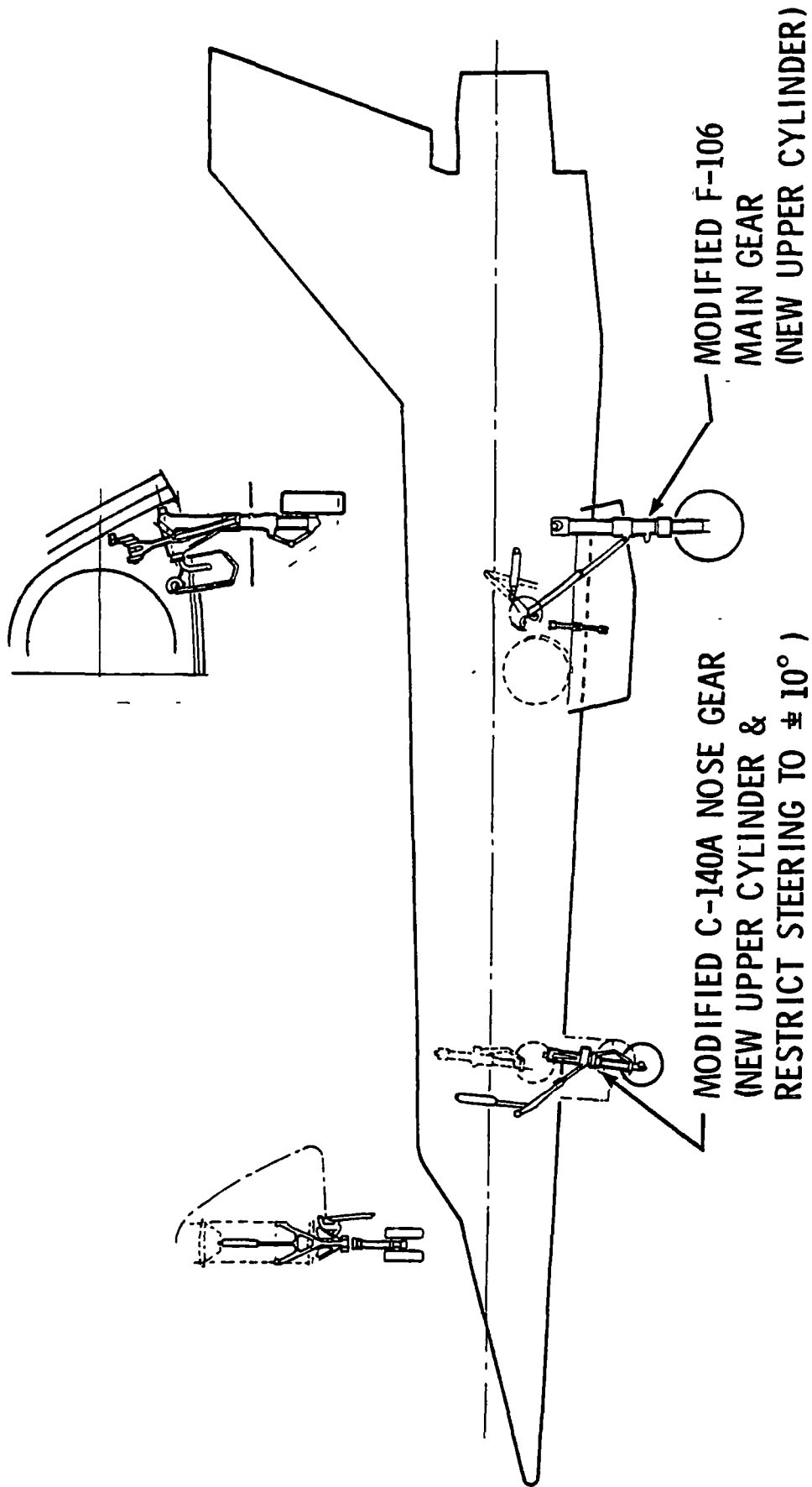


Figure 141 - Landing Gear Arrangement



Location of the NLG aft of the cockpit will permit the nose area to use as an equipment bay, enhancing both installation and servicing of these systems due to the ease of access afforded by this location.

NLG Selection - The C-140A NLG, Figure 142, was selected as (1) the lightest of the candidates, (2) over-all dimension fit the requirement/vehicle best, (3) its stroke/piston fit the requirements and has a 20% growth potential, and (4) is presently in production and available.

MLG Selection - The F-106 MLG, Figure 143, was selected (1) because of its availability from USAF inventory, (2) its stroke/piston fit the requirements and has a 30% growth potential, and (3) its over-all dimensions and single tire fit the requirement/vehicle. Even though the selected concept was the third lightest of the four candidates the lightest, the Grumman design, incorporates a dual tire arrangement which could not be accommodated within the X-24C envelope. The second lightest, the F-102 concept, was found to have marginal strength and shock absorption capability, therefore has no growth capability.

Gear Modification - All gears reviewed, including the selected concepts assumed that the internal parts will be retained as is, but a new outer cylinder would be required. Also, for the MLG, a new retracting mechanism must be adapted to the vehicle. The new outer cylinder is necessary, for both NLG and MLG, to provide trunnion points compatible with the X-24C structure.

Selected gears will not require drop of strength testing (qualification), since X-24C loads and energy absorption are lower than the proven gear requirements.

#### Propulsion System Installation

No particular problems were uncovered during installation development of the proposed propulsion system for either of the three structural concepts. Installation concepts are typical for all three vehicle structural arrangements with minor differences due to the difference in frame spacing or skin/TPS concepts. The following installation considerations apply to the propulsion systems.

Payload Bay Fwd Frame

Cockpit Aft Frame

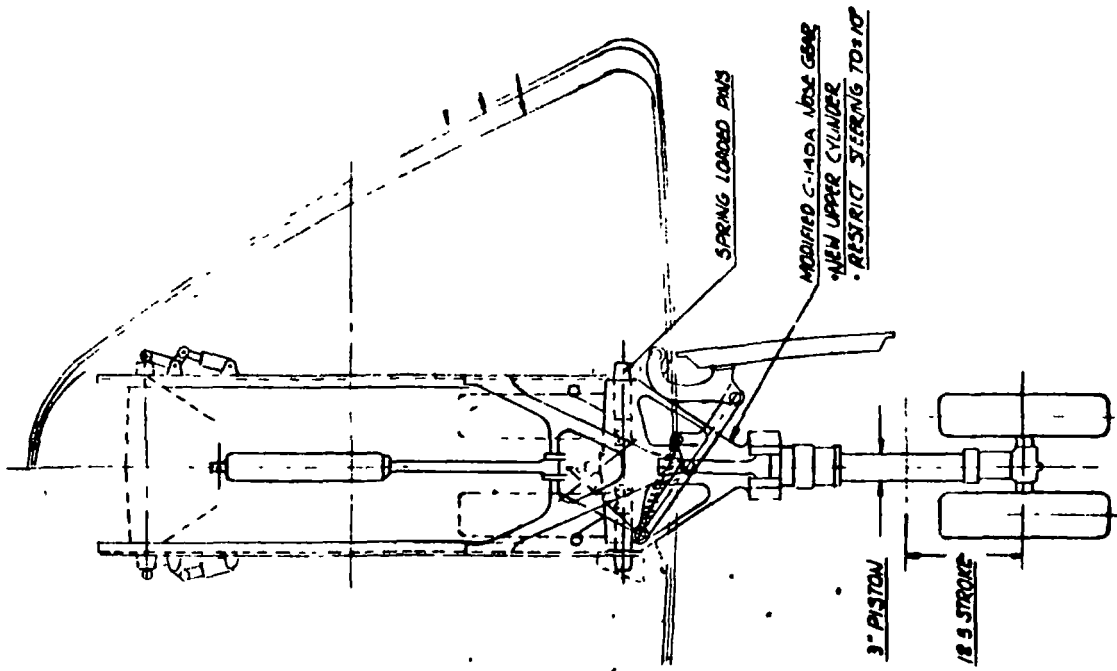
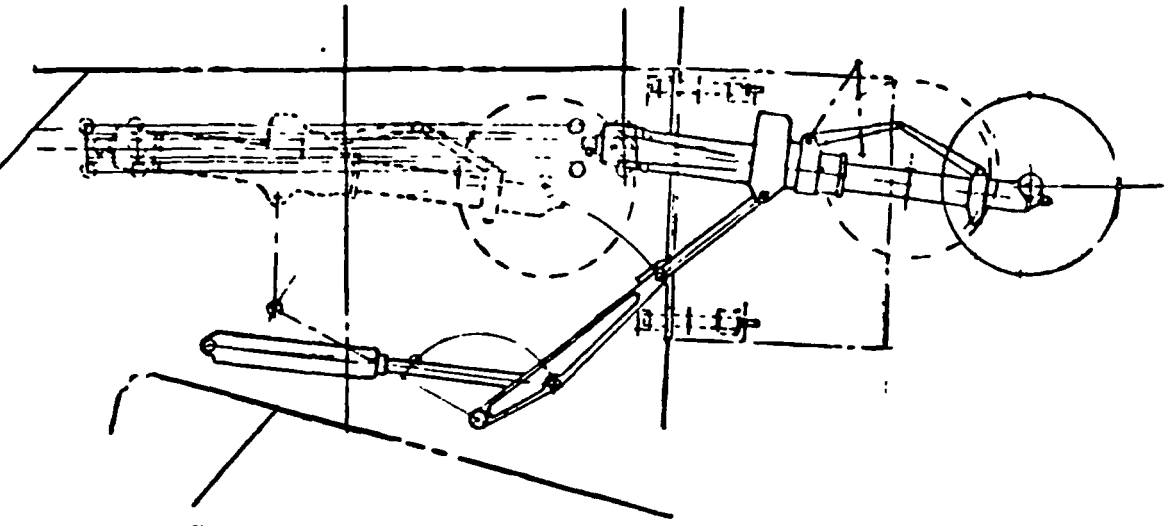


Figure 142 - Nose Gear Installation

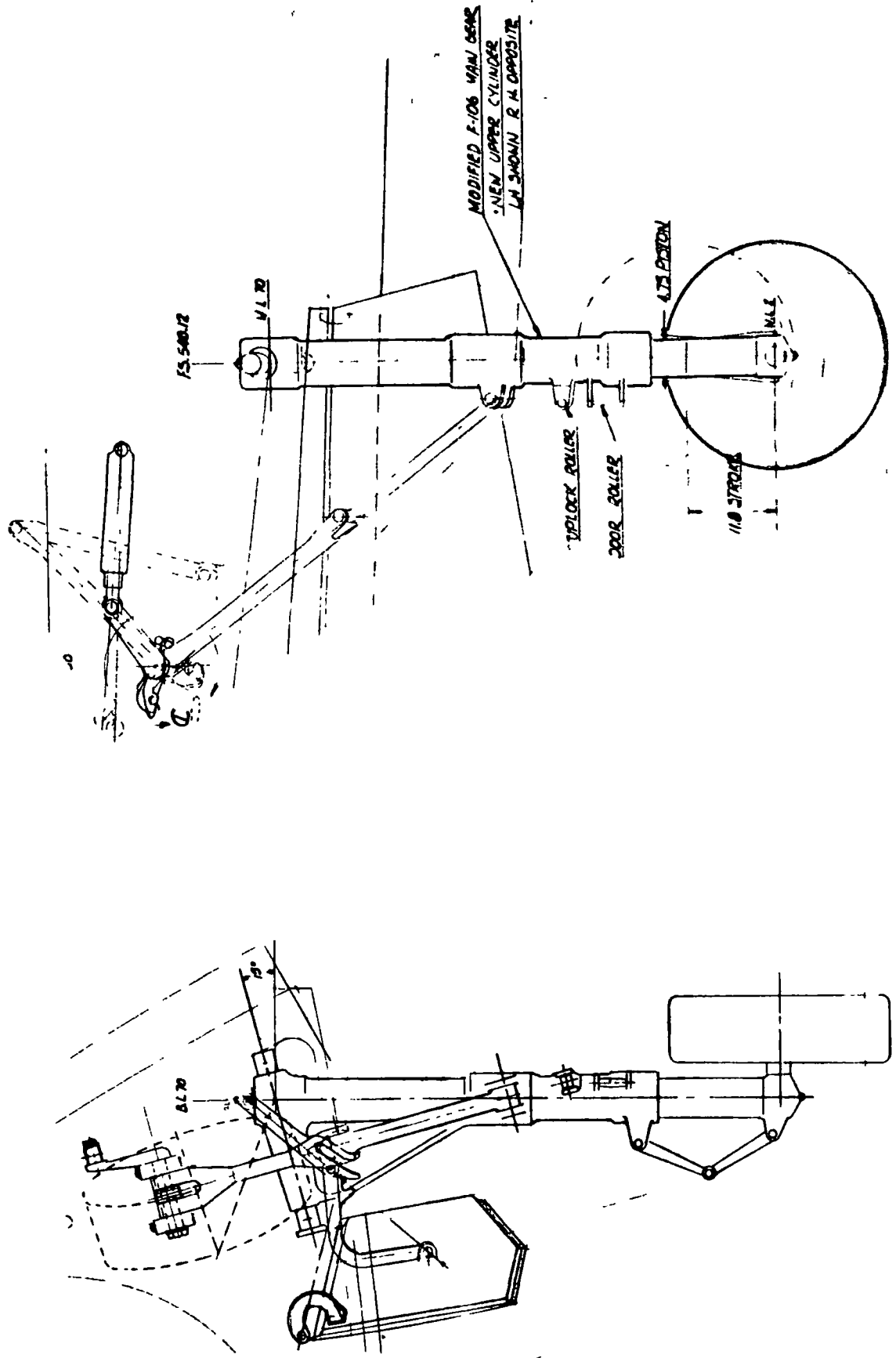


Figure 143 - Main Landing Gear Installation

LR-105 Rocket Engine - Engine installation, conceptual installation reflected in Figure 144, will utilize the same mounting provisions, on the engine, used in the Atlas rocket installation. To stabilize the aft end of the engine in the horizontal position on the X-24C, as opposed to the vertical position on the Atlas installation, and to reduce the vibratory deflections between the engine and aircraft structure, a modification to the engine is required. Two ears must be added to the engine exhaust shroud to provide additional means of attachment to the vehicle.

LR-99 Rocket Engine - Engine installation, conceptual installation reflected in Figure 145, will utilize a mounting scheme similar to the concept employed on the X-15. The volumetric differences between the X-24C and X-15 around the engine prevent use of the X-15 mount. However, the X-24C engine mount will be similarly constructed and configured to fit the X-24C structure. The rearward shift of the engine depicted in Figure 145 represents the shift required to accommodate the fuel cell change discussed in the "Propellant Tankage Volumetric Analysis." Its only impact on the engine installation is the foreshortening of the engine mount tubular legs.

LR-11 and LR-101 Sustainer and Vernier Engines - Conceptual installation depicted in Figures 146 and 147 will position these engines on either side of the main engine mounted to the aft vehicle frame. Engine exhaust nozzles are positioned so that their exhaust plumes do not impinge on the main engines.

Engine and Vehicle Seals - An engine shroud, Figure 147, extending from the aft vehicle frame will enclose both main engines and sustainer or vernier engines. Openings are provided at the aft end for the engine(s) exhaust ports. To compensate for engine(s) expansion and deflections and the shroud opening a thermal seal, depicted conceptually in Figure 148, is required. This seal requirement applies to all three structural concepts.

Scramjets - Structural provisions, Figure 149, for installation of the baseline three (3) module scramjet assembly were based on the criteria set forth in

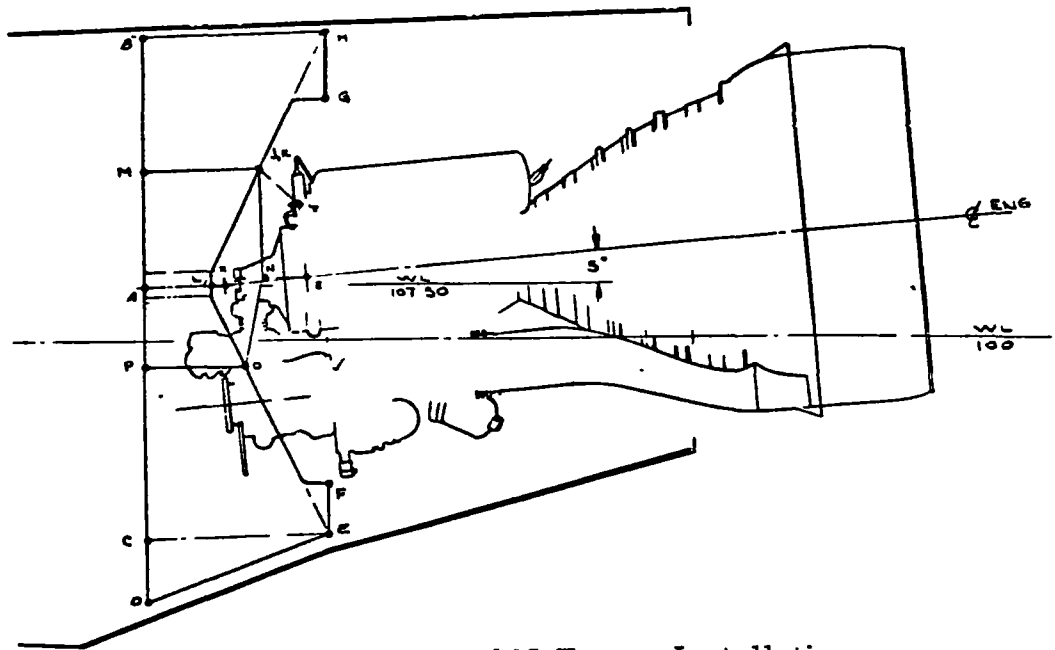


Figure 144 - LR-105 Engine Installation

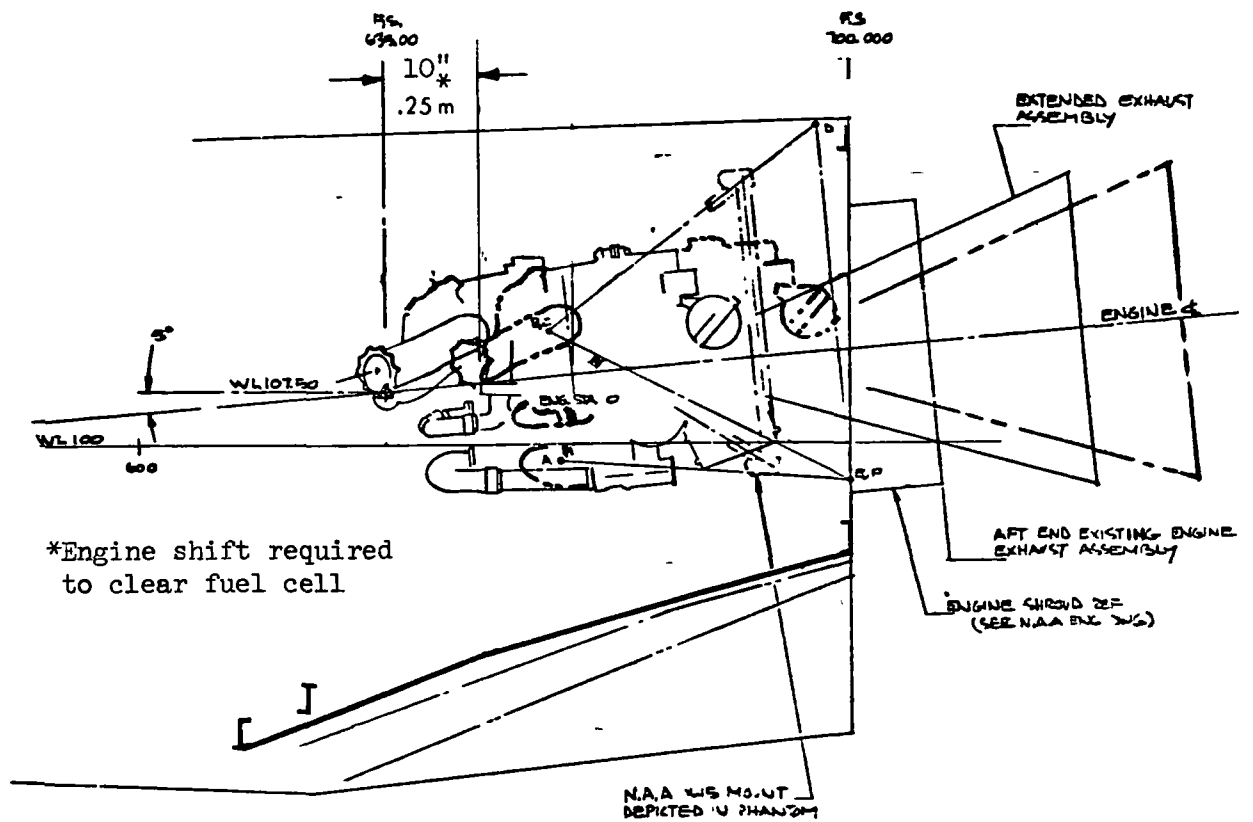
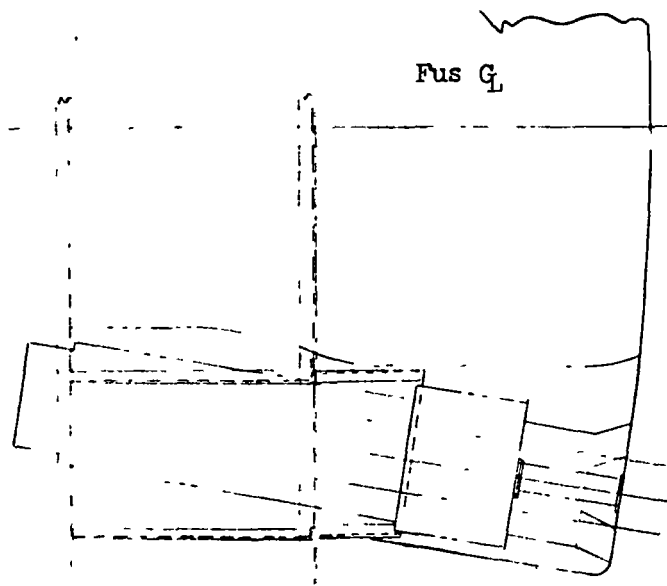


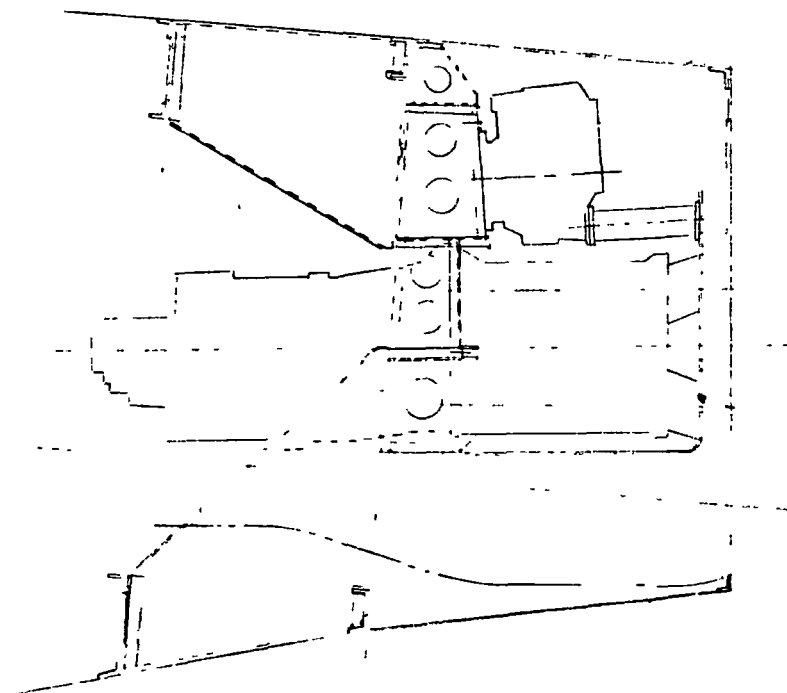
Figure 145 - LR-99 Engine Installation



LR-11 Engine - 2 Req.

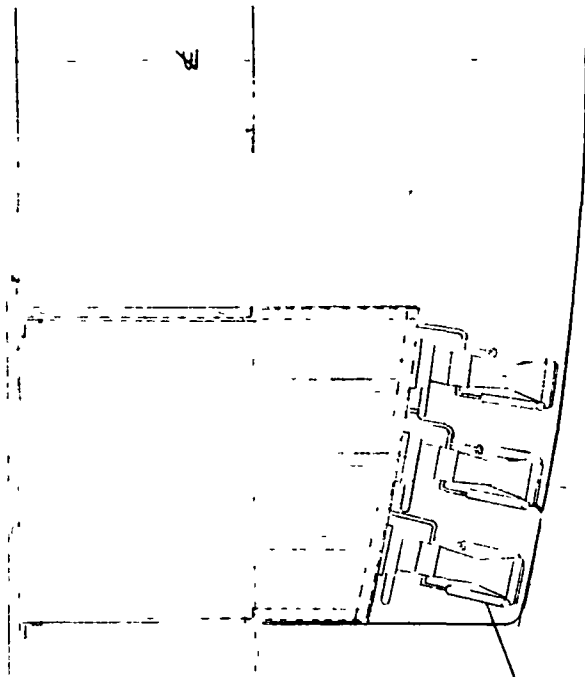
Shroud

Turbo pump - 2 Req.



Fus. Sta. 700

Figure 146 - LR-11 Engine Installation



LR-101 Engine - 12 Req.

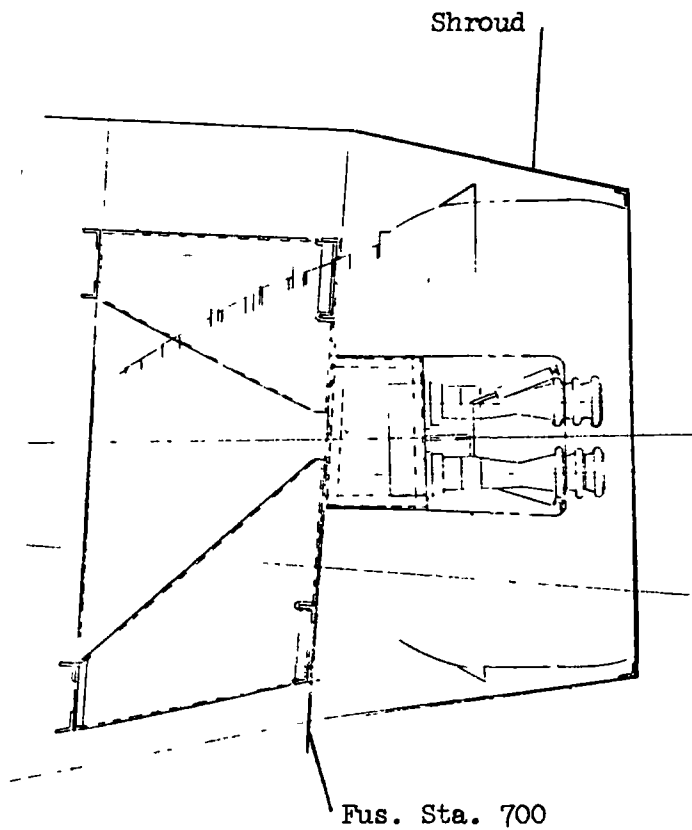


Figure 147 - LR-101 Engine Installation

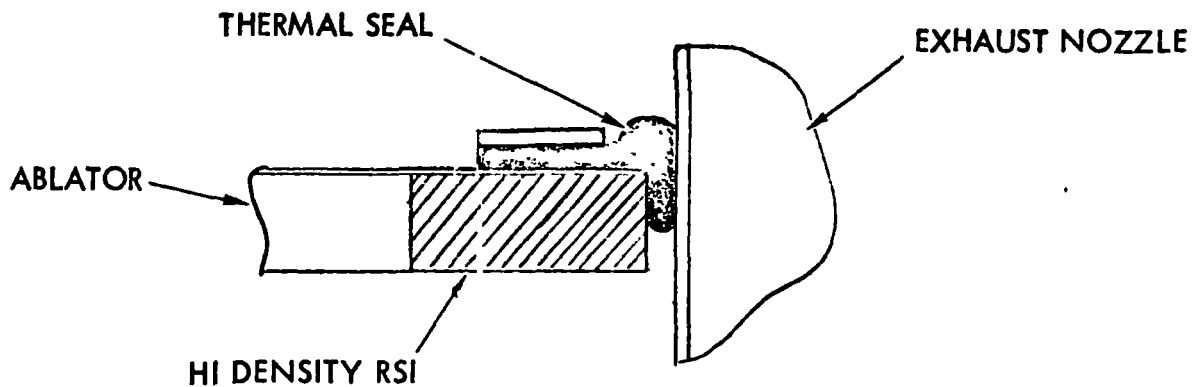


Figure 148 - Engine Seal Criteria

Appendix A. Due to the lack of precise scramjet envelope data it was necessary to coordinate with engineering, from the Garrett Corporation, to assure the recommended provisions would be compatible with the final study activity on scramjets by Garrett. The Garrett program is independent of the X-24C program reported herein and appears schedule-wise to be lagging behind the X-24C study. Numerous meetings between Garrett and Lockheed were held on this subject. The first few consisted primarily of updating Garrett on the X-24C and constraints that could affect them. The last were to discuss changes to the scramjet structural concept that would tend to assure a satisfactory X-24C installation Figure 150 depicts the present scramjet module structure concept and the mount method agreed upon during these discussions.

The structural provisions, Figure 149, were configured for the three module concept for the baseline vehicle and can be modified to accommodate scramjet



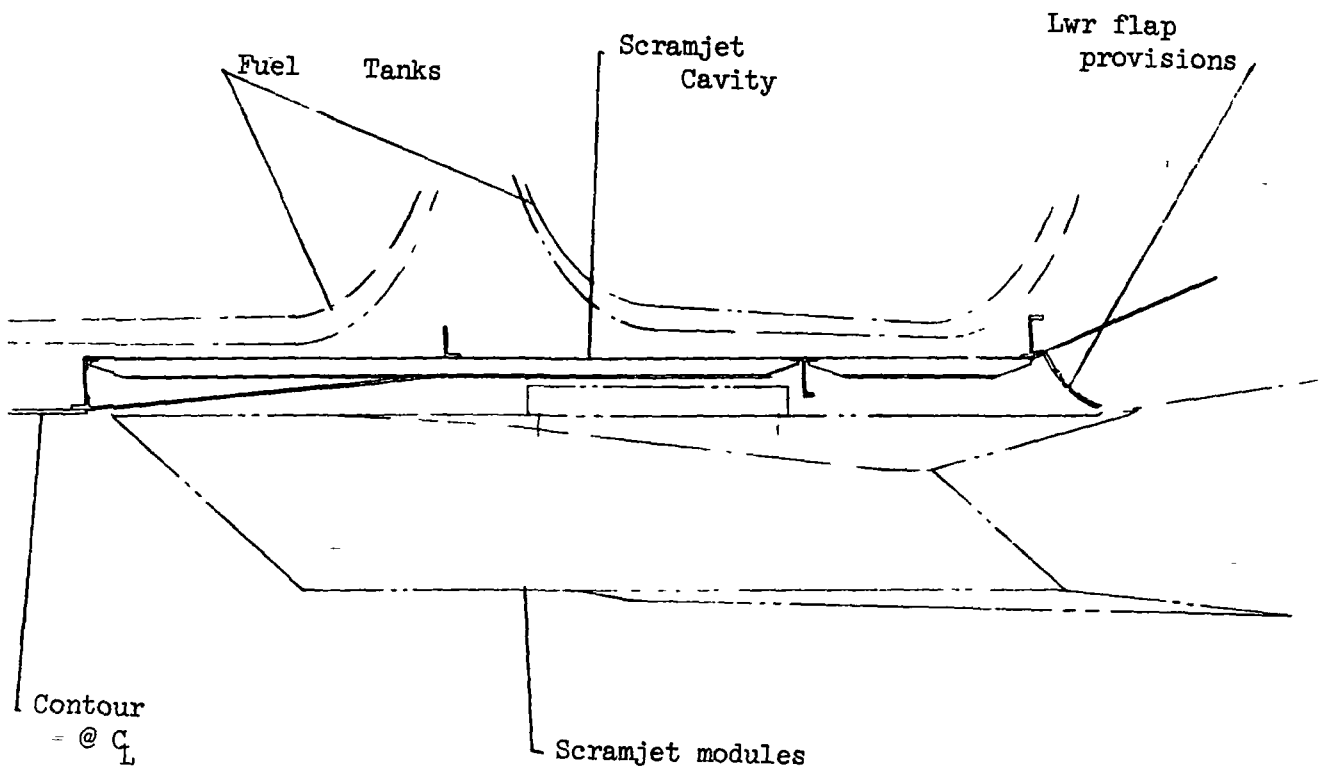


Figure 149 - Scramjet Structural Cavity

growth. The installation is similar for all three vehicle structural concepts. LI-900, Ablator or Lockalloy will line the walls of the cavity to protect the vehicle from heat radiating from the scramjet during its operation.

Thermal seals are provided between the scramjet walls and vehicle structural cavity. In addition to providing for expansion of the scramjet body the seal must also allow for scramjet deflection caused by relationship of the scramjet mounts to the ends of the scramjet body. Figure 151 depicts the requirements

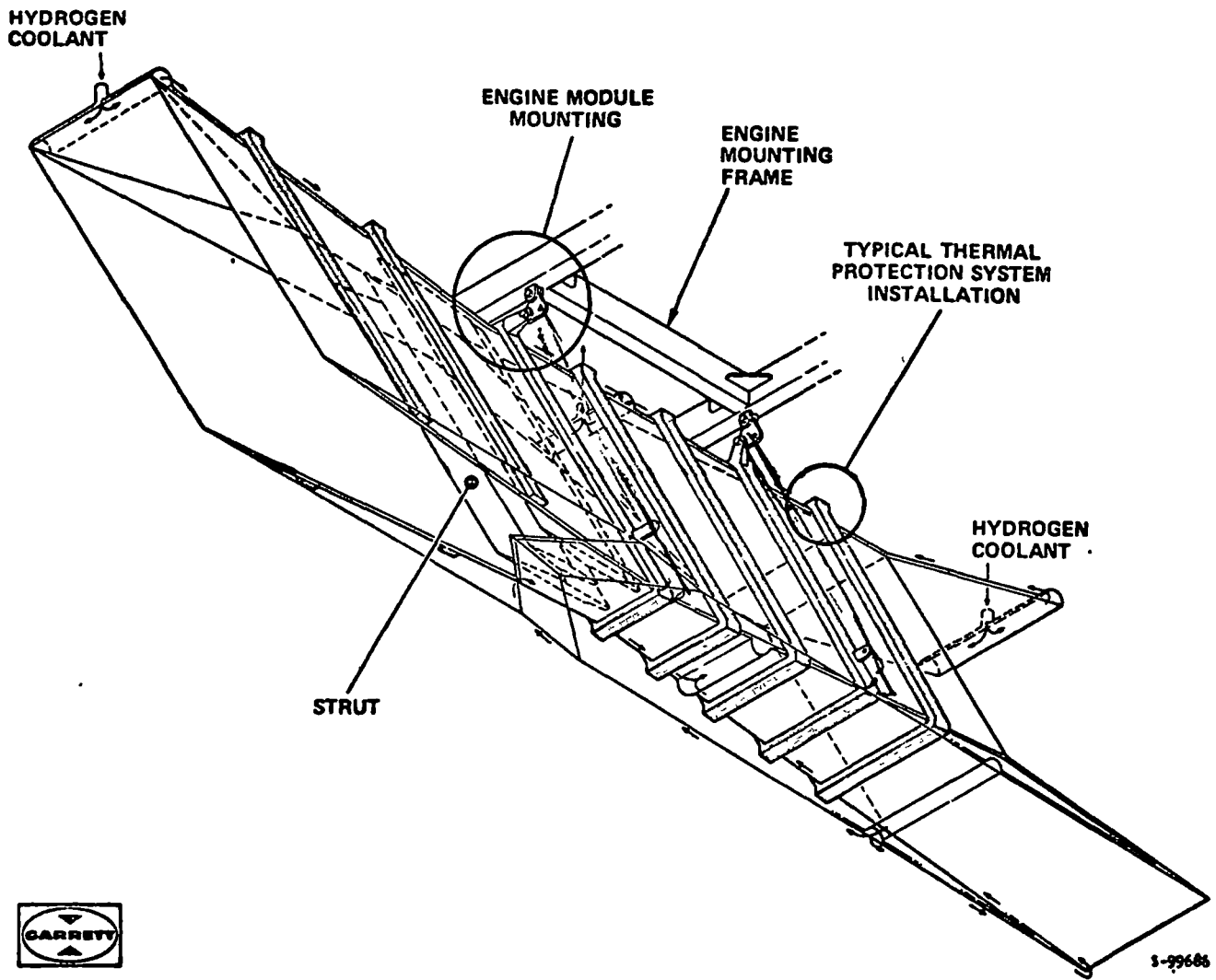


Figure 150 - Scramjet Module Installation

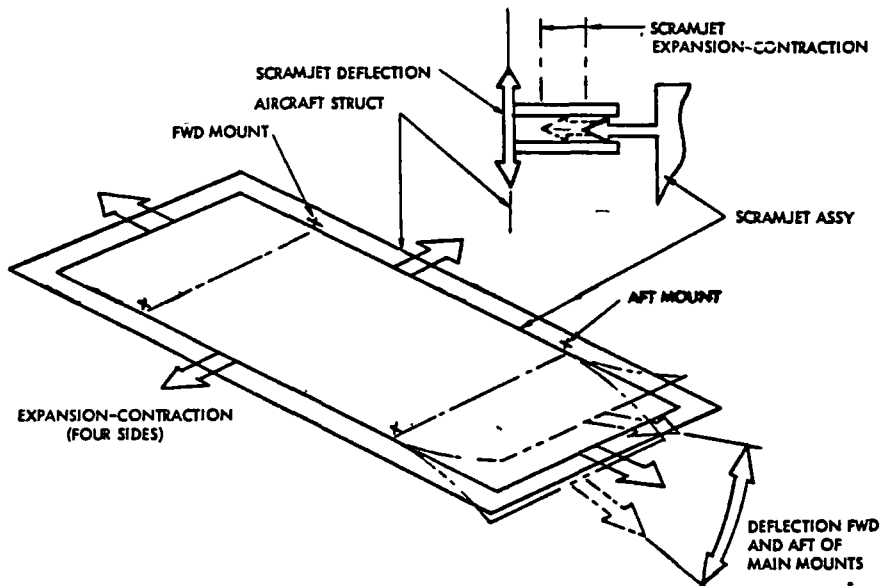


Figure 151 - Scramjet Seal Criteria

for the thermal seal. Complexity of the seal can be reduced by changing the scramjet mounts further apart, front to rear. Garrett indicated that at this stage of investigation a further scramjet change appeared doubtful. Based on a limited study on the seal it appears that due to the requirements the LI-900 and Ablator vehicle concept must use an RSI in lieu of LI-900 or Ablator for the seal. In the Lockalloy vehicle, while still presenting a complex design problem, the seal can be configured using Lockalloy.

#### Propellant Tankage Volumetric Analysis

Tankage concepts were developed for each of the vehicle structural/propulsion system combinations. In addition to the basic fuel load required for the mission allowances were made for fuel temperature variations, ullage, tank shrinkage, tank insulation, tank oscillation, vehicle structure deformation from airloads and thermal variations.

Tank Concepts - Figures 152, 153 and 154 depict the tankage concepts for the rocket engine combination along with the fuel load and volumes used in sizing the tanks. In addition to the fuel volumes, allowances also were included for ullage 5%, 36 mm of insulation around the lox tanks and 7.7 mm around the ammonia tanks (LR-99 engine configuration). Also included were 31.8 mm between the tank insulation to inside of the vehicle shell structure for structural deflection due to airloads and/or thermal variations.

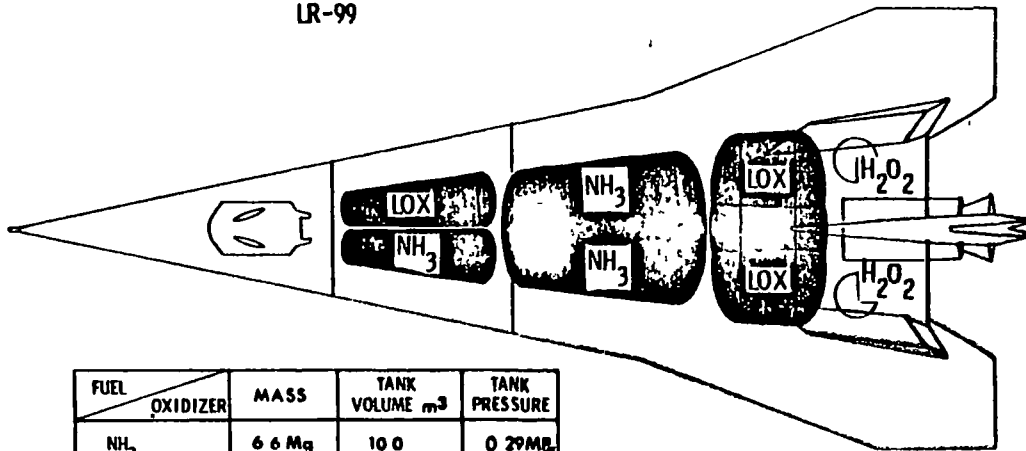
Initially the Figure 152 combination was found incapable of accommodating the fuel required for the mission. Later analysis supported by shifting the LR-99 engine aft 0.25 m, Reference Figure 144, made it possible to accommodate proper tank volumes.

Fuel tank construction will be of 2219 aluminum with internal substructure capable of transmitting fuel loads, through links into the vehicle. An investigation was conducted on a tank concept using nested frames capable of carrying both fuel loads and vehicle shell airloads. The investigation determined the concept would result in an increase in volume available for propellant, but would result in an increase in tank suspension loads.

Detail analysis are required to determine whether separate tanks, as shown in Figures 152, 153 and 154 are better than nested tanks with a structural tie between domes.

Tank mounting for all configurations, aluminum vehicle structure shown in Figure 155, will use a series of suspension links, between tank frame and shell structure to permit expansion between the vehicle and tank to occur without increasing tank stresses. Link attachment, to the aluminum shell structure, will utilize intercostals between frames as shown in Figure 155. In the Lockalloy heat-sink construction further analysis is required to develop an attachment concept that minimizes the thermal stresses which will occur at the point of contact of the link at the skin surface. Where possible the links will terminate at a hard point on the main frame and as near the outer skin as possible. If the arrangements

LR-99

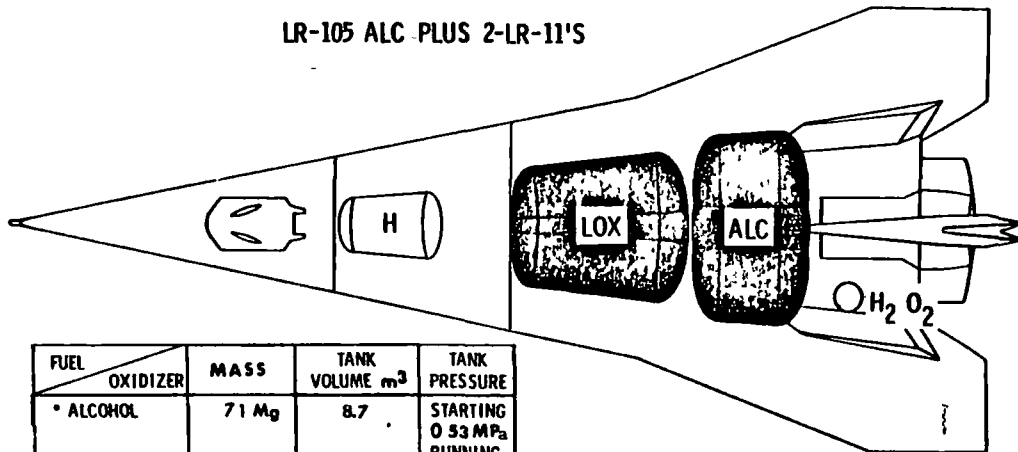


FUEL	OXIDIZER	MASS	TANK VOLUME m <sup>3</sup>	TANK PRESSURE
NH <sub>3</sub>		6.6 Mg	10.0	0.29 MPa
	MAIN			
	AUXILIARY	0.7	1.0	
LOX		8.3	7.6	0.29
	MAIN			
	AUXILIARY	0.8	0.8	
H <sub>2</sub> O <sub>2</sub>		0.6	2 TANKS 0.2 ec	3.8
PRESSURIZATION AND PURGING	H <sub>2</sub>	33.6 kg	0.4	20.7

NOTE: PAYLOAD BAY  
UNAVAILABLE FOR  
SCRAM JET FUEL.

Figure 152 - Propellant Tankage Arrangement - LR-99

LR-105 ALC PLUS 2-LR-11'S

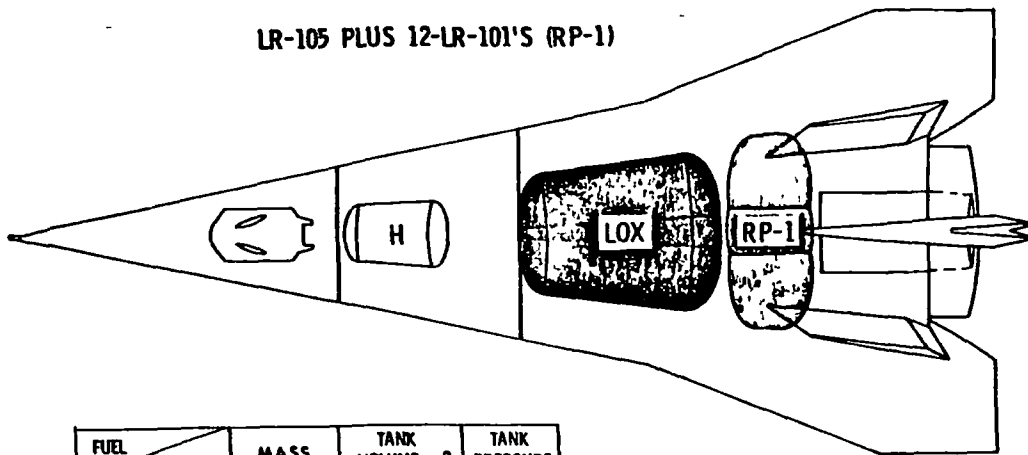


FUEL	OXIDIZER	MASS	TANK VOLUME m <sup>3</sup>	TANK PRESSURE
* ALCOHOL		7.1 Mg	8.7	STARTING 0.53 MPa RUNNING 0.12
LOX		8.7	8.1	STARTING 0.37 RUNNING 0.23
H <sub>2</sub> O <sub>2</sub> (LR-11'S)		0.07	0.05	3.3
PRESSURIZATION AND PURGING	H <sub>2</sub>	0.06	0.7	20.7

\* ALCOHOL PLUS 2% WATER

Figure 153 - Propellant Tankage Arrangement - LR-105

LR-105 PLUS 12-LR-101'S (RP-1)



FUEL OXIDIZER	MASS	TANK VOLUME m <sup>3</sup>	TANK PRESSURE
RP-1	4.7 Mg	6.2	STARTING 0.53 MPa RUNNING 0.29
LOX	10.4 Mg	9.7	STARTING 0.37 RUNNING 0.21
PRESSURIZATION AND PURGING H <sub>2</sub>	55.6 kg	0.6	20.7 MPa

Figure 154 - Propellant Tankage Arrangement - LR-105

necessitates use of intercostals, their design will be capable of transmitting shear loading into the Lockalloy skin while allowing skin thermal expansion to occur without increasing the thermal stress.

### Structural Arrangement

In conjunction with structural, thermal, and flutter analysis structural concepts were developed. Three versions, one each for the different thermal protection systems (TPS) were configured taking into account predetermined factors, such as, aerodynamic envelope, fuel tankage volumes, landing system location, cockpit, payload bay, replaceable wings and fins, scramjet provisions, TPS provisions, and launch vehicle interfacing provisions.

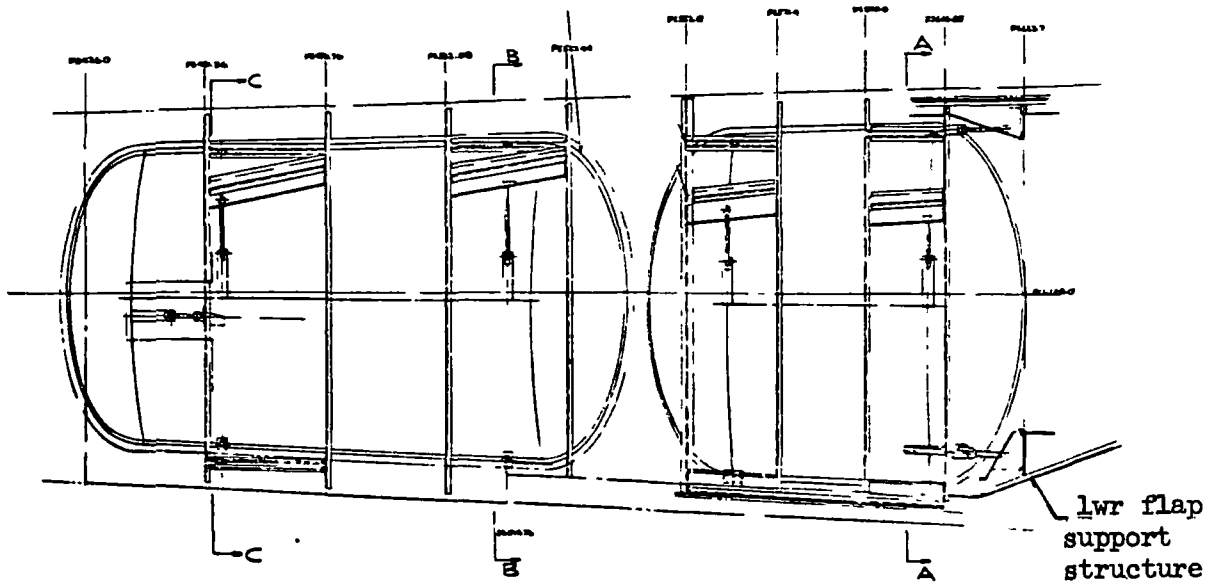
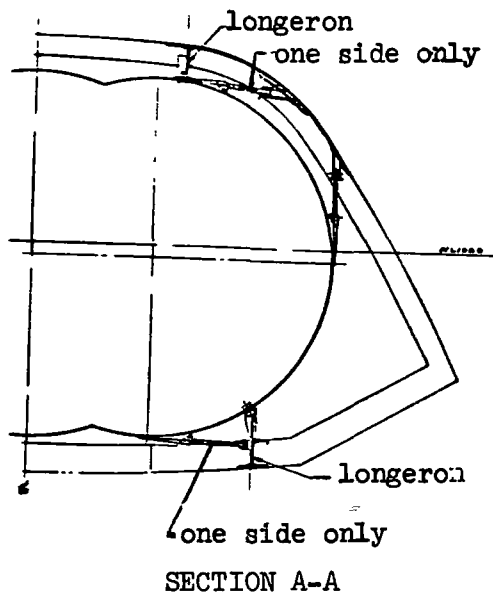
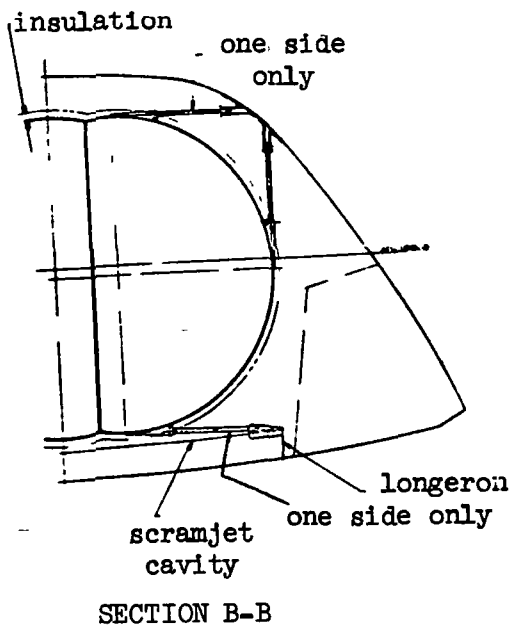
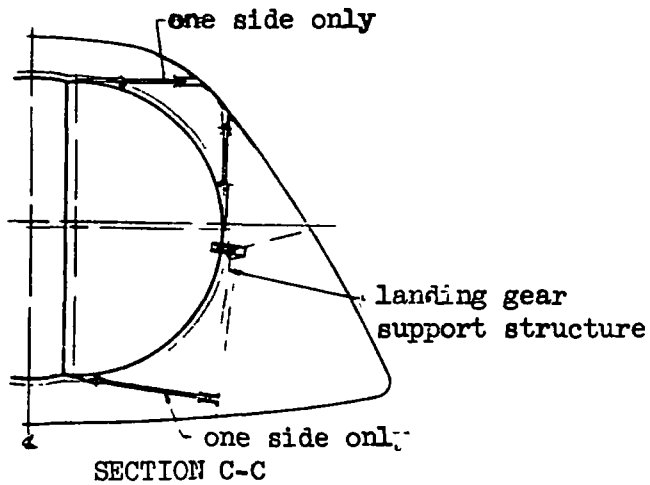


Figure 155 - Typical Tank Mounting

Aluminum Structure - LI-900/Ablator - The structural concept shown in Figures 156, 157, 158 and 159 is based on a nominal 76 mm stringer interval, for the LI-900 TPS, and 84 mm interval for the Ablator TPS, and 0.61 m frame intervals, with a 0.81 mm skin thickness. These dimensions were selected by considering surface pressure loads and panel flutter criteria for flat panels at a nominal design dynamic pressure at 47.9 kPa and nonbuckling skin criteria. Major bulkhead frames are provided at the forward face of the cockpit shell, at the forward and aft end of the payload bay, at the rear attachment points to the launch vehicle, at the contour transition point on the lower surface, and at the rear of the vehicle; the aft frame also serves as the aft beam for the wing and vertical rudder. The frame at the contour transition serves as the hinge point for the lower fuselage flap, Reference Figure 160. Vertical shear webs extend forward along the sides of the main and nose wheel wells. Longitudinal beams extend on the sides of the scramjet provisions and at the lower flap hinge point on the lower surface. On the top surface beams extend fore and aft of the launch vehicle aft latch points. The payload bay provides a double wall concept, Figure 161, depicts the aluminum construction, with inner surface set under contour 0.15 m on the lower centerline and 0.10 m on the sides and top. The payload bay outer shell can be completely replaced with alternate panels for experimental purposes. The wings shown in Figure 162 are designed for rapid replacement. Structure provisions for attaching the wing to the main fuselage has been configured, Figure 163, so that each attachment joint allows for thermal deflections that replacement hot-structure assemblies present as well as rapid assembly/disassembly of replacement assemblies. Aerodynamic controls are provided by wing elevons, split vertical fin rudders, and potentially by the lower fuselage flap. The canopy is configured similarly to the SR-71 aircraft canopy and will use a number of SR-71 canopy components for latching, ejection and sealing. Cockpit pressure vessel will be similar to the F-104A aircraft cockpit.

Heat-Sink Structure - Lockalloy - The structural concept shown in Figures 164, 165, 166 and 167 is based on varying thickness Lockalloy skin panels and 0.48 m frame intervals. Skin panel thicknesses were designed by thermal



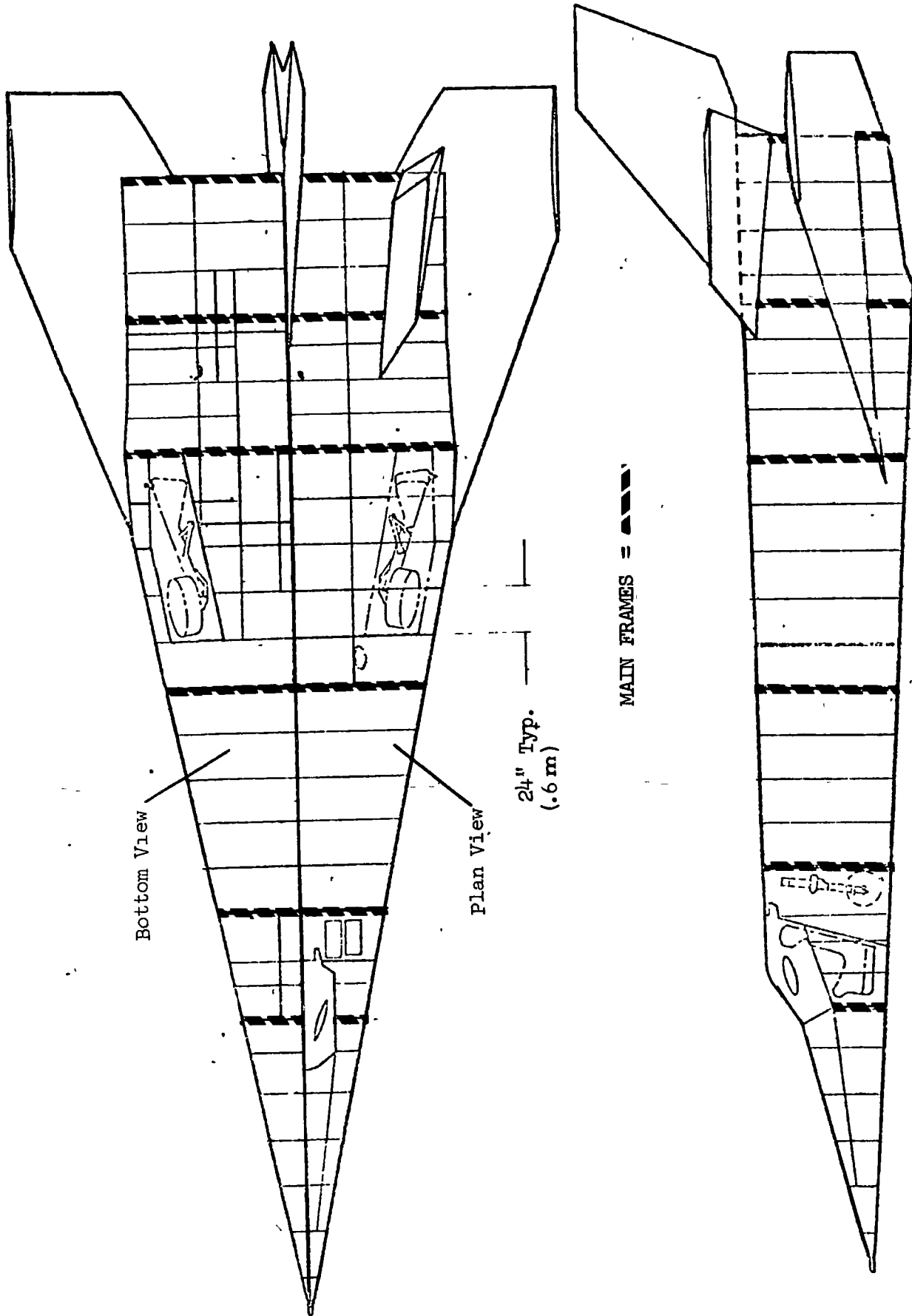


Figure 156 - General Arrangement - Aluminum Design

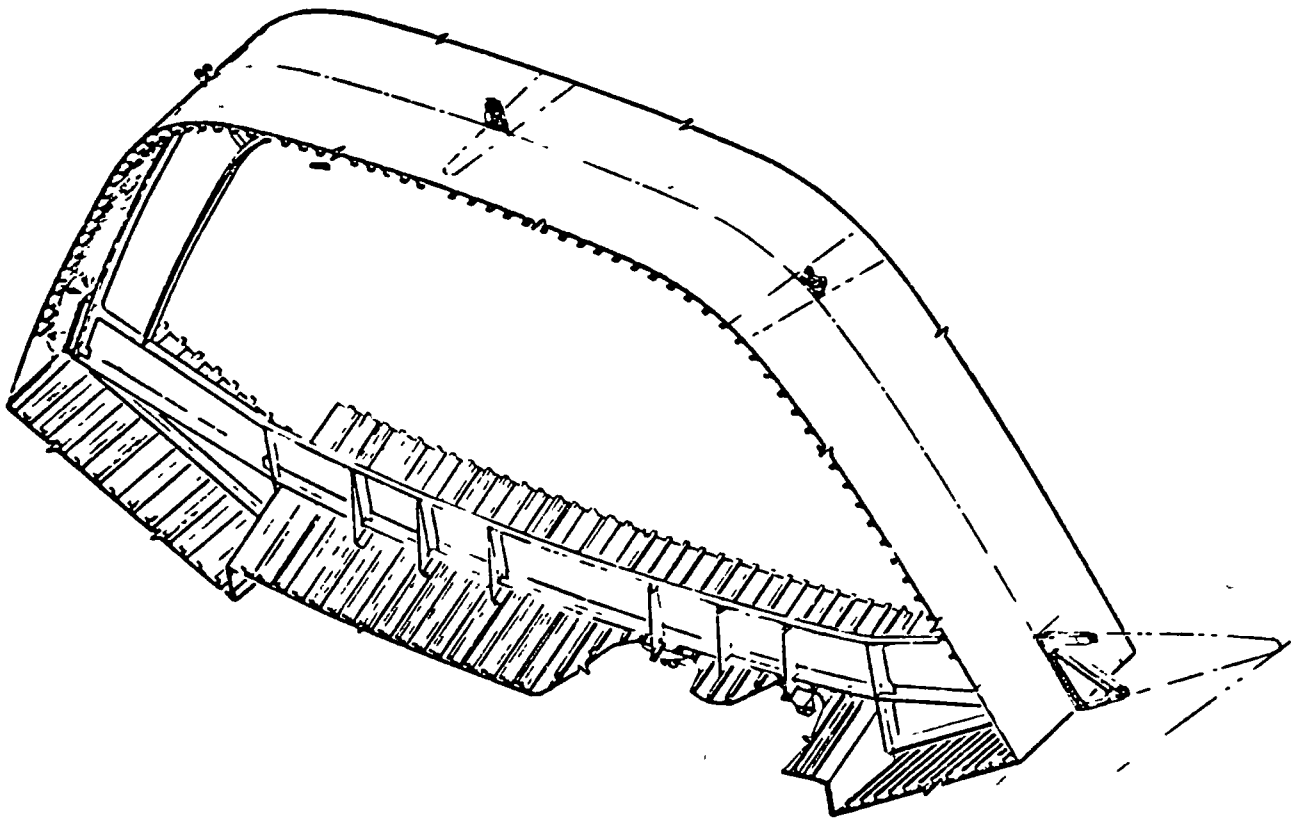


Figure 157 - Typical Frame - Aluminum Design

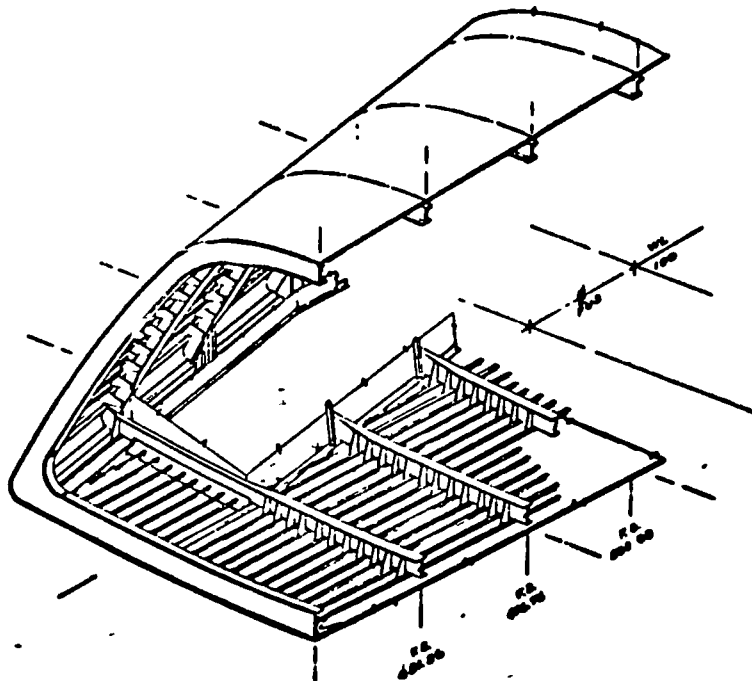


Figure 158 - Mid-body Section - Aluminum Design

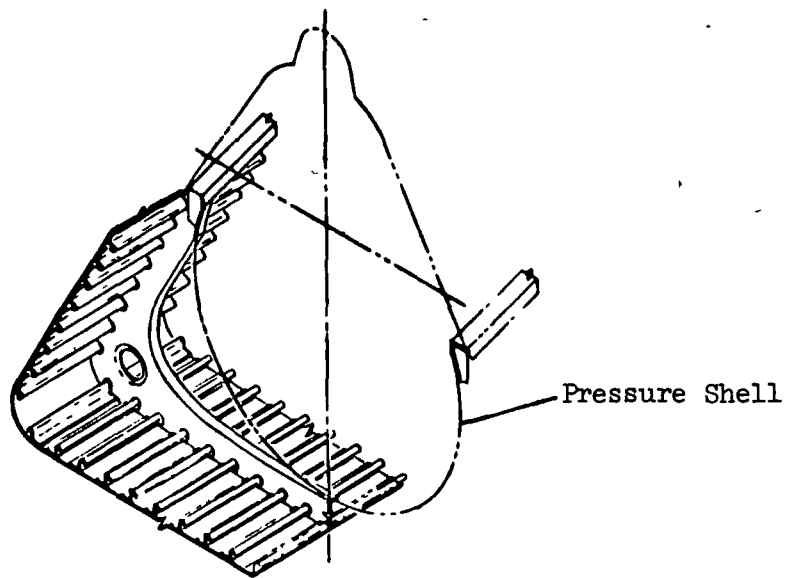


Figure 159 - Cockpit Area Structure - Aluminum Design

considerations in most cases rather than structural requirements. Frames from the payload bay aft are constructed, Figure 166, using a truss concept with a series of aluminum links bridging between a titanium angle against the Lockalloy panel and an aluminum tee serving as the inboard cap member. Frames forward of the payload bay will employ a stainless steel or titanium sheet metal zee-section in lieu of the truss concept. Major bulkhead frames, vertical shear webs, and longitudinal beams are placed similarly to the aluminum vehicle concept and likewise serve the same roles. Wing concept, Figure 168 is designed for rapid replacement as was the aluminum design. The side fins and vertical fin are similarly constructed and attached to the fuselage as the wing assembly. Wing elevons, split vertical fin rudders, and the fuselage lower flap are identical to the aluminum structure concept except for the construction materials. Cockpit pressure vessel is identical to the aluminum vehicle except for possible relocation of

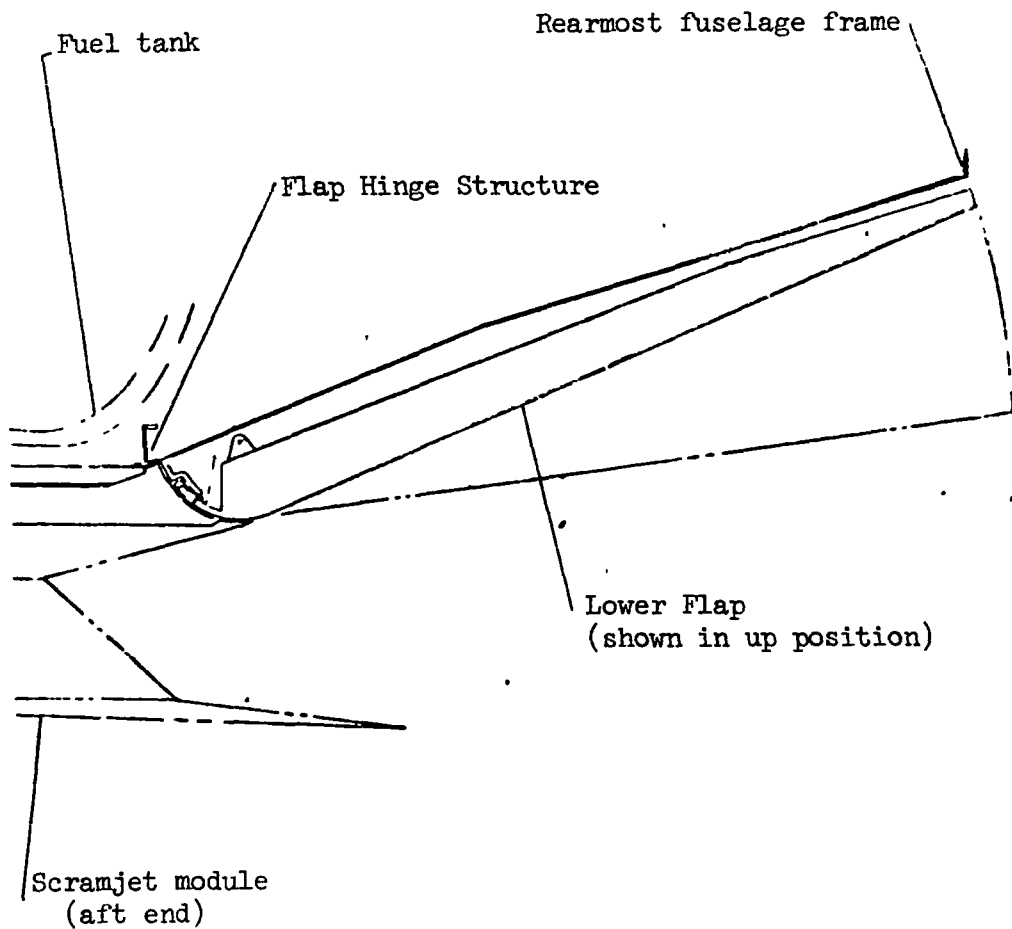


Figure 160 - Lower Flap Installation

pressure vessel frames to clear the Lockalloy skin panel frames. Excepting for the Lockalloy skin surface the canopy will be configured similarly to the SR-71 canopy using the X-15 type high-temperature window panes. SR-71 latching, actuating, and sealing components will also be used where possible. The payload bay, like in the aluminum vehicle, is double walled to permit the outer surface panels to be completely replaced with test thermal protection system such as advanced radiative TPS. The payload bay primary structure has a field splice at each end to test advance structures under the existing TPS or advanced TPS.

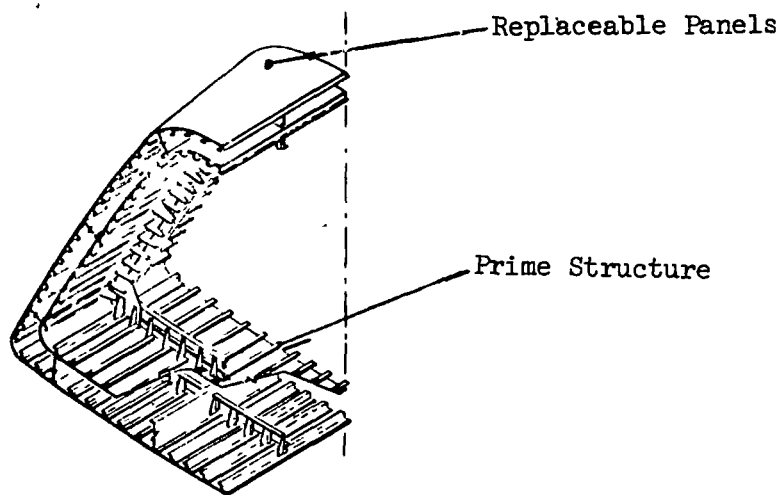


Figure 161 - Payload Bay Structure - Aluminum Design

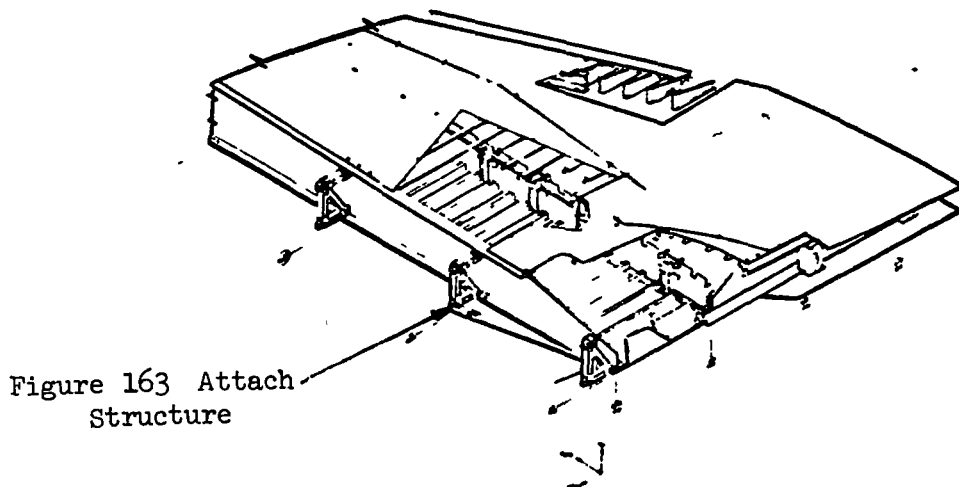


Figure 162 - Wing Arrangement - Aluminum Design

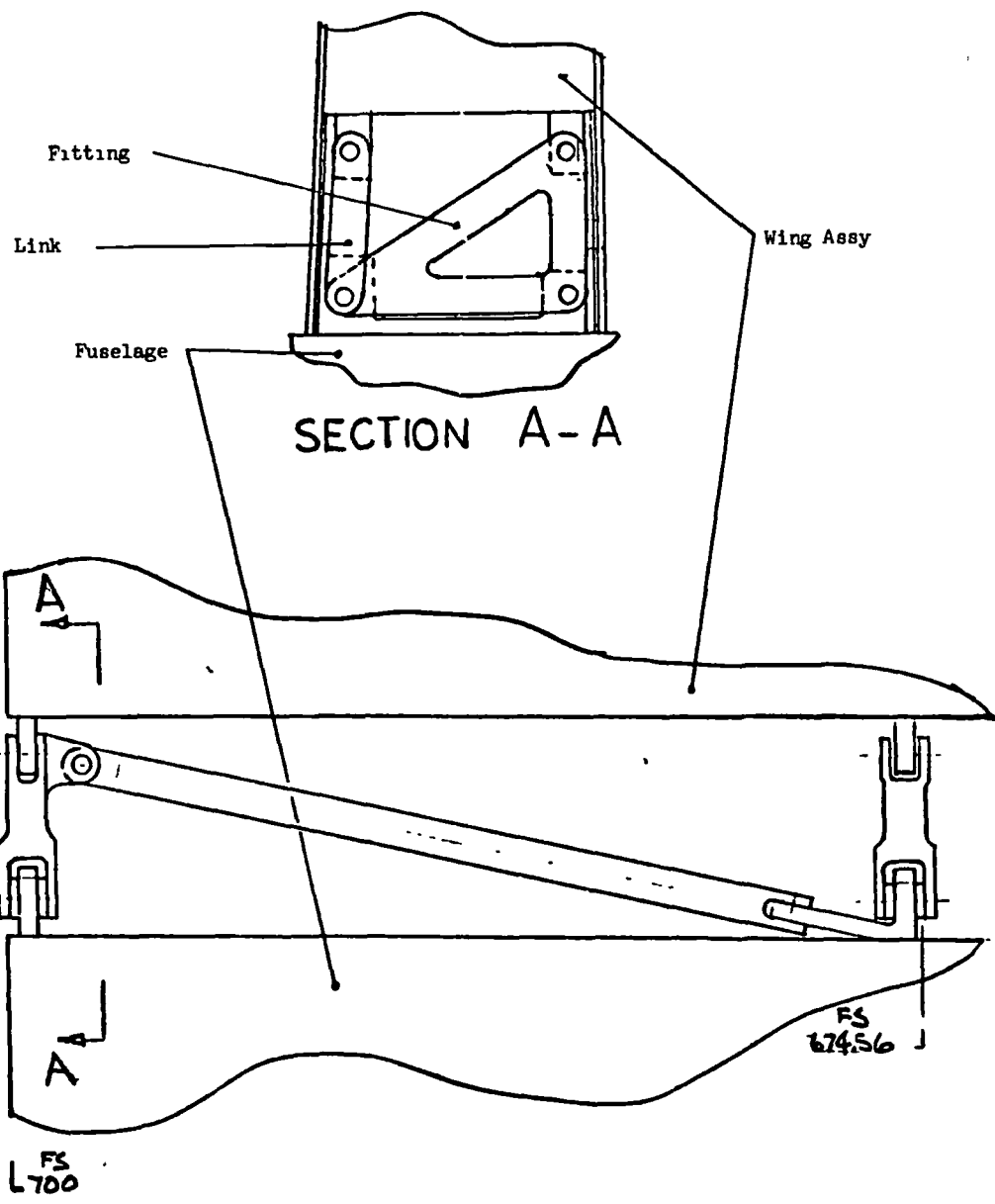


Figure 163 - Wing Attachment

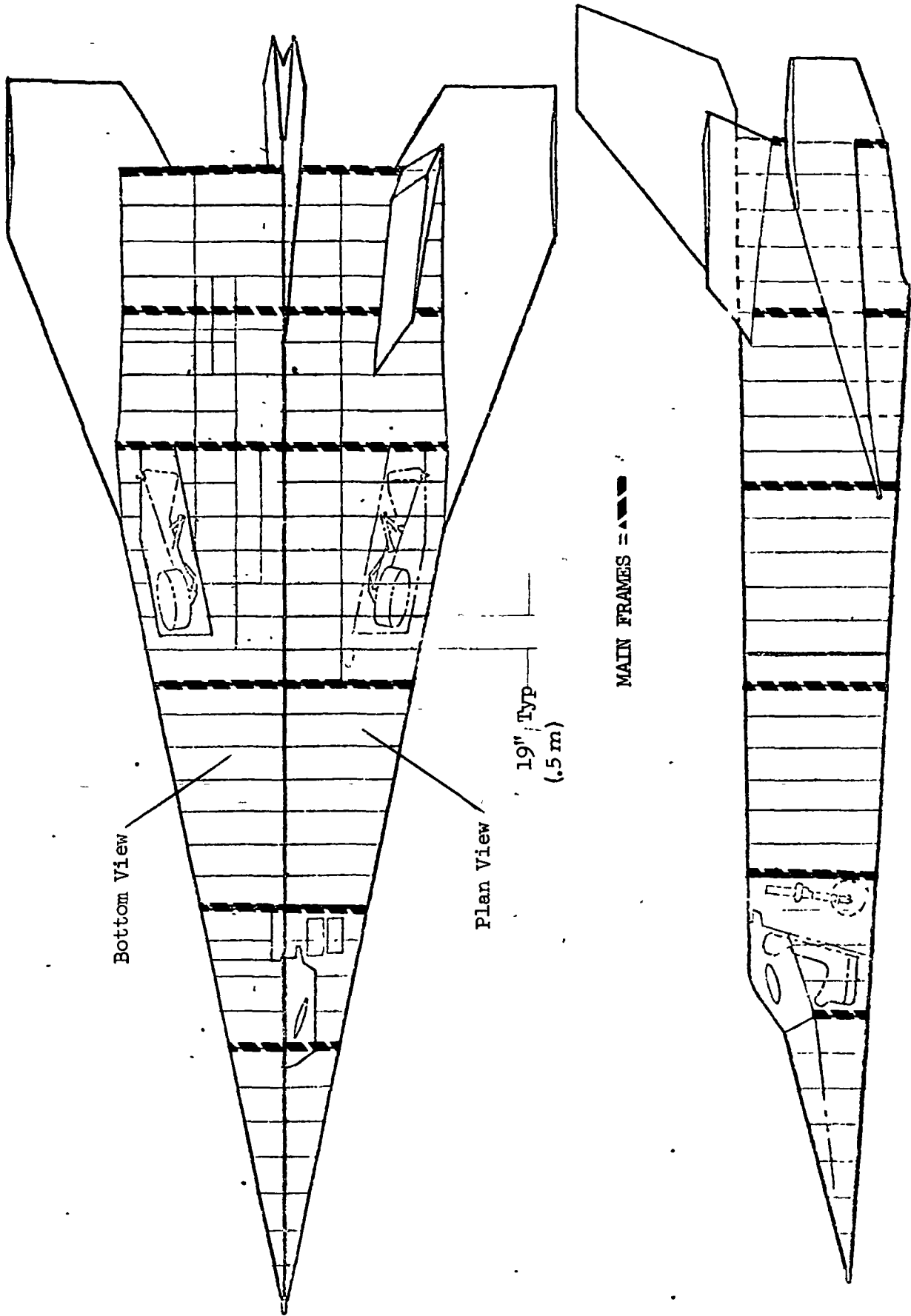


Figure 164 - General Arrangement - Lockalloy Design

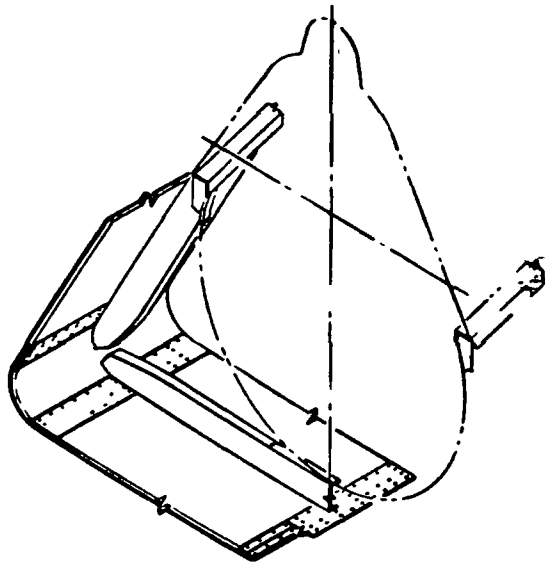


Figure 165 - Cockpit Area Structure - Lockalloy Design

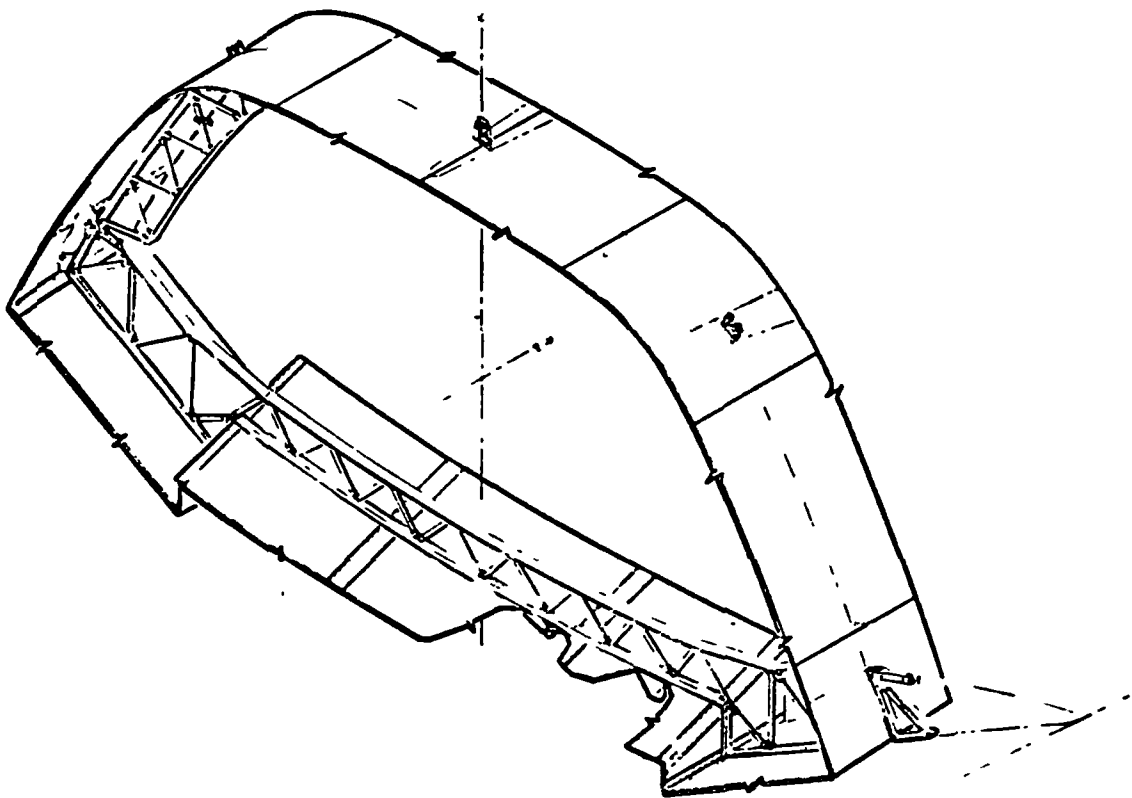


Figure 166 - Typical Fuselage Frame - Lockalloy Design



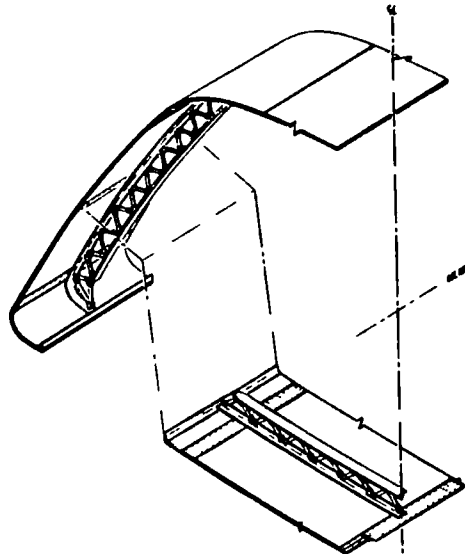


Figure 167 - Mid-body Structure - Lockalloy Design

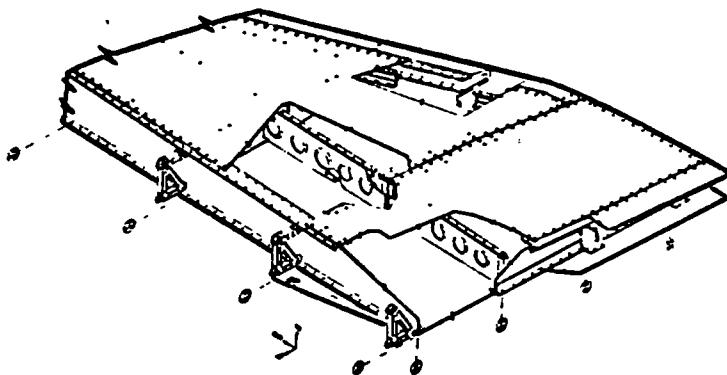


Figure 168 - Wing Arrangement - Lockalloy Design

Installation TPS - LI-900 - The entire external surface of the vehicle, less the canopy glass area, will be covered with the LI-900 tiles sized and tailored to fit the vehicle shape and thermal envelope. Installation of the individual tiles will utilize the procedure developed for the Space Shuttle program, depicted in Figure 169, which will consist of a coating of RTV 560, on the vehicle surface, a 4.06 mm nomex felt isolator pad, followed by a coating of RTV 560 and the LI-900 tile. Tile(s) will be held in place during the bonding/curing cycle utilizing tooling which will be similar to that used on the Space Shuttle for tile assembly and installation. It may be possible that Space Shuttle tooling for tile preparation, assembly, etc. can be adapted for use on the X-24C program. However,

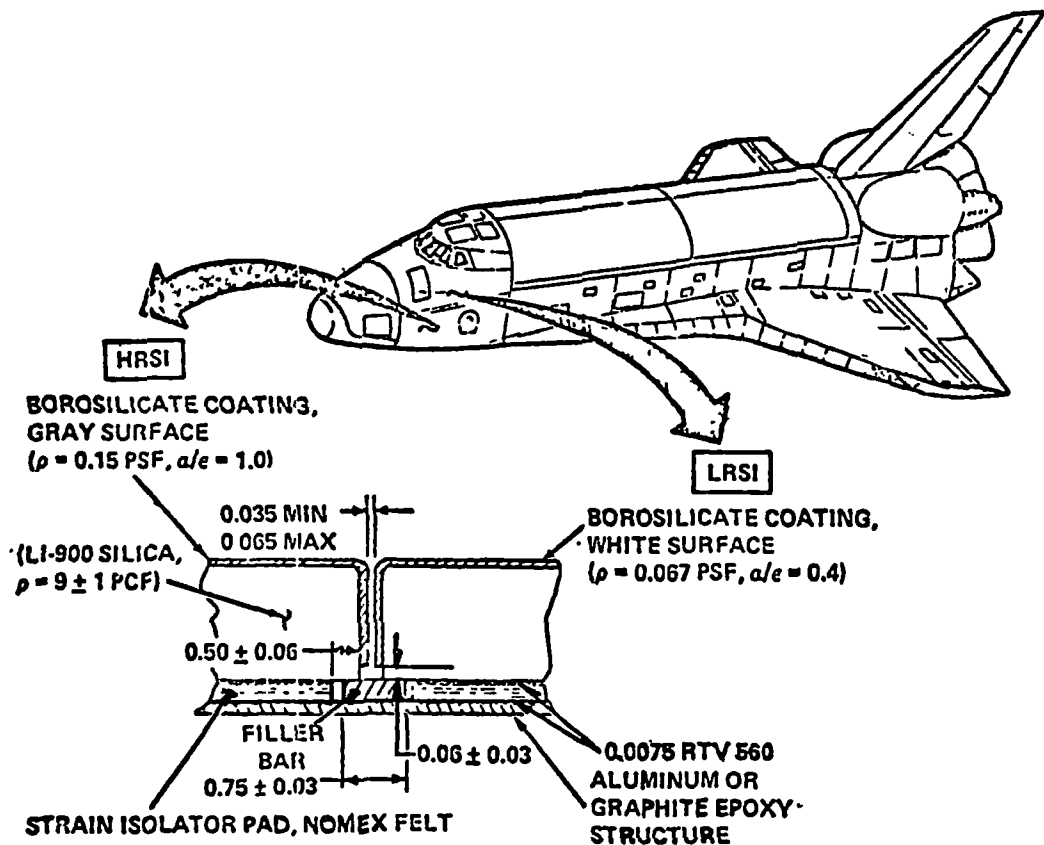


Figure 169 - Space Shuttle - LI-900 RSI Installation

time constraints on Phase I of this study prevented a detail review of a potential cost saving. The use of high density RSI, like on the Space Shuttle, will be used as edging member wherever the LI-900 RSI may be subject to damage during ground servicing, air launch or flight operations. This high density RSI which can be molded and/or machined will be used as edging on all access openings and panels, i. e., service areas, landing gear doors, and canopy/sill interfacing surface edges. On control surfaces, i. e., elevons, speed brake flaps, and scram-jet exhaust flap, where the leading edges are subject to rubbing by the thermal seal, high density RSI will also be used. Thermal seals, to prevent heating of the aluminum structure will be given careful design consideration. To avoid the possible loss of the seal during flight, as demonstrated during the Langley NASA aerothermal testing, the seal design will be configured so that it is trapped by the access/door panel while swelling to fill the gap between the side of the panel and vehicle opening. Attachment of structural access panels, other than MLG and NLG doors, will use the fastener-plug concept considered in the Space Shuttle study, Reference 36. A much simpler approach does not require the use of a plug to seal the cavity for the fastener. This latter approach will be looked at in more detail together with aerothermal testing to verify suitability with the X-24C environment. Monitoring of the Space Shuttle program, in regards to the TPS efforts, is highly recommended to take advantage of those TPS improvements developed for the Space Shuttle that can likewise enhance the X-24C program.

Installation TPS - Ablator - The entire external surface of the vehicle, less window areas, will be covered with the Ablator insulation. On vehicle surface areas with gradual contour variations Ablator panels, approximately 0.91 by 1.22 m and sized for the vehicle thermal envelope, will be bonded directly to the aluminum skin using a coating of RTV. Vacuum pressure will be used to restrain the Ablator against the vehicle during curing. On areas subject to rapid contour changes, i. e., wing, fin, and elevon leading edges molded or machined Ablator segments will be used in lieu of basic panels. These segments will, likewise, be bonded directly to the aluminum skin. Thermal Analysis results indicates the

low density Ablator will not sustain the heating environment, of the X-24C mission profile, on leading edges and shock impingement regions. Prior Ablator studies, Reference 10, bears out the analysis results. Subsequently, approximately 20% of the X-24C wetted surface will be insulated with high density RSI (1.05 kPa Reusable Surface Insulation) on those regions subject to the high aerodynamic heating rates. High density RSI will also be used as an edging member on areas, i. e., canopy interface, access areas, service joints, landing gear doors, slip joints, and thermal expansion joints where the low density Ablator edges will be subject to damage during servicing and operational cycling. RSI will also be used in lieu of the Ablator whenever test instrumentation, i. e., pressure sensors, etc., require skin surface measurements. Due to the precise surface position required by these sensors, approximately 200 plus have been estimated, charring and erosion of the Ablator surface can have an invalidating effect on test results due to the change in aerodynamic flow. Additionally the sensors can also draw in char particles which also invalidates test measurement. The amount of RSI around each test sensor will require further analysis after each test point has been established and located on the vehicle. For this study it was assumed that a 38 mm diameter button per sensor would eliminate the noted potential test instrumentation problem.

Thermal seals will be used on all interfaces subject to service or operation opening. The seal will be trapped by the access panel/door and expand to fill the gap between the interfacing edges. Attachments through the Ablator surfaces panel/doors, where required, will utilize the fastener-plug concept considered in the Space Shuttle study, Reference 36. A simpler approach not requiring a plug to seal the fastener cavity will also be looked at in more detail with further aerothermal testing to verify suitability with the X-24C environmental and structural envelope.

Thermal Protection - Lockalloy - No TPS is required for the Lockalloy heat-sink vehicle concept. Panel thicknesses and leading edges and control surface exposed into the airstream are sized to function within the structural/thermal envelope of the mission.

Access-Installation and Maintenance - In establishing the accessibility requirements for the X-24C vehicle two types of access needs were considered: (1) manufacturing installation, and (2) maintenance access. For manufacturing it has been assumed structural panels will be provided to support installation activity associated with electrical, controls, fuel tankage, fuel system, and hydraulic system and subsequently TPS (LI-900 or Ablator) will be bonded directly over these access panels. Unscheduled maintenance requiring access for servicing into these areas will require TPS removal and replacement using the TPS refurbishment technique developed for these materials. For scheduled maintenance access a conservative panel acreage of  $3.0 \text{ m}^2$  amounting to approximately 32.6 m of panel edging is anticipated. Because of the complexity associated with panel edges (i. e., using higher density materials, sealing requirements, etc.) as well as the potential increase in maintenance due to the panel fastener limitations produced by the LI-900 and Ablator TPS, further study will be required for grouping of functional systems requiring scheduled maintenance to reduce panel footage. On the Lockalloy concept most panels can be removed for maintenance access since the complexity associated with the TPS edging and fastener concept do not apply. However, functional system grouping will still be considered with the Lockalloy vehicle due to its enhancement of the maintenance of the vehicle.

Slip Joints - Parts of the vehicle have been developed for potential replacement (i. e., wings, side fins, vertical fin and scramjet package) with like assemblies but of materials not thermally similar to the vehicle. The attachment surface between these replacement items and basic vehicle shell must accommodate thermal expansion or contraction due to material differences. Approximately 38.1 m of possible slip joint length are anticipated which will produce design as well as maintenance complexity. The Ablator and LI-900 system will be more of a challenge than the Lockalloy due to the inability of the TPS material to withstand structural loading as might be introduced at the slip joint. The Lockalloy concept can accommodate a slip joint concept much more easily with effecting the material. Criteria for the slip joint between the scramjet body and vehicle

structure are depicted in Figure 151. Slip joint criteria between replaceable assemblies is depicted in Figure 170.

Ablator and LI-900 Thickness Cutoff - Structural and thermal analysis established the minimum thickness of Ablator TPS and LI-900 RSI required on the X-24C to perform the required mission. However, overriding effects to these materials required a cutoff of the minimum thicknesses with a resultant increase to mass and cost.

- LI-900 RSI Thickness - Minimum thickness of 5.0 mm, in certain areas, were found compatible with the mission requirements. However, discussions with LMSC and Rockwell International engineering disclosed that even though the yield on space shuttle tile (breaking during installation) was yet unknown, tile thickness below 10.0 mm would not be practical. Subsequently, in final analysis, mass and cost studies were adjusted for a minimum tile thickness cutoff of 10.0 mm.

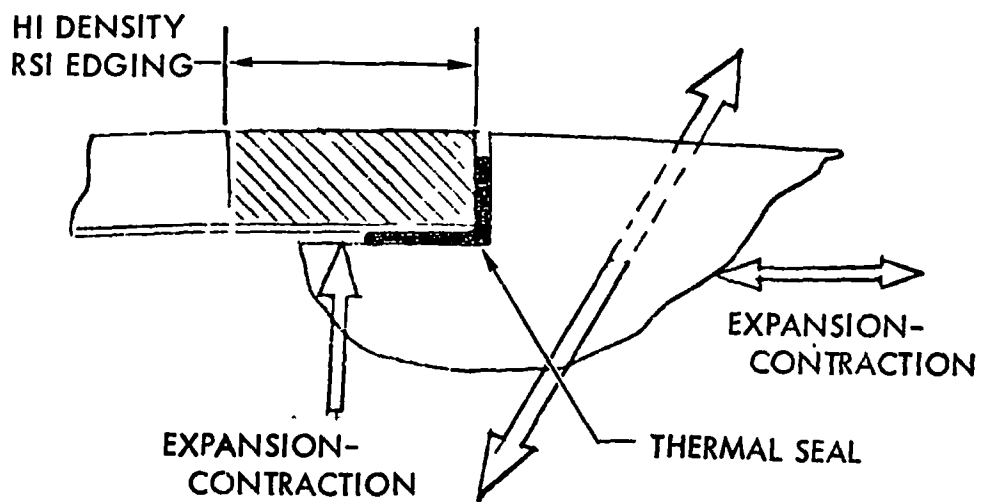


Figure 170 - Slip Joint Criteria

- Ablator TPS Thickness - Thermal and structural analysis determined a minimum 5.0 mm thickness, in certain areas, of Ablator would support the X-24C mission profile over the 100 mission life cycle. Results of previous Ablator studies and tests, Reference 43, indicate a potential Ablative defect such as material cracking resulting from unsupported handling as a very real possibility. Residual stresses, cold soak strain, and thermal stresses during flight can reduce overall panel stiffness and under flight induce buffeting and vibration loads. Under these conditions the Ablator would be susceptible to crack propagation leading to excessive loading of the panel loss with catastrophic results to the X-24C vehicle. It was therefore necessary that this study take into account a potential hazard associated with this material and provide a safety factor which established a minimum thickness cutoff of 10.0 mm. The minimum thickness was accounted for in both cost and mass analysis.

Fuselage Pressure Sealing - Both cockpit and fuselage shell will be provisioned for standard sealing to retain cockpit and fuselage internal pressures. On the aluminum framed vehicle, for the Ablator TPS and LI-900 RSI, all skin stringers, clips, etc. will be sealed against the skin using a high temperature silicone base RTV. Doors and access panels into these areas will require the use of a wet sealant each time door/panel access is required. The Lockalloy configured vehicle likewise will be sealed wherever the frames, longerons, etc. come in contact with the Lockalloy panels. A wet seal will be used on those designated panels required for vehicle access. A determining point in cutoff of maximum temperature allowables used for the Lockalloy configuration was based on the desire to maximize the utilization of system experience and materials, i. e., sealants, etc., developed for the YF-12 and SR-71 aircraft which are applicable to the X-24C.

Vehicle Parts Count - Estimation of the structural parts for each of the structural configurations as reflected in Table 56 and described under the section titled: 'Complexity Factors' was based on the structural concepts described under aluminum structure and heat-sink structure section herein. Excluded from the parts count were elements common to all configurations; i. e., fuel tanks and support structure, main longerons, cockpit pressure structure, main engine and mounts, sustainer/cruise engines and mounts, nose and main landing gears and their support structure.

### Functional Systems

Conceptual designs of the X-24C Functional Systems were developed to determine their mass, size, and cost as they affect the program cost and risk analysis. Criteria which all systems were required to meet is discussed in "Basis for Design Trade" included:

- Maximum emphasis was placed on locating and specifying GFE for the vehicle. The term GFE is defined as being available to this program from any Government program, either NASA or the U. S. Military.
- Use of existing NASA owned X-24B/X-15 hardware with minimum modification (cost).
- All functional systems to be common to all candidate configurations to be evaluated.

The functional systems developed and evaluated for the X-24C included:

- Avionics
- Flight controls
- Electrical
- Hydraulics



- Cockpit and furnishings
- Tank pressurization and feed system

Avionics - The avionic system complement shown in Figure 171 is composed of the following elements:

- 1) Air Data System,
- 2) Inertial Navigation System,
- 3) Communication Equipment,
- 4) Intercommunication Equipment, and
- 5) Radar Beacon

- Air Data System - The air data system measures pneumatic pressures and converts these pressures into electrical analog outputs of angle-of-attack, side-slip angle, Mach number, dynamic pressure, altitude and speed. The air data system consists of three components: a fixed

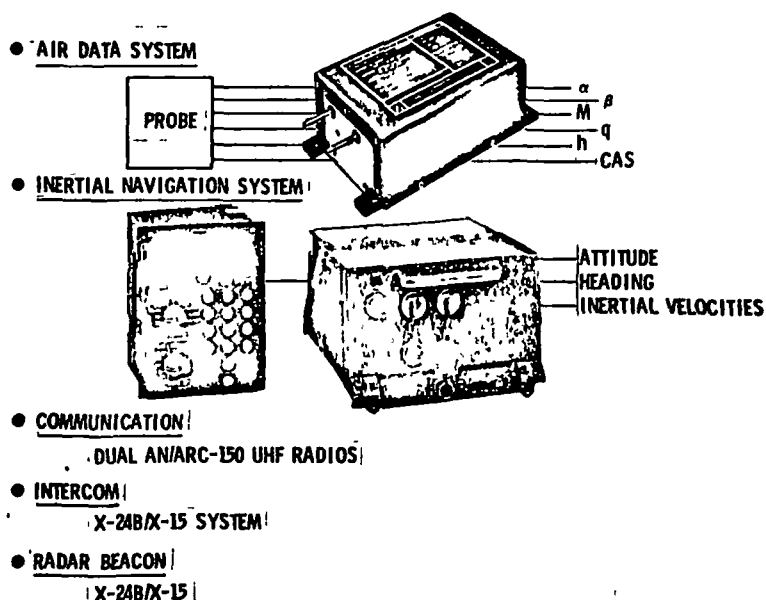


Figure 171 - Avionic System

hemispherical probe located in the nose of the vehicle, and two matched converters which output the electrical analog parameters. Because of the unique flight envelope of the X-24C, no existing air data system is available, and consequently this system is CFE. Rosemont Engineering Corporation is the potential manufacturer of this equipment.

- Inertial Navigation System - The inertial navigation system provides attitude and heading outputs and inertial velocities for display on the instrument panel and for use by the flight control system. The inertial system consists of two units: the input keyboard located in the cockpit, and the combined inertial measurement unit and digital computer. This system, manufactured by Litton Industries, is installed in an F-5E aircraft and consequently can be GFE. For use in the X-24C, however, it is required that the software program of its computer be modified to generate the longitudinal and vertical velocity signals and the digital to analog conversion in order to output these signals to the instruments and flight control system. The cost of these modifications is included in the Cost Analysis section of this report.
- Communication Equipment - The UHF radio communication equipment allows the X-24C pilot to communicate with neighboring aircraft and ground stations. Two AN/ARC-159 radios are used. The second radio serves as a back-up in the event of failure of the primary transceiver. The AN/ARC-159 UHF radio is the standard used in NASA's Dryden Flight Research Center F-104 fleet. These UHF radios are compatible with the antennas used in the X-15 program.
- Intercommunication Equipment - The intercom allows the pilot to communicate, on the ground, with the crew, and also with the B-52 crew prior to launch. The X-24B/X-15 intercom is proposed for use in the X-24C.

- Radar Beacon - The radar beacon enhances ground air air-borne radar acquisition and tracking of the X-24C. The X-24B/X-15 beacon is proposed for use in the X-24C.

Flight Control System - In developing conceptual flight control system designs, several trade-offs were required by the NASA Statement of Work, Appendix A. The first involved the use of fly-by-wire vs. conventional mechanical control means and the second addressed digital vs. analog flight control computational techniques. During the studies it was determined that fly-by-wire (FBW) was a more attractive choice for two reasons:

- Interchangeable payload bay, and
- Temperature effects.

The interchangeable payload bay requires that a mechanical control system be re-rigged everytime that this section of the aircraft is removed and replaced. This applies to the pitch, roll and yaw axes of control as well as the speed brakes. With FBW this rather precise time consuming task, mechanical re-rigging, can be minimized. The second reason is that the effects of vehicle elongation due to high temperature and the attendant complex cable tension devices can be eliminated. With respect to digital vs. analog computation methods, the availability of analog GFE equipment as opposed to digital GFE equipment resulted in the analog approach being selected.

As a result of the flight control system conceived for the X-24C features FBW in all three axes of control (including speed brakes), the use of a two axis side-arm controller, an analog mechanization, and has a triple channel redundancy level.

Control surfaces and their functions include: (1) pitch control by symmetrical operation of the left and right elevons, (2) roll control by differential operation of these same elevons (3) directional control (yaw) via the rudder on the central vertical fin, and (4) speed control employing the split surfaces on the central fin rudder.

The major elements of the flight control system shown diagrammatically in Figure 172 are:

- Side-arm controller (pitch and roll),
  - Rudder pedal position transducers,
  - Inertial Navigation System,
  - Flight Control Computer,
  - Air Data System,
  - Rate and Acceleration Sensors,
  - Triplex servo actuators, and
  - The surface actuation systems.
- Side-arm Controller - The side-arm controller converts pilot commands relative to pitch and roll rate and attitude changes into electrical analog signals to the Flight Control Computer. The side-arm controller

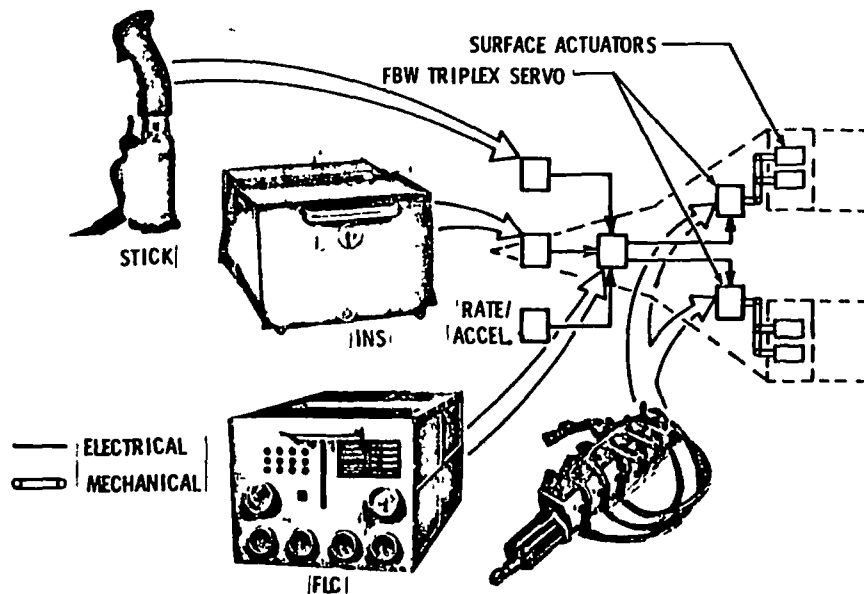


Figure 172 - Flight Control System Pitch and Roll Axis

proposed for the X-24C is a modified F-16 controller, developed for the USAF by the Lear Siegler Astronics Division, Santa Monica, CA. Lear Siegler has also supplied side-arm controllers to both NASA Dryden Flight Research Center and NASA Ames. This controller requires minor modification from a quadraflex to a triplex configuration. The side-arm controller will be available as GFE for the X-24C program, modified from its existing 4 channel operation to a 3 channel.

- Rudder Pedal Position Transducer - These transducers supply an electrical signal proportional to rudder pedal position to the Flight Control Computer. They would be supplied by Lear Siegler, and have triple channel outputs, left and right.
- Inertial Navigation System - The inertial navigation system was described earlier as part of the Avionics equipment. Although the flight control system is primarily mechanized triply redundant, the inertial system is singular. The reason for not requiring additional inertial systems is its demonstrated reliability, built-in-test, and the rather short flying time of the X-24C (compared to the F-5E).
- Flight Control Computer - The flight control computer performs the required computation of external signals which in turn are supplied to the surface control system through the triplex actuators as a function of predetermined control laws. The flight control computer is a modification of that being supplied to USAF for the F-16 program. This computer is also manufactured by Lear Siegler, and the modifications consist of elimination of the fourth channel required for the F-15, and the internal implementation of the analog X-24C control laws. This computer contains extensive built-in-test which allows complete end-to-end testing of the flight control system from sensors to aircraft control surfaces, As part of the F-16 program it is required to demonstrate a high level of reliability; much higher than required for the relatively short flying time, per mission, of the X-24C.

- Air Data System - The air data system provides scheduling functions as well as commands to the flight control system. The air data system was described earlier in the Avionic Systems portion of this report.
- Rate and Acceleration Sensors - Rate gyros and accelerometers sense the aircraft motion and provide signals to the flight control computer. These devices are CFE because of the unique characteristics of the X-24C. Pitch, roll, and yaw rate gyros, triplicated, and normal and lateral accelerometers, triplicated, are included. These devices have self test features to enable the flight control computer to assess their availability and reliability prior to and during flight. Lear Siegler would provide these sensors.
- Triplex Servo Actuators - During the development of the U.S. Army's Heavy Lift Helicopter (HLH) program, Berteau, Inc., developed a triplex servo actuator which underwent successful laboratory and flight testing as part of the HLH program. This actuator is proposed for the X-24C as the electro-mechanical link between the flight control computer and the surface actuation system. The triplex actuator provides for completely independent triple inputs, and mechanically summed hydraulic force/position outputs, which are capable of operating directly into the surface control actuators hydraulic valves. The triplex actuator operates from three 10 MPa hydraulic systems, two of which are the primary 21 MPa hydraulic systems powering the surface actuators. The third system is an independent hydraulic system (see Hydraulic System). Four of these actuators would be required for the X-24C. Two are needed for the pitch and roll axes, one for yaw control and the fourth for the speed brake control. Because these actuators have already been developed, though in limited quantities, their design and test data is available at minimum cost to support the X-24C program, requiring only the manufacturing costs of the needed additional actuators.

- Surface Actuation System - The surface actuation system consists of those actuators which move the X-24C control surfaces in response to the triplex servo actuators. It is anticipated that although the X-24B surface actuation system is available, it will require modification to accommodate the hinge moments associated with the higher Mach number and dynamic pressures.

Electrical System - The electrical system for the X-24C provides the power for the flight control system, the instruments, hydraulic system, communications, and for the ignition system. Figure 173 is a block diagram of the electrical system, and indicates that there are four battery assemblies which provide the prime electrical power. As shown on this figure, three batteries are devoted exclusively to the fly-by-wire flight control system. The fourth battery provides the power for instruments, navigation, communication, and engine ignition. Batteries were chosen as the source of electrical power over other means, e. g., a-c generators, monopropellant generators, etc., because of the simplicity and reliability they

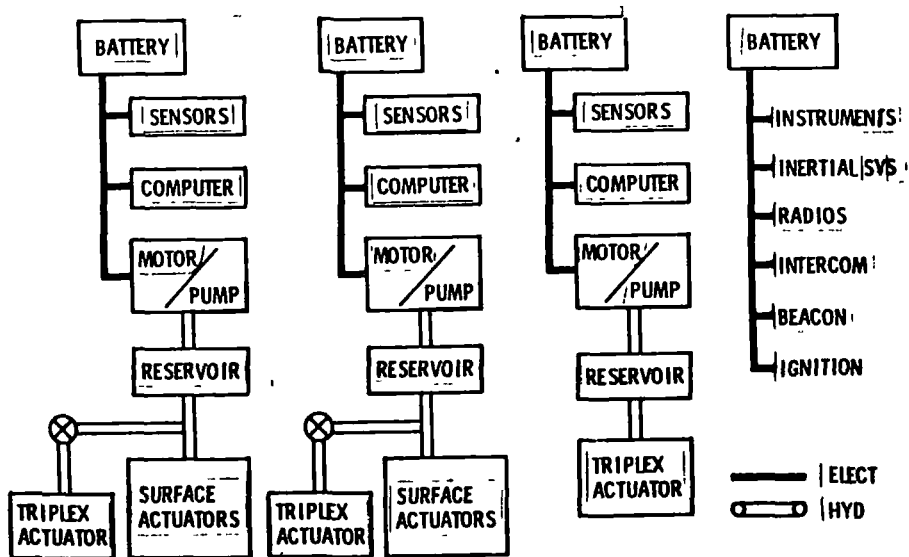


Figure 173 - Electrical and Hydraulic System

offer, and the fact that these battery units are available through the Federal Stock Number System (FSN). In addition, NASA's Dryden Flight Research Center has available support equipments, such as chargers, which can be fully utilized with no additional cost to the program.

The three batteries associated with the flight control system are located adjacent to the three hydraulic pumps to minimize line losses. The fourth battery is located in the nose of the vehicle. In addition to the four battery assemblies shown, a fifth assembly has been included for the exclusive use of the flight test instrumentation system. Prior to the launch of the vehicle it is required that these batteries be heated because of the cold temperatures anticipated internal to the X-24C during the climb-out and ascent to the launching altitude. Blanket heaters will be installed to maintain battery temperatures conducive to long battery life. The electrical power for these heaters will be supplied from the B-52. After launch, and during the acceleration to the cruise Mach number and descent for landing, the batteries will require cooling. Cooling will be provided by the X-24C environmental control system.

Hydraulic System - The hydraulic system for the X-24C consists of two 21 MPa power sources and a single 10 MPa source. The two 21 MPa systems power the X-24C surface actuators; the single 10 MPa system is devoted exclusively to the third channel of the flight control system (see Flight Control System). The hydraulic pumps for all three systems are powered by d-c motors. Each system is completely independent from the others having its own pump, accumulator, reservoir and plumbing lines. Such an arrangement guarantees the functional reliability of the fly-by-wire flight control system.

Cockpit and Furnishings - The cockpit and furnishings for the X-24C consist of the following:

- Instrument panel,
- Egress system,
- Side-arm controller,



- Rudder pedal arrangement,
- Console equipment,
- Canopy, and
- Environmental control system.

The instrument panel contains the instruments tabulated in Appendix D. In general, most of the instruments are available from the X-15/X-24B program. The egress system consists of the NASA YF-12 ejection seat. Although other ejection systems can be used, this seat was chosen because of its high "q" capability. It was also assumed that the pilot's pressure suit would also be of the YF-12 type available to NASA. The side-arm controller, mounted on the right hand console, is a modified USAF F-16 controller. The modification consists of the deletion of the fourth channel of electronics. The rudder pedal arrangement is that from the X-24B. This includes the rudder pedal force spring. Mounted to this assembly are the three force (or position) transducers. Console equipment includes the normal and emergency UHF radio control panels, the engine throttle controls and the Inertial Navigation System control panel, as major items. The canopy utilizes the X-15 fused silica quartz windows (2). Canopy deployment during emergency egress is provided through initiators and thrusters available from the YF-12 program. The environmental control system is composed of major components from the X-15/X-24B system.

### Structural Dynamics

#### Panel Flutter

Structural panel design for the SR-71 program used the design criteria presented in References (24) and (25). After the X-24C study contract award, NASA recommended that ADP update their panel flutter methods and suggested References (26) and (27) for this purpose. These two references were examined in detail, and prompted further study of panel flutter using References (4) and (28) through (33).

Reference (26) was used as the primary reference for study of the basic equations for panel flutter with the other references providing material for the implementing of the solution of those equations. The equations found in Reference (26) solve for the lateral deflection of thin isotropic plates as a function of the lateral loading. The lateral loading has two components, 1) inertial and 2) applied loadings (aerodynamic), etc. These equations can be solved directly only for very simple configurations and special applied loadings. In general, an approximate solution by either an energy approach using Lagrange's dynamical equation or by means of a Galerkin-type solution. In either method, the deflection is expanded in a series where the terms of the series are products of time dependent coefficients and the appropriate modal shapes. Reference (31) as well as others have modified the equations for an isotropic plate to accommodate an orthotropic plate.

Examination of the X-24C structural panel design indicated the flutter design criteria of Reference (26), which included the effects of edge support, in-plane stress ratio and structural damping, could be applied to the Lockalloy panels. The design criteria was calculated for a typical Lockalloy wing panel with a length and width of 0.46 m for a panel aspect ratio of one and with the minimum design thickness of 3.6 mm. Using the flutter criteria of Reference (26), the panel is flutter free for clamped edges, but requires structure damping,  $g = 0.01$ , for stability of the simple support case. The actual panel edge support will be somewhere in between.

The flutter criteria for a panel aspect ratio of one showed large changes for very small changes in panel aspect ratio with even more pronounced changes for panel aspect ratios less than one that represent the fuselage panels. Sensitivity of the flutter criteria as shown here would make it impractical to establish flutter safety on the basis of the criteria only. The assessment of the edge conditions, in-plane stress ratios, and orthotropic stiffness characteristics of the stiffened aluminum panel with either TPS candidate would be difficult for selecting the proper flutter criteria of Reference (31). The conclusions stated above led to the

decision to determine the panel flutter safety by analysis. The method of Reference (34) was considered for forming the structural model until it was determined that considerable modification would be required for its use. NASTRAN, as described in Reference (35) has many features that are needed to build a representative panel structure, and was thus chosen for the structural modeling. Two dimensional quasi-steady aerodynamics described in Reference (26) are used in the flutter analysis. The points in the flight envelope selected for the panel flutter analysis use a criterion  $f(m)$  from Reference (27) in place of  $\beta$  for the calculation of the parameter  $\beta E/q$ .

- Analysis

Stiffness - Representative panels of the wing and fuselage structure were modeled using the finite element NASA Structural Analysis Program (NASTRAN). Adequate structural definition was obtained using conditions of symmetry combined with substructuring feature of the NASTRAN program to construct a fine mesh structural grid. The analytical models featured detailed structural networks with an average of approximately 500 node points on a surface, and with  $z$ ,  $\theta_x$ , and  $\theta_y$  retained degrees of freedom.

The structural skin of each panel was built up of  $6 \text{ cm}^2$  homogeneous quadrilateral membrane and bending elements (QUAD 2). Skin panel mass, and TPS mass where applicable, were input with the QUAD 2 element data as non-structural mass.

Stiffeners and frames were represented by single beam elements (BAR) with the appropriate offsets such that out of plane shear center effects were included. Shear clips and connectors were modeled using scalar spring elements (ELAS 2).

Inertia - The inertia data is calculated using NASTRAN. This is done to ensure that the mass matrices are reduced in numbers of degrees of freedom in the same way as the stiffness matrices.

Material density for the BAR elements was input so that NASTRAN could calculate the appropriate mass distribution for these elements internally. Mass values for the shear clips and connectors are considered to be negligible.

Aerodynamics - The aerodynamics to be used for flutter analysis are the same as those noted in Reference (27). The two aerodynamic terms are as follows:

$$\frac{2q}{\beta} \frac{dw}{dx} + \rho c \frac{dw}{dt} = 0$$

The first term gives the aerodynamic forces as a function of stream-wise slope and the second term represents the aerodynamic damping. These terms were obtained from two dimensional quasi-steady aerodynamic theory.

Vibration - The vibration analysis is concerned with obtaining approximate modes of the plates that represent the first 10 modes in the stream direction combined with only the first mode in the crosstream direction. These modes, although approximate, must be close enough to the exact modes such that the frequency error is within one percent. This is required since these modes are used in the flutter analysis to reduce the computational times without loss in the mode quality.

Flutter - The panel flutter equation of Reference (26) was the starting point for the panel flutter analysis. The capability of including the effect of structural damping on the stiffness terms was retained in the equation modified for use in the Lockheed FAMAS computer program. The inplane panel loadings,  $N_x$  and  $N_y$ , will not be included in the initial analyses to reduce the time required for program checkout. The aerodynamic dampint term will not be included in the initial analysis for the same reason. The X-24C structural panels will be designed to show freedom from flutter to values of dynamic pressures,  $q$ , equal

to 1.32 times the  $q$  values at the selected, critical points of the flight envelope.

### Vibroacoustics

The vibroacoustic investigation of the X-24C study covers three areas of the flight envelope. The first area of concern is the captive flight segment from take-off to launch point. The second area of concern is the launch phase of the X-24C flight envelope. The third concern is primarily the panels in the exit area of the scramjet. The structural panels during these three phases are exposed to the broad band sound pressure levels due to jet and rocket engine exhausts. The analysis of panel fatigue for this load time history environment is very difficult due to the broad frequency band of force input. Normally the force input is treated as a random function and the panel response is obtained using power spectral techniques. Lockheed ADP developed a program in the FAMAS computer system that obtains transfer functions of aeroelastic analytical models due to sinusoidal force inputs at discrete speeds and frequencies. A scheme for using this program to investigate vibroacoustic panel effects is under study, and will be explained in the analysis. If the proposed scheme is not feasible, the random forcing function with power spectral analysis will be used.

- Analysis

The method of analysis under study for the vibroacoustics investigation uses the basic flutter equation except that the sum of the inertial, stiffness, and aerodynamic forces are set equal to a sinusoidal force input that is a function of frequency. The equation is solved for a given dynamic pressure,  $q$ , and a sequence of discrete input frequencies. The center frequency corresponds to a resonant frequency of the system. The response of the system is obtained in displacement, velocity, or acceleration as directed by the engineer. These responses can be converted to panel loads for evaluation of the fatigue characteristics of the panel.

The major disadvantage is the wide frequency bandwidth with numerous resonant frequencies of the panels that can be excited by the broad spectrum of sound pressure input from the rocket, jet, or scramjet engines. To analyze the structural panels, an almost infinite number of modes would need to be checked using the frequency response method. If the structural damping present increased for each succeeding higher order vibration mode, perhaps only a small number of lower frequency modes would have to be evaluated from a fatigue standpoint.

Some recent data on Lockalloy shows that the specific damping energy increases by a factor approximately equal to the stress level change ratio. Stress level is directly proportional to load level which in turn is inversely proportional to load level which in turn is inversely proportional to the radius of curvature of the deflected elastic element. Observation of vibration modes has shown that radius of curvature decreased as the order of vibration modes goes from the fundamental to the higher modes, which in turn means the stress level increases steadily as the vibration modes move from the fundamental mode to the higher order modes. The results of this study now in progress may in fact prove the predicted theoretical trends, but from a practical engineering standpoint indicate that the size of the computational problem can not be reduced because of the minimal effect in actual structures.

If the effect being investigated is negligible from an engineering standpoint, the random function/power spectral method would be used.

### Mass Analysis

Group mass predictions found in Table 27 were developed by using all the various applicable methods available. Thermal Protection System (TPS) mass were derived partly by minimum and average thicknesses bonded to wetted areas of wing, tail and fuselage; and partly by calculations from thermal tables of required typical panel thicknesses over typical areas. Wing, Tail, and Fuselage

	Group Mass Breakdowns - kg										
	LR-99 Engine (Throttled)				LR-105 + 2 LR-11 Sustainers				LR-105 + 12 Atlas Verniers		
	-109 Ablator	-108 LI-900	-107 Lockalloy	-106 Ablator	-105 LI-900	-104 Lockalloy	-103 Ablator	-102 LI-900	-101 Lockalloy		
T. P. S.	820	417	-	820	417	-	820	417	417	-	-
Wing	356	361	476	356	361	388	356	361	388	388	388
Tail	279	279	482	246	246	423	246	246	423	423	423
Fuselage	3285	3350	3987	3390	3455	4092	3359	3424	4068	4068	4068
Landing Gear	590	590	590	590	590	590	590	590	590	590	590
Propulsion	497	497	497	866	866	866	658	658	658	658	658
Propellant System	1202	1202	1202	1043	1043	1043	998	998	998	998	998
Systems	1143	1143	1154	1135	1135	1148	1135	1135	1148	1148	1148
Contingencies	-	-	-	-	-	-	-	-	-	-	-
Mass Empty	8172	7839	8383	8446	8113	8850	8162	7829	8273	8273	8273
Useful Load	186	186	186	186	186	186	186	186	186	186	186
Flight Test Instrumentation	454	454	454	454	454	454	454	454	454	454	454
Operating Mass Empty	8812	8479	9028	9086	8753	9190	8802	8469	8913	8913	8913
Payload	64	397	-152	894	1227	790	1957	2290	1846	1846	1846
Three Scramjets	-	-	-	-	(1225)	-	(1225)	(1225)	(1225)	(1225)	(1225)
Other	-	-	-	-	(2)	-	(732)	(1065)	(621)	(621)	(621)
Maximum Allowable Z. F. Mass	8876	8876	8876	9980	9980	9980	10759	10759	10759	10759	10759
Required Propellant	16979	16979	16979	15875	15875	15875	15096	15096	15096	15096	15096
Launch Mass	25855	25855	25855	25855	25855	25855	25855	25855	25855	25855	25855
DCPR	7037	6705	7254	7013	6681	7117	5938	6605	7049	7049	7049

Table 27 - Group Mass Properties Breakdown

Structure mass were generated by use of NASTRAN output loads information for skins, stiffeners, rings, and bulkheads. Doors and access panel cutout penalties were then hand calculated, as were wing leading edges, elevons, and rudder. Landing Gear mass was obtained from actual mass reports of the C-140A and F-106 airplanes with slight modification. Engine mass were taken from engine specifications and X-15 data. Propellant System mass were calculated from tank size requirements plus preliminary information as to fuel system, plumbing, equipment and insulation. Systems mass were coordinated with the preliminary equipment list and rounded out by use of historical comparative data. Useful Load is made up of pilot, pressurized suit, oxygen and unusable fluids, plus a 454 kg allotment for flight test instrumentation. SCRAMJET mass were estimated from verbal information and substantiated by a copy of the preliminary version of a report entitled: "Scramjet Module Experiment Weight and Payload Bay Volume" by Ernest A. Mackley.

Results - Table 27 reflects the results of the detail mass analysis, described herein, for each of the candidate configurations using the methods described above.

Starting with the Baseline Launch Mass of 25.85 Mg, established by NASA, and subtracting the mass of propellant, required by the candidate propulsion systems to accomplish the Baseline mission, the Maximum Allowable Zero Fuel Mass is derived for each of the candidate configurations. This then establishes the 'not' to exceed mass limit the candidate configurations must meet in order to become viable candidates.

Using the propellant mass required for each configuration, to complete a specific mission, this then established the fuel cell volumes and size required to fit within the aerodynamic shape, predetermined by NASA, and the candidate structural concepts for the X-24C. Mass analysis on each of the major structural segments of the vehicle as well as the associated subsystems established the Mass Empty of each of the candidate configurations. Adding a uniform Useful Load, a predetermined Flight Test Instrumentation Load to the established Mass Empty for each configuration established the Operating Mass Empty for each



configuration. The difference between the determined Allowable Zero Fuel Mass and the established Operating Mass Empty determined a payload mass allowance. If the payload allowance turned out to be a negative number, as the case of configuration X-24C-107 of Table 27, this determined that configuration as not a viable candidate. Having determined the Payload mass the mass of the three (3) scramjets, another NASA Baseline requirement, is subtracted resulting in a term identified as Other in Table 27. A positive number implies a viable candidate, one which can do the mission within an established mass constraint while meeting all Baseline requirements. A negative number, as occurred with configuration -104, -106, -107, -108 and -109 of Table 27 implies a 'not viable concept.' Four of the nine configurations -101, -102, -103 and -105 of Table 27 were found to be viable concepts capable of meeting the Baseline requirements and with capability of additional, 'Other,' payload. However only three configurations, utilizing the same propulsion system met the Baseline requirements while providing a good load range for payload or future growth potential. These configurations were -101, -102 and -103 of Table 27.

Wing Mass Analysis - A detailed stress analysis of the wing structural box was conducted for the following three types of wing structure:

- Aluminum design with LI-900 TPS
- Aluminum design with Ablator TPS
- Lockalloy heat sink skin panels

Results of the wing stress analysis was used in the mass analysis for the wing structural box. A fourth design consideration applies only to the elevons, for the Lockalloy wing on the LR-99 vehicle. The heat sink material on the lower surface has a different thickness requirement because of the constant 15° down elevon at cruise required to trim the vehicle with speed brakes deployed during rocket cruise.

### Aluminum Wing LI-900 Configuration:

- Structural box upper and lower surface panels - Table 28 and 29. The lower surface skin panels were analyzed by the method used on the upper surface.
- Spars and Ribs - For the substructure components (caps and webs), Figure 174, the internal loads from the structural model runs were reviewed. The loads from the most critical load condition were used to size these components for their critical failure modes. Local areas were sized for strength and this data was expanded to the total wing by the following:

$$\text{cap mass}_{(\text{up./lwr.})} = \left[ \left( t_{e(\text{skin})} \times 1.5 \right) 0.0478 \text{ m} + 0.00127 \text{ m} \right. \\ \left. \times 0.0142 \text{ m} \right] \text{span} \times \rho \times 1.15 \times 2$$

$$\text{web mass} = h \times \text{span} \times 0.00127 \text{ m} \times \rho \times 1.15 \times 2 - (\text{Table 30})$$

- Leading Edge - The leading edge has a buildup of 0.81 mm unstiffened skin panels with formers at each wing frame station. The leading edge beam caps have a cross sectional area of 61 mm<sup>2</sup>. Mass properties depicted in Table 31.
- Elevons - Use 9.03 kg/m<sup>2</sup> for spars and ribs, including elevon attach fittings and supports. Skin panels, upper and lower, have an average  $t_e$  of 2.36 mm<sup>2</sup>/mm including doublers, splices, and hardware. Mass properties depicted in Table 32.
- Wing Summary - LI-900 - See Table 33.
- Aluminum Wing-Ablator Configuration - Surface panels are designed for non-buckling at 80% limit load for these vehicles. This design concept for these vehicles changes the  $t_e$  requirement for the structural box

Frame Station/ Butt Line	Panel L/R Area (m <sup>2</sup> )	$t_e$ ( $\times 10^{-3}$ m <sup>2</sup> /m)	Volume ( $\times 10^{-3}$ m <sup>3</sup> )	Mass (kg) +15% NOF
<b>Upper Surface Panels</b>				
(Mass = Volume $\times \rho \times 1.15$ )				
<u>B L 72 - 107.8</u>				
<u>F S</u>				
552.8 - 590.0	0.7804	1.42	1.11	3.6
590.0 - 623.7	0.7830	1.42	1.11	3.6
623.7 - 649.1	0.5906	1.85	1.09	3.5
649.1 - 674.6	0.5908	2.24	1.32	4.3
674.6 - 700.0	0.5906	2.36	1.39	4.5
<b>Material to Transfer End Plane Surface Panel Loads to Adjacent Body Structure</b>				
(Mass = $t_e \times \text{Span} \times 0.36 \text{ m} \times \rho \times 2$ )				
552.8 - 590.0		0.00142 $\times$ 0.945 $\times$ 0.36 $\times$ 2800 $\times$ 2		2.7
590.0 - 623.7		0.00142 $\times$ 0.856 $\times$ 0.36 $\times$ 2800 $\times$ 2		2.4
623.7 - 649.1		0.00185 $\times$ 0.646 $\times$ 0.36 $\times$ 2800 $\times$ 2		2.4
649.1 - 674.6		0.00224 $\times$ 0.646 $\times$ 0.36 $\times$ 2800 $\times$ 2		2.9
674.6 - 700.0		0.00236 $\times$ 0.646 $\times$ 0.36 $\times$ 2800 $\times$ 2		3.0
<u>B L 107.8 - 123.6</u>				
<u>F S</u>				
590.0 - 623.7	0.4355	1.42	0.618	2.0
623.7 - 649.1	0.5797	1.65	0.957	3.1
649.1 - 674.6	0.5908	2.11	1.25	4.0
674.6 - 700.0	0.5906	1.93	1.14	3.7
<u>B L 123.6 - 139.4</u>				
<u>F S</u>				
623.7 - 649.1	0.0545	1.42	0.077	0.2
649.1 - 674.6	0.4021	2.01	0.808	2.6
674.6 - 700.0	0.5906	1.73	1.02	3.3
<b>Chordwise Splices at Rib Joints</b>				
Mass = $[t_e(\text{Inboard}) + t_e(\text{Outboard})] \times 0.102 \text{ m} \times \text{Span} \times \rho \times 1.15 \times 2$				
<u>B L 92</u>		(0.00186 + 0.00186) $\times$ 0.102 $\times$ 3.737 $\times$ 2800 $\times$ 2.30		9.1
<u>B L 107.8</u>		(0.00197 + 0.00178) $\times$ 0.102 $\times$ 2.794 $\times$ 2800 $\times$ 2.30		2.8
<u>B L 123.6</u>		(0.0019 + 0.00172) $\times$ 0.102 $\times$ 1.622 $\times$ 2800 $\times$ 2.30		3.9
<b>Spanwise Splices at Spars</b>				
Mass = $[2t_{(\text{skin})} \times 0.0635 \text{ m} + 0.019 \text{ m} (t_1 - t_2)] \times \text{Span} \times \rho \times 1.15 \times 2$				
<u>F S</u>				
590.0		[(2 $\times$ 0.00142 $\times$ 0.0635) + 0 $\times$ 0.019] $\times$ 0.43 $\times$ 2800 $\times$ 2.30		0.5
623.7		[(2 $\times$ 0.00159 $\times$ 0.0635) + (0.00066 $\times$ 0.019)] $\times$ 0.81 $\times$ 2800 $\times$ 2.30		1.1
649.1		[(2 $\times$ 0.00188 $\times$ 0.0635) + (0.00048 $\times$ 0.019)] $\times$ 1.09 $\times$ 2800 $\times$ 2.30		1.7
674.6		[(2 $\times$ 0.00191 $\times$ 0.0635) + (0.00033 $\times$ 0.019)] $\times$ 1.37 $\times$ 2800 $\times$ 2.30		2.2
700.0		[(2 $\times$ 0.0019 $\times$ 0.0635) + (0 $\times$ 0.019)] $\times$ 1.37 $\times$ 2800 $\times$ 2.30		2.1
<b>Removable Panels (Fairing) Inboard of B L 92</b>				
Use same $t_e$ as next outboard panel				
Mass = 0.165 (0.00142 $\times$ 1.801) + (0.00185 $\times$ 0.645) + (0.00224 $\times$ 0.645) + (0.00236 $\times$ 0.645) $\times$ 2800 $\times$ 1.15 $\times$ 2				
<b>Hardware</b>				
Mass = Mass <sub>(Panels)</sub> $\times$ 0.05 = 86.3 $\times$ 0.05				
<b>TOTAL UPPER SKIN PANELS</b>				<b>90.6</b>

Table 28 - Wing Structural Box - LI-900

Item	Mass (kg)
Lower Surface Panels	31.1
Load Transfer Material Added to Panels	11.3
Chordwise Spllices	15.4
Spanwise Spllices	4.0
Removable Lower Panels	6.0
Hardware	3.4
<b>Total Lower Skin Panels</b>	<b>● 71.2</b>

Table 29 - Lower Skin Panels - LI-900

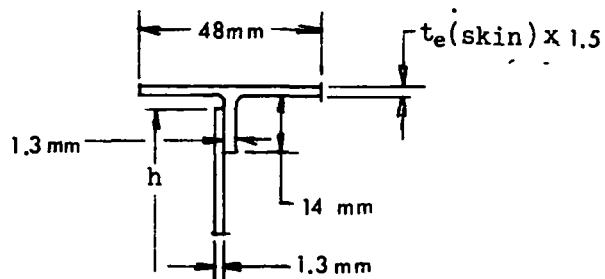


Figure 174 - Spars and Ribs

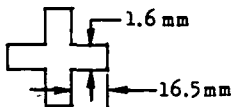
Item	Mass (kg)
Spars	19.6
Ribs	37.7
Ribs to Spar Spllices	2.2
 Area = 1.03 mm <sup>2</sup> Use h = 0.20 m Ave	
$\text{Mass} = A \times h_{(\text{web})} \times \rho \times \text{Number Required}$ $= 1.03 \times 10^{-4} \times 0.20 \times 2800 (19 \times 2)$	
Hardware	2.9
$\text{Mass} = (\text{Mass}_{(\text{Spars \& Ribs})} \times 0.05)$ $= 57.3 \times 0.05$	
<b>TOTAL SPARS AND RIBS</b>	<b>● 62.4</b>

Table 30 - Spars and Ribs

Item	Mass (kg)
Skin Panels	9.5
Formers	3.5
Leading Edge Beams	6.5
Hardware	1.4
Total Leading Edge	● 20.9

Table 31 - Leading Edge Mass - LI-900

Item	Mass (kg)
Spars and Ribs	38.0
Skin Panels	63.8
Aft and Side Closing Members	5.3
Total Elevon	● 107.1

Table 32 - Elevon Mass - LI-900

surface panels from the LI-900 vehicles. The rib/spar portion of the wing is the same for all aluminum vehicles. See Figures 65 and 66 for the surface panel  $t_e$  required.

- Ablator Configuration - Wing Summary - See Table 34.
- Lockalloy Wing - LR-105/12 LR-101 Engine Configuration - The wing was analyzed for 0.46 m spar and rib spacing. Skin panel thicknesses are shown in Figure 69.
- Structural Box Upper and Lower Surface Panels (Tables 35 and 36) - The lower surface panels were analyzed by the same method used on the upper surface.

Item	Mass (kg)
Structural Box	224.2
Upper Skin Panels	90.6
Lower Skin Panels	71.2
Spars and Ribs	62.4
Leading Edge	20.9
Wing Attach Structure	9.5
Elevons	107.1
Total Wing	●361.7

Table 33 - Wing Summary - LI-900

Item	Mass (kg)
Structural Box	213.2
Upper Skin Panels	80.7
Lower Skin Panels	70.1
Spars and Ribs	62.4
Leading Edge	20.9
Wing Attach Structure	9.5
Elevons	107.1
Total Wing	●350.7

Table 34 - Wing Summary - Ablator

- Spars and Ribs - Use data from Figure 62 for determining titanium spars and ribs. (Use 0.46 m rib spacing.)

$$\begin{aligned}
 \text{Mass}_{(\text{SPARS AND RIBS})} &= 7.62 \text{ kg/m}^2 \times S_{(\text{STRUCTURAL BOX})} \\
 &= 7.62 \times 7.63 \text{ m}^2 \\
 &= \bullet 58.1 \text{ kg}
 \end{aligned}$$

Frame Station/Butt Line	Panel L/R (Area m <sup>2</sup> )	$t_e$ ( $\times 10^{-3}$ m <sup>2</sup> /m)	Volume ( $\times 10^{-3}$ m <sup>3</sup> )	Mass (kg) +5% NOF
Upper Surface Panels. (Mass = Volume $\times \rho \times 1.05$ )				
<u>B. L. 92 - 107.8</u>				
<u>F. S.</u>				
552.8 - 590.0	0.7804	3.56	2.78	6.1
590.0 - 623.7	0.7830	3.71	2.90	6.4
623.7 - 661.9	0.8843	4.39	3.88	8.5
661.9 - 680.9	0.4398	4.19	1.84	4.0
680.9 - 700.0	0.4421	4.01	1.77	3.9
<u>B. L. 107.8 - 123.6</u>				
<u>F. S.</u>				
590.0 - 623.7	0.3881	3.56	1.38	3.0
623.7 - 661.9	0.8798	3.63	3.19	7.0
661.9 - 680.9	0.4376	3.94	1.72	3.8
680.9 - 700.0	0.4399	3.81	1.68	3.7
<u>B. L. 123.6 - 139.4</u>				
<u>F. S.</u>				
623.7 - 661.9	0.4409	4.32	1.90	4.2
661.9 - 680.9	0.4386	5.46	2.39	5.2
680.9 - 700.0	0.4409	3.43	1.51	3.3
Removable Panels at B. L. 92.				
<u>B. L. 86.0 - 92.0</u>				
<u>F. S.</u>				
552.8 - 700.0	1.1776	3.05	3.59	7.9
Spanwise and Chordwise Splices*				
(Mass = 0.711 kg/m $\times$ ) = 0.711 $\times$ 24.1				17.1
Fasteners*				
(Mass = Mass <sub>(panels + Splices)</sub> $\times$ 0.075) = (67.0 + 17.1) $\times$ 0.075				6.3
<b>TOTAL UPPER SKIN PANELS</b>				<b>● 90.4</b>

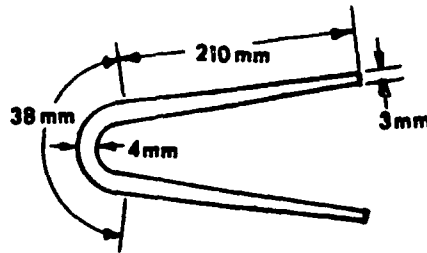
Table 35 - Wing Structural Box - Lockalloy

Item	Mass (kg)
Lower Surface Panels	63.3
Removable Panels	8.7
Splices	17.1
Fasteners	6.8
<b>Total Lower Skin Panels</b>	<b>● 95.1</b>

Table 36 - Lower Skin Panels - Lockalloy

- Leading Edge - Use peak temperature data for 70° swept wing from Figure 118.

LEADING EDGE F. S. 552.8 - 662.2



Mass summary depicted in Table 37:

Item	Mass (kg)
Leading Edge:	
F. S. 552.8 - 662.2	22.3
$\text{Mass} = 3.17 \text{ m} \left[ 0.00381 \times 0.038 + 0.211 \left( \frac{0.00381 + 0.00305}{2} \right) \right]$ $\times 2 \times 2090 \times 1.05$	
F. S. 662.2 - 700.0	4.5
Same as F. S. 552.8 - 622.2 except tapered section is 0.135 m	
$\text{Mass} = 0.096 \text{ m} \left[ 0.00381 \times 0.038 + 0.135 \left( \frac{0.00381 + 0.00305}{2} \right) \right]$ $\times 2 \times 2090 \times 1.05$	
Hardware	2.0
Total Leading Edge	●28.8

Table 37 - Leading Edge Mass - Lockalloy



- Elevons - Table 38 shows the skin thickness required for the various vehicles. Use  $9.03 \text{ kg/m}^2$  for elevon spars and ribs, including attach. fittings and supports. Area/elevon is  $2,105 \text{ m}^2$ .

Elevon mass breakdown - LR-105/12 LR-101 Engine and LR-99T Engine Vehicles - Table 39.

Vehicle	Panel Thickness	
	Upper	Lower
LR-105/12 - LR-101	3.8 mm	3.8 mm
LR-99T	3.8 mm	6.35 mm

Table 38 - Elevon Panel Thickness - Lockalloy

Item	Mass (kg)
<b>Elevon - LR-105 Vehicle</b>	
Skin Panels - Upper and Lower	
$\text{Mass}_{(\text{skin})} = 2t \times S \times \rho \times 2 \times 1.05$ $= 2 \times 0.00381 \times 2,105 \times 2090 \times 2 \times 1.05$	70.8
$\text{Mass}_{(\text{splices})} = l \times 0.711$ $= 25.6 \times 0.711$	18.1
Spars and Ribs	
$\text{Mass}_{(\text{spars \& ribs})} = 9.03 \times S$ $= 9.03 (2,105) 2$	38.0
<b>TOTAL ELEVON - LR-105 VEHICLE</b>	<b>● 126.9</b>
<b>Elevon - LR-99T Vehicle</b>	
Skin Panels - Upper and Lower	
$\text{Mass}_{(\text{skin})} = (t_{\text{upper}} + t_{\text{lower}}) S \times \rho \times 2 \times 1.05$ $= (0.00381 + 0.00635) 2,105 \times 2090 \times 2 \times 1.05$	94.3
$\text{Mass}_{(\text{splices})} = (\text{same as above})$	18.1
$\text{Mass}_{(\text{spars \& ribs})} = (\text{same as above})$	38.0
<b>TOTAL ELEVON - LR-99T VEHICLE</b>	<b>● 150.4</b>

Table 39 - Elevon Mass - Lockalloy

- Lockalloy Vehicles - Wing Summary (Table 40).
- Wing Mass Summary - Wing structure mass summary for all configurations is shown in Table 41.

Tail Mass Analysis - The tail group in the following mass analysis is broken down into the following three major categories:

- Vertical fin
- Rudder/speed brakes
- Side fins

The speed brake capability required designs the vertical tail so the following design criteria is presented to support the tail mass substantiation.

- Speed Brake Design Consideration - Table 42 shows the overthrust at cruise and the drag required at the start of descent. (All design conditions are at max. q.)

A split rudder design was selected for use as the energy management system for the X-24C in flight operations. The critical design conditions for the speedbrakes is the drag load shown in the above chart. Figure 175 depicts rudder.

$$S_{(\text{speedbrakes})} = \frac{D}{q C_D}$$

Where:

$$D = 101.4 \text{ kN (LR-99T); } 44.5 \text{ kN (LR-105)}$$

$$q = 47.9 \text{ kPa}$$

$$C_D = 1.0$$

Item	Mass (kg)	
	LR-105	LR-99T
Structural Box	243.6	243.6
Upper Skin Panels	90.4	90.4
Lower Skin Panels	96.1	96.1
Spars and Ribs	58.1	58.1
Leading Edge	28.8	28.8
Wing Attach Structure	17.6	17.6
Elevons	126.9	150.4
Total Wing	416.9	440.4

Table 40 - Wing Summary - Lockalloy

Item	Vehicle Configurations								
	LR-105 + 12 Atlas Verniers			LR-105 + 2 LR-11 Sustainers			LR-99 Throttled		
	Lockalloy kg	LI-900 kg	Ablator kg	Lockalloy kg	LI-900 kg	Ablator kg	Lockalloy kg	LI-900 kg	Ablator kg
Structural Box	243.6	224.2	213.2	243.6	224.2	213.2	243.6	224.2	213.2
Upper Skin Panels	90.4	90.6	80.7	90.4	90.6	80.7	90.4	90.6	80.7
Lower Skin Panels	95.1	71.2	70.1	95.1	71.2	70.1	95.1	71.2	70.1
Spars and Ribs	58.1	62.4	62.4	58.1	62.4	62.4	58.1	62.4	62.4
Leading Edge	28.8	20.9	20.9	28.8	20.9	20.9	28.8	20.9	20.9
Wing Attach Structure	17.6	9.5	9.5	17.6	9.5	9.5	17.6	9.5	9.5
Elevons	126.9	107.1	107.1	126.9	107.1	107.1	150.4	107.1	107.1
<b>TOTAL WING STRUCTURE</b>	<b>417</b>	<b>362</b>	<b>351</b>	<b>417</b>	<b>362</b>	<b>351</b>	<b>440</b>	<b>362</b>	<b>351</b>

Table 41 - Wing Structure Mass Summary

Design Condition	Main Engines	
	LR-99T	LR-105
<b><u>CRUISE PHASE</u></b>		
Min. throttle - main engine (thrust = kN)	132.6 kN	0 kN
Scramjets (3) (kg)	40.0	40.0
Sustainer Engines	-	31.1
X-24C Drag (Clean)	71.2	71.2
<b>EXCESS CRUISE THRUST</b>	101.4	0
<b><u>START OF DESCENT</u></b>		
In addition to X-24C drag	44.5	44.5
<b>DESIGN SPEED BRAKES TO</b>	101.4	44.5

Table 42 - Speed Brake Design Conditions

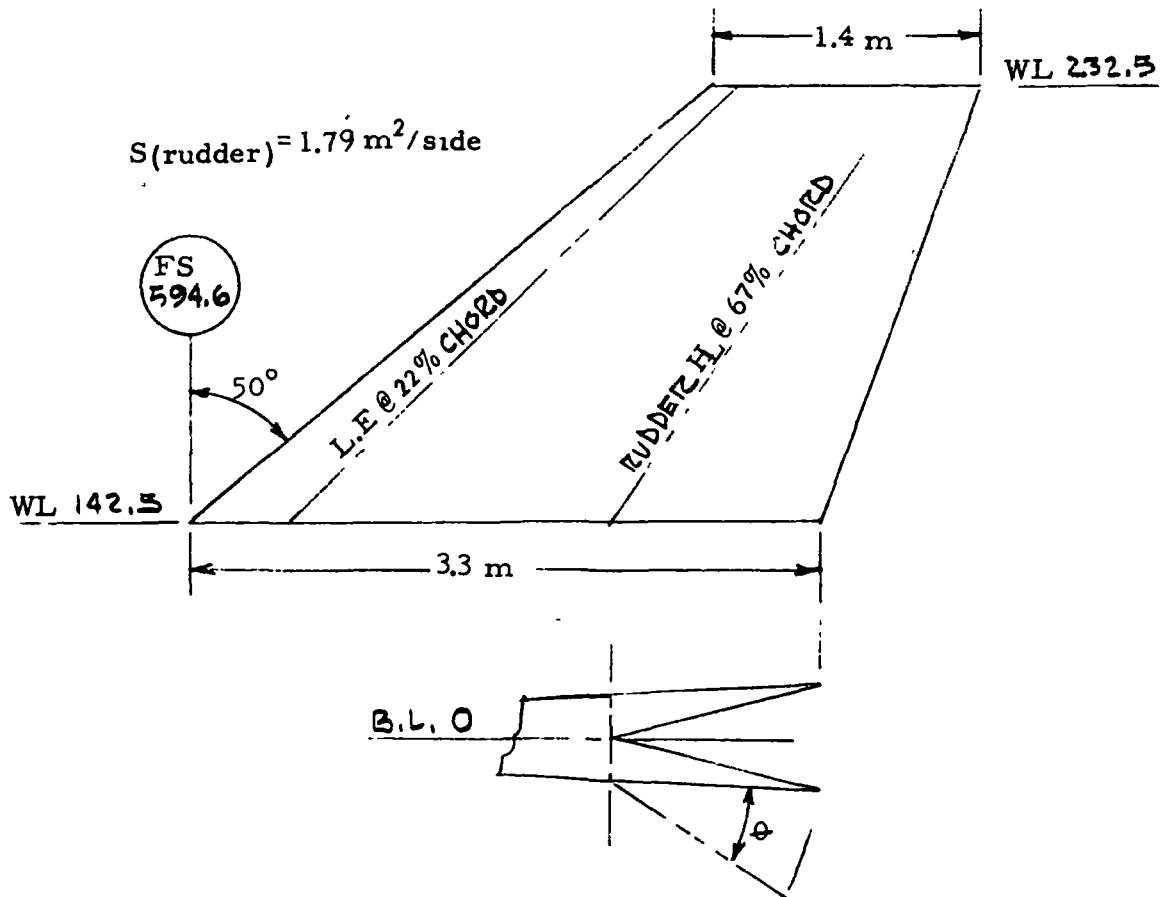


Figure 175 - Rudder Envelope

$$S_{(\text{speedbrakes})} = 2.12 \text{ m}^2 \text{ (LR-99T); } 0.929 \text{ m}^2 \text{ (LR-105)}$$

Determine speed brake open angle required for the two drag conditions, Figure 176.

$$S_{(\text{effective})} = 2S_{(\text{rudder})} \sin \theta$$

The tail system (vertical fin including speed brakes and side fins, was not covered by stress analysis, so a parametric analysis for this system was used.

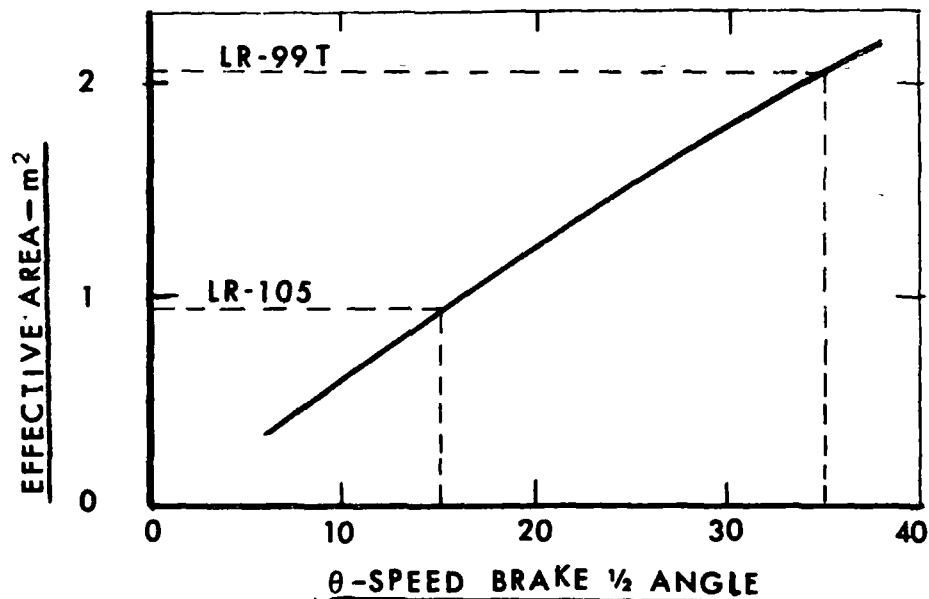


Figure 176 - Speed Brake Limit

• Vertical Fin Analysis - Aluminum Configuration

$$\text{Mass}_{(\text{basic shell})} = 0.650 \left( \frac{N}{m^2} \right)^{0.3} (m^2) + 6.84 (m^2) \\ + 1.35 \left( \frac{N}{m^2} \right)^{0.2} (m^2)$$

Where

$$F_V = 3.8869 (N M_{DES})^{0.891} \quad \text{Ultimate vertical tail load}$$

$$F_V = 3.8869 (3.75 \times 25.85 \text{ Mg})^{0.891} = 107.8 \text{ kN}$$

$$\text{Mass}_{(\text{basic shell})} = 0.650 \left( \frac{107.8}{5.44} \right)^{0.3} (1.2) + 6.84 (2.45) \\ + 1.35 \left( \frac{107.8}{5.44} \right)^{0.2} (1.79) \\ = 49.4 \text{ kg}$$

$$\text{Mass}_{(\text{bending material})} = 0.000111 \left( \frac{2F_V}{t_R} \right)^{0.7} (2b')^{1.4} \\ (1 + \lambda)^{0.35} (2S_{SB})^{0.3}$$

Where

$$b' = \text{Structural span @ 50\% chord (2.87 m)}$$

$$t_R = \text{Maximum thickness @ root (0.357 m)}$$

$$\lambda = C_T/C_R \text{ planform taper ratio (0.426)}$$

$$\begin{aligned}
 \text{Mass}_{\text{(bending material)}} &= 0.000111 \left( \frac{2 \times 107.8}{0.357} \right)^{0.7} \\
 &\quad (2 \times 2.87)^{1.4} (1 + 0.426)^{0.35} \\
 &\quad \times (2 \times 2.45)^{0.3} \\
 &= 26.0 \text{ kg (Use 39.0 kg for LR-99 and} \\
 &\quad \quad \quad 36.1 \text{ kg for LR-105 Engine} \\
 &\quad \quad \quad \text{Configuration)}
 \end{aligned}$$

Sweep back kick load:

$$\text{Mass} = 5.79 \times 10^{-6} \left( \frac{4F_V b'}{t_R} \times \frac{S_{VO}}{S_{VT}} \sin \Lambda \quad 0.5 C \right)^{0.92}$$

$$\text{Use } \frac{S_{VO}}{S_{VT}} = 1.0$$

$$\text{Mass} = 5.79 \times 10^{-6} \left( \frac{4 \times 107.8 \times 2.87}{0.357} \times 1 \sin 38.5^\circ \right)^{0.92}$$

$$= 3.9 \text{ kg (Add to above bending material to get total spar and rib mass)}$$

Since the critical design loads aft of hinge line on the vertical fin are caused by overthrust conditions the 67% to 100% chord section is analyzed as a speed brake:

$$\text{Mass}_{\text{(speed brake + support structure)}} = 0.146 (N_{SB} S_{SB})^{0.98} (q C_D S_{SB})^{0.49}$$

Where:

$$N_{SB} = \text{number required (2)}$$

$$S_{SB} = \text{speed brake area/brake (1.79 m}^2\text{)}$$

q = design dynamic pressure (47.9 kPa)

$C_D$  = drag coefficient (Use  $1 \times \sin \theta$ )

LR-99T Engine Configuration:

$$\begin{aligned} \text{Mass}_{(\text{speed brake})} &= 0.146 (2 \times 1.79)^{0.98} (47.9 \sin 35^\circ \times 1.79)^{0.49} \\ &= 101.4 \text{ kg (Use 92.3 kg) See Note 1.} \end{aligned}$$

LR-105 Engine Configuration:

$$\begin{aligned} \text{Mass}_{(\text{speed brake})} &= 0.146 (2 \times 1.79)^{0.98} (47.9 \sin 15^\circ \times 17.9)^{0.49} \\ &= 68.7 \text{ kg (Use 62.5 kg) See Note 1.} \end{aligned}$$

Total Primary Structure Mass Vertical Fin:

LR-99T Engine Configuration    180.7 kg

LR-105 Engine Configuration    148 kg

- Vertical Fin Analysis - Lockalloy Vehicles - The Lockalloy skin panels are sized by thermal requirements on the windward side and on the inner surface of the speed brakes a panel thickness of 5.08 mm was used.

Substructure mass for the Lockalloy configurations was estimated by the following:

**NOTE 1:** Use 9% of speed brake mass in main box as increased support structure to support the speed brakes.



$$\text{Mass}_{(\text{spars \& ribs})} = \frac{f_{tu} (394 \text{ K Al.})}{f_{tu} (478 \text{ K Ti.})} \times \text{Al. Mass (394 K)} \times \frac{\rho (\text{Ti.})}{\rho (\text{Al.})}$$

Skin panel estimate, see Table 43.

Surface area breakdown:

$$\text{L. E. (0 - 0.22 chord)} = 1.20 \text{ m}^2/\text{side}$$

$$\text{Main (0.22 - 0.67 chord)} = 2.45 \text{ m}^2/\text{side}$$

$$\text{Speed brakes (0.67 - 1.0 chord)} = 1.79 \text{ m}^2/\text{surface}/\text{side}$$

$$\text{Mass}_{(\text{skin panels})} = S(\text{m}^2) \text{ Thickness} \times \rho \times 1.025 = \text{Table 44}$$

Spars and inner ribs - main box; (see tail mass breakdown summary for aluminum bending material mass).

$$\begin{aligned} \text{LR-99T Mass}_{(\text{spars \& ribs})} &= \frac{4.0 \times 10^8}{9.31 \times 10^8 \times 0.84} \times 41.4 \times \frac{4510}{2800} \\ &= 34.1 \text{ kg} \end{aligned}$$

$$\begin{aligned} \text{LR-105 Mass}_{(\text{spars \& ribs})} &= \frac{4.0 \times 10^8}{7.82 \times 10^8} \times 38.8 \times \frac{4510}{2800} \\ &= 32.0 \text{ kg} \end{aligned}$$

Ribs and attach linkage - speed brakes:

$$\text{LR-99 Mass}_{(\text{ribs and attach linkage})} = \frac{4.0 \times 10^8}{7.82 \times 10^8} \times 31.1 \times \frac{4510}{2800} = 25.6 \text{ kg}$$

$$\text{LR-105 Mass}_{(\text{ribs and attach linkage})} = \frac{4.0 \times 10^8}{7.82 \times 10^8} \times 17.6 \times \frac{4510}{2800} = 14.5 \text{ kg}$$

Main Engine	Skin Panel Location/Average Thickness			
	L. E.	Main Box	Rudder	
			Inner	Outer
LR-99T	8.9	6.4	6.0	13.3
LR-105	8.9	6.4	5.0	7.6

Table 43 - Skin Panel Thickness ~ mm

Main Engine	Skin Panel Mass (kg)		
	L. E.	Main Box	Rudder
LR-99T	45.7	66.7	141.2
LR-105	45.7	66.7	97.4

Table 44 - Skin Panel Mass

Total primary structure mass, vertical fin:

LR-99T Engine Configuration 313.3 kg

LR-105 Engine Configuration 256.3 kg

- Side Fins Analysis - Aluminum Vehicles - See Figure 177.

Design criteria - side fin:

Areas:

$$S_{(\text{side fin})} = \frac{2.79 + 2.36}{2} \times 1.12 = 2.88 \text{ m}^2/\text{fin}$$

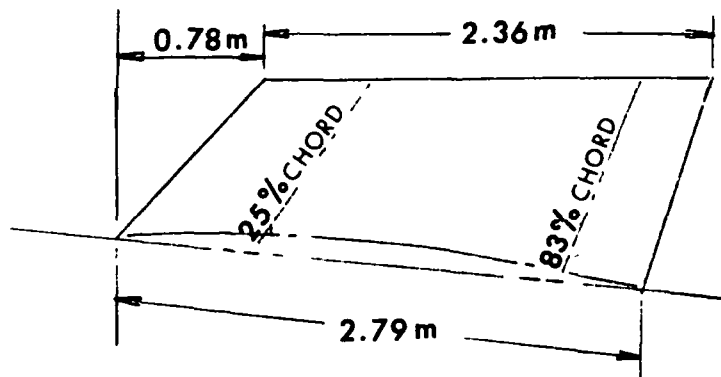


Figure 177 - Side Fin Envelope

$$S_{(L.E.)} = 0.25 \times 2.88 = 0.721 \text{ m}^2/\text{fin}$$

$$S_{(S.B.)} = (0.83 - 0.25) \times 2.88 = 1.673 \text{ m}^2/\text{fin}$$

$$S_{(T.E.)} = 2.88 - (0.720 + 1.673) = 0.491 \text{ m}^2/\text{fin}$$

$$b' = 1.12 \text{ m}$$

$$= \frac{C_T}{C_R} = 0.845$$

$$\Lambda_{0.5C} = 27^\circ$$

$$P_y = 1406 \text{ kg limit load} \times 1.5 = 2.1 \text{ Mg (Ultimate design load/side fin)}$$

Use the same method for analyzing the side fins as was used to analyze the structural box and leading edge of the vertical fin.

$$\text{Mass}_{(\text{basic shell})} = 22.0 \text{ kg/fin}$$

$$\text{Mass}_{(\text{kick load})} = 2.5 \text{ kg/fin}$$

$$\text{Mass}_{(\text{bending material})} = 10.9 \text{ kg/fin}$$

Slip joint fairing mass:

$$\text{Use } t_e = 1.8 \text{ mm}^2/\text{mm}$$

wrap width = 0.20 m

$$\begin{aligned} \text{Mass}_{(\text{slip joint})} &= 2 \ell w t_e \rho \\ &= 2 \times 2.93 \text{ m} \times 0.20 \text{ m} \times 0.0018 \text{ m}^2/\text{m} \times 2800 \text{ kg/m}^3 \\ &= 5.9 \text{ kg/fin} \end{aligned}$$

Total side fin mass (all aluminum vehicles) 82.6 kg.

- Side Fin Analysis - Lockalloy Vehicles - All skin panels are sized to fit the area between spars and ribs so there is no necessity for splice joints. Skin panel thermal design requirements depicted in Table 45.

$$\text{Mass}_{(\text{skin panels})} = (\Sigma S \times \text{Thickness}) \rho \times 1.025$$

$$\begin{aligned} \text{Mass}_{(\text{L. E. skin})} &= 2 (0.691 \times 0.0089 + 0.749 \times 0.0053) \times 2090 \\ &\quad \times 1.025 \\ &= 43.4 \text{ kg} \end{aligned}$$

$$\text{Mass}_{(\text{main box skin})} = 2 (3.345 \times 0.0053) \times 2090 \times 1.025 = 76.0 \text{ kg}$$

$$\text{Mass}_{(\text{T. E. skin})} = 2 (0.975 \times 0.0051) \times 2090 \times 1.025 = 21.3 \text{ kg}$$

Position	% Chord	Area/Fin m <sup>2</sup>	Thickness mm
L. E.	0-12	0.671	8.9
L. E.	12-25	0.749	5.3
Main Box	25-83	3.345	5.3
T. E.	83-100	0.975	5.1

Table 45 - Skin Panel Criteria

Substructure mass (spars and ribs)

$$\text{Use Mass}_{(\text{spars \& ribs})} = \frac{f_{tu} (394 \text{ K Al})}{f_{tu} (478 \text{ K Ti})} \times \text{Al. Mass (394 K)}$$

$$\times \frac{\rho (\text{Ti.})}{\rho (\text{Al.})}$$

Where

$$\text{Al. Mass} = 2 (10.9 + 2.5) \text{ (see preceding page)}$$

$$\text{Mass}_{(\text{spars \& ribs})} = \frac{4.0 \times 10^8}{7.82 \times 10^8} \times 26.8 \times \frac{4510}{2800} = 22.1 \text{ kg}$$

Total side fin mass

All Lockalloy vehicles 162.8 kg

- Secondary Structure Analysis - The secondary structure consists of equipment access panels. On the aluminum vehicles these panels are assumed to be 10% of the primary structure mass of the vertical fin. On the Lockalloy vehicles no secondary structure mass is required because panels can be removed as required for access.

- Tail Mass Summary - Tail structure mass summary for all configurations is shown in Table 46.

Fuselage Analysis - Fuselage skin panels and main frames have been stress analyzed for the critical load conditions. The design load conditions were applied to the structural model showing no cutouts for nonstructural doors, scramjet opening, or access panels. All cutout penalties have been analyzed separately and is included in the mass breakdown as added mass to frames and skin panels.

The fuselage is divided into three main sections, forebody (F.S. 100-306); payload bay (F.S. 306-426); and aftbody (F.S. 426-700).

The forebody section will show a detailed mass derivation of all forebody structure for the various vehicles and for expediency the payload bay and aftbody will show a mass summary table only for all vehicles.

Forebody Primary Structure Analysis - LI-900 Vehicles:

- Covering mass - Table 47.

Use  $\bar{t}$  data from Figure 59 for the nonbuckled skin requirements with a minimum manufacturing  $\bar{t}$  of  $1.42 \text{ mm}^2/\text{mm}$ .

Cutout penalty for access doors - Figure 178, left and right sides.

Mass penalty - shear material:

$$\text{Mass} = \rho t_e \left( 0.8 \beta x e + \frac{e^2 + 2\beta^2}{2} \right)$$

Where:

$$t_e = \frac{(0.025 + 0.013 \times 2) 0.00102}{0.076} + 0.00127$$

$$= 1.95 \text{ mm}^2/\text{mm}$$

Item	Vehicle Configurations - Mass in kg									
	LR-105 + 12 Atlas Verners		LR-105 + 2 LR-11 Sustainers		LR-99 Throttled					
	Lockalloy	LI-900	Ablator	Lockalloy	LI-900	Ablator	Lockalloy	LI-900	Ablator	Lockalloy
Vertical Fin	256.3	162.8	162.8	256.3	162.8	162.8	313.3	198.8	198.8	198.8
Main Box	98.7	75.6	75.6	98.7	75.6	75.6	100.8	78.5	78.5	78.5
Covering	66.7	39.5	39.5	66.7	39.5	39.5	66.7	39.5	39.5	39.5
Spars and Ribs	32.0	36.1	36.1	32.0	36.1	36.1	34.1	39.0	39.0	39.0
Leading Edge	45.7	9.9	9.9	45.7	9.9	9.9	45.7	9.9	9.9	9.9
Rudder/Speed Brakes	111.9	62.5	62.5	111.9	62.5	62.5	166.8	92.3	92.3	92.3
Covering	97.4	41.6	41.6	97.4	41.6	41.6	141.2	61.4	61.4	61.4
Ribs and Attach Linkage	14.5	20.9	20.9	14.5	20.9	20.9	25.6	30.9	30.9	30.9
Secondary Structure (10% of Primary Structure)	0	14.8	14.8	0	14.8	14.8	0	18.1	18.1	18.1
Side Fins - L and R	162.8	82.6	82.6	162.8	82.6	82.6	162.8	82.6	82.6	82.6
Main Box	98.1	55.9	55.9	98.1	55.9	55.9	98.1	55.9	55.9	55.9
Covering	76.0	34.1	34.1	76.0	34.1	34.1	76.0	34.1	34.1	34.1
Spars and Ribs	22.1	21.8	21.8	22.1	21.8	21.8	22.1	21.8	21.8	21.8
Leading Edge	43.4	8.3	8.3	43.4	8.3	8.3	43.4	8.3	8.3	8.3
Trailing Edge	12.3	6.6	6.6	21.3	6.6	6.6	21.3	6.6	6.6	6.6
Slip Joint Fairing	0	11.8	11.8	0	11.8	11.8	0	11.8	11.8	11.8
TOTAL TAIL STRUCTURE	419	245	245	419	245	245	476	281	281	281
TOTAL TAIL STRUCTURE (Detail Mass Breakdown)	423	245	245	423	245	245	482	279	279	279

Table 46 - Tail Mass Properties Summary

Fuselage Station	Wetted Area (m <sup>2</sup> )	$\bar{t}$ ( $\times 10^{-3}$ m <sup>2</sup> /m)	Volume ( $\times 10^{-3}$ m <sup>3</sup> )	Mass (kg) +15% NOF
<b>Skin Panels: (Mass = Volume <math>\times</math> <math>\rho</math> <math>\times</math> 1.15)</b>				(73.3)
108.4 - 133.4	0.6815	1.42	0.9677	3.1
133.4 - 158.4	1.677	1.42	2.381	7.7
158.4 - 208.4	3.145	1.42	4.466	14.4
208.4 - 230.0	2.156	1.42	3.062	9.9
230.0 - 278.0	4.095	1.42	5.815	18.7
278.0 - 299.0	2.117	1.42	3.006	9.7
299.0 - 306.0	2.136	1.42	3.003	9.8
<b>Shear Material Required for Offset Load Path @ F.S. 306.0:</b>				(10.0)
(Mass = $\bar{t} \times .36 \text{ m} \times l \times \rho \times 1.15$ )				
= 0.00142 $\times$ 0.36 $\times$ 6.10 $\times$ 2800 $\times$ 1.15				
<b>Longitudinal and Peripheral Splices:</b>				
(Mass = $\bar{t} \times 0.0635 \text{ m} \times l \times \rho \times 1.15$ )				(19.8)
= 0.00142 $\times$ 0.0635 (31.128 + 37.226) 2800 $\times$ 1.15				
<b>Hardware: (Mass = Mass<sub>(Skin + Splices)</sub> <math>\times</math> 0.05)</b>				(5.2)
= (83.3 + 19.8) 0.05				
<b>Panel and Door Cutout Penalties: (See Following Analysis)</b>				
133.4 - 208.4	Access Doors - Right Side		(8.9)	
230.0 - 278.0	Access Doors - L & R Side		(15.6)	
278.0 - 306.0	Access Doors - L & R Side		(12.5)	
278.0 - 306.0	Nose Landing Gear Door		(3.1)	
<b>TOTAL SKIN PANEL MASS</b>				<b>• 148.4</b>

Table 47 - Forebody Skin Panel Mass - LI-900

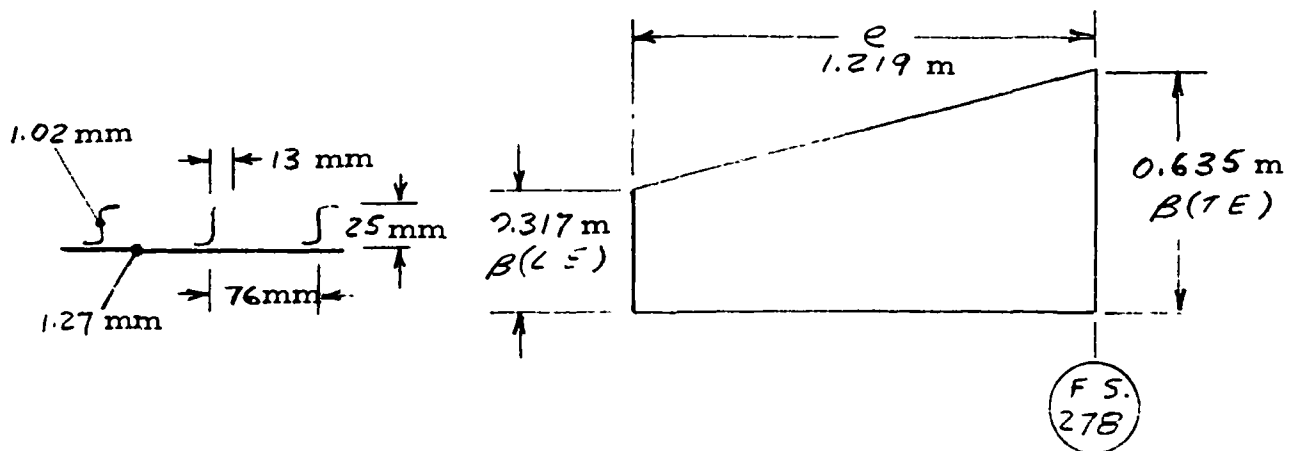


Figure 178 - Access Door Cutout



$$\begin{aligned} \text{Mass} &= 2800 \times 0.00195 \left[ 0.8 \left( \frac{0.317 + 0.635}{2} \right) 1.219 \right. \\ &\quad \left. + \left( \frac{1.219^2 + 2 \times 0.476^2}{2} \right) \right] \\ &= 7.8 \text{ kg/side (add to covering mass)} \end{aligned}$$

Mass penalty - frame material:

$$\text{Mass} = 4.25 \times 10^{-4} N_y e^2 + 3.2 \times 10^{-4} N_y \beta e$$

$$\text{Use: } N_y = 70.1 \text{ kN/m}$$

$$\begin{aligned} \text{Mass} &= 4.25 \times 10^{-4} \times 70100 \times 1.219^2 + 3.27 \times 10^{-4} \\ &\quad \times 7140 \times 0.476 \times \frac{1.219}{9.81} \\ &= 5.9 \text{ kg/side (add to frame mass)} \end{aligned}$$

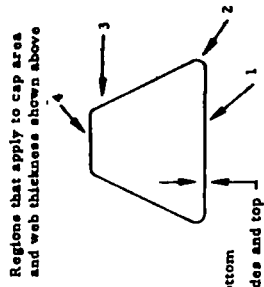
All other door and panel cutouts in the fuselage are analyzed in the same manner.

- Frame and Bulkhead Mass - The frames were analyzed for requirements based on stability and pressure only. Cut frames due to doors and access panels are added as a frame mass penalty.

See Figure 91 for frame cap and web requirements.

Frame to surface panel attachment brackets in Figure 87 is considered as part of the frame mass and is included in this section of the mass analysis, as shown in Table 48.

Frame Station	Frame Caps										Web/Bulkhead				Total Volume ( $\times 10^{-3} \text{ m}^3$ )	Mass (kg) $\times 1.05$
	Area - Inner + Outer ( $\text{m}^2$ )/Length (m)					4					@ 3 and 4		@ 1 and 2			
	1 and 2	3	4	5	6	7	8	9	10	11	12	13	14	15		
108 4	0.194	0.103	0.103	0.148	0.508	0.103	0.203	1.52	0.076	0.711	1.52	0.102	0.457	0.236	0.7	
133 4	0.194	0.103	0.103	0.148	0.965	0.103	0.254	1.52	0.076	1.219	1.52	0.102	0.711	0.338	1.0	
156 4	0.194	0.103	0.103	0.148	1.511	0.103	0.356	1.52	0.076	1.867	1.52	0.102	0.940	0.558	1.6	
183 4	0.194	0.103	0.103	0.148	1.905	0.103	0.406	1.52	0.076	2.311	1.52	0.102	1.034	0.804	2.4	
208.4	0.194	0.103	0.103	0.148	1.194	0.103	0.406	1.52	0.076	1.94	1.52	0.102	1.270	1.034	3.0	
230 0	0.194	0.103	0.103	0.148	1.194	0.103	0.406	1.52	0.076	1.94	1.52	0.102	1.334	0.804	2.4	
247 8	0.232	0.155	0.155	0.194	1.651	0.155	0.651	1.52	0.076	1.651	1.52	0.102	1.854	1.229	3.6	
263 6	0.252	0.206	0.206	0.229	1.956	0.229	0.696	1.52	0.076	1.956	1.52	0.102	2.032	1.501	4.4	
278 0	0.277	0.232	0.232	0.255	2.591	0.255	0.699	1.52	0.076	2.591	1.52	0.102	2.057	1.849	5.4	
306 0	0.342	0.284	0.284	0.313	3.505	0.313	0.699	1.52	0.076	3.505	1.52	0.102	2.057	4.422	13.0	
<p>This Frame Has Special Hook-up to Pitot System - Use Volume = <math>2.36 \times 10^{-4} \text{ m}^3</math></p> <p>Cockpit Canopy Area</p>											Bulkhead $t = 0.00193 \text{ m}$ , Area = $1.239 \text{ m}^2$					



Regions that apply to cap area and web thickness shown above

$h_{web} = 0.102 \text{ mm}$  - bottom  
 $0.076 \text{ mm}$  - sides and top

- F S. 306 0 is a bulkhead using single outer cap
- Frame to surface panel attaching brackets
  - Use 0.10 m c-c spacing
  - Angle =  $0.0445 \text{ m} \times$  (frame web depth + 0.0508 m)
  - Material gage =  $t$  of skin panels
- Mass =  $0.0445 \times t_{(skin)} (h_{(web)} + 0.0508) \left( \frac{f_{(Frames)}}{0.10} \right) 2800 \times 1.15$ 
  - =  $0.0445 \times 0.00127 \times 0.0869 + 0.0508 \times \frac{30.109}{0.10} \times 2800 \times 1.15$
- Frame Splices and Hardware
  - Use 10% of Frame Mass above
- Frame Cutout Mass Penalty for Doors and Panels
  - F S 133 4 - 208 4 access panel - right side
  - F S 230 0 - 278 0 access panel - L and R side
  - F S 278.0 - 306 0 access panel - L and R side
  - F S. 278 0 - 306 0 Nose landing gear door

TOTAL FRAME AND BULKHEAD MASS

Table 48 - Frame and Bulkhead Mass Table - LI-900 Vehicles

- Longerons - There was insufficient time to completely analyze the longerons by detail drawings or through the NASTRAN model. Statistical data from existing aircraft was used to estimate the mass of the longerons at 10% of total fuselage mass. This allows a total of 6 aluminum intercostal/longeron combination running full length - 15.2 m - of the vehicle at an average cross sectional area of 13 cm<sup>2</sup>, plus a 1.25 factor for fittings, discontinuities and non-optimum factors. It is estimated that about 47.6 kg would be in the forebody, 102.1 kg for the 3.0 m payload bay section, and 258.5 kg for the aft body section, for a total of 408.2 kg for all configurations.
- Pressurized Cockpit - Design requirements for the X-24C pressurized cockpit are:

21 kPa ultimate cockpit pressure

crash loads -  $N_z \pm 2.35$ ;  $N_x - 4.68$ ;  $N_y \pm 0.82$  (kN/m)

The F-104A cockpit design requirements are:

34 kPa ultimate cockpit pressure

crash loads -  $N_z \pm 2.22$ ;  $N_x - 5.20$ ;  $N_y \pm 0.79$  (kN/m)

Since the total design requirements are almost equal the following structural mass (Table 49) for the cockpit has been scaled by size only.

- Nose Gear Well Side Support Structure - This structure is to be designed to support 47.9 kPa (limit) air loads at max. q in case of nose gear door failure at cruise.

The side wall structure, Figure 179, is in the area between the cockpit aft canted bulkhead and the bulkhead at F.S. 360.0, on B.L. 10.5 left and right. Mass is summarized in Table 50.

Primary Structure Items	Mass (kg)
Skin Panels	27.8
Forward Pressure Bulkhead	5.2
Aft Pressure Bulkhead (Canted)	8.9
Sill and Lower Longerons	10.2
Crash Load Attach Structure (Pressurized Cockpit to Forebody Frames)	8.1
Non Optimum Factor (10% of Structure Mass)	6.0
<b>Total Primary Structure (Pressurized Cockpit)</b>	<b>● 66.2</b>

Table 49 - Cockpit Structure Mass

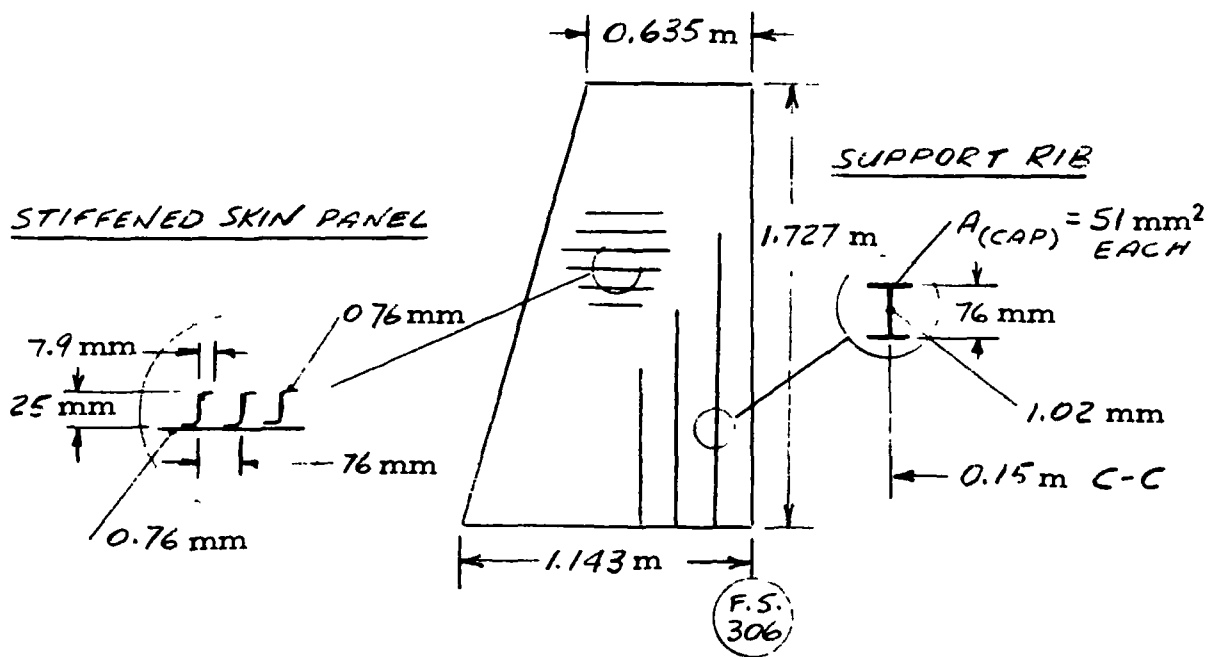


Figure 179 - Side Wall Structure

Item	Mass (kg)
Shear Panels	10.5
Support Ribs and Edge Members	12.2
Hardware	1.1
Total Nose Gear Well Side Support Structure	● 23.8

Table 50 - Sidewall Structure

- Mass Summary (Table 51) - Forebody primary structure, LI-900 vehicles.
- Forebody Primary Structure Analysis - Ablator Vehicles - The only differences that occur between the LI-900 vehicles and the Ablator vehicles are:
  - Skin panel stiffener requirement
  - Body sealing requirement (secondary structure)

$$\begin{aligned}
\text{Mass}_{(80\% \text{ buckled panels})} &= \left( \frac{80\%}{100\%} \right)^{1/2} \times \text{Mass}_{(\text{nonbuckled panels})} \\
&= 0.89 \times 83.1 \text{ kg} \\
&= 74 \text{ kg}
\end{aligned}$$

- Mass Summary (Table 52) - Forebody primary structure, Ablator vehicles.

#### Lockalloy Vehicles

- Covering Mass - The fuselage skin panel thickness requirements are obtained from the structural thickness requirement curves shown in

Primary Structure	Mass (kg)
Covering	148.4
Frames and Bulkheads	73.2
Longerons	47.6
Pressurized Cockpit	66.2
Nose Gear Well Side Support Structure	23.8
Total	(359.2)

Table 51 - Forebody Structure - LI-900

Primary Structure	Mass (kg)
Covering	139.2
Frames and Bulkheads	73.2
Longerons	47.6
Pressurized Cockpit	66.2
Nose Gear Well Side Support Structure	23.8
Total	(350.0)

Table 52 - Forebody Structure - Ablator

Figures 82, 83 and 84 for thickness required due to panel loading. The heat sink thickness requirements shown on Figures 104 and 105 were used as data points plotted on the fuselage loft drawing. These points were transferred into isothickness lines to cover the entire fuselage. From a review of the strength and heat requirements the maximum thickness values were selected and transferred onto the gross area curve (fish) Figure 140. The material thickness is now described at every position on the fuselage, and panel splice length can also be determined. Table 53 summarizes forebody panel mass.



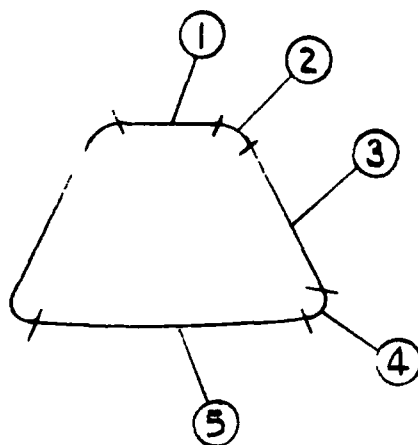
Fuselage Station	Wetted Area (m <sup>2</sup> )	Thickness (x 10 <sup>-3</sup> m)		Material Volume (x 10 <sup>-3</sup> m <sup>3</sup> )	Mass +5% NOF (kg)
		Range	Average		
Skin panels ② through ⑤, F.S. 108.4 - 133.4:					
Mass = Volume x Density x 1.05					
108.4 - 120.0	0.257	7.62 - 6.99	7.30	1.88	4.1
120.0 - 133.4	0.424	6.99 - 6.35	6.67	2.83	6.2
Skin panels ⑤, F.S. 133.4 - 306.0:					
133.4 - 183.4	0.726	6.35 - 5.33	5.84	4.24	9.3
183.4 - 230.0	0.421	5.33 - 5.08	5.21	2.19	4.8
183.4 - 230.0	0.812	6.86 - 5.33	6.10	4.95	10.9
230.0 - 306.0	0.588	5.08	5.08	2.99	6.6
230.0 - 306.0	1.594	5.08 - 5.33	5.21	8.30	18.2
230.0 - 306.0	1.226	6.86 - 5.33	6.10	7.48	16.4
Skin panels ④, F.S. 133.4 - 306.0:					
133.4 - 306.0	1.559	7.62	7.62	11.88	26.1
Skin panels ③, F.S. 133.4 - 306.0:					
133.4 - 230.0	3.138	4.32 - 3.81	4.06	12.74	28.0
230.0 - 306.0	0.392	3.81	3.81	1.49	3.3
230.0 - 306.0	0.588	3.81 - 3.05	3.43	2.02	4.4
230.0 - 306.0	3.757	3.05	3.05	11.46	25.1
Skin panels ②, F.S. 133.6 - 306.0:					
133.6 - 306.0	2.222	4.32	4.32	9.60	21.1
Skin panel splices - longitudinal and peripheral:					
Mass = 0.711 kg/m x $\ell$ = 0.711 x 56.21 m					40.0
Fasteners:					
Mass = (Mass <sub>skin</sub> + Mass <sub>splices</sub> ) x 0.075					
= (184.5 + 40.0) x 0.075					16.8
Panel and door cutout penalties: (See following analysis)					
230.0 - 278.0	Access Doors - L & R Sides				12.2
(All other structural panels can be removed as required for access - no penalty)					
Total Skin Panel Mass					● 253.5

Table 53 - Forebody Panel Mass



The forebody skin panels are sized for 644 K, payload bay and aft body are sized for 589 K.

Regions that apply to skin panel thickness are shown in the following chart:



Cutout penalty for nonstructural access doors - F.S. 230.0 to 278.0, left and right sides.

Door size is the same as shown for the LI-900 Configuration.

Mass penalty-shear material:

$$\begin{aligned} \text{Mass} &= 2090 \times 0.00203 \left[ 0.8 \left( \frac{0.317 + 0.635}{2} \right) 1.219 \right. \\ &\quad \left. + \left( \frac{1.219^2 + 2 \times 0.476^2}{2} \right) \right] \\ &= 6.1 \text{ kg/side} \end{aligned}$$

- Frame and Bulkhead Mass - Use the data from Structure Analysis, Figure 94 for fuselage frame areas using the curve for steel. Table 54 summarizes the frame and bulkhead masses.

Frame Station	Lower Surface 1 and 2		Upper Surface 3 and 4		Frame Volume (x 10 <sup>-4</sup> x m <sup>3</sup> )	Mass +20% (kg)
	A (x 10 <sup>-4</sup> m <sup>2</sup> )	ℓ (m)	A (x 10 <sup>-4</sup> m <sup>2</sup> )	ℓ (m)		
$Mass_{(Frames)} = Volume \times \rho (0.05 + 1.15)$						
Where:						
$\rho = 7920 \text{ kg/m}^3 \text{ (S. Stl.)}$						
0.05 = Add to Stabilize Inner Cap						
1.15 = Non Optimum Factor						
108.4	0.77	0.406	0.65	0.356	0.544	0.5
120.9	0.77	0.813	0.65	0.686	1.072	1.0
133.4	0.77	1.143	0.65	0.737	1.359	1.3
145.9	0.77	1.461	0.65	0.940	1.736	1.6
158.4	0.77	1.842	0.65	1.270	2.244	2.1
170.9	0.77	2.210	0.65	1.511	2.684	2.6
183.4	0.77	2.527	0.65	1.689	3.044	2.9
195.9	0.77	2.921	0.65	1.905	3.487	3.3
208.4	0.77	3.277	0.65	2.096	3.886	3.7
219.4	0.77	3.594	0.65	2.438	4.352	4.1
230.0	0.77	1.727	0.65	1.219	2.122	2.0
242.0	0.87	1.930	Cockpit Canopy Area		1.679	1.6
254.0	0.90	2.134			1.921	1.8
266.0	1.00	2.286			2.286	2.2
278.5	1.03	2.286	0.65      3.874		2.355	2.2
292.3	1.13	2.311			5.130	4.9
F.S. 306 is a Bulkhead						
Cap	1.16	2.388	0.65	4.001	19.5	18.5
Web	(t = 0.00114 m) (A = 1.239 m <sup>2</sup> )					
Splices and Hardware: (Mass = Mass <sub>(Frames)</sub> x 0.125)						7.0
= 56.3 x 0.125						
Mass Penalty - Doors and Panels:						
F.S. 230.0 - 278.0 Access Doors - L & R Side						5.1
F.S. 278.0 - 306.0 Nose Landing Gear Door						2.5
<b>TOTAL FRAME AND BULKHEAD MASS</b>						<b>● 70.9</b>

Table 54 - Frame/Bulkhead Mass - Lockalloy

- Mass Summary Table - Forebody primary structure, Lockalloy vehicles, Table 55.
- Forebody Secondary Structure Analysis - Pressurized cockpit - following is a mass breakdown to be used for all vehicles, Table 56.
- Doors and Nonstructural Panels - Aluminum vehicles, Table 57.
- Doors and Nonstructural Panels - Lockalloy vehicles, Table 58.  
All equipment access panels are readily removable for quick access on the Lockalloy vehicles.
- Mass Summary Table - Forebody secondary structure, LI-900, Ablator and Lockalloy vehicles, Table 59.
- Payload Bay Summary, Table 60 - Primary and secondary structure, all vehicles.
- Aft Body Summary - Summary of primary and secondary structure mass for all vehicle configurations is shown in Table 61.
- Fuselage Mass Summary - Total fuselage mass summary for all vehicles is shown in Table 62.

T. P. S. Mass Summary - The Ablator configuration mass was derived by using a density of  $224 \text{ kg/m}^3$  over most of the surface areas, plus  $352 \text{ kg/m}^3$  to  $897 \text{ kg/m}^3$  for leading edges. A bonding agent of  $1410 \text{ kg/m}^3$  density was used at 0.13 mm thick. For the wing wetted area of  $29.7 \text{ m}^2$ , an average thickness of 14 mm gives a mass of 118 kg which includes a 20% margin. Similarly the tail of  $27.9 \text{ m}^2$  area at an average thickness of 15 mm gives a mass of 120 kg. The Ablator on the fuselage was calculated from panel thickness requirements established by thermal calculations and amounted to 582 kg. Total Ablator mass for configurations 103, 106 and 109 is 820 kg as shown on Table 27. The LI-900 @  $144 \text{ kg/m}^3$  and 10 mm thick was used over the entire vehicle wetted area along

Primary Structure	Mass (kg)
Covering	253.5
Frames and Bulkheads	70.9
Longerons	47.6
Pressurized Cockpit	66.2
Nose Gear Well Side	
Support Structure	23.8
Total	(462.0)

Table 55 - Forebody Structure Mass - Lockalloy

Item	Mass (kg)
Canopy	(36.5)
Structure	27.0
Glass	4.4
Insulation	5.1
Canopy Operating Mechanism	17.3
Plumbing and Seals	3.8
Jettison Mechanism	3.4
Cockpit Floor	5.3
Sealing Compound	2.7
Total Pressurized Cockpit	69.0

Table 56 - Cockpit Secondary Structure Mass

with a layer of sponge-like material and two coatings of bonding agents with a total unit mass of  $2.45 \text{ kg/m}^2$  and a total mass of 417 kg.

Landing Gear Mass - The following data shows the basis for the off-the-shelf existing gear of 590 kg used on all configurations.

Item	Mass (kg)
F.S. 133.4 - 208.4 Access Panels	4.8
F.S. 230.0 - 278.0 Access Panels	8.6
F.S. 278.0 - 306.0 Access Doors	12.3
F.S. 278.0 - 306.0 Nose Gear Door	6.8
Total Doors and Panels	● 32.5

Table 57 - Doors/Nonstructure Panels Mass - Aluminum

Item	Mass (kg)
F.S. 278.0 - 306.0 Access Doors	12.0
F.S. 278.0 - 306.0 Nose Gear Door	9.9
Total Doors	● 21.9

Table 58 - Doors/Nonstructural Panels Mass - Lockalloy

Secondary Structure	Mass (kg)		
	LI-900	Ablator	Lockalloy
Pressurized Cockpit	69.0	69.0	69.0
Doors and Panels	32.5	32.5	21.9
Body Sealant	7.8	5.5	5.0
Total	(109.3)	(107.0)	(95.9)

Table 59 - Forebody Secondary Structure Mass

Item	Mass (kg)		
	LI-900	Ablator	Lockalloy
Primary Structure:	558.9	535.4	885.1
Covering	343.1	319.6	602.2
Frames	113.7	113.7	180.8
Longerons	102.1	102.1	102.1
Secondary Structure:	50.8	44.0	9.2
Access Panels	27.2	27.2	0
Body Sealant	23.6	16.8	9.2
Total Payload Bay	609.7	579.4	894.3

Table 60 - Payload Bay Mass Summary

From a mass report on the F-106B:

Main Gear	477 kg
Nose Gear	<u>93 kg</u>
Total	570 kg

From a mass report on the C-140A:

Main Gear	390 kg
Nose Gear	<u>100 kg</u>
Total	490 kg

Therefore, for the X-24C use:

F-106B Main Gear	477 kg
C-140A Nose Gear	100 kg
Allowance for Modification	<u>13 kg</u>
Total	590 kg

Item	Vehicle Configurations (kg)									
	LR-105 + 12 Atlas Verniers		LR-105 + 2 LR-11 Sustainers			LR-99 Throttled				
	Lockalloy	LR-900	Ablator	Lockalloy	LI-900	Ablator	Lockalloy	LI-900	Ablator	LI-900
<b>PRIMARY STRUCTURE</b>										
Covering	2402 4	2169 4	2143 2	2425 1	2199 8	2173 6	2320 3	2095 0	2068 8	
Frames	1205 4	665 0	638 8	1205 4	665 0	638 8	1205 4	665 0	638 8	
Bulkheads	601 9	928 4	928 4	606 6	928 1	928 1	606 6	928.1	928 1	
Aft Tank Support BHD	183 1	164 0	164 0	184 1	177 7	177 7	138 3	131 9	131.9	
F.S 700 BHD. and Fairing	100 1	81.0	81 0	91.1	84.7	84 7	91 1	84 7	84 7	
Longerons/Intercostals	83 0	83 0	83.0	93 0	93 0	93 0	47 2	47 2	47 2	
Main Gear Well Support Structure	258 5	258.5	258 5	258 5	258 5	258 5	258 5	258 5	258 5	
Sustainer Engine Structure	111 5	111 5	111 5	111 5	111 5	111 5	111 5	111 5	111 5	
	42 0	42.0	42 0	59.0	59.0	59.0	0	0	0	
<b>SECONDARY STRUCTURE</b>										
Doors and Panels	227 8	177 2	165 6	227 8	177 2	165 6	227 8	177.2	165 6	
Main Landing Gear Doors	49 4	40 5	40 5	49 4	40 5	40 5	49 4	40 5	40 5	
Production Joint Access Panels	49 4	31 9	31 9	49 4	31 9	31 9	49 4	31.9	31 9	
Engine Compartment Access Panels	0	2 9	2 9	0	2 9	2 9	0	2.9	2 9	
Aft Body Lower Flap	0	5 7	5 7	0	5 7	5 7	0	5 7	5 7	
Body Sealant	158 8	96.2	96 2	158 8	96 2	96 2	158.8	96 2	96.2	
	19.6	40.5	28.9	19 6	40 5	28.9	19 6	40 5	28 9	
<b>Total Aft Body</b>	2630 2	2346 6	2308 8	2652 9	2377 0	2339 2	2548 1	2272 2	2234 4	

Table 61 - Aft Body Mass Summary





Propulsion Mass Summary - The following table gives the breakdown of the three engine configurations. Engine mass were taken from latest available engine specifications. LR-99 mounts and controls were taken from X-15 data while nozzle extension and engine shroud were calculated in detail. The LR-105 engine mounts and controls were estimated while the sustainer mounts and shrouds were detail calculated as part of the fuselage mass and are listed here only as a reference input in Table 63.

Propellant System Mass Summary - This system includes the tank mass required to contain the mission fuel, plus insulation where needed and the plumbing, valves and controls necessary to pressurize and purge the fuel system. Table 64 shows a combination of actual, calculated and estimated mass for the three engine configurations.

Systems Mass Summary - Since speed brakes were a major variable among the various configurations, 1126 kg was used as a base for comparison and delta mass are listed in the table below to account for surface control actuation differences. The mass for the seven systems of the vehicle were derived from actual analysis of existing equipment plus estimates based on comparative data and shown in Table 65.

Item \ System	LR-105 Plus (2) Atlas	LR-105 Plus (2) LR-11	LR-99
Engine	413 kg	413 kg	413 kg
Mounts, and Controls	136	136	65
Nozzle Extension			19
Sustainer Engines	109	317	
Mounts	(42)	(59)	
Engine Shrouds	(83)	(113)	(47)
Totals	658 kg	866 kg	497 kg

Table 63 - Propulsion System Mass Summary

Item \ System	LR-105 Engine with Atlas (kg)	LR-105 Engine with LR-11 (kg)	LR-99 Engine (kg)
Tanks			
Lox	244	211	205
RP-1	188		
Helium	57	68	73
Alcohol		243	
H <sub>2</sub> O <sub>2</sub>		10	48
Amonia			256
Lox-Aux			49
Amonia-Aux			59
Helium	23	27	34
Insulation			
Lox Tank	57	49	51
Lox Aux Tank			14
Amonia Tank			17
Amonia Aux Tank			4
H <sub>2</sub> O <sub>2</sub> Tank		0.45	
Other	14	14	14
Plumbing, Valves, Controls, Regulators	400	400	358
Contingencies	16	21	19
<b>Total</b>	<b>999</b>	<b>1043</b>	<b>1203</b>

Table 64 - Propellant System Mass Summary

Surface Controls	△ 1	318 kg	△ 1	Vehicle 101 add 23 kg
Instruments		36 kg	△ 1	Vehicle 102 add 10 kg
Hydraulics		136 kg	△ 1	Vehicle 103 add 10 kg
Electrical		227 kg	△ 1	Vehicle 104 add 23 kg
Avionics		91 kg	△ 1	Vehicle 105 add 10 kg
Furnishings		136 kg	△ 1	Vehicle 106 add 10 kg
Air Conditioning		<u>182 kg</u>	△ 1	Vehicle 107 add 30 kg
	△ 1	1126 kg		
Adjustment due to speed brake requirement △ 1				

Table 65 - Systems Mass Summary

<u>USEFUL LOAD MASS SUMMARY</u>	<u>kg</u>
PILOT	82
PRESSURE SUIT, HELMET AND SHOES	15
PARACHUTE AND SURVIVAL KIT	33
OXYGEN - 10 LITERS	11
RESIDUAL FUELS, ESTIMATED	<u>45</u>
TOTAL	186 kg

#### COST ANALYSES

The cost and man-hours data prepared to support the X-24 Phase I Design Trade Studies have been developed by experienced estimating personnel using techniques refined as the result of many years of work on experimental and research and development vehicle programs. These efforts were supported by inputs from Lockheed-ADP engineering, manufacturing and flight test organizations and by consultation with NASA and other contractors. The estimates presented in this study reflect experience gained on the YF-12, SR-71, U-2, F-104,

X-15, and B-70 development and test programs, to name a few. Initial vehicle cost estimates for the alternative configurations are presented in addition to the vehicle flight support and maintenance man-hours estimates.

Estimates have been prepared for the nine X-24C vehicle configurations which can be summarized as follows:

<u>Configuration Number</u>	<u>Airframe/TPS</u>	<u>Propulsion System</u>
X-24C-101	Lockalloy Heat-Sink Structure	LR-105/Atlas Vernier
-102	Aluminum/LI-900 TPS	LR-105/Atlas Vernier
-103	Aluminum/Ablator TPS	LR-105/Atlas Vernier
-104	Lockalloy Heat-Sink Structure	LR-105/LR-11
-105	Aluminum/LI-900 TPS	LR-105/LR-11
-106	Aluminum/Ablator TPS	LR-105/LR-11
-107	Lockalloy Heat-Sink Structure	LR-99
-108	Aluminum/LI-900 TPS	LR-99
-109	Aluminum/Ablator TPS	LR-99

Initial Vehicle Costs - Vehicle program costs are set forth in this section which provide a basis for measuring the relative costs of the alternative propulsion system installations and thermal protection systems. These cost estimates, when considered together with other factors including technical performance and risk and system maintenance costs, offer a means to select the more promising configuration concepts to be evaluated in Phase II of the contract.

Costing Assumptions - Costing assumptions set forth under the section Basis For Design Trades were used in preparing initial vehicle cost estimates.

Basis for Estimates - The primary factors used as the basis for vehicle cost estimates are listed in Table 66.

BASIS FOR ESTIMATES

	LOCKALLOY HEAT-SINK STRUCT.	ALUMIN. STRUCT. LI-900 RSI TPS	ALUMIN. STRUCT. ABLATOR TPS
TPS	<ul style="list-style-type: none"> <li>• YF-12 LOCKALLOY VENTRAL FIN ACTUAL COST</li> <li>• ADP ENGR. &amp; MFG. ESTIMATES</li> <li>• KBI FIRM PRICE QUOTATION</li> </ul>	<ul style="list-style-type: none"> <li>• PUBLISHED DATA, MARTIN-MARIETTA ROCKWELL LMSC</li> <li>• CONSULTATION WITH LMSC ROCKWELL NASA HOUSTON</li> <li>• ADP ESTIMATES</li> </ul>	<ul style="list-style-type: none"> <li>• PUBLISHED DATA MARTIN-MARIETTA ROCKWELL AVCO</li> <li>• ADP ESTIMATES</li> </ul>
CONVENTIONAL STRUCTURES AND SYSTEMS	<ul style="list-style-type: none"> <li>• ADP &amp; INDUSTRY PRIOR EXPERIENCE</li> <li>• MAN-HOURS PER DCPR POUND</li> <li>• COMPLEXITY FACTORS DERIVED FROM MATERIAL TYPE PARTS COUNT ENGINEERING ESTIMATES</li> <li>• SUPPLIER QUOTATIONS</li> </ul>		
<ul style="list-style-type: none"> <li>• PRICED LIKE A CONTRACT PROPOSAL</li> </ul>			

Table 66 - Phase I Costing Tradeoff Study

- Thermal Protection Systems - Actual engineering, testing, material characterization, tooling and manufacturing experience has been gained by ADP in the development of a Lockalloy ventral fin assembly for a NASA YF-12 aircraft. This experience, together with other detailed engineering and manufacturing estimates provides the basis for costing of the Lockalloy vehicles. The Lockalloy supplier, Kawecki Berylco Industries, Inc. (KBI) has submitted a firm priced proposal for material quantities for one or two X-24C vehicles. The costs of procurement and installation of the alternative forms of TPS reflect consideration by ADP of the data published by the contractors as noted in Table 66. In addition, ADP consulted with other competent sources and applied its own experience and judgment factors where appropriate. Where possible, TPS estimates were developed on a cost per square meter basis.

- Conventional Structures and Systems - In the case of design, testing, tooling and manufacturing effort for more conventional materials (e. g., aluminum, titanium, steel), including those materials as used on the Lockalloy vehicle, and for functional systems, the more traditional means of developing cost estimates were used. A concentrated effort was made to derive complexity factors which would provide a basis for comparing the costs of alternative configurations. Supplier quotations have been obtained on some of the more significant system equipment items (e. g., flight control system).
- Priced Like a Contract Proposal - With the exception of the LI-900 RSI and elastomeric Ablator TPS costs (where sufficient hard data and experience do not exist in order to permit such an approach), all estimates have been prepared in the same manner and to the degree of accuracy and contractor confidence as for a Lockheed/ADP firm priced proposal to the Government.

Vehicle Price Summaries - Table 67 summarizes the "bottom line" price estimates for two X-24C vehicles in each of the nine configurations. These estimates are presented in January 1976 dollars. The costs of a single vehicle for each configuration and more detailed breakdowns by element are provided below. Costs in January 1975 dollars and other data relating to economic escalation factors can be found in Appendix C.

The exclusions listed at the bottom of Table 67 are significant in that such factors will have to be added in order to arrive at total program costs. Initial spares, AGE and tech data estimates which are a part of the initial investment costs are covered under Initial Spares, AGE and Data Section, and added to arrive at the acquisition or initial investment costs summarized under the Total Initial Investment Cost Section.

## TWO X-24C VEHICLES-PRICE SUMMARY

(JAN. 1976 DOLLARS IN THOUSANDS)

ROCKET PROPULSION OPTIONS \	STRUCTURE/TPS OPTIONS	LOCKALLOY HEAT-SINK STRUCTURE	ALUMINUM STRUCT. LI - 900 RSI TPS	ALUMINUM STRUCT. ABLATOR TPS
LR-105/ATLAS VERNIER		\$53,061 (-101)	\$62,176 (-102)	\$54,076 (-103)
LR-105/LR-11		\$54,391 (-104)	\$63,503 (-105)	\$55,404 (-106)
LR-99		\$53,074 (-107)	\$61,778 (-108)	\$53,678 (-109)

### EXCLUDES

- AERO CONFIGURATION DEVELOPMENT
- FLIGHT TEST INSTRUMENTATION & PAYLOAD/EXPERIMENT DEVELOPMENT
- B-52 MODIFICATION
- FLIGHT TEST & SUPPORT AFTER DELIVERY
- ROCKET PROPULSION SYSTEMS ( COSTS TO BE PROVIDED BY NASA)

Table 67 - Vehicle Price Summary

Costs by Element - The cost breakdowns by major element for one or two vehicles for each of the nine configurations are set forth in Tables 68 through 76. The effort included in each of these elements includes:

- Engineering Design and Development Testing - This element includes the basic design of the X-24C vehicle, the propulsion system installation and sufficient design effort to define the TPS installations in adequate detail to permit the manufacture of either the LI-900 or Ablator by the supplier as a finished product essentially ready to be installed on the aluminum vehicle. Also included are the related design support functions of aerodynamics, thermodynamics, stress, mass properties, etc. Structural testing consisting of component testina dna complete vehicle proof and shake test and functional system testing (controls simulation,

( JAN. 1976 DOLLARS IN THOUSANDS )

	BASELINE AIRFRAME	PROPULSION SYSTEM Δ	TPS Δ	TOTAL VEHICLE
<u>ONE VEHICLE</u>				
ENGINEERING	\$ 11,054	\$ 3,204	INCLUDED	\$ 14,258
TOOLING	6,965	2,750		9,715
MFG. LABOR	6,794	2,712	IN BASELINE	9,506
MFG. MATERIAL & EQUIPMENT	5,405	985		6,390
GFAE	327	0		327
TOTALS	\$ 30,545	\$ 9,651	—	\$ 40,196
<u>TWO VEHICLES</u>				
ENGINEERING	\$ 11,829	\$ 3,319	INCLUDED	\$ 14,688
TOOLING	7,287	2,868		10,155
MFG. LABOR	12,218	4,892	IN BASELINE	17,110
MFG. MATERIAL & EQUIPMENT	8,766	1,688		10,454
GFAE	654	0		654
TOTALS	\$ 40,794	\$ 12,767	—	\$ 53,061

Table 68 - X-24C-101 Summary

( JAN. 1976 DOLLARS IN THOUSANDS )

	BASELINE AIRFRAME	PROPULSION SYSTEM Δ	TPS Δ	TOTAL VEHICLE
<u>ONE VEHICLE</u>				
ENGINEERING	\$ 9,417	\$ 3,172	\$ 3,334	\$ 15,923
TOOLING	7,851	2,701	995	11,327
MFG. LABOR	7,832	2,813	862	11,507
MFG. MATERIAL & EQUIPMENT	2,683	575	3,815	7,082
GFAE	327	0	0	327
TOTALS	\$ 27,815	\$ 9,345	\$ 9,006	\$ 46,166
<u>TWO VEHICLES</u>				
ENGINEERING	\$ 9,762	\$ 3,287	\$ 3,623	\$ 16,672
TOOLING	7,902	2,898	1,083	11,893
MFG. LABOR	14,093	5,070	1,647	20,810
MFG. MATERIAL & EQUIPMENT	3,610	917	7,630	12,157
GFAE	654	0	0	654
TOTALS	\$ 36,021	\$ 12,172	\$ 12,983	\$ 62,176

Table 69 - X-24C-102 Summary



( JAN. 1976 DOLLARS IN THOUSANDS )

	BASILINE AIRFRAME	PROPULSION SYSTEM Δ	TPS Δ	TOTAL VEHICLE
<u>ONE VEHICLE</u>				
ENGINEERING	\$ 9331	\$ 3172	\$ 2293	\$ 14,796
TOOLING	7435	2781	292	10,508
MFG LABOR	7705	2813	253	10,771
MFG MATERIAL & EQUIPMENT	2689	579	1499	4,761
GFAE	327	0	0	327
TOTALS	\$ 27481	\$ 9345	\$ 4337	\$ 41,163
<u>TWO VEHICLES</u>				
ENGINEERING	\$ 9676	\$ 3287	\$ 2524	\$ 15,487
TOOLING	7786	2898	321	11,005
MFG LABOR	13865	5070	180	19,415
MFG MATERIAL & EQUIPMENT	3601	917	2997	7,515
GFAE	654	0	0	654
TOTALS	\$ 35582	\$ 12172	\$ 6322	\$ 54,076

Table 70 - X-24C-103 Summary

( JAN. 1976 DOLLARS IN THOUSANDS )

	BASILINE AIRFRAME	PROPULSION SYSTEM Δ	TPS Δ	TOTAL VEHICLE
<u>ONE VEHICLE</u>				
ENGINEERING	\$ 11059	\$ 3508	INCLUDED IN BASELINE	\$ 14,562
TOOLING	6965	3045		10,010
MFG. LABOR	6794	3041		9,835
MFG. MATERIAL & EQUIPMENT	5405	1039		6,444
GFAE	327	0	0	327
TOTALS	\$ 30545	\$ 10633	—	\$ 41,178
<u>TWO VEHICLES</u>				
ENGINEERING	\$ 11369	\$ 3652	INCLUDED IN BASELINE	\$ 15,021
TOOLING	7287	3191		10,478
MFG. LABOR	12218	5474		17,692
MFG. MATERIAL & EQUIPMENT	876	1780		10,546
GFAE	654	0	0	654
TOTALS	\$ 40294	\$ 14097	—	\$ 54,391

Table 71 - X-24C-104 Summary

( JAN. 1976 DOLLARS IN THOUSANDS )

	BASELINE AIRFRAME	PROPULSION SYSTEM Δ	TPS Δ	TOTAL VEHICLE
<u>ONE VEHICLE</u>				
ENGINEERING	\$ 9417	\$ 3477	\$ 3334	\$ 16228
TOOLING	7551	3074	995	11,620
MFG. LABOR	7892	3142	862	11,836
MFG. MATERIAL & EQUIPMENT	2688	632	3815	7,135
GFAE	327	0	0	327
TOTALS	\$ 27815	\$ 10325	\$ 9006	\$ 47,146
<u>TWO VEHICLES</u>				
ENGINEERING	\$ 9762	\$ 3621	\$ 3622	\$ 17,005
TOOLING	7902	3219	1083	12,204
MFG. LABOR	14093	5652	1647	21,392
MFG. MATERIAL & EQUIPMENT	3610	1008	7630	12,248
GFAE	654	0	0	654
TOTALS	\$ 36021	\$ 13500	\$ 13982	\$ 63,503

Table 72 - X-24C-105 Summary

( JAN. 1976 DOLLARS IN THOUSANDS )

	BASELINE AIRFRAME	PROPULSION SYSTEM Δ	TPS Δ	TOTAL VEHICLE
<u>ONE VEHICLE</u>				
ENGINEERING	\$ 9331	\$ 3477	\$ 2293	\$ 15,101
TOOLING	7435	3074	291	10,800
MFG. LABOR	7705	3142	254	11,101
MFG. MATERIAL & EQUIPMENT	2688	632	1499	4814
GFAE	327	0	0	327
TOTALS	\$ 27481	\$ 10325	\$ 4337	\$ 42,143
<u>TWO VEHICLES</u>				
ENGINEERING	\$ 9676	\$ 3621	\$ 2524	\$ 15,821
TOOLING	7786	3219	320	11,325
MFG. LABOR	13868	5652	480	19,997
MFG. MATERIAL & EQUIPMENT	3601	1008	2998	7,607
GFAE	654	0	0	654
TOTALS	\$ 35582	\$ 13500	\$ 6322	\$ 55,404

Table 73 - X-24C-106 Summary

( JAN. 1976 DOLLARS IN THOUSANDS )

	BASELINE AIRFRAME	PROPULSION SYSTEM Δ	TPS Δ	TOTAL VEHICLE
<u>ONE VEHICLE</u>				
ENGINEERING	\$ 11054	\$ 3150	INCLUDED IN BASELINE	\$ 14,204
TOOLING	6985	2576		9541
MFG. LABOR	6794	2662		9456
MFG. MATERIAL & EQUIPMENT	5405	1155		6560
GFAE	327	0		327
TOTALS	\$ 30545	\$ 9573	—	\$ 40,088
<u>TWO VEHICLES</u>				
ENGINEERING	\$ 11369	\$ 3265	INCLUDED IN BASELINE	\$ 14,634
TOOLING	7287	2694		9981
MFG. LABOR	12218	1790		17,008
MFG. MATERIAL & EQUIPMENT	8766	2031		10,797
GFAE	654	0		654
TOTALS	\$ 40294	\$ 12780	—	\$ 53,074

Table 74 - X-24C-107 Summary

( JAN. 1976 DOLLARS IN THOUSANDS )

	BASELINE AIRFRAME	PROPULSION SYSTEM Δ	TPS Δ	TOTAL VEHICLE
<u>ONE VEHICLE</u>				
ENGINEERING	\$ 9417	\$ 3061	\$ 3333	\$ 15,811
TOOLING	7551	2664	996	11,211
MFG. LABOR	7832	2737	862	11,431
MFG. MATERIAL & EQUIPMENT	2688	560	3815	7,063
GFAE	327	0	0	327
TOTALS	\$ 27815	\$ 9022	\$ 9006	\$ 45,843
<u>TWO VEHICLES</u>				
ENGINEERING	\$ 9762	\$ 3176	\$ 3622	\$ 16,560
TOOLING	7902	2782	1083	11,767
MFG. LABOR	14093	4917	1648	20,658
MFG. MATERIAL & EQUIPMENT	3610	899	7630	12,139
GFAE	654	0	0	654
TOTALS	\$ 36021	\$ 11774	\$ 13983	\$ 61,778

Table 75 - X-24C-108 Summary

( JAN. 1976 DOLLARS IN THOUSANDS )

	BASELINE AIRFRAME	PROPULSION SYSTEM Δ	TPS Δ	TOTAL VEHICLE
<u>ONE VEHICLE</u>				
ENGINEERING	\$ 9331	\$ 3061	\$ 2292	\$ 14,684
TOOLING	7435	2664	232	10,391
MFG. LABOR	7705	2737	253	10,695
MFG. MATERIAL & EQUIPMENT	2683	560	1500	4,743
GFAE	327	0	0	327
TOTALS	\$ 27481	\$ 9022	\$ 4337	\$ 40,840
<u>TWO VEHICLES</u>				
ENGINEERING	\$ 9676	\$ 3176	\$ 2524	\$ 15,376
TOOLING	7786	2782	320	10,898
MFG. LABOR	13865	4917	480	19,262
MFG. MATERIAL & EQUIPMENT	3601	899	2998	7,498
GFAE	654	0	0	654
TOTALS	\$ 35682	\$ 11,774	\$ 6322	\$ 53,678

Table 76 - X-24C-109 Summary

Propellant system, canopy ejection, etc.) are a part of this element. In addition, sufficient supplemental wind tunnel testing as required to support detailed design (determination of hinge moments, etc.) and full scale mockups of critical areas such as the cockpit, equipment bays and engine compartments are included. Engineering mockup and development testing requirements which are included as a basis for estimating X-24C costs are the result of ADP experience in the design and development of advanced airframes and systems. The extent of the test of structures, materials and systems is entirely adequate to assure that the X-24C vehicle will perform its intended mission. Other items in this element are initial flight test planning assistance to NASA, engineering liaison with ADP shops and suppliers and the cost of all engineering test parts, materials and scientific computer usage. Under the

TPS alternative, costs are included for vehicle application testing and evaluation, although the basic materials characterization of both the LI-900 and Ablator are assumed to be already essentially completed for purposes of this study. Lockalloy vehicle structural testing includes adequate engineering testing to complete material characterization to the degree necessary for use on the X-24C.

- Tooling - This element includes the cost of all project tooling and manufacturing aids, both labor and material, necessary for the manufacture of the baseline vehicle, the propulsion system installation provisions and to support the installation of the TPS. Where necessary, tool design effort is also included.
- Manufacturing Labor - This element includes the cost of all manufacturing labor, both in-plant and outside production, for the fabrication, assembly and checkout of the baseline vehicle, the propulsion system installation provisions and the actual installation of the LI-900 or Ablator TPS. Also included are the related manufacturing planning and quality assurance efforts for each vehicle configuration.
- Manufacturing Material and Equipment - Included in this element are the costs of all raw materials, purchased parts, and CFE system equipment necessary for the manufacture of the vehicle. Allowances for design growth, shop usage, and scrap are included based on Lockheed/ADP experience and/or engineering estimates for new types of materials. TPS materials are included on a cost per square meter basis as further described below. Raw material costs, including the costs of Lockalloy, LI-900 and Ablator TPS materials are shown in Table 77 in the amounts which are included in the total vehicle prices.

The principle items of CFE systems (including their respective non-recurring costs) which are included are:

One Vehicle	-101	-102	-103	-104	-105	-106	-107	-108	-109
Raw materials, parts and TPS	\$ 3,539	\$ 4,231	\$1,910	\$ 3,545	\$ 4,236	\$1,915	\$ 3,730	\$ 4,233	\$1,913
Purchased system equipment	\$ 2,851	2,851	2,851	2,899	2,899	2,899	2,830	2,830	2,830
Totals	\$ 6,390	\$ 7,082	\$4,761	\$ 6,444	\$ 7,135	\$4,814	\$ 6,560	\$ 7,063	\$4,743
Two Vehicles									
Raw materials, parts and TPS	\$ 6,759	\$ 8,462	\$3,820	\$ 6,769	\$ 8,471	\$3,830	\$ 7,125	\$ 8,467	\$3,826
Purchased system equipment	3,695	3,695	3,695	3,777	3,777	3,777	3,672	3,672	3,672
Totals	\$10,454	\$12,157	\$7,515	\$10,546	\$12,248	\$7,607	\$10,797	\$12,139	\$7,498

Table 77 - Material and Equipment Cost Summary  
(January 1976 Dollars in Thousands)

- FBW Flight Control System - Electronics, actuators and servos.
- Inertial Navigation System
- Propellant System - Helium tanks, pumps, and valves.
- SR-71 Ejection System components
- Air Data System

The costs for these items as well as other functional system purchased equipment are also shown in Table 77.

- Government Furnished Aeronautical Equipment - The maximum use of GFAE from existing and prior NASA/USAF research vehicle programs such as the X-15 and X-24B is assumed. Costs are included in all configurations for the following items which are assumed to be GFAE but which may have to be paid for by NASA by transfer of funds to other Government programs.

<u>Item</u>	<u>Quantity per Vehicle</u>
F-106 Main Landing Gear (FSN 1620-00-592-9638)	2 ea.
C-140A Nose Landing Gear (No. FSN - P/N JL1501-1)	1 ea.
AN/ARC-150 UHF Radio	2 ea.

A more detailed list of GFAE items to be used from the X-15 and X-24B programs is included in Appendix D. In addition to the cost of the items noted above, an allowance of approximately \$235,000 has been included for the modification and refurbishment of GFAE.

- DCPR Mass Data - One of the primary tools used in estimating the costs of the X-24C vehicle configurations which were defined for the Phase I study is the man-hours per DCPR kilogram of airframe mass

relationship. The Defense Contractors' Planning Report (DCPR) formula, formerly known as AMPR, provides a widely accepted and reliable way of reflecting comparative efficiencies between airframe contractors. Consequently the DCPR air vehicle mass can be used as a prime point of reference in preparing manhours and cost estimates and comparisons. Prior Lockheed and ADP experience as well as industry average data were considered in arriving at cost estimating factors for use in this study. In addition, these factors were adjusted up or down, as appropriate, to reflect the relative complexity of systems as set forth in other sections of this report. Breakdowns of airframe mass (to the DCPR definition) for each X-24C configuration are shown in Tables 78 through 86. Man-hours per pound relationships were utilized in the estimating of engineering design, tooling and manufacturing effort.

Propulsion System Alternatives - The delta costs of each of three alternative propulsion system installations was estimated for the Phase I Trade Study.

- Complexity Factors - In order to arrive at the relative costs of installing each propulsion system, several factors which contributed to system complexity were utilized. The more significant ones are listed in Table 87, and their relative values shown.
- Costs - Using the Lockalloy heat-sink skin vehicle as a baseline airframe, the costs of installing each of the alternative propulsion systems in two vehicles are shown in Table 88. These estimates are the net result of using the various derived complexity factors in arriving at total system cost. Propulsion installation provisions include engine mounts and shrouds, the complete propellant system, tanks, etc. and other structural items that are significantly affected by the rocket engine selection (e. g., speed brakes, aft body flaps and elevons). The relative value of the three systems are shown in Table 88 with the LR-105 and LR-11 combination costing 10 percent more than either



(AS DEFINED BY DCPR-DEFENSE CONTRACTORS PLANNING REPORT)

ELEMENT	BASELINE AIRFRAME	PROPULSION RELATED	TPS RELATED	TOTAL AIRFRAME
<u>STRUCTURE:</u>				
TPS	N/A		Included	
LOCKALLOY	4681	693	IN	5374
TITANIUM	1188	495	BASELINE	1683
STEEL	2417	9		2426
ALUMINUM & MISC	1277			1277
LANDING GEAR	600			600
<b>SUB-TOTAL STRUCT.</b>	<b>10163</b>	<b>1197</b>		<b>11360</b>
<u>SYSTEMS:</u>				
PROPULSION		300		300
PROPELLANT		2200		2200
SURF CONTROLS	750			750
INSTRUMENTS	20			20
HYDRAULIC	300			300
ELECTRICAL	50			50
AVIONICS	50			50
FURNISHINGS	300			300
AIR, COND.	210			210
<b>SUB-TOTAL SYS</b>	<b>1680</b>	<b>2500</b>		<b>4180</b>
<b>TOTAL AIRFRAME</b>	<b>11843</b>	<b>3697</b>		<b>15540</b>

Table 78 - X-24C-101 Mass Breakdown \*

(AS DEFINED BY DCPR-DEFENSE CONTRACTORS PLANNING REPORT)

ELEMENT	BASELINE AIRFRAME	PROPULSION RELATED	TPS RELATED	TOTAL AIRFRAME
<u>STRUCTURE:</u>				
TPS	N/A		919	919
LOCKALLOY				
TITANIUM	80	276		356
STEEL	51			51
ALUMINUM & MISC	7883	600		8483
LANDING GEAR	600			600
<b>SUB-TOTAL STRUCT.</b>	<b>8614</b>	<b>876</b>	<b>919</b>	<b>10409</b>
<u>SYSTEMS:</u>				
PROPULSION		300		300
PROPELLANT		2200		2200
SURF CONTROLS	722			722
INSTRUMENTS	20			20
HYDRAULIC	300			300
ELECTRICAL	50			50
AVIONICS	50			50
FURNISHINGS	300			300
AIR, COND.	210			210
<b>SUB-TOTAL SYS</b>	<b>1652</b>	<b>2500</b>		<b>4152</b>
<b>TOTAL AIRFRAME</b>	<b>10266</b>	<b>3376</b>	<b>919</b>	<b>14561</b>

Table 79 - X-24C-102 Mass Breakdown \*

(AS DEFINED BY DCPR - DEFENSE CONTRACTORS PLANNING REPORT)

ELEMENT	BASELINE AIRFRAME	PROPULSION RELATED	TPS RELATED	TOTAL AIRFRAME
<b>STRUCTURE:</b>				
TPS	N/A		1807	1807
LOCKALLOY				
TITANIUM	80	276		356
STEEL	51			51
ALUMINUM & MISC	7729	600		8329
LANDING GEAR	600			600
<b>SUB-TOTAL STRUCT.</b>	<b>8460</b>	<b>876</b>	<b>1807</b>	<b>11143</b>
<b>SYSTEMS:</b>				
PROPULSION		300		300
PROPELLANT		2100		2100
SURF CONTROLS	722			722
INSTRUMENTS	20			20
HYDRAULIC	300			300
ELECTRICAL	50			50
AVIONICS	50			50
FURNISHINGS	300			300
AIR. COND.	210			210
<b>SUB-TOTAL SYS.</b>	<b>1652</b>	<b>2500</b>		<b>4152</b>
<b>TOTAL AIRFRAME</b>	<b>10112</b>	<b>3376</b>	<b>1807</b>	<b>15295</b>

Table 80 - X-24C-103 Mass Breakdown \*

(AS DEFINED BY DCPR - DEFENSE CONTRACTORS PLANNING REPORT)

ELEMENT	BASELINE AIRFRAME	PROPULSION RELATED	TPS RELATED	TOTAL AIRFRAME
<b>STRUCTURE:</b>				
TPS	N/A		included	
LOCKALLOY	4681	693	IN	5374
TITANIUM	1188	594	BASELINE	1742
STEEL	2417			2417
ALUMINUM & MISC	1277			1277
LANDING GEAR	600			600
<b>SUB-TOTAL STRUCT.</b>	<b>10163</b>	<b>1247</b>		<b>11410</b>
<b>SYSTEMS:</b>				
PROPULSION		300		300
PROPELLANT		2300		2300
SURF CONTROLS	750			750
INSTRUMENTS	20			20
HYDRAULIC	300			300
ELECTRICAL	50			50
AVIONICS	50			50
FURNISHINGS	300			300
AIR. COND.	210			210
<b>SUB-TOTAL SYS.</b>	<b>1680</b>	<b>2600</b>		<b>4280</b>
<b>TOTAL AIRFRAME</b>	<b>11843</b>	<b>3847</b>		<b>15690</b>

Table 81 - X-24C-104 Mass Breakdown \*

(AS DEFINED BY DCPR-DEFENSE CONTRACTORS PLANNING REPORT)

ELEMENT	BASELINE AIRFRAME	PROPULSION RELATED	TPS RELATED	TOTAL AIRFRAME
<b>STRUCTURE:</b>				
TPS	N/A		919	919
LOCKALLOY				
TITANIUM	80	335		415
STEEL	51			51
ALUMINUM & MISC	7883	608		8491
LANDING GEAR	600			600
<b>SUB-TOTAL STRUCT.</b>	<b>8614</b>	<b>943</b>	<b>919</b>	<b>10476</b>
<b>SYSTEMS:</b>				
PROPULSION		300		300
PROPELLANT		2300		2300
SURF CONTROLS	722			722
INSTRUMENTS	20			20
HYDRAULIC	300			300
ELECTRICAL	50			50
AVIONICS	50			50
FURNISHINGS	300			300
AIR, COND.	210			210
<b>SUB-TOTAL SYS.</b>	<b>1652</b>	<b>2600</b>		<b>4252</b>
<b>TOTAL AIRFRAME</b>	<b>10266</b>	<b>3543</b>	<b>919</b>	<b>14728</b>

Table 82 - X-24C-105 Mass Breakdown \*

(AS DEFINED BY DCPR-DEFENSE CONTRACTORS PLANNING REPORT)

ELEMENT	BASELINE AIRFRAME	PROPULSION RELATED	TPS RELATED	TOTAL AIRFRAME
<b>STRUCTURE:</b>				
TPS	N/A		1807	1807
LOCKALLOY				
TITANIUM	80	335		415
STEEL	51			51
ALUMINUM & MISC	7129	608		8337
LANDING GEAR	600			600
<b>SUB-TOTAL STRUCT.</b>	<b>8460</b>	<b>943</b>	<b>1807</b>	<b>11210</b>
<b>SYSTEMS:</b>				
PROPULSION		300		300
PROPELLANT		2300		2300
SURF CONTROLS	722			722
INSTRUMENTS	20			20
HYDRAULIC	300			300
ELECTRICAL	50			50
AVIONICS	50			50
FURNISHINGS	300			300
AIR, COND.	210			210
<b>SUB-TOTAL SYS.</b>	<b>1652</b>	<b>2600</b>		<b>4252</b>
<b>TOTAL AIRFRAME</b>	<b>10112</b>	<b>3543</b>	<b>1807</b>	<b>15462</b>

Table 83 - X-24C-106 Mass Breakdown \*

(AS DEFINED BY DCPR-DEFENSE CONTRACTORS PLANNING REPORT)

ELEMENT	BASELINE AIRFRAME	PROPULSION RELATED	TPS RELATED	TOTAL AIRFRAME
<b>STRUCTURE:</b>				
TPS	N/A			
LOCKALLOY	4681	1016	Included	5697
TITANIUM	1188	924	N	1512
STEEL	2417		BASELINE	2417
ALUMINUM & MISC.	1277			1277
LANDING GEAR	600			600
<b>SUB-TOTAL STRUCT.</b>	<b>10163</b>	<b>1340</b>		<b>11503</b>
<b>SYSTEMS:</b>				
PROPULSION		144		144
PROPELLANT		2650		2650
SURF CONTROLS	750	15		765
INSTRUMENTS	20			20
HYDRAULIC	300			300
ELECTRICAL	50			50
AVIONICS	50			50
FURNISHINGS	300			300
AIR. COND.	210			210
<b>SUB-TOTAL SYS</b>	<b>1680</b>	<b>2809</b>		<b>4489</b>
<b>TOTAL AIRFRAME</b>	<b>11843</b>	<b>4149</b>		<b>15992</b>

Table 84 - X-24C-107 Mass Breakdown - \*

(AS DEFINED BY DCPR-DEFENSE CONTRACTORS PLANNING REPORT)

ELEMENT	BASELINE AIRFRAME	PROPULSION RELATED	TPS RELATED	TOTAL AIRFRAME
<b>STRUCTURE:</b>				
TPS	N/A		919	919
LOCKALLOY				
TITANIUM	80	104		184
STEEL	51			51
ALUMINUM & MISC.	7883	680		8563
LANDING GEAR	600			600
<b>SUB-TOTAL STRUCT.</b>	<b>8614</b>	<b>784</b>	<b>919</b>	<b>10317</b>
<b>SYSTEMS:</b>				
PROPULSION		144		144
PROPELLANT		2650		2650
SURF CONTROLS	722	18		740
INSTRUMENTS	20			20
HYDRAULIC	300			300
ELECTRICAL	50			50
AVIONICS	50			50
FURNISHINGS	300			300
AIR. COND.	210			210
<b>SUB-TOTAL SYS.</b>	<b>1652</b>	<b>2812</b>		<b>4464</b>
<b>TOTAL AIRFRAME</b>	<b>10266</b>	<b>3596</b>	<b>919</b>	<b>14781</b>

Table 85 - X-24C-108 Mass Breakdown - \*

(AS DEFINED BY DCPR - DEFENSE CONTRACTORS PLANNING REPORT)

ELEMENT	BASELINE AIRFRAME	PROPULSION RELATED	TPS RELATED	TOTAL AIRFRAME
<b>STRUCTURE:</b>				
TPS	N/A		1807	1807
LOCKALLOY				
TITANIUM	80	104		184
STEEL	51			51
ALUMINUM & MISC	7729	680		8409
LANDING GEAR	600			600
<b>SUB-TOTAL STRUCT.</b>	<b>8460</b>	<b>784</b>	<b>1807</b>	<b>11051</b>
<b>SYSTEMS:</b>				
PROPULSION		144		144
PROPELLANT		2650		2650
SURF CONTROLS	722	18		740
INSTRUMENTS	20			20
HYDRAULIC	300			300
ELECTRICAL	50			50
AVIONICS	50			50
FURNISHINGS	300			300
AIR. CNB.	210			210
<b>SUB-TOTAL SYS.</b>	<b>1652</b>	<b>2812</b>		<b>4464</b>
<b>TOTAL AIRFRAME</b>	<b>10112</b>	<b>3596</b>	<b>1807</b>	<b>15515</b>

Table 86 - X-24C-109 Mass Breakdown \*

\*Mass breakdown depicted in pounds and reflected in kilograms (pounds) in Table 95.

**COMPLEXITY FACTORS**

	<u>LR-105/ATLAS</u>	<u>LR-105/LR-11</u>	<u>LR-99</u>
BY INSTALLATION PROVISIONS MASS	1.00	1.04	1.10
BY ENGINEERING ESTIMATE OF SYSTEM COMPLEXITY (NO. TANKS, PLUMBING, CONTROLS, ETC.)	1.10	1.20	1.00
COST OF PROPELLANT SYSTEM PURCHASED EQUIPMENT	1.05	1.15	1.00

Table 87 - Propulsion System Alternatives

	<u>-101 LR-105/ATLAS</u>	<u>-104 LR-105/LR-1</u>	<u>-107 LR-99</u>
(DOLLARS IN THOUSANDS)			
AIRFRAME _____	\$ 40,294	\$ 40,294	\$ 40,294
PROPULSION SYSTEM INSTALLATION AND RELATED ITEMS _____	<u>12,767</u>	<u>14,097</u>	<u>12,780</u>
TOTALS _____	<u>\$ 53,061</u>	<u>\$ 54,391</u>	<u>\$ 53,074</u>
COST PROPULSION INSTALLATION ALTERNATIVES	1.00	1.10	1.00

NOTE: EXCLUDES COST OF ROCKET PROPULSION ENGINES

Table 88 - Propulsion System Alternatives -  
Lockalloy Configuration

of the other two alternatives. This propulsion system cost relationship is also valid for the other two TPS configurations.

Thermal Protection System Alternatives - Considerable attention was given in this phase of the study to providing realistic and comparable cost estimates for the alternative TPS. Since Lockalloy is an integral part of the vehicle structure, it is not broken out separately to the same degree as for the LI-900 and Ablator. However, some Lockalloy cost factors are provided for comparison purposes and to furnish a basis for field maintenance estimates.

- Complexity Factors - As in the case of the propulsion systems, various complexity factors were derived to provide a basis for determining the relative costs of both the baseline structural vehicles and the TPS. Some of these are illustrated in Table 89. It should be noted from these data that the number of significant structural parts in the Lockalloy vehicle is approximately one half of the parts count in either aluminum vehicle. It is this relative simplicity of design and construction which is a major contributing factor to offsetting the high cost of the Lockalloy material as compared to aluminum. It should also be noted, that due to the requirements to provide 100 percent of limit load nonbuckling skin structure for the LI-900 and 80 percent for the Ablator, the parts count is some two percent greater for the LI-900 airframe over the Ablator; and some six percent greater for the Ablator airframe over a conventional aluminum fighter-type aircraft. ADP does not believe that a Mach 6 vehicle with these TPS surface installation requirements can be produced, within these mass and performance constraints, for any significantly less part count.
- Costs - Table 90 lists the costing factors used to develop the estimates for LI-900 and Ablator procurement and installation. The Lockalloy data is shown for reference. RSI and Ablator materials are assumed to be delivered from the supplier to the airframe manufacturer in finished form ready for installation. As noted in the Engineering Design and

**COMPLEXITY FACTORS**

<u>FUSELAGE/WING/TAIL NUMBER STRUCTURAL PARTS (1)</u>	<u>LOCKALLOY HEAT-SINK STRUCTURE</u>	<u>ALUMINUM STRUCT. LI-900 RSI TPS</u>	<u>ALUMINUM STRUCT. ABLATOR TPS</u>
	5,500	11,340 (2)	11,080 (2)
<u>TPS PARTS</u>			
<u>APPROX. NUMBER</u>	500 (3)	5,000	500
<u>AVERAGE SIZE</u>	0.51 x 0.76 m PANEL	0.20 x 0.20 m TILE	0.51 x 0.76 m SHEET
<u>STRUCTURE MASS-kg</u>			
<u>LOCKALLOY</u>	2438	NONE	NONE
<u>OTHER</u>	2714	4305	4235
<u>SUB-TOTAL</u>	5153	4305	4235
<u>TPS</u>	(INCL. ABOVE)	417	819
<u>TOTAL</u>	5153	4722	5054

NOTES: (1) EXCLUDES MISC. SMALL PARTS AND FASTENERS  
 (2) CONVENTIONAL FIGHTER TYPE ALUMINUM STRUCTURE- 10,350 PARTS  
 (3) ALSO INCLUDED IN STRUCTURE ABOVE

Table 89 - Thermal Protection System Alternatives

Testing Section, the costs for detail design of the TPS installation and testing of TPS application to the X-24C vehicle (hinge lines, slip joints, etc.) are included in the ADP portion of the TPS cost breakdown. Basic materials characterization for use of either LI-900 or Ablator materials is assumed to be already accomplished or included in the cost per square meter of delivered TPS materials. The cost of Ablator type material includes allowances for the RSI type material that will be used on leading edges and other areas of shock impingement. Man-hours for field installation for the RSI and Ablator are greater than the in-plant hours



because of the need for removal of damaged material prior to replacement. Lockalloy field replacement is substantially less because panel replacement is a simple operation of removing fasteners and reinstalling an interchangeable predrilled part. The scrap and usage factors listed consider the vulnerability of each material to damage during transportation, handling, and storage as well as during installation. The results of estimating alternative TPS configurations is shown in Table 91 using the LR-105/Atlas vernier propulsion airframe as a baseline. Lockalloy structure is an integral part of the vehicle and therefore it is not feasible to break it out separately. The aluminum airframes can be treated as theoretical complete fly-away vehicles without TPS, therefore the separate cost for TPS engineering, tooling, material procurement, and installation can be clearly segregated. Considering the Lockalloy vehicle as a base, the Ablator cost for two vehicles is only 2 percent greater, whereas the LI-900 cost is 17 percent greater.

- Correlation to Other Contractor Estimates - Because there is relatively little industry experience with the installation and use of either the LI-900 or the Ablator, and because ADP could not obtain as much hard cost data on these TPS as desired; we have attempted to correlate the ADP estimates for total cost of each TPS (on a per square meter basis) to other published industry data. The comparisons are shown in Table 92. In each case data from other companies have been adjusted by ADP to escalate to January 1976 dollars and to include the 10 percent contractor fee. If the Martin Marietta Ablator estimate is further adjusted to add installation cost based on the NASA Houston estimate of 183 man-hours per sq. meter , the total cost would be \$29,060 per sq. meter . Lockheed believes that this illustrates a reasonable correlation between the various contractor data, particularly when the range of accuracy of the estimates as defined in the Analysis Conclusion Section below.

	LOCKALLOY PANELS*	RSI (LI-900 TYPE)	ABLATOR (MM SLAZZO TYPE)
<u>INSTALLATION MAN-HOURS PER m<sup>2</sup></u>			
IN FACTORY			
FIRST VEHICLE	116	183	54
SECOND VEHICLE	93	165	48
IN FIELD (INCL. REMOVAL AND REPLACEMENT)	22	215	65
COST OF TPS PANELS DELIVERED TO AIRFRAME READY FOR INSTALLATION	\$16 430/m <sup>2</sup>	\$14080/m <sup>2</sup>	\$5870/m <sup>2</sup>
INSTALLATION USAGE AND SCRAP FACTOR (APPLY TO PROCURED PANELS/ TILES)	5%	33%	25%

\*HOT STRUCTURE HEAT-SINK

Table 90 - TPS Comparison

TWO X-24C AIRFRAMES - LR-105/ATLAS VERNIER CRUISE

(DOLLARS IN THOUSANDS)	-101 LOCKALLOY	-102 LI-900	-103 ABLATOR
AIRFRAME _____	\$53,061	\$48,193	\$47,754
TPS _____	(INTEGRAL ABOVE)	13,983	6,322
TOTALS _____	\$53,061	\$62,176	\$54,076
TPS AVERAGE COST PER m <sup>2</sup>	(INCLUDED IN STRUCTURE)	\$37630	\$17020
COST OF ALTERNATIVES COMPARED TO LOCKALLOY	1.00	1.17	1.02

ASSUMES ALL VEHICLE CONFIGURATIONS HAVE 186 m<sup>2</sup> SURFACE AREA

Table 91 - TPS Alternatives

<u>DIRECT BOND ABLATOR</u>	<u>CONTRACTOR ESTIMATES</u> <u>AVERAGE PRICE PER</u>	
	<u>M<sup>2</sup></u>	<u>(FT<sup>2</sup>)</u>
MARTIN-MARIETTA _____	\$10,190	(\$ 947*)
ROCKWELL _____	\$15,120	(\$1,405*)
LOCKHEED-ADP CURRENT STUDY _____	\$17,020	(\$1,581)
 <u>DIRECT BOND RSI</u>		
MARTIN-MARIETTA (EXCLUDING INSTL) _____	\$24,700	(\$2,295*)
ROCKWELL _____	\$44,250	(\$4,111*)
LOCKHEED-ADP CURRENT STUDY _____	\$37,630	(\$3,496)

\*BASED ON PUBLISHED DATA ESCALATED BY ADP TO COMMON BASELINE OF JAN. 1976 DOLLARS AND TO INCLUDE 10% CONTRACTOR FEE.

Table 92 - TPS Cost Comparison

Initial Spares, AGE and Data - Part of the Phase I cost trade task was to include the estimated value of initial spare parts, AGE and technical data in order to develop the total initial investment cost.

- Initial Spares - The provisioning of spare parts to support the first year of flying operations (plus procurement lead time) is estimated as follows:

	<u>Lockalloy</u> <u>Heat-Sink</u> <u>Structure</u>	<u>Aluminum</u> <u>Structure</u> <u>LI-900 TPS</u>	<u>Aluminum</u> <u>Structure</u> <u>Ablator TPS</u>
One Vehicle	\$2,300,000	\$5,400,000	\$3,200,000
Two Vehicles	\$2,600,000	\$6,000,000	\$3,600,000

Premises used in developing spares costs are shown in Table 93. Structural items and TPS materials generally fall under the category of "insurance" spares and are included in the amounts shown based on their estimated vulnerability to field damage and replacement. The three alternative propulsion system installations do not contribute to any significant difference in initial spares provisioning costs.

- Aerospace Ground Equipment - Table 93 also discussed AGE provisioning premises. It should be noted that none of the TPS concepts are penalized with the cost of excessive specialized equipment or field

**SPARES PROVISIONING:**

ALL CONFIGURATIONS \_\_\_\_\_ FUNCTIONAL SYSTEMS 100% ONE VEHICLE  
 \_\_\_\_\_ STRUCTURAL COMPONENTS 10% ONE VEHICLE  
 (INCLUDES LOCKALLOY)  
 TPS LOCKALLOY \_\_\_\_\_ ADDITIONAL 10% OF ONE VEHICLE MATERIAL  
 ABLATOR \_\_\_\_\_ 100% OF ONE VEHICLE MATERIAL \*  
 LI-900 \_\_\_\_\_ 100% OF ONE VEHICLE MATERIAL

**AGE:**

ALL CONFIGURATIONS \_\_\_\_\_ AIRFRAME HANDLING AND SYSTEMS  
 CHECKOUT EQUIPMENT

NOTE: PRIMARY CAPABILITY FOR TPS MANUFACTURE AND FORMING  
 RETAINED AT SUPPLIER FACILITY.  
 IF SPECIALIZED EQUIPMENT IS REQUIRED AT DRC FOR TPS  
 REFURBISHMENT/REPLACEMENT, IT SHOULD BE AVAILABLE  
 FROM X-24C PROJECT TOOLING.

\* Ref: Martin Marietta Corp. report AFFDL-TR-75-37,  
 dated 5 May 1975

Table 93 - Initial Spares and AGE Premises

facilities for the refurbishment of TPS. The estimated cost of initial AGE is \$300,000 for one vehicle and \$500,000 for two vehicles for all configurations.

- Technical Data - The cost of development and supply of pilot operating handbook data, airframe and system maintenance manuals and other maintenance tech data has been estimated based on experience from the YF-12 and other programs. For purposes of this study, the cost of data was assumed to be the same for all nine configurations at \$900,000.
- Total Initial Investment Cost - Table 94 summarizes the total initial investment cost for two X-24C vehicles including spares, AGE and technical data. The relative costs of the three alternative thermal protection systems are shown based on the vehicle with a LR-105/Atlas vernier propulsion system. Total initial investment cost through delivery for the three TPS concepts rank as follows:

Lockalloy Heat-Sink Structure	1.00
Aluminum Structure/Ablator TPS	1.04
Aluminum Structure/LI-900 RSI	1.22

Initial investment cost for one or two vehicles in each of the nine configurations is summarized in Table 95, which also include the estimate of annual TPS maintenance man-hours for each.

Initial Vehicle Cost Analyses Conclusions - An assessment of the range of accuracy of the cost estimates in this study is presented in Table 96. This indicates that ADP has the least confidence in the LI-900 estimates, particularly because of the lack of experience and uncertainty regarding tooling and installation costs. While it is not anticipated that they will reduce significantly (at least until the Space Shuttle program gains experience) they could increase substantially. The potential spread of Ablator costs is also greater than for either the Lockalloy vehicle or the aluminum vehicles exclusive of TPS. As noted, ADP does not

TWO VEHICLES - JAN, 1976, DOLLARS

	LOCKALLOY HEAT-SINK STRUCT.	ALUMIN. STRUCT. LI-900 RSI TPS	ALUMIN. STRUCT. ABLATOR TPS
AIRFRAMES _____	\$53.1M	\$62.2M	\$54.1M
INITIAL SPARES _____	2.6M	6.0M	3.6M
AGE _____	.5M	.5M	.5M
DATA _____	.9M	.9M	.9M
INITIAL INVESTMENT THROUGH DELIVERY	\$57.1M	\$69.6M	\$59.1M

NOTE: ● EXCLUDING CONFIGURATION DEVELOPMENT, PROPULSION SYSTEMS,  
B-52 MODIFICATION AND INSTRUMENTATION/PAYLOAD/EXPERIMENT  
DEVELOPMENT

● BASED ON LR-105/ATLAS PROPULSION ALTERNATIVE

Table 94 - Initial Investment

believe that this affects the Phase I study conclusions. For example, if Ablator TPS costs are overstated by 25 percent, the Aluminum vehicle with Ablator would cost on the order of one percent less than the Lockalloy vehicle.

The conclusions drawn from the Phase I costing tradeoff study are summarized in Table 97.

### FLIGHT SUPPORT AND MAINTENANCE ANALYSIS

Vehicle flight support and maintenance man-hours estimates were based on the following sources:

NUMBER OF VEHICLES	STRUCTURE/TPS OPTIONS		ALUMINUM STRUCTURE ELASTOMERIC ABULATOR TPS				ALUMINUM STRUCTURE LI-1900 R-1 TPS				MAGNESIUM/BERYLLIUM HEAT-SINK STRUCTURE		
	ROCKET PROPULSION OPTIONS		DCPR AIRFRAME MASS (kg) (Lb)	INITIAL AIRFRAME COST (K\$)	ANNUAL TPS MAINT MAN-HOURS	DCPR AIRFRAME MASS (kg) (Lb)	INITIAL AIRFRAME COST (K\$)	ANNUAL TPS MAINT MAN-HOURS	DCPR AIRFRAME MASS (kg) (Lb)	INITIAL AIRFRAME COST (K\$)	ANNUAL TPS MAINT MAN-HOURS	DCPR AIRFRAME MASS (kg) (Lb)	INITIAL AIRFRAME COST (K\$)
1	XLR-99*		7017 (15,315)	\$45,240	10,000	6705 (14,761)	\$52,443	24,000	7254 (15,992)	\$43,588	1,000		
	THROTTLED LR-105		7013 (15,462)	\$46,543	10,000	6681 (14,728)	\$53,746	24,000	7117 (15,690)	\$44,678	1,000		
	LR-105 (NO THROTTLE) ATLAS VERNIER (CRUISE)		6938 (15,295)	\$45,563	10,000	6605 (14,561)	\$52,766	24,000	7049 (15,500)	\$43,696	1,000		
2	XLR-99*			\$58,678	15,000		\$69,178	36,000		\$57,074	1,500		
	THROTTLED LR-105			\$60,404	15,000		\$70,903	36,000		\$58,391	1,500		
	LR 105 (NO THROTTLE) ATLAS VERNIER (CRUISE)			\$59,076	15,000		\$69,576	36,000		\$57,061	1,500		

ASSUMPTIONS:

1. 100 TOTAL FLIGHTS PER VEHICLE AVERAGING 12 PER YEAR
2. B-52B S/N 008 LAUNCH CONSTRAINTS SAME AS WITH X-15A-2 (25.85 MPa - 57,000 Lb)
3. OPERATING PERFORMANCE SHALL BE MACH 6.0 WITH 40 SECONDS OF ROCKET CRUISE AT 47.9 MPa (1000 PSFD) DYNAMIC PRESSURE (INCLUDING DRAG AND WEIGHT OF A 3-MODULE SCRAMJET TEST PACKAGE)

\*WITH NOZZLE EXTENSION

Table 95 - Initial Investment Cost Summary

**OBJECTIVE:**

PROVIDE COST ESTIMATES IN  $\pm 10\%$  RANGE OF ACCURACY

**ADP ESTIMATE — RANGE OF ACCURACY ACHIEVED:**

LOCKALLOY VEHICLE	-----	$\pm 10\%$
ALUMINUM VEHICLES (EXCL. TPS)	-----	$\pm 10\%$
TPS - ABLATOR	-----	$\pm 25\%$
TPS - LI-900	-----	{ +40%
		{ -10%

NOTE: APPLYING UPPER AND LOWER LIMITS OF TPS ESTIMATES DOES NOT CHANGE COST STUDY CONCLUSIONS.

Table 95 - Cost Estimate Accuracy

VEHICLE ACQUISITION COST CONCLUSIONS
● THERE IS NO SIGNIFICANT DIFFERENCE BETWEEN THE INITIAL COST OF A LOCKALLOY HEAT-SINK STRUCTURE VEHICLE AND AN ALUMINUM VEHICLE WITH DIRECT BOND ABLATOR TPS.
● AN ALUMINUM VEHICLE WITH DIRECT BOND LI-900 TYPE RSI TPS WILL COST APPROXIMATELY 20% OR \$12 MILLION MORE THAN THE OTHER TPS ALTERNATIVES.
● THE LR-105/LR-11 PROPULSION SYSTEM IS MORE COSTLY TO INSTALL THAN EITHER THE LR-105/ATLAS OR LR-99; HOWEVER, ALL FALL WITHIN A $\pm 10\%$ RANGE (EXCLUDING ROCKET ENGINE COSTS).

Table 97 - Vehicle Acquisition Cost Conclusion



- Published reports, U. S. Government and Contractors.
- Correspondence with personnel currently working for either NASA or a contractor in the field of interest.
- In-house data and experience at Lockheed and Lockheed Missiles and Space Co.
- Consulting services of Mr. Jim Love, X-15 NASA FRC Program Manager.

The effort of determining Thermal Protection System (TPS) manpower for one and two vehicles was expanded to include manpower required for flight line, base support, contractor support and B-52 support. A summary of this manpower is shown in Figures 180 and 181.

Turnaround Time Influence on Maintenance - The X-24C program is now planned to take approximately eight years to complete 190 flights per vehicle. This requires 12 flights per year per vehicle. Experience accumulated on other programs and in particular the X-15 program shows that to accomplish an average of one flight per month, it is necessary to complete the turnaround activity within ten working days. Turnaround within this time span is required in order to compensate for delays caused by weather, vehicle modifications, holidays, unscheduled maintenance, flight aborts, etc. (References 37 and 38).

A breakdown of the ten day turnaround shows the following time allotment for the various tasks:

- 1 day to preflight the X-24C
- 1 day to load on the B-52
- 1 day to fly
- 1 day to postflight

This assignment uses four days leaving only six days for vehicle maintenance. Any maintenance activity that causes an extension of the ten day turnaround time runs the risk of causing a calendar time stretch out of the eight year program.

ONE VEHICLE, MAN-YEARS PER YEAR

	ABLATIVE			LI-900			LOCKALLOY		
	LR-99	LR-105 + 2 LR11	LR-105 + 12 VERN	LR-99	LR-105 + 2 LR11	LR-105 + 12 VERN	LR-99	LR-105 + 2 LR11	LR-105 + 12 VERN
FLIGHT LINE	14.5	14.5	14.0	14.5	14.5	14.	13.5	13.5	13.
BASE SUPPORT	10.0	10.0	9.5	10.0	10.0	9.5	10.0	10.0	9.5
VEHICLE SUB-TOTAL	24.5	24.5	23.5	24.5	24.5	23.5	23.5	23.5	22.5
MANAGEMENT AND SYSTEM ENGR.	8.5	8.5	8.5	8.5	8.5	8.5	8.5	8.5	8.5
LOCKHEED SUPPORT	10	10	10	10	10	10	10	10	10
CONTRACTOR TPS	5	5	5	12	12	12	0.5 FROM BASE SUPPORT	0.5	0.5
B-52 SUPPORT	7	7	7	7	7	7	7	7	7
*TOTAL	55	55	54	62	62	61	49.5	49.5	48.5

\*DOES NOT INCLUDE PROPULSION SYSTEM CONTRACTOR SUPPORT

Figure 180 - Manpower Summary

	ABLATIVE			LI-900			LOCKALLOY		
	LR-99	LR-105 + 2 LR-11	LR-105 + 12 VERN	LR-99	LR-105 + 2 LR-11	LR-105 + 12 VERN	LR-99	LR-105 + 2 LR-11	LR-105 + 12 VERN
FLIGHT LINE	29	29	28	29	29	28	27	27	26
BASE SUPPORT	15	15	14.5	15	15	14.5	14.5	14.5	14
SUB-TOTAL	44	44	42.5	44	44	42.5	41.5	41.5	40
MANAGEMENT SYS. ENGR	11	11	11	11	11	11	11	11	11
LOCKHEED SUPPORT	12	12	12	12	12	12	12	12	12
CONTRACTOR TPS	7.5	7.5	7.5	18	18	18	.5 FROM BASE SUPPORT	.5	.5
B-52 SUPPORT	7	7	7	7	7	7	7	7	7
*TOTAL	81.5	81.5	80.0	92	92	90.5	72	72	70.5

\*DOES NOT INCLUDE CONTRACTOR PROPULSION SYSTEM SUPPORT

Figure 181 - Manpower Summary - Two Vehicles

TPS Influence on Maintenance - Most of the published data reviewed on Ablative and RSI TPS is related to entry vehicles, primarily the Space Shuttle. One exception is the data published on the X-15 (References 39 and 40). The X-15 experience provides one source of information where ablative TPS was exposed to an operational environment very similar to the environment the X-24C will experience. The X-15 using a spray-on ablative material required 700 man-hours and two weeks in a dedicated facility to refurbish after one flight. (Reference 40.)

Although ablative materials available today may be much improved over the material used on the X-15 (in that they may be more compatible with LOX, fuels, hydraulic fluids, less ablative, etc.) many of the problems and precautions added to the X-15 maintenance effort will still exist for an X-24C covered with an external TPS. It should be pointed out that only direct bonded TPS has been considered during this study since cost studies already completed on TPS systems consistently show this to be the lightest and lowest cost way to attach TPS. (References 41, 42 and 10.)

When an external TPS is added to an aluminum structured vehicle, it adds to the cost of maintaining that vehicle in two significant ways:

- 1) Increased manhours expended by systems maintenance personnel due to TPS related delays and increased care that must be exercised by personnel working on or around the vehicle.
- 2) Postflight/preflight inspections and any necessary TPS refurbishment.

Item 1 above takes into consideration the delays maintenance people will experience because more protective covers, masking, and sealing must take place prior to removing access panels, climbing in and out of the cockpit, opening up fuel or hydraulic lines, etc. It is also not likely that maintenance personnel will be permitted to walk on a TPS covered vehicle nor will other maintenance work be permitted on the vehicle during the same time that the TPS is being refurbished. (Reference 43.) Therefore an increase of 5% in maintenance time over a Lockalloy vehicle has been included, Figures 182, 183, and 184.

MAINT. HOURS ASSIGNMENT - ONE VEHICLE

	BASELINE LOCKALLOY		LOCKALLOY	
	% PER SYS.	LR-105 +12 VERN. MAN-HR YEAR	LR-99 MAN-HR YEAR	LR-105 +2 LR-11 MAN-HR YEAR
1. AIRFRAME	15.8	6,162	7,265	7,265
2. ENGINES	13.5	5,265		
3. COCKPIT	3.3	1,287		
4. PROPELLANTS	30.0	11,700		
5. ELECTRICAL	8.6	3,354		
6. HYDRAULICS	9.1	3,549		
7. ENVIRONMENTAL	1.9	741		
8. FLIGHT CONTROLS	3.5	1,365		
9. LANDING GEAR	6.1	2,379		
10. AVIONICS	8.2	3,198		
SUB-TOTAL	100.0	39,000	41,000	41,000
△ 11. MISSION SUPPORT		6,000	6,000	6,000
12. TPS		1,000	1,000	1,000
TOTAL		46,000	48,000	48,000

△ MISSION SUPPORT = LOADS LAB, OPERATIONS ENG'R, DATA SYSTEMS TECH.

Figure 182 - Maintenance Hours Assignment -  
Lockalloy

MAINT. HOURS ASSIGNMENT - ONE VEHICLE

	LI-900		LI-900	
	% PER SYS.	LR-105 +12 VERN MAN-HR YEAR	LR-99 MAN-HR YEAR	LR-105 +2 LR-11 MAN-HR YEAR
1. AIRFRAME	15.8	6,470	7,528	7,528
2. ENGINES	13.5	5,528		
3. COCKPIT	3.3	1,351		
4. PROPELLANTS	30.0	12,285		
5. ELECTRICAL	8.6	3,522		
6. HYDRAULICS	9.1	3,726		
7. ENVIRONMENTAL	1.9	778		
8. FLIGHT CONTROLS	3.5	1,433		
9. LANDING GEAR	6.1	2,498		
10. AVIONICS	8.2	3,358		
SUB-TOTAL	100.0	40,950	42,950	42,950
△ 11. MISSION SUPPORT		6,000	6,000	6,000
12. TPS		24,000	24,000	24,000
TOTAL		70,950	72,950	72,950

△ MISSION SUPPORT = LOADS LAB, OPERATIONS ENG'R., DATA SYSTEMS TECH.

Figure 183 - Maintenance Hours Assignment -  
LI-900

MAINT. HOURS ASSIGNMENT - ONE VEHICLE

	ABLATIVE		ABLATIVE	
	% PER SYS.	MAN-HR YEAR	LR-99 MAN-HR YEAR	LR-105 +2 LR-11 MAN-HR YEAR
1. AIRFRAME	15.8	6,470	7,528	7,528
2. ENGINES	13.5	5,528		
3. COCKPIT	3.3	1,351		
4. PROPELLANTS	30.0	12,285		
5. ELECTRICAL	8.6	3,522		
6. HYDRAULICS	9.1	3,726		
7. ENVIRONMENTAL	1.9	778		
8. FLIGHT CONTROLS	3.5	1,433		
9. LANDING GEAR	6.1	2,498		
10. AVIONICS	8.2	3,358		
SUB-TOTAL	100.0	40,950	42,950	42,950
△ 11. MISSION SUPPORT		6,000	6,000	6,000
12. TPS		10,000	10,000	10,000
TOTAL		56,950	58,950	58,950



MISSION SUPPORT = LOADS LAB, OPERATIONS ENG'R., DATA SYSTEMS TECH.

Figure 184 - Maintenance Hours Assignment -Ablative

The postflight/preflight inspections for an insulated vehicle require more time than for a Lockalloy vehicle. In a refurbishment cost study, Reference 44, conducted by McDonnell Douglas Astronautics Co. - East, it was determined that 18 minutes per sq. meter and 23 minutes per sq. meter were required to visually inspect ablative and RSI insulation respectively. Additional time must be spent verifying the condition of the RTV bond through the use of sonic, ultrasonic, infra-red, x-ray or some other technique. It is the lack of a quick, simple, and fool-proof method for checking bond condition that may cause a large variation in the time required to complete a postflight/preflight inspection. TPS must also be

inspected for internal cracks, delaminations, moisture infiltration, condition of emissivity coating, and inclusions from ground debris. In a proposal on the use of LI-900 for the Space Shuttle, Reference 45, submitted by LMSC to Rockwell International it was pointed out that a major LI-900 maintenance item would be post-mission and post-repair inspection.

Inspection of Lockalloy closely resembles conventional aircraft postflight/preflight inspections, consisting primarily of a visual scanning for dings, cracks, or temperature induced damage. Suspect areas can be dye checked or x-rayed as done on aluminum aircraft.

Therefore, in recognizing both the magnitude of the postflight/preflight inspection effort and the need to establish realistic inspection times compatible with a ten day turnaround schedule, it is felt that 80 hours for ablative, 100 hours for LI-900, and 8 hours for Lockalloy would be a reasonable inspection time.

In considering TPS refurbishment estimates, it becomes quickly apparent that ablative of LI-900 long time (8 to 10 years) multiple thermal exposure data based on actual flight experience is not available. On the basis of research data accumulated, it can be concluded that both ablative and LI-900 TPS have extensive reuse capability but some refurbishment will be required for each TPS concept including Lockalloy.

An early Space Shuttle TPS study conducted by LMSC, estimated for the Space Shuttle using LI-1500 (similar to LI-900) that a 2 to 5% refurbishment per flight might be expected and 70 to 100% refurbishment per flight using an ablative TPS. It is recognized that entry heating for the Space Shuttle is a much more severe exposure than the X-24C will experience. A study conducted by Rockwell International, Reference 42, on an X-24C type vehicle made an estimate of tile damage that might be expected primarily due to ground handling damage. Following telephone discussions with Rockwell International engineering personnel, involved with the development of Reference 42, an adjustment to the Reference 42 data was made. Using the revised Rockwell International data it was determined that tile

estimated damage per-flight turnaround would equal 3.3% of the vehicle wetted area. Ablative insulation was estimated as being subjected to the same amount of turnaround damage plus an undetermined amount of flight damage due to ablation. Martin Marietta Corporation, in Reference 46, also indicates that a spare shipset of ablative TPS should be procured for an ablative covered X-24C vehicle.

Although it may not be possible to establish a scheduled maintenance requirement for TPS, it is expected that some refurbishment will be required in the form of unscheduled maintenance due to TPS damage incurred during flight or the turnaround activity and deterioration on wear due to aging. The amount of refurbishment per flight is estimated to be as follows:

- Ablative - 0.62% to 2.5%
- LI-900 - 0.375% to 1.5%
- Lockalloy - 0.05% to 0.2%

The one percent higher refurbishment rate required to ablative material over LI-900 is felt necessary since ablative material will not tolerate thermal overruns as well as LI-900, is not as tolerant of fluid contamination such as hydraulic oils, has a very fragile char layer, and may experience some ablation and erosion, not anticipated for LI-900.

TPS Repair Times - As has already been stated very little experience from an operational standpoint is available on TPS maintenance. X-15 experience, while valuable in pointing out the need to seal and protect aircraft systems and openings such as vents, filler lines, and static air sources during TPS refurbishment, does not permit the direct equating of refurbishment manhours for repairing a sq. meter of X-15 TPS to X-24C TPS. The X-15 used a sprayed on material while the X-24C will use ablative panels bonded directly to the aircraft skin.

A study on removal methods for ablative TPS was conducted by Martin Marietta Aerospace, Denver Division, Reference 47, using a lifting body vehicle as a test bed with ablative TPS bonded directly to its skin. Although this study

was conducted with the Space Shuttle the intended beneficiary, much of the experience gained can be applied to X-24C requirements.

McDonnell Douglas has also conducted studies on ablative panel refurbishment and results of their study is available in Reference 45.

It is obvious that unless refurbishment is limited to repairing removable doors or panels that the vehicle must be placed in a facility where a power source is available for hand tools, dust and vapor control equipment, and a vacuum source for applying pressure to hold replacement material in place during the RTV bond cure.

Utilizing the information from References 45, 42, 10 and 47, the following time allotment has been established as reasonable to refurbish ablative TPS:

● Remove damaged TPS	16 hour per m <sup>2</sup>
● Prefit and install	38 hour per m <sup>2</sup>
● Q. Ac.	5 hour per m <sup>2</sup>
● Direct supervision	<u>5 hour per m<sup>2</sup></u>
TOTAL	64 hour per m <sup>2</sup>

In a memorandum received from the Lyndon B. Johnson Space Center, it was stated that the first orbiter (OV102) will require approximately 183 manhours per sq. meter to install LI-900 tile. The time is made up of 11 hours of tile prefit time, 151 hours of installation operation, and 19 hours of vacuum leak checking of both the installation tool vacuum seal and for leaks through the aluminum skin. It includes a 51.5% factor for personnel fatigue, delays, some overhead and a modest amount of "out of scope" changes. It assumes that individual tiles have been selected and brought to the work site, but not individually fit. It also includes the use of a "picture frame" array tool in which 20 to 30 tiles are correctly spaced and already have nomex felt strain isolator pads attached. The 183 manhours does not include quality assurance time.



On a refurbishment basis, the array tool would not be used since tiles would be fitted and installed one at a time. Although damaged tiles will normally be removed and replaced with new ones, NASA has developed a scheme to repair some types of tile damage by fitting prefabricated plugs of the tile material into cavities made by removing the damaged area of the tile, Reference 49.

In the pursuit of more information on LI-900 tile installation and refurbishment costs, Mr. Don Greene of Rockwell International was contacted. It was his opinion that it would take more than 16 man-hours to install tiles on a one at a time basis and more than 16 hours per square meter to remove damaged tile. It is therefore estimated that refurbishing LI-900 tile will take approximately 215 man-hours per square meter.

Lockalloy offers a much more durable surface than either ablative or RSI material and will resemble the X-15 when it was flown as a heat sink machine. Thermal expansion will be a primary design consideration in X-24C development to avoid the type of structural damage (permanent buckles) experienced by the X-15.

Lockalloy will also be exposed to ground handling damage during mission turnaround. Minor dings or scratches can be polished out but, generally, damaged panels will be removed and replaced. Since the Lockalloy skin panels will be attached with screws instead of rivets; this will be a comparatively low man-hour activity. 22 hours per square meter is estimated for replacing damaged panels.

Annual TPS Refurbishment Manhours - Annual maintenance manhours for each TPS concept can now be computed. A surface area of  $186 \text{ m}^2$  will be used for all three concepts. This may not be the final area, but it will permit comparison. Therefore, using the percentages of area requiring refurbishing and hours per square meter:

$$\text{Ablator: } 186 \text{ m}^2 \times 2.5\% \text{ per flight} \times 64.6 \text{ hr per m}^2 = 300 \text{ hours per flight}$$

$$\text{For 12 flights per year} = 3600 \text{ hours}$$

This equals less than 2 men per year until the ten day turnaround cycle is considered. With a maximum of six maintenance working days available, it requires the following manpower:

One man work 6 days = 48 hours per man per turnaround,

$$\frac{300 \text{ HR}}{48 \text{ HR}} = 6^+ \text{ men per day for six days to do the TPS}$$

If the equivalent of 1 man is used from the base support crew then 5 TPS contractor personnel must be used.

Five contractor personnel times 2000 hours per year = 10,000 manhours as shown on the manpower summary chart, Figure 180.

$$\text{LI-900 RSI: } 186 \text{ m}^2 \times 1.5\% \text{ per flight} \times 215 \text{ hr per m}^2 = 600 \text{ hours per flight for 12 flights per year}$$

$$12 \text{ flights} = 7200 \text{ manhours}$$

For the 10 day turnaround:

$$\frac{600 \text{ HR}}{48 \text{ HR}} = 12^+ \text{ men per day for six days,}$$

twelve TPS contractor personnel at an annual cost of 24,000 manhours as shown in Figure 180.

$$\text{Lockalloy Heat-Sink: } 186 \text{ m}^2 \times 0.2\% \text{ per flight} \times 21.5 \text{ hr per m}^2 = 8 \text{ hours per flight}$$

This is the estimated maintenance time that will be required, averaged for the life of the vehicle, to correct thermally caused problems similar to those experienced by the X-15. ADP experience estimates that a 0.5 man-year effort will be adequate to handle unscheduled exterior surface maintenance. This level

of effort will be handled by shop personnel, already accounted for in the Base Support Manpower, Figure 185.

Annual Maintenance Manpower - Manpower forecasts for flightline, base support, contractor support, and B-52 support are shown on Figure 180 and Figure 181 for one and two vehicles respectively. The following conditions and assumptions were applied:

- One-shift, 5 day work week
- 5 - 10 day turnaround time
- All systems in quasi-operational status
- USAF maintains pilots pressure suits
- B-52 and PSTS contractor operated
- Average manpower shown for years three through six. Years one and two require approximately 10% more. Seventh and eighth years require approximately 10% less.

BASE SUPPORT

ONE X-24C, MANYEARS PER YEAR

	ABELATIVE			LI-900			LOCKALLOY		
	LR-99	LR-105 +12 VERN	LR-105 +2 LR-11	LR-99	LR-105 +12 VERN	LR-105 +2 LR-11	LR-99	LR-105 +12 VERN	LR-105 +2 LR-11
*ROCKET SHOP TECH	2 0	1 5	2	2 0	1 5	2 0	2 0	1 5	2 0
TPS TECH	5	5	5	5	5	5	-	-	-
TPS ENGR	0	0	0	0	0	0	0	0	0
BATTERY TECH	1	1	1	1	1	1	1	1	1
FLIGHT SYS. TECH. SUP.	2	2	2	2	2	2	2	2	2
FAB SHOP	1	1	1	1	1	1	1 5	1 5	1 5
LIFE SUPPORT	1	1	1	1	1	1	1	1	1
INSTRU MAINT	0.5	0.5	0.5	0.5	0.5	0.5	0.5	0.5	0.5
LOADS LAB	1	1	1	1	1	1	1	1	1
Q A	1	1	1	1	1	1	1	1	1
ONE VEH TOTAL	10.0	9.5	10.0	10.0	9.5	10.0	10.0	9.5	10.0
TWO VEH TOTAL	15.0	14.5	15.0	15.0	14.5	15.0	14.5	14.0	14.5
LOCKHEED SUPPORT									
LIAISON & DESIGN	3	3	3	3	3	3	3	3	3
STRUCT/FUNCT ANALYSIS	7	7	7	7	7	7	7	7	7
ONE VEHICLE TOTAL	10.0	10.0	10.0	10.0	10.0	10.0	10.0	10.0	10.0

\*DOES NOT INCLUDE CONTRACTOR PSTS - G P E

Figure 185 - Base Support Summary

The manloading shown in Figures 180 and 181 are essentially in agreement with a manpower estimate submitted by Mr. Jack Kolf, X-24C Project Manager, Dryden Flight Research Center, Edwards, California except in the area of TPS technicians required to accomplish ablative or RSI refurbishments. As part of Mr. Kolf's assumptions in compiling his estimate, he did not estimate the number of people required, but rather the number of man-years. TPS contractor manpower shown in Figures 180 and 181 does consider the influence of the ten day turnaround effort and consequently shows considerably more manpower, for TPS maintenance than Mr. Kolf's estimate.

The manpower estimated for Lockheed support is less firm than the other manpower estimates due to the vagueness of just how much participation the airframe contractor will contribute to the research experiments which the X-24C will perform.

## RESEARCH CAPABILITIES

In compliance with the Research Requirements all candidate structural configurations were integrated with vehicle features including:

- 1) A full depth 3 m payload bay, Figure 70, extending between the cockpit and propellant tanks. The bay is joined to the cockpit assembly and aft body through service joints which permit the bay to be replaced in the field. The payload bay is double walled constructed allowing the outer wall to be completely or partially replaced with panels of an advanced thermal protection system. The inboard wall is designed to retain structural integrity in the event of failure to the advance TPS panels being tested. Alternatively, the entire inboard wall may be replaced by an advanced demonstration structure. Service panels are provided for installation or servicing of test payloads within the bay.

- 2) Wings, side fins and vertical fin were developed so that interface at the fuselage junction will accommodate replacement assemblies of advanced aerodynamic surface structures for testing. The fuselage junction has been developed to permit field replacement of the surfaces and provide for thermal deflections resulting from differences between the vehicle and the advance structures.
- 3) Structural provisions are also provided on the lower surface of the vehicle for scramjet module integration. The rear segment of the vehicle is provided with an adjustable (ground adjustment) flap to act as an external nozzle expansion surface. A structural plug is provided to cover over these provisions whenever the scramjet modules are not employed.

Research Capabilities Assessment - In determining the payload mass allowance based on the difference between the maximum allowable zero fuel mass and operating mass empty, one of the nine configurations, -109 of Table 27, and one using the LR-99 engine in conjunction with the Lockalloy heat-sink structure, produced a negative payload allowance. This means that even with no payload the vehicle could not accomplish the basic mission.

Using an estimated mass allowance of 1225 kg for a three module scramjet plus coolant, for the mission, four of the remaining eight configurations were capable of the scramjet mission load, in addition to providing an excess for additional research payload. The four configurations found incapable of the scramjet role exhibited payload mass allowances of 64 to 894 kg. All insufficient for the scramjet role. Of the four potential configurations one exhibited a minimal excess of 1.8 kg; the remaining three ranged from 621 kg to 1065 kg.

Research Capabilities Results - The three configurations exhibiting the maximum payload capability used the LR-105 engines in conjunction with 12 LR-101 sustainer engines, are (1) the aluminum structure with the LI-900 RSI provides a payload allowance of 2290 kg; (2) the aluminum structure with the Ablator provides

1957 kg; and (3) the Lockalloy Heat-Sink Configuration provides 1846 kg of payload capability.

## RISK ASSESSMENT

Analysis results from technical development, cost estimates, and system maintenance costs were the basis for comparison of the relative program risks, for each of the candidate configurations, and was the means by which the most promising configuration was selected for evaluation in Phase II of the study. The analysis produced elements of risk that each configuration was weighed against, (1) flight program risks affecting all configurations the same, (2) propulsion and functional system risks affecting all configurations, and (3) risks peculiar to a given configuration.

Flight Program Risks - An important element for reducing risk during the flight operation is to schedule:

- Complete vehicle proof and shake testing to 80% of limit load.
- Functional system testing including controls simulation, propellant system, and canopy ejection.
- Select components for structural testing to failure.
- Computer simulation of critical performance areas.
- Installation of strain gages and thermocouples during fabrication in critical areas.
- Flight readiness reviews.
- TM monitoring of performance during flight.
- A cautious approach to Mach number and cruise duration to evaluate operation.

Propulsion and Functional System - Even though procurement and pricing of the propulsion rockets is a NASA option there are certain elements of risk that must be considered in selecting the most cost effective configuration in conjunction with the most technically viable as exposed by the study. They are:

- The LR-105 engine is not man rated for horizontal operations. A vendor development program will be required.
- The LR-105 engine purging from a horizontal orientation is a possible problem. If the engine vendor cannot readily solve the problem, aircraft complexity (cost) will rise extensively.
- The LR-105 engine may be in short supply due to other program requirements.
- The LR-99 and LR-11 engines are not in current production. Available supplies of engines and spare parts may not be adequate to support the life cycle of the X-24C program.

Functional systems present the following risk elements:

- Modification of existing functional system components for X-24C usage is not a major risk but one that must be timely introduced.
- The fixed hemispherical probe, located in the nose, must be developed for compatibility with the air data system and the thermal loads on the vehicle and probe location.

Flight Operations and Related Technical Risks - Flight operational and related technical risks include:

- Potential hazard or burn through to aluminum structure resulting from inflight loss/failure of Ablator or LI-900 RSI. This calls for extensive nondestructive test (NDT) for TPS airworthiness verification to be developed.

- Degradation of Ablator and LI-900 RSI from fuels, oils, and personnel. This calls for protective coatings, over the TPS, protective shields over areas exposed to maintenance activity and double sealing of fuel and hydraulic oil ports during maintenance periods.
- Degradation of Ablator and LI-900 RSI at hinge lines, between rubbing surfaces, and complexity factor between the scramjet package and air-vehicle interface gap. This calls for use of TPS of higher densities with resultant higher vehicle costs.
- Potential hazard resulting from damage to the aluminum structure beneath the TPS. Air-worthiness verification inspection must be developed that is both cost effective and falls within the minimum turn-around schedule.
- Potential breaking/cracking of LI-900 RSI tiles of thicknesses below 10 mm. Use of thicker tiles to overcome potential problem increases vehicle mass unnecessarily.
- Unnecessary mass impact associated with splicing together of small Lockalloy panels. Welding panels together will alleviate this risk.
- Potential health hazard associated with Lockalloy manufacture (machining). This calls for continuation of improving safety procedures and working with the material vendor to consider all aspects including backup procedures.
- Procurement of sufficient quantities and the relatively high cost of Lockalloy calls for continued moderate procurement and coordinated efforts with the material vendor to reduce the cost of production.
- Limited experience with Ablators and Lockalloy requires continuation of test programs like the Langley (NASA) aerothermal panel tests and the YF-12 ventral fin program.



Relative TPS Program Technical Risks - The assessment of the TPS technical aspects lead to a matrix by which each of the TPS configurations were ranked from the highest to lowest risk to the X-24C program. The highest turned out to be the LI-900 RSI followed by the Ablator and the lowest, the Lockalloy Heat-Sink. Figures 186, 187 and 188 show the risk elements used in the combined ranking shown in Figure 189.

## TRADE STUDY RESULTS

The Phase I analytical study of candidate X-24C configurations has been performed based on the systematic assessment of realistic detail designs and technical analysis. The study has produced results that have narrowed the design options and, together with cost analysis, provide the rationale for selection, (Table 94) of viable configurations recommended for refinement in Phase II of the study. Results of the Phase I study include:

- LR-105 with 12 Atlas Sustainers using JP Fuel and Lox is significantly better than the LR-99 for the X-24C on a performance basis.
- The Lockalloy airplane and the elastomeric Ablator covered aluminum airplane are approximately equal in acquisition cost and in mass.
- The LI-900 Shuttle type insulator covered aluminum airplane is more expensive and only a few kilograms lighter in mass than the Lockalloy or elastomeric Ablator airplane.
- The risks using Lockalloy are procurement oriented and are pretty well out of the way before flight.
- The risks in using elastomeric Ablator are both procurement oriented and with us throughout the life use cycle.
- Phase II and Phase III can be done satisfactorily without coming to a firm selection on the type of TPS, all forms result in approximately the same vehicle mass.

LI-900 - HIGHEST RISK

- HIGH INITIAL COST
- HIGHEST MANHOURS PER SQUARE METER REFURBISHMENT
- JEOPARDIZES THE TWO-WEEK TURNAROUND TIME SCHEDULE
- THIN (< 10 MM) TILE FOR X-24C ENVIRONMENT - CRACKS EASILY
- DIFFICULTY IN ASSESSING INTEGRITY OF BASIC STRUCTURE
- REQUIRES NON-BUCKLING SURFACE STRUCTURE
- THERMAL EXPANSION JOINTS ARE DIFFICULT TO MAKE SO AS TO PROTECT AGAINST TENDENCY TO OPEN GAPS AT EDGE OF THE INSULATION ALONG APPROXIMATELY 95 LINEAR METERS PER VEHICLE
- TPS AT HINGE LINES DIFFICULT TO MAINTAIN

Figure 186 - Risk Elements

ABLATIVE - MIDDLE RISK

- HIGH INITIAL COST - REQUIRES DIE BLOCKS OR MACHINING FOR FORMING TPS SHEETS PRIOR TO INSTALLATION
- HIGHEST PROBABLE PERCENTAGE OF REFURBISHMENT PER FLIGHT
- JEOPARDIZES TWO-WEEK TURNAROUND SCHEDULE - MAY REQUIRE DEDICATED WORK AREA
- DIFFICULTY IN ASSESSING INTEGRITY OF BASIC STRUCTURE
- THERMAL EXPANSION JOINTS ARE DIFFICULT TO MAKE SO AS TO PROTECT AGAINST TENDENCY TO GAP AT EDGE OF INSULATION ALONG APPROXIMATELY 95 LINEAR METER PER VEHICLE
- TPS AT HINGE LINES DIFFICULT TO MAINTAIN

Figure 187 - Risk Elements

LOCKALLOY - LOWEST RISK

- HIGHEST INITIAL MATERIAL COST
- MUST USE SAFETY PROCEDURES TO AVOID HEALTH HAZARD
- LARGE NUMBER OF JOINTS REQUIRED BECAUSE MILL SIZE PANELS ARE RELATIVELY SMALL
- LOWEST PROBABLE PERCENTAGE REFURBISHMENT AND MAINTENANCE COST
- INTEGRITY OF BASIC STRUCTURE EASILY ASSESSED VISUALLY
- THERMAL EXPANSION JOINTS - CAN USE LOCKALLOY SLIP JOINTS SEALED INTERNALLY
- LOCKALLOY AT HINGE LINES REQUIRES LITTLE MAINTENANCE
- HEAVIEST OF TPS CANDIDATES

Figure 188 - Risk Elements















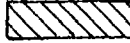







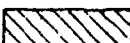




<u>SUMMARY</u>			
	<u>LI-900</u>	<u>ABLATIVE</u>	<u>LOCKALLOY</u>
INITIAL COST			
MANHOURS FOR REFURBISHMENT			
TWO-WEEK TURNAROUND CAPABILITY			
DEDICATED REFURBISHMENT AREA REQUIRED			
INSPECTION OF BASIC STRUCTURE			
EXPANSION JOINTS PROVISIONS			
PROTECTION AT HINGE LINES			
MASS			
			 — DIFFICULT, UNACCEPTABLE, OR COSTLY  — MARGINAL  — ACCEPTABLE OR NO PROBLEM

Figure 189 - Risk Elements Summary

## TRADE STUDY RECOMMENDATIONS

This study has identified promising configurations of the X-24C, which have the capability to perform the mission and research requirements specified for Phase I of the X-24C Study. The Phase II Study will include the viable configurations developed around the following recommendations:

- 1) Carry both Lockalloy and the elastomeric Ablator into Phase II for growth potential.
  - Either TPS system can be a viable approach for the X-24C and will be approximately equivalent in acquisition costs.
  - The life cycle maintenance costs, projected in Phase I, are based on some very broad assumptions which may or may not be conservative.
  
- 2) Consider the LR-105 with 12 Atlas sustainers, fueled with Kerosene and Lox, as the prime propulsion candidate for Phase II.
  - This engine will show the best vehicle growth potential because of its performance advantage.
  - This engine will allow sufficient mass growth so as to determine an optimum launch mass for Phase III.
  
- 3) Use the LR-99 with LR-11's fueled with  $\text{NH}_3$  and Lox as a back-up engine for Phase II.
  - This engine will show the effect of somewhat lesser propulsion performance in Phase II trades.
  - This engine can be considered somewhat interchangeable with the LR-105 and 2 LR-11's fueled with Alcohol and Lox.

## PREVIEW OF PHASE II AND III STUDIES

- 1) Phase II will evaluate the effect of varying the launch mass from 25.85 Mg to 31.75 Mg for the recommended configurations which will result in selection of:
  - A recommended launch mass to be used in Phase III.
  - A recommended configuration to be carried into Phase III.
  
- 2) Phase III will evolve a candidate vehicle configuration which takes into account simultaneously the results of Phase I and II studies, a comprehensive assessment of B-52 constraints, and all available hypersonic gechnology.

## REFERENCES

1. Miranda, L. & Elliot, R. "A Unified Non-Planar Vortex Lattice Method for Subsonic and Supersonic Flow," Lockheed-California Co. Report LR 26299, 8 Aug. 1974.
2. Gentry, A.E., "Hypersonic Arbitrary-Body Aerodynamic Computer Program," Douglas Aircraft Report DAC 61552, April 1968.
3. The NASTRAN User's Manual; National Aeronautics and Space Administration, Washington D.C., NASA SP-222, 1969.
4. Timoshenko, S.; and Wionowsky-Krieger, S.: Theory of Plates and Shells, McGraw-Hill Book Company, New York, 1959.
5. Wittrick, W.H.: Correlation Between Some Stability Problems for Orthotropic and Isotropic Plates under Bi-axial and Uni-axial Direct Stress. The Aeronautical Quarterly, Volume IV, August 1952.
6. Jackson, L.R. and Taylor, A.H.: A Structural Design for Hypersonic Research Aircraft, Paper No. 76-906, AIAA Aircraft Systems and Technology Conference, Dallas, Texas, Sept. 1976.
7. Aerospace Structural Metals Handbook, USAF AFML-TR-68-15, March 1976.
8. YF-12 Lockalloy Ventral Fin, Program Final Report NASA-CR-144971, Jan. 1976.
9. Edwards, C.L.W., "Forebody Design Techniques for Highly Integrated Bottom Mounting Scramjets with Application to a Hypersonic Research Airplane," NASA TM-X 71971, November 1974.

10. Brackeen, R.E. and Marcy, W.L., "X-24B Growth Version Feasibility Study," Technical Report AFFDL-TR-73-116, October 1973.
11. Beckwith, I., Similar Solutions for the Compressible Boundary Layer on a Yawed Cylinder with Transpiration Cooling, NASA TR-R-42, 1959.
12. Lees, L., Laminar Heat Transfer Over Blunt Nosed Bodies at Hypersonic Speeds, Jet Propulsion, April 1956.
13. Token, K.H., "Heat Transfer Due to Shock Wave Turbulent Boundary Layer Interactions on High Speed Weapon Systems," AFFDL-TR-74-77, April 1974.
14. Hiers, R.S., "Heat Transfer to Protuberances Partially Immersed in a Hypersonic, Turbulent Boundary Layer," AEDC-TDR-62-66, April 1962.
15. Watts, J.D., "Flight Experiences with Shock Impingement and Interference Heating on the X-15-2 Research Airplane", NASA TM X-1669, October 1968.
16. Royall, J.F., Jr., "Investigation of Heat Transfer on a Finned Body in the Region of Fin-Body Interference in Free Flight at Mach Numbers Up to 11", NASA TM X-737, November 1962.
17. Spægle, Katherine C., "Heat-Transfer Measurements of Two Wing-Body Combinations at  $8^\circ$  Angle of Attack from a Flight Test for Mach Numbers to 4.86 and Reynolds Numbers to  $19.2 \times 10^6$ ", NASA Memo 10-25-58L, December 1958.
18. Price, E.A., Howard, P.W., and Stallings, R.L., Jr., "Heat-Transfer Measurements on a Flat Plate and Attached Fins at Mach Numbers of 3.51 and 4.44", NASA TN D-2340, June 1964.

19. Burbank, P.G., Newlander, R.A., and Collins, I.K., "Heat-Transfer and Pressure Measurements on a Flat-Plate Surface and Heat-Transfer Measurements on Attached Protuberances in a Supersonic Turbulent Boundary Layer at Mach Numbers of 2.65, 3.51, and 4.44", NASA TN D-1372, December 1962.
20. Needham, D.D., Stollery, J.L., "Boundary Layer Separation in Hypersonic Flow," AIAA Paper No. 66-455, Jan. 1966.
21. Hamilton, H.W., Dearing, J.D., "Effect of Hinge-Line Bleed on Heat Transfer and Pressure Distributions Over a Wedge-Flap Combination at Mach 10.4," NASA TN D-4686, Aug. 1968.
22. Holden, M.S., "Shock Wave-Turbulent Boundary Layer Interaction in Hypersonic Flow," ARL 73-0137, Oct. 1973.
23. Popinski, Z., and Ehrlich, C.E., "Development of Design Methods for Predicting Hypersonic Aerodynamic Control Characteristics," Lockheed-Calif. Co., LR 19460, April 1966.
24. Kordes, E.; Tuovila, Weiner, J.F, and Guy, Lawrence D., "Flutter Research on Skin Panels," NASA TN D-451, September 1960.
25. Guy, Lawrence D., "The Effects of Aerodynamic on Panel Flutter," Symposium Proceedings, Structural Dynamics on High Speed Flight, Sponsored by Aircraft Industries Associated Office of Naval Research, Los Angeles, Calif., April 1961.
26. Shore, Charles P., "Flutter Design Charts for Bi-Axially Loaded Isotropic Panels," Journal of Aircraft, Vol. 7, No. 4, July-Aug. 1970, pp. 325-329.



27. Lemley, C., "Design Criteria for the Prediction and Prevention of Panel Flutter," AFFDL-TR-67-140; Volume I: Criteria Presentation, Volume II Background and Review of State of the Art, 1968.
28. Libove, C., and Batdorf, S.B., "A General Small Deflection Theory for Flat Sandwich Plates," NACA Report 899 (1948).
29. Hedgepeth, J.M., "Flutter of Rectangular Simply-Supported Panels at High Supersonic Speeds," J. Aerospace Sci. 24, pp. 563-573, 586 (1957).
30. Kordes, E. and Noll, Richard B., "Theoretical Flutter Analysis of Flat Rectangular Panels in Uniform Coplanar Flow with Arbitrary Direction," NASA TN D-1156, January 1962.
31. Stroud, W. Jefferson, "Elastic Constants for Bending and Twisting of Corrugation - Stiffened Panels," NASA TR R-166, December 1963.
32. Bohon, H.L. and Anderson, M.S., "Role of Boundary Conditions on Flutter of Orthotropic Panels," AIAA Journal, Vol. 4, No. 7, July 1966, pp 1241-1248.
33. Shore, Charles P., "Effects of Structural Damping on Flutter of Stressed Panels," NASA TN D-4990, January 1969.
34. Bohon, H.L., Anderson, M.S.; and Heard, W.L., Jr.,; "Flutter Design of Stiffened-Skin Panels for Hypersonic Aircraft," NASA TN D-5555, Dec. 1969.
35. MacNeal, R.H., "The Solution of Elastic Plate Problems by Electrical Analogies," Journal of Applied Mechanics, March 1951, pp. 59-67.
36. Summary Refurbishment Cost Study of Thermal Protection System of a Space Shuttle Vehicle, NASA CR-111833, March 1971.

37. Study of Critical Defects in Ablative Heat Shield Systems for the Space Shuttle, NASA CR-2336, dated Feb. 1974.
38. Love, James E. and Young, William R., "Survey of Operation and Cost Experience of the X-15 Airplane as a Reusable Space Vehicle," NASA TN-D-3732.
39. Capasso, Vicent No., Jr., Space Shuttle Related Maintenance Experience with the X-15 Aircraft, NASA FRC, Edwards, Calif., date unknown.
40. Cary, John P., Experience with a Charring Ablator Heat Shield on the X-15-2 Airplane to Mach 6.7, NASA TM-X-1745, September 1968.
41. Armstrong, Johnny G., Flight Planning and Conduct of the X-15A-2 Envelope Expansion Program, FTC-TD-69-4, July 1969.
42. Williams, E.T. and Coakley, R.C., Costing Methodology for High Speed Research Airplanes Including Parametric Cost Trend Evaluations, NASA CR-132658, January 1975.
43. Seiferth, Rolf W., "Ablative Heat Shield Design for Space Shuttle," Final Report, NASA CR-132282, Aug. 1973.
44. Thompson, J.T. and Price, A.B., "Application and Refurbishment Procedures X-15A-2 Thermal Protection System," NASA - CR-96000, January 1968.
45. Haas, D.W., "Final Report Refurbishment Cost Study of the Thermal Protection System of a Space Shuttle Vehicle," NASA CR-111832, 1 March 1971.
46. Plank, Paul P.; Marcy, William L, Hacfeld, Rudolph, C., "Experiments Impact on X-24C," AFFDL Report AFFDL-TR-75-37.

47. King, W.E., "A Study of Ablator Producibility and Refurbishment Methods," Martin-Marietta Aerospace Corp. Paper No. 44, Seventh Conference on Space Simulation Symposium, Los Angeles, Calif., November 1972.
48. Kirkham, F.S.; Jones, R.A.; Buck, M.L.; Zima, W.P., "Joint USAF/NASA Hypersonic Research Aircraft Study," AIAA Paper, AIAA Aircraft Systems and Technology Meeting, Los Angeles, Calif., August 1975.
49. "Repair of Damaged Insulation Tiles," NASA Tech. Brief, Lyndon B. Johnson Space Center, B75-10321, Dec. 1975.
50. Sechler, E.E. and Dunne, L.G., "Airplane Structural Analysis and Design," John Wiley and Sons In., New York, 1942.
51. Hubka, R.E., "Structural Optimization of Six Different Types of Rectangular Plates Subjected to Combined Shear and Bi-Axial Compressive Loading," Lockheed-California Company Report, LR 21662, Sept. k968.
52. Gerard, George, Handbook of Structural Stability, Part V - Compressive Strength of Flat Stiffened Panels, NACA TN 3785, Aug. 1957.

APPENDIX A  
CONFIGURATION DEVELOPMENT STUDY  
OF THE  
X-24C HYPERSONIC RESEARCH AIRPLANE

STATEMENT OF WORK

1.0 INTRODUCTION

The purpose of this contract effort is to accomplish an in-depth study and refinement of the X-24C aerodynamic configuration, taking into consideration the impact of various structural design, systems, and propulsion options. The study is expected to narrow the range of design options, tighten the specifications on vehicle configuration and performance, and provide program cost estimates with a much higher degree of accuracy than those currently available.

2.0 OBJECTIVES

The study is intended to accomplish the following tasks:

2.1 Cost and weight trade studies of several structure/propulsion design combinations, as indicated in Table I, and major subsystem trades (Phase I).

2.2 Determination of performance growth potential of promising design concepts and the costs associated with increased performance (Phase II).

2.3 Refinement of the X-24C aerodynamic configuration and conceptual design of the vehicle which evolves from the design trades and growth potential evaluation (Phase III).

2.4 Design and fabrication of a 1/30-scale precision wind tunnel model of the contractor's conceptual design of the X-24C for government testing at the NASA Langley Research Center (LRC) (Phase III).

### 3.0 PHASE I - DESIGN TRADES

The contractor shall determine initial vehicle costs, vehicle weight breakdowns, certain operational manpower requirements, and relative program risks of all X-24C structure/propulsion combinations indicated in Table I.

3.1 Aerodynamic Configuration. - For the basis of the design trades, the aerodynamic configuration shall be assumed to be the concept shown in attachment I. The aerodynamic characteristics of this configuration shall be assumed to be satisfactory for the purposes of the Phase I design trades. The government will supply untrimmed lift, drag, and aerodynamic center characteristics as a function of Mach number and angle of attack for this configuration concept.

3.2 Performance. - For the design trades, the performance for the vehicle shall be held constant at the following conditions:

40 seconds cruise at Mach 6.0 on rocket power  
with a 3-module scramjet package installed.

Test capability at 1000 lb/sq ft dynamic pressure  
throughout the Mach range.

A payload bay shall be reserved in the fuselage for research experiments including scramjet hydrogen tanks. Two payload bay options shall be considered: (a) all rocket propellants to meet the above performance requirements must be carried in the primary propellant tanks and (b) a portion of the rocket propellant may be carried in the payload section.

3.3 Firm Research Requirements.- Research requirements dictate the following vehicle features to be maintained through all three phases of this contract:

3.3.1 The vehicle shall have a full-depth, replaceable, 10-foot long research payload bay provided by a section of the body structure between the cockpit and rocket propellant tanks.

3.3.2 The volume within the payload bay shall be used for research payloads, research structures, integral and nonintegral experimental hydrogen tanks, research instrumentation and equipment, and fuel for research propulsion systems such as the scramjet.

3.3.3 The payload bay structure may be of conventional construction compatible with the rest of the vehicle and have transition sections at both ends to allow a load path offset for the requirements of 3.3.4. Field splices will be provided at each end of the bay to allow replacement of the bay structure with advanced research structure.

3.3.4 The payload bay shall have a heat shield type stand-off thermal protection system (TPS) with the same TPS concept as the vehicle itself and a mold line recessed four inches on the upper and side surfaces and six inches on the lower surface. This arrangement will allow partial or complete replacement of the payload bay stand-off TPS with advanced research TPS concepts.

3.3.5 The vehicle shall have removable and replaceable wings, strakes, and stabilizers to allow testing of advanced aerodynamic surface structures. Slip joints or other appropriate interface structure shall be provided at the fuselage junction to enable testing of hot structures.

3.3.6 The vehicle shall have a lower surface designed to allow efficient aerodynamic integration of LRC scramjet modules of sufficient size to cruise the aircraft at Mach 6. The integrated design concept utilizes the forebody of the vehicle as an inlet precompression surface and the afterbody as an external nozzle expansion surface. Additional information on the scramjet is contained in Attachment II.

3.4 Vehicle Operations. - It shall be assumed that the X-24C aircraft will be operated in the following manner during the flight research program:

3.4.1 B-52 Air-Launch - The vehicle will be air-launched from B-52B S/N 008 at 45,000 feet altitude and a Mach number of 0.85. For the present, the assumption shall be made that weight, c.g., and clearance constraints are the same as with the X-15A-2 vehicle.

3.4.2 Test Range - The NASA High Range test corridor in the Utah-Nevada-California area will be utilized for X-24C in the same manner as with the X-15. Existing radar, telemetry, and communications stations at Edwards AFB and Ely, Nevada, shall be considered satisfactory for the X-24C program.

3.4.3 Flight Frequency - For planning purposes and operational cost estimating, an average of 12 flights per year shall be assumed for the X-24C per vehicle unless refurbishment or other characteristics of a particular design concept make this an unrealistic assumption. This number is based on past experience with rocket-powered research aircraft at the Flight Research Center. The flight research program shall be assumed to consist of 100 flights per vehicle.

3.4.4 Energy Management - For the purposes of energy management in the flight operations of X-24C, a speed brake system will be required.

3.5 Costing Assumptions.- The following assumptions shall be made regarding the cost determinations to be made in Phases I, II, and III.

3.5.1 The entire X-24C program philosophy is based on the need by both NASA and USAF to keep program costs to a minimum commensurate with accomplishing the research objectives.

3.5.2 The management approach used by the government in this program shall be in the form of prototype management wherein the contractor who builds the vehicle is given considerable freedom to accomplish his task with minimal government control.



3.5.3 The contractor shall be assumed to operate in a "classical" experimental shop mode wherein the engineering, design, and fabrication team is separated from normal corporate operations and located in an atmosphere which is conducive to close communication and minimum red tape and paperwork.

3.5.4 All cost estimates and breakdowns (actuals) shall be provided in terms of January 1975 and January 1976 dollars. The purpose of this requirement is to provide a basis for comparison with past cost estimates.

3.5.5 Maximum usage of government-furnished equipment and off-the-shelf hardware is to be made in this program in the interest of minimizing cost. In the contractor's vehicle cost estimates, he will include the cost of all government-furnished equipment and identify the source and availability. The only exception to this requirement is the rocket engine or engines. The rocket engines will be procured and the costs estimated separately by the government. However, the contractor shall include in his design effort and cost estimates all other components of the primary propulsion system including installation of the rocket engines.

3.6 Initial Structural Design Criteria.- The contractor shall use the Preliminary Design Criteria for X-24C structure contained in Attachment III. However, these criteria are to be considered only as a starting point and the contractor should recommend changes in the criteria as appropriate as the study progresses. The design concepts shall provide for the structural and system interfaces of the airframe/SCRAMJET, airframe/removable surfaces, and airframe/payload bay.

3.7 TPS Annual Maintenance Manpower.- The contractor shall thoroughly study the problem of field maintenance of all TPS system concepts. Pre-flight inspection, quality assurance, post-flight assessment of TPS damage or wear and corrective action, total or partial refurbishment, and recertification for flight shall be included among items considered when estimating TPS maintenance manpower requirements. Where real experience is missing, the contractor shall use his initiative in utilizing the experience of other TPS programs and in devising experimental means of determining these manpower requirements.

3.8 Assessment of Relative Program Risks.- The contractor shall devise a means of comparing the relative program technical risks of the various concepts and rank them from lowest to highest risk. A full explanation of the contractor's reasoning used in the evaluation shall be given.

3.9 Validation of Design Trade Results.- The contractor shall validate all detailed aerodynamic, structural, weight, heating, and cost trade results with in-depth analyses and test data in the appropriate reports.

3.10 Selection of Promising Design Concepts.- From the trade study results of Phase I, the contractor shall select (jointly with the technical monitor) the most promising design concept or concepts for further study of growth potential in Phase II.

#### 4.0 PHASE II - DESIGN CONCEPT REFINEMENT FOR GROWTH POTENTIAL

The primary objective of Phase II is to determine the performance growth potential of the promising design concepts resulting from Phase I. Performance desires are aimed at not only assessing the impact of using the rocket cruise fuel to boost to higher Mach numbers but also to

determine the feasibility and cost of obtaining higher boost Mach numbers and correspondingly longer cruise times at intermediate Mach numbers. Efforts to increase performance must be constrained by limits on fuel volume, TPS limits, and vehicle costs.

4.1 Configuration. - For purposes of the growth potential evaluation the vehicle configuration concepts shall be considered (1) clean without a SCRAMJET test package, and (2) with cruise SCRAMJETS.

4.2 Launch Weights. - Launch weight limits of 57,000 lbs. (present B-52 limit) and 70,000 lbs. shall be assumed for this growth potential evaluation. The 70,000 lb. weight is a theoretical weight that may be attainable through modifications to the B-52 launch aircraft, which is being assessed separately.

4.3 Phase II Results. - The contractor shall determine the maximum boost Mach number, the vehicle dry weight, initial vehicle cost, and an assessment of TPS annual maintenance manpower and relative program risks of each concept studied in Phase II. The contractor shall then, jointly with the technical monitor, select a concept for Phase III.

#### 5.0 PHASE III - VEHICLE CONCEPT REFINEMENT

With the design concept selected in Phase II and all available X-24C wind tunnel data, the contractor shall perform a conceptual aerodynamic, structural, and vehicle refinement of the X-24C.

5.1 The contractor shall utilize the firm research requirements listed in Section 3.3 in addition to the following general vehicle design criteria in performing the design task:

5.1.1 SCRAMJET Cruise - The contractor shall design the vehicle in such a manner as to couple the SCRAMJET with the airframe and formulate the design (insofar as this is consistent with the other requirements) to cruise the vehicle on SCRAMJET power alone at a Mach number to be selected by the technical representative at the end of Phase II.

5.1.2 Stability - The vehicle shall be statically stable without stability augmentation. However, an appropriate stability augmentation system for the integrated design shall be included in the total system.

5.1.3 Subsonic L/D Goal - The subsonic lift-to-drag ratio of the vehicle in the dirty configuration (landing gear down, nonthrusting cruise SCRAMJET installed) in the final approach attitude shall not be lower than 3.5. It is desired to have this landing L/D higher if possible.

5.1.4 Launch Weight - The contractor shall be supplied with the allowable launch weight at the beginning of Phase III.

5.1.5 Phase III Cost Constraints - At the beginning of Phase III, the contractor shall be supplied with a total initial cost figure. With this cost figure, the contractor shall apply the "design to cost" approach to the Phase III conceptual design.

5.2. Wind Tunnel Model Design and Fabrication.- The contractor shall design and fabricate a 1/30-scale precision wind tunnel model of the contractor's final configuration for government wind tunnel testing at the NASA Langley Research Center. The model design shall be in accordance with model specifications contained in Attachment IV.

5.2.1 Pre-fabrication Plan Submittal - When the drawings and stress analysis are complete for the mode, they shall be submitted to the Contracting Officer for review and approval before fabrication is started.

## 6.0 REPORTING

6.1 Monthly Progress Reports. - The contractor shall submit an informal monthly progress report in letter form which summarizes the accomplishments of the preceding month, indicates any major conclusions reached, and outlines the planned work for the following month. In addition, the contractor shall include in each monthly report at least two viewgraphs which summarize the month's progress and significant results.

6.2 Oral Presentations at NASA-LRC. - The contractor shall provide the following oral presentations at the Langley Research Center during the course of the contract. These presentations shall be open to personnel from other agencies.

6.2.1 At the end of Phase I the contractor shall report the results of the trade studies in Phase I. In addition, the contractor and the Technical Representative of the Contracting Officer shall jointly select the design concepts with which the contractor shall accomplish Phase II.

6.2.2 At the end of Phase II the contractor shall report the results of the growth potential evaluation made in Phase II. In addition, the contractor and the Technical Representative of the Contracting Officer shall jointly select the single design concept with which the contractor shall accomplish Phase III.

6.2.3 At the end of Phase III the contractor shall make the final oral presentation, giving the results of the configuration refinement and conceptual design effort of Phase III.

6.2.4 The contractor shall repeat the final oral presentation for the Air Force Flight Dynamics Laboratory and other interested Air Force personnel at Wright-Patterson AFB, Ohio, following the Langley presentation.

6.3 Written Reports.- The final written reports required in this contract will be published as a high-number NASA Contractor Report in three volumes and consist of the following:

6.3.1 Volume I, Design Trade Results - The first volume of the report will contain the results of Phase I of the contract. This first volume shall be submitted in draft form 30 days following the completion of Phase I.

6.3.2 Volume II, Conceptual Design Report - Volume II of the written report will include all results of Phases II and III. This volume shall be submitted in draft form 30 days following the completion of Phase III.

6.3.3 Volume III, Executive Summary - Volume III of the written report will be an executive summary of all major results, conclusions, and contractor recommendations. This volume shall be submitted in draft form concurrently with Volume II.

NUMBER OF VEHICLES	STRUCTURE / TPS OPTIONS		ALUMINUM STRUCTURE ELASTOMERIC ABLATOR TPS			ALUMINUM STRUCTURE LI-1500 RSI TPS			LOCKALLOY / BERYLLIUM HEAT-SINK STRUCTURE		
	ROCKET PROPULSION OPTIONS		AIRFRAME WEIGHT	INITIAL AIRFRAME COST (\$)	ANNUAL TPS MAINT. MAN-HOURS	AIRFRAME WEIGHT	INITIAL AIRFRAME COST (\$)	ANNUAL TPS MAINT. MAN-HOURS	AIRFRAME WEIGHT	INITIAL AIRFRAME COST (\$)	ANNUAL TPS MAINT. MAN-HOURS
1	YLR-99 *										
	THROTTLED LR-105										
	LR-105 (NO THROTTLE) ATLAS VERNIER (CRUISE)										
2	XLR-99 *										
	THROTTLED LR-105										
	LR-105 (NO THROTTLE) ATLAS VERNIER (CRUISE)										

NOTE: CONTRACTOR SHALL DETERMINE THE NUMBER OF ROCKET ENGINES AND SPARE PARTS REQUIRED FOR THE TOTAL FLIGHT PROGRAM IN ALL CASES.

ASSUMPTIONS:

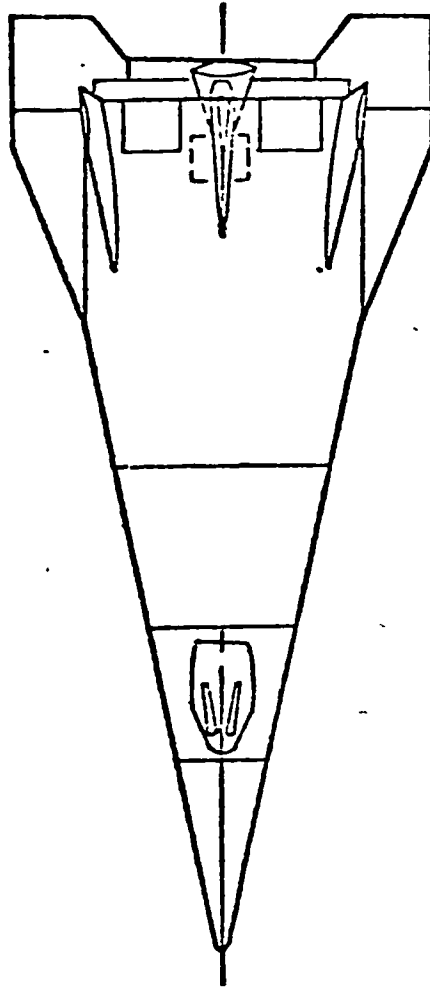
1. 100 TOTAL FLIGHTS PER VEHICLE AVERAGING 12 PER YEAR.
2. B-52B S/N 008 LAUNCH CONSTRAINTS SAME AS WITH X-15A-2 (57,000 LB LOAD LIMIT)
3. OPERATING PERFORMANCE SHALL BE MACH 6.0 WITH 40 SECONDS OF ROCKET CRUISE AT 1000 PSF DYNAMIC PRESSURE. (INCLUDING DRAG AND WEIGHT OF A 3-MODULE SCRAMJET TEST PACKAGE)

\* With Nozzle Extension

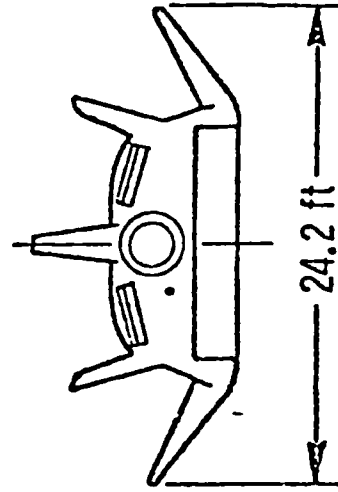
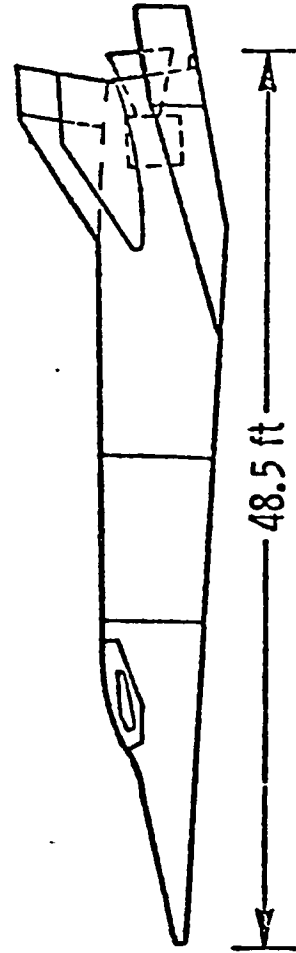
TABLE I

X-24C PROPULSION / STRUCTURE DESIGN TRADES

USAF-NASA X-24C CONCEPT  
GENERAL ARRANGEMENT



- WING-BODY CONFIGURATION
- B-52 LAUNCHED
- MAX. USE OF GFE PROPULSION GEAR SUBSYSTEMS





## SCRAMJET PERFORMANCE

The airframe-integrated scramjet currently under development at Langley Research Center is described in Enclosure 2. The sidewalls of the inlet combustor, and fuel struts are formed by swept compression and expansion planes aligned at 48 degree sweep angle. The current scramjet geometry is shown in Enclosure 1. The nozzle starts at the swept combustor exit plane and would utilize the vehicle aft lower surface as an external expansion surface.

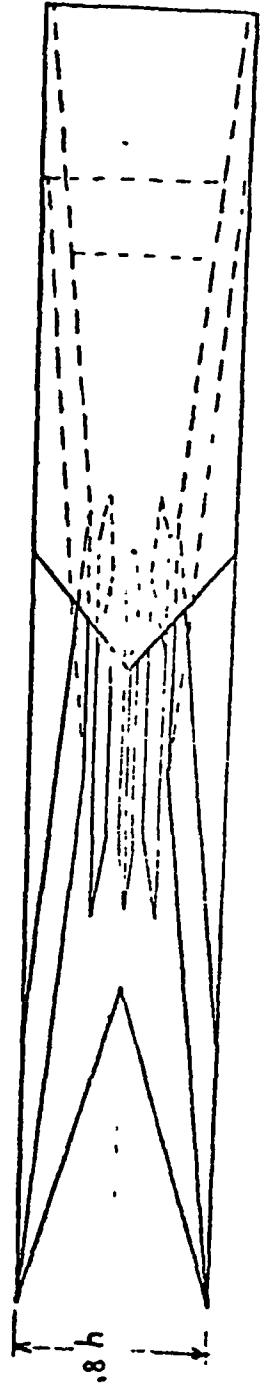
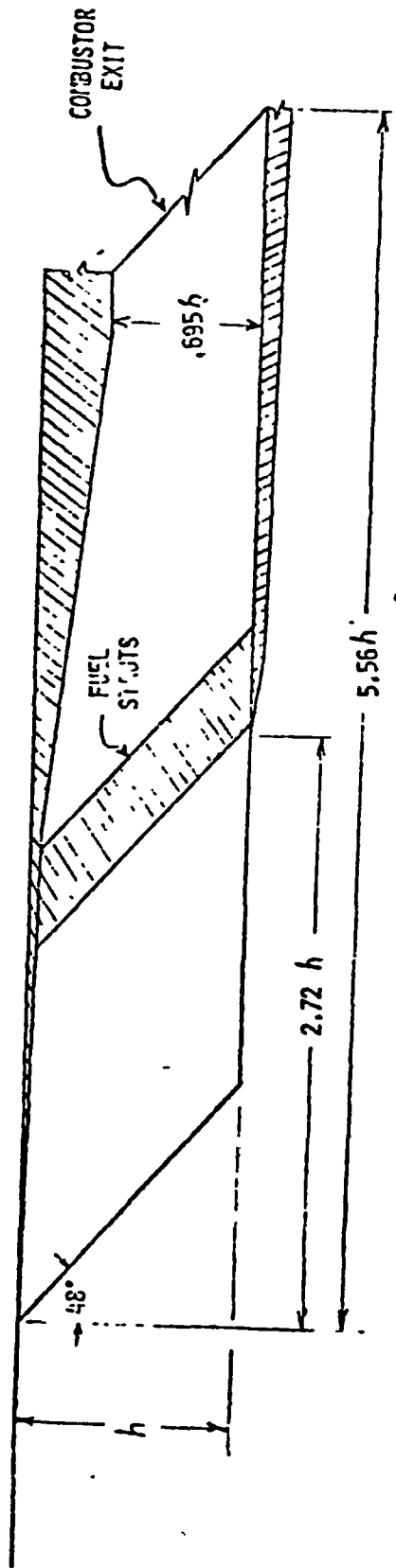
Current estimates of scramjet inlet and combustor performance will be available to the contractor over a range of hypersonic Mach numbers, fuel-to-air-ratio, flight dynamic pressure, and vehicle angle of attack. This data will include flow properties ahead of and within the engine as illustrated in Table 1 of Enclosure 3. Stream thrust and net thrust from the engine can be determined from these data. These data along with estimates of external cowl and spillage forces can form the basis of an integration analysis as illustrated in Enclosure 3.

A definition of scramjet weight and a structural concept for the scramjet is given in Enclosure 4. Any information on changes in the scramjet weight or structural integration requirements will be available to the contractor.

### Enclosures:

- (1) Figure defining scramjet geometry.
- (2) Henry, J. R. and Anderson, G. Y.: Design Considerations for the Airframe-Integrated Scramjet. NASA TM X-2895, December 1973.
- (3) Small, W. J., Weidner, J. P. and Johnston, P. J.: Scramjet Nozzle Design and Analysis as Applied to a Highly Integrated Hypersonic Research Airplane. NASA TM X-71972, November 1974.
- (4) Weiting, A. R. and Guy, Robert W.: Preliminary Thermal-Structural Design and Analysis of an Airframe-Integrated Hydrogen-Cooled Scramjet. Presented at the AIAA 13th Aerospace Sciences Meeting, Pasadena, California, January 20-22, 1975.

INLET & COMBUSTOR SECTION OF SCRAMJET MODULE



## Attachment III

## PRELIMINARY STRUCTURAL CRITERIA

The structure and thermal protection system shall be designed and tested to demonstrate a safe-life of at least four times the specified service life.

Limit load factors are tabulated as follows:

<u>Case</u>	<u>Condition</u>	<u>N<sub>z</sub></u>	<u>N<sub>x</sub></u>	<u>N<sub>y</sub></u>
1	B-52 Taxi at 60K	2.0	<u>+2.5</u>	0
2	B-52 Taxi at 60K	1.0	0	<u>+3</u>
3	B-52 Maneuver & Gust (M=.6, q=240)	+1.5 -1.0	0	<u>+3</u>
4	B-52 Maneuver & Gust (M=.6, q=240)	1.8	<u>+2.5</u>	0
5	B-52 Launch & Nose over Near Max Mach	-1.0	+3.0 -0.5	<u>+5</u>
6	Pull-up after B-52 Launch	2.5	+1.5 -.5	<u>+5</u>
7	Pull-up or Turn at Max Mach	3.0	<u>+5</u>	<u>+5</u>
8	Drag Brakes & No Thrust at Max Mach	0	-2.0	0
9	Subsonic Flight	+2.5 -1.0	<u>+5</u>	<u>+5</u>
10	Landing (10 ft/sec Sink Rate)	2.0	-1.0	<u>+5</u>
11	Crash - Crew Compartment	<u>+13.4</u>	-26.7	<u>+4.67</u>
12	Crash - Equipment Supports	+3.0 -1.3	+1.0 -6.0	+1.0

A limit load pressure difference of +1.0 psi shall apply to vented cavities.

Factors of safety are tabulated as follows:

<u>Component</u>	<u>Factor of Safety</u>		
	<u>Yield</u>	<u>Ultimate</u>	<u>Proof</u>
Unpressurized Structure	1.0	1.5	-
Crew Compartment	-	3.0	2.0
Propellant Tanks	1.1	1.4	1.05
Other Pressure Vessels	-	2.0	1.5
Pressurized Lines & Fittings	-	2.5	1.5

Vehicle flutter shall have a factor of 1.32 applied to the maximum dynamic pressure at all Mach numbers encountered.

Panel flutter shall have a factor of 1.5 applied to the maximum local dynamic pressure at all Mach numbers encountered.

The vehicle shall be designed to prevent coupling between the propellants (slosh) and structure and between propellants - propulsion system and structure (pogo) for all mission conditions.

B-52 and ascent rocket engine noise shall be 158 dB random frequency. Boundary layer noise in areas of laminar and turbulent flow are subject to root-mean-square sound pressure levels equal to 0.70 percent of free-stream dynamic pressure ( $.007q$ ). Areas subject to transition flow are subject to a sound pressure level of  $0.022q$ .

Thermal stresses shall be combined with stresses due to ultimate airloads when the stresses are of the same sign. Thermal stresses shall be ignored when the stresses are of opposite sign. No factor of safety shall be applied to thermal stress; however, the worst combination of air load induced stress (ultimate) and thermal stress shall be determined considering

all trajectories including limit trajectory variations indicated in the load factor table.

A maximum permanent deformation of 0.2 percent due to creep shall be accumulated during the service life of the vehicle.

A total permanent set of 0.2 percent shall be permitted at limit airload and limit thermal stress.

For compression members the ultimate allowable stress shall be the critical buckling stress (based on appropriate plasticity reduction factors) of the members supporting primary loads.

Uncertainty factors on heat transfer rates are 1.10 for laminar heating, 1.25 for turbulent heating and 1.50 for interference and separated flow heating. However, maximum temperature gradients shall be based on a factor of 1.0 for determining the lower temperature on the colder side of a structure, such as a wing.

The maximum mismatch and gaps between separate surface panels shall be 0.050 inch. Only aft facing steps shall be acceptable; forward facing deflections tapered to less than 3° deflection may be used to eliminate forward facing steps. Protrusions due to fasteners, etc., shall not exceed 0.005 inch.

The structure and thermal protection system shall sustain rain, dust, sand from dry lake landings, humidity, and freezing environments as specified in NASA SP-8057.

Boundary layer air leakage into the vehicle is prohibited except that flow required to equalize pressure in the vented cavities on return glide.

APPENDIX B

NASTRAN Output-Unit Surface Loading and Shear Flow

FUSELAGE F S 227 UNIT LOADS AND SHEAR FLOWS (ULT.)											
ROD ELEMENT	SHEAR PANEL	2g TAXI + Rx		2g TAXI - Rx		2 W LNDG		M - 6 CRUISE		2.5 g PULLUP AFTER LAUNCH	
		Nx	q	Nx	g	Nx	g	Nx	q	Nx	g
2001		-59		-48		-24		-33		12	
	2021		6		3		2		4		2
2002		-55		-47		-23		-33		12	
	2022		9		18		6		17		8
2003		-62		-48		-25		-30		9	
	2023		25		29		11		31		12
2004		-64		-49		-25		-24		5	
	2024		84		86		38		65		4
2007		-16		-5		-8		-6		-5	
	2027		140		138		70		82		7
2008		65		63		27		31		-8	
2010		223		224		117		127		-10	
FUSELAGE F S 277 UNIT LOADS AND SHEAR FLOWS (ULT.)											
2501		-39		-33		-17		-18		6	
	2521				2		1		5		2
2502		-52		-40		-22		-27		9	
	2522				7		2		11		6
2503		-103		-87		-48		-63		10	
	2523				50		27		18		6
2504		-156		-130		-69		-90		6	
	2524				191		102		130		4
2507		-44		-31		-22		-28		-2	
	2527				203		110		164		18
2508		109		112		55		67		-8	
	2528				205		104		150		12
2509		264		265		137		180		-18	
2510		247		242		118		163		2	

FUSELAGE F S 336 UNIT LOADS AND SHEAR FLOWS (ULT )											
ROD ELEMENT	SHEAR PANEL	2g TAXI +nx		2g TAXI Nx		2 W LNDG.		M - 6 CRUISE		2.5g PULLUP AFTER LAUNCH	
		Nx	g	Nx	g	Nx	q	Nx	q	Nx	q
3101		-86		-90		-13		37		-12	
	3121		44		48		3		28		8
3102		-68		-78		-33		3		8	
	3122		120		144		44		16		1
3103		-142		-145		-111		-100		45	
	3123		159		198		104		10		39
3104		-218		-197		-168		-231		59	
	3124		45		59		166		95		138
3107		17		29		-1		-27		4	
	3127		13		100		208		180		149
3108		73		111		110		101		-61	
	3128		90		62		36		32		52
3109		331		336		191		256		-40	
	3129		74		34		46		15		66
3110		447		478		307		388		-93	
FUSELAGE F S. 396 UNIT LOADS AND SHEAR FLOWS (ULT )											
3601		-40		-73		-44		-7		24	
	3621		68		47		25		58		36
3602		-50		-60		-8		13		-11	
	3622		161		141		49		28		2
3603		-77		-114		-121		-101		75	
	3623		262		201		58		35		22
3604		-61		-111		-283		-244		223	
	3624		379		201		218		58		345
3607		-1		25		-8		-26		1	
	3627		393		177		195		22		325
3608		68		163		186		154		-138	
	3628		296		112		220		23		278
3609		74		257		408		334		-293	
	3629		51		113		118		122		78
3610		120		125		141		155		-57	

FUSELAGE F S 462 UNIT LOADS AND SHEAR FLOWS (ULT )															
ROD ELEMENT	SHEAR PANEL	2		3		21		11				31			
		2 g TAXI	+nx	2 g TAXI	-nx	2 g TAXI	-nx	M = 6 CRUISE				2.5 g PULLUP AFTER LAUNCH			
		Nx	q	+nx	q	Nx	q	Nx	T*	Nx tot	q	Nx	T**	Nx tot	q
4201	4221	297	240	263	218	-84	47	-105	-79	-184	63	204	-229	-25	150
4202	4222	78	373	48	306	-81	167	-51	-79	-130	131	110	-229	-119	324
4302	4273	-1	412	-52	300	-165	285	-74	-79	-153	137	152	-229	-77	451
4204	4224	-235	127	-312	288	-255	311	-62	-79	-141	102	170	-229	-59	336
4207	4227	-53	250	40	389	43	78	17			227	-30	-229	-259	161
4208	4228	66	125	225	224	255	9	124			178	-206	-229	-435	150
4209	4229	12	32	249	95	323	43	124			33	-331	-229	-560	97
4210		23		224		246		69				-285	-229	-514	
*CRUISE THRUST	** MAX THRUST														

FUSELAGE  
F S 525 5 UNIT LOADS AND SHEAR FLOWS (ULT)

BOTTOM €	5001		343		316		-102		-124	-89	-213		283	-255	
		5021		221		240		38			58				98
5002			23		-62		-134		-34		-123		129		
		5022		594		630		71			183				278
5003			-38		-93		-168		-50		-139		176		
		5023		702		748		199			236				371
5004			-737		-854		-316		113				-8		-263
5005			10		-45		-295		-135		-224		467		
5006			-35		-75		-235		-101		-190		332		
		5024		737		859		116			116				3
5007			-76		-47		140		27		-62		-83		-338
		5027		623		769		75			12				38
5008			228		377		304		59		-30		-280		-535
		5028		376		623		7			75				153
5009			156		609		275		38		-51		-292		-547
		5029		199		93		15			18				80
TOP €	5010		246		467				39	-89	-50		-315	-255	-570



FUSELAGE F S 571 UNIT LOADS AND SHEAR FLOWS (ULT )															
ROD ELEMENT	SHEAR PANEL	2 g TAXI +nx		2 g TAXI -nx		2 W LNDG		M - 6 CRUISE				2.5 g PULLUP AFTER LAUNCH			
		Nx	q	Nx	q	Nx	q	Nx	T*	Nx tot.	q	Nx	T**	Nx tot.	q
BOTTOM	5501	341		327		14		-134	-91	-225		283	-262		
	5521		295		290		141				79				155
	5502	-276		-62		-134		59		-32		6		-256	
	5522		131		123		179				27				1
	5503	-18		-61		-87		52		-143		176			
	5523		410		416		311				39				99
	5504	-178		-854		-316		-49		-140		189			
	5524		1083		1121		928				180				161
	5505	-445		-510		-244		64		-27		467			
	5525		847		888		565				1				75
	5506	-103		-75		-235		-42		-133		99		-153	
	5526		594		602		497				135				345
	5507	9		38		121		5		-86		-83		-345	
	5527		902		886		306				207				326
	5508	280		377		303		15		-76		-243		-505	
	5528		816		622		121				158				20
	5509	476		231		239		24		-67		-292		-554	
	5529		102		243		36				37				1
TOP	5510	347		467		274		31	-91	-60		-222	-262	-484	
	*CRUISE THRUST														
	**MAX. THRUST														

FUSELAGE  
F S. 607 UNIT LOADS AND SHEAR FLOWS (ULT )

5901		392		391		94		-115	-93	-208		322	-267		
	5921		251		266		32				123				205
5902		-162		-183		-38		48				21		-246	
	5922		334		334		201				32				10
5902		62		37		-17		-46		-139		194			
	5923		299		306		285				65				145
5904		-41		-73		-54		-46		-139		172			
	5924		122		134		223				180				152
5905		-287		-315		-237		80				-75		-342	
	5925		361		374		301				111				127
5906		-177		-191		-156		6				-63		-330	
	5926		532		547		434				65				314
5907		71		96		72		20				-82		-349	
	5927		538		508		351				62				357
5908		188		199		161		-2		-95		-113		-380	
	5928		307		219		180				47				220
5909		159		75		162		-25		-118		-188		-455	
	5929		95		113		51				15				60
5910		193		169		156		-3	-93	-96		-172	-267	-439	
	*CRUISE THRUST														
	**MAX THRUST														

FUSELAGE  
F S 662.5 UNIT LOADS AND SHEAR FLOWS (ULT )

ROD ELEMENT	SHEAR PANEL	2 g TAXI + nx		2 g TAXI - nx		2 W LNDG.		M - 6 CRUISE		2.5 g PULLUP AFTER LAUNCH	
		Nx	q	Nx	q	Nx	q	Nx	q	Nx	q
6501		114		100		53		-10		81	
	6521		55		70		24		18		45
6502		54		54		34		-11		58	
	6522		115		134		76		24		115
6503		10		2		7		-4		63	
	6523		158		164		124		8		230
6512		30		9		73		96		156	
	6522		453		453		349		97		888
6504		-65		-80		-48		41		214	
	6524		26		30		10		44		360
6505		-68		-68		-96		-4		-108	
	6525		109		111		137		108		77
6506		-69		-71		-69		-13		-114	
	6526		286		291		310		14		347
6507		21		28		21		5		-67	
	6527		219		202		247		59		263
6508		28		23		37		-14		-41	
	6528		135		96		139		32		155
6509		53		39		50		-2		-20	
	6529		42		33		47		7		54
6510		55		44		60		-7		-56	

APPENDIX C

X-24C Phase I Cost Trade Studies - Escalation Factors

The primary cost data in this study are shown in January 1976 dollars. In order to provide a basis for comparison to past cost estimates, the summary vehicle costs for each configuration are presented in this Appendix in January 1975 dollars. In addition, the average economic escalation which takes into account both Lockheed experience and the U.S. Consumer Price Index, is estimated at:

January 1973	73%
January 1974	80%
January 1975	92%
January 1976	100% (Base)

The estimated program costs for each of the nine configurations in January 1975 dollars is summarized in Table 1.

APPENDIX C, TABLE 1  
X-24C VEHICLE COST SUMMARY  
(JANUARY 1975 DOLLARS IN THOUSANDS)

	-101	-102	-103	-104	-105	-106	-107	-108	-109
<b>ONE VEHICLE</b>									
ENGINEERING	\$13,080	\$14,608	\$13,574	\$13,360	\$14,888	\$13,854	\$13,031	\$14,506	\$13,472
TOOLING	8,913	10,392	9,640	9,183	10,660	9,908	8,753	10,285	9,533
MFG. LABOR	8,721	10,597	9,882	9,023	10,859	10,184	8,675	10,487	9,812
MFG. MATERIAL & EQUIP.	5,863	6,497	4,368	5,912	6,546	4,417	6,019	6,480	4,351
CFRAN	300	300	300	300	300	300	300	300	300
SUB-TOTAL	\$36,877	\$42,394	\$37,764	\$37,778	\$43,253	\$38,663	\$36,778	\$42,058	\$37,468
INITIAL SPARES, AGM, AND DATA	3,120	6,020	3,920	3,120	6,020	3,920	3,120	6,020	3,920
INITIAL INVESTMENT	\$40,027	\$48,404	\$41,714	\$40,928	\$49,303	\$42,613	\$39,928	\$48,108	\$41,418
<b>TWO VEHICLES</b>									
ENGINEERING	\$13,475	\$15,295	\$14,208	\$13,781	\$15,601	\$14,514	\$13,426	\$15,193	\$14,106
TOOLING	9,317	10,902	10,096	9,613	11,196	10,390	9,157	10,795	9,989
MFG. LABOR	15,697	19,092	17,812	16,231	19,626	18,346	15,604	18,952	17,672
MFG. MATERIAL & EQUIP.	9,591	11,153	6,895	9,675	11,237	6,978	9,905	11,137	6,879
CFRAN	600	600	600	600	600	600	600	600	600
SUB-TOTAL	\$48,680	\$57,042	\$49,611	\$49,900	\$58,260	\$50,829	\$48,692	\$56,677	\$49,246
INITIAL SPARES, AGM, AND DATA	3,620	6,720	4,220	3,620	6,720	4,220	3,620	6,720	4,220
INITIAL INVESTMENT	\$52,330	\$63,792	\$54,161	\$53,520	\$65,010	\$55,379	\$52,342	\$63,427	\$53,796

APPENDIX D

X-24C Major Equipment Items

<u>SYSTEM</u>	<u>GFAE</u>		<u>GFAE</u>	<u>CFE</u>
	<u>QTY</u>	<u>SOURCE</u>	<u>QTY</u>	<u>QTY</u>
<u>COCKPIT &amp; FURNISHINGS</u>				
ATTITUDE DIRECTOR IND.	1	X-15/X-24B		
ANGLE OF ATTACK IND.	1	X-15/X-24B		
SIDE SLIP IND.	1	X-15/X-24B		
BAROMETRIC ALTIMETER	1	X-15/X-24B		
AIRSPEED/MACH IND.	1	X-15/X-24B		
DYNAMIC PRESSURE IND.	1	X-15/X-24B		
ELAPSED TIME IND.	1	X-15/X-24B		
CLOCK	1	X-15/X-24B		
"G" METER	1	X-15/X-24B		
VERTICAL VELOCITY IND.	1	X-15/X-24B		
LONGITUDINAL VELOCITY IND.	1	X-15/X-24B		
INERTIAL HEIGHT IND.	1	X-15/X-24B		
CABIN PRESSURE IND.	1	X-15/X-24B		
WHISKEY COMPASS	1	X-15/X-24B		
HYDRAULIC PRESSURE IND.	3	X-15/X-24B		
STANDBY ATTITUDE IND.	1	X-15/X-24B		
DUAL ELEVON POSITION IND.	1	X-15/X-24B		
RUDDER POSITION IND.	1	X-15/X-24B		
SPEED BRAKE POSITION	1	X-24B		
D.C. VOLTMETER	4	X-15/X-24B		
LOX TANK PRESSURE IND.	1	X-15/X-24B		
① RP-1 TANK PRESSURE IND.	1	X-15/X-24B		
② ALCOHOL TANK PRESSURE IND.	1	X-15/X-24B		
② H <sub>2</sub> O <sub>2</sub> GAS TURBINE PRESSURE IND.	1	X-15/X-24B		
③ AMMONIA TANK PRESS. IND.	1	X-15/X-24B		
③ H <sub>2</sub> O <sub>2</sub> GAS TURBINE PRESSURE IND.	1	X-15/X-24B		
EJECTION SEAT				1
LOX CONVERTER				1

<u>SYSTEM</u>	<u>QTY</u>	<u>GFAE</u> <u>SOURCE</u>	<u>GFAE</u> <u>QTY</u>	<u>CFE</u> <u>QTY</u>
<u>AVIONICS</u>				
UHF RADIO AN/ARC-159			2	
AIR DATA PROBE				1
AIR DATA MODULES				2
INERTIAL NAV. SYSTEM				1
INTERCOMM. SET	1	X-15/X-24B		
RADAR BEACON	1	X-15/X-24B		
<u>HYDRAULIC SYSTEM</u>				
DC PUMP MOTORS	3	X-15/X-24B		
HYDRAULIC PUMPS	3	X-15/X-24B		
ACCUMULATORS				3
PRESSURE REGULATORS				3
FILTER ASSEMBLY				3
SHUT-OFF VALVES				3
RELIEF VALVES				3
<u>ELECTRICAL SYSTEM</u>				
BATTERY	5	X-15/X-24B		
<u>FLIGHT CONTROL SYSTEM</u>				
RUDDER PEDALS (SET)	1	X-15/X-24B		
YAW FEEL SPRING ASSY.	1	X-15/X-24B		
YAW TRIM ACTUATOR	1	X-15/X-24B		
MACH/ALPHA TRIM ACT.	1	X-15/X-24B		
RUDDER POWER ACT.	1	X-15/X-24B		
LEFT ELEVON POWER ACT.	1	X-15/X-24B		
RIGHT ELEVON POWER ACT.	1	X-15/X-24B		
PITCH BIAS ACTUATOR	1	X-15/X-24B		
SPEED BRAKE ACTUATOR	1	X-15/X-24B		
LOWER FLAP POWER ACT.	1	X-24B		
TRIPLEX SERVO ACT'S.				4
SIDE-ARM CONTROLLER				1
FLIGHT CONTROL COMP.				1

<u>SYSTEM</u>	<u>QTY</u>	<u>GFAE</u> <u>SOURCE</u>	<u>GFAE</u> <u>QTY</u>	<u>CFE</u> <u>QTY</u>
<u>FLIGHT CONTROL SYSTEM (CONT'D)</u>				
CONTROL PANEL				1
RUDDER PEDAL POS. XDCR.				1
RATE/ACCELERATION ASSY.				3
STATUS PANEL				1
<u>COCKPIT ENCLOSURE</u>				
CANOPY JETTISON INIT.				1
CANOPY JETTISON THRSTR				1
CANOPY WINDSCREEN	2	X-15		
GAS GENERATOR				1
ACTUATING CYLINDER				1
<u>LANDING GEAR</u>				
C-140 NOSE GEAR			1	
F-106 MAIN GEAR (SET)			1	
NOSE GEAR AIR BOTTLE				2
MAIN GEAR AIR BOTTLE				4
REGULATOR VALVES				3
CROSS OVER VALVES				1
<u>ENVIRONMENTAL CONTROL</u>				
DEWAR, 50 LITER LN <sub>2</sub>				1
CONTROL PANEL	1	X-15/X-24B		
LN <sub>2</sub> GAGE	1	X-15/X-24B		
REGULATOR				1
TRANSDUCER				1
VALVE				1
SWITCH				1

NOTE: 1 LR-105/LR-101 Configuration Only.  
2 LR-105/LR-11 Configuration Only.  
3 LR-99 Configuration Only.